INFORMATION TO USERS

This manuscript has been reproduced from the microfilm master. UMI films the text directly from the original or copy submitted. Thus, some thesis and dissertation copies are in typewriter face, while others may be from any type of computer printer.

The quality of this reproduction is dependent upon the quality of the copy submitted. Broken or indistinct print, colored or poor quality illustrations and photographs, print bleedthrough, substandard margins, and improper alignment can adversely affect reproduction.

In the unlikely event that the author did not send UMI a complete manuscript and there are missing pages, these will be noted. Also, if unauthorized copyright material had to be removed, a note will indicate the deletion.

Oversize materials (e.g., maps, drawings, charts) are reproduced by sectioning the original, beginning at the upper left-hand corner and continuing from left to right in equal sections with small overlaps. Each original is also photographed in one exposure and is included in reduced form at the back of the book.

Photographs included in the original manuscript have been reproduced xerographically in this copy. Higher quality 6" x 9" black and white photographic prints are available for any photographs or illustrations appearing in this copy for an additional charge. Contact UMI directly to order.

UMI

A Bell & Howell Information Company
300 North Zeeb Road, Ann Arbor MI 48106-1346 USA
313/761-4700 800/521-0600

THE INTERNAL STRUCTURE OF LAVA FLOWS: INSIGHTS FROM AMS MEASUREMENTS

A DISSERTATION SUBMITTED TO THE GRADUATE DIVISION OF THE UNIVERSITY OF HAWAII IN PARTIAL FULFILLMENT OF THE REQUIREMENTS FOR THE DEGREE OF

DOCTOR OF PHILOSOPHY

IN

GEOLOGY AND GEOPHYSICS

MAY 1996

By

Edgardo Cañón-Tapia

Dissertation Committee:

George Walker, Chairperson
Barry Lienert
Emilio Herrero-Bervera
Klaus Keil
Michele Teng

UMI Number: 9629814

UMI Microform 9629814
Copyright 1996, by UMI Company. All rights reserved.

This microform edition is protected against unauthorized copying under Title 17, United States Code.

UMI
300 North Zeeb Road
Ann Arbor, MI 48103

© Copyright 1996

by

Edgardo Cañón-Tapia

To P.P. for bearing the bad times,
and sharing the, fortunately not so few, good times.

To my parents.

ACKNOWLEDGEMENTS

Financial support for the completion of this work was granted by CONACyT. Some travel and field-related expenses were funded by the Jaggar Bequest fund. The collaboration of all the memebers of my committee in different stages of the research was always of incalculable value, but the companionship and help provided by George Walker deserves special acknowledgement. Also, the support shown by Prof. Ed Berg during hard times is greatly appreciated. Figures of Chapter 3 were made possible through the help of the members of the publications' department of the Department of Geology and Geophysics; and the photographs of Chapter 6 were taken by Dr. José Guerrero. Carlos Cañón Amaro provided the means for the completion of many of the remaining figures. Finally, I want to acknowledge the important task of all those that opposed the realization of this work by raising barriers of one kind or another. Unfortunately, their persistent anonymousness precludes a more detailed mention.

ABSTRACT

Lava flows are complex multicomponent systems, the details of emplacement of which are understood but in more than general terms. Anisotropy of magnetic susceptibility (AMS) is an until now unexploited technique that can yield important information to increase our understanding of such processes. Despite its successful application in inferring flow direction in pyroclastic deposits and intrusives, its utility in lava flows remains controversial as the result of some unjustified basic assumptions. For instance, the hypothesis of a single-grain dominant anisotropy is untenable if it is acknowledged that most of the magnetic grains observed in thin sections of pristine igneous rocks are not elongated (flattened), but are almost equant and probably crystallized after movement of lava had stopped. An alternative, suggested by several authors through time, has been that magnetic interactions among neighboring grains is the main source of the measured AMS. The relationship among the movement of melted rock / pyroclastic material, the final grain distribution and the measured AMS, however, had not received much attention. A model linking all this aspects is developed in this work based on the evidence gathered for more than 25 lava flows. The consequences of the new model are far reaching, requiring additional effort in the interpretation of results and a careful planning in the sampling strategy. For example, it has been possible to infer through magnetic measurements a) the location of the points where maximum velocity and/or plug structure has been attained, b) approximate vertical and horizontal velocity profiles across complete units, c) whether cooling occurred under static conditions or rather movement continued until temperature had fallen near the complete solidification of the flow, d) the occurrence of endogenous growth of flow units, and e) the direction of local movement of lava. In addition, magnetic measurements clearly reflect the internal differences of various morphologies (S-type pahoehoe, P-type pahoehoe, Toothpaste lava and A'a) that include aspects such as shear rate and cooling mechanisms. The intimate relationship that AMS bears with the fluid behavior of lava results in the almost universal applicability of the method, or in other words, it is to some extent independent of the preservation of other structures in the outcrop that have been used traditionally to infer the same information, which may be of special interest in the study of older, eroded flows, or of units lacking good exposures displaying their internal structure.

TABLE OF CONTENTS

ACKNOWLEDGEMENTS v

ABSTRACT vi

LIST OF TABLES xi

LIST OF FIGURES xii

CHAPTER 1: INTRODUCTION 1

CHAPTER 2: WHAT IS AMS? 4

MAGNETIC SUSCEPTIBILITY 4

ANISOTROPY OF MAGNETIC SUSCEPTIBILITY 5

Crystalline Anisotropy 8

Shape Anisotropy 10

Magnetic-Domain Anisotropy 12

Textural Anisotropy 15

Specimen-Shape Anisotropy 17

Relative Importance Of The Various AMS Sources 17

FIELD AND LABORATORY METHODS 18

Collection of specimens and instrument for AMS measurement 18

Bulk (volume) susceptibility. 19

Degree of anisotropy 19

Magnetic fabric 19

Mean directions and regions of confidence around them 20

CHAPTER 3: MAGNETIC FABRIC AND FLOW DIRECTION IN BASALTIC PAHOEHOE LAVA OF XITLE VOLCANO, MEXICO 21

INTRODUCTION 21

SAMPLING LOCATIONS 21

RESULTS 22

Bulk susceptibility. 22

Degree of Anisotropy. 25
Magnetic Fabrics. 25
Directions of the Principal Susceptibilities. 32
DISCUSSION 32
AMS and Flow Direction. 32
Internal Variation Within Single Units. 36
SUMMARY 38

CHAPTER 4: NEAR VENT A'A 41
INTRODUCTION 41
GEOLOGY OF THE LAVA FLOWS 45
RESULTS 46
Bulk susceptibility and direction of the principal susceptibilities. 46
a) Xitle flow 46
b) Mauna Kea flow 46
Magnetic fabrics and degree of anisotropy 54
ORIGIN OF THE FOLIATION PATTERNS 60
The origin of AMS 60
Foliations due to fluid motion 61
VELOCITY PROFILES 63
Flow conditions and rheology 63
DISCUSSION 67
CONCLUSIONS 72

CHAPTER 5: HAWAIIAN PAHOEHOE, TOOTHPASTE AND A'A 73
INTRODUCTION 73
FIELD AND LABORATORY METHODS 73
BULK SUSCEPTIBILITY 78
Variation within units 78
Variation between units 78
Discussion 89
DEGREE OF ANISOTROPY 91

Variation within units 91
Variations between units 91
Discussion 98
MAGNETIC FABRIC 101
Variation within units 101
Variations between units 112
Discussion 112
ORIENTATION OF PRINCIPAL SUSCEPTIBILITIES 113
Directions of mean principal susceptibilities and regions of confidence around them 113
Directions of the mean susceptibilities and flow direction .. 121
Vertical variation of the direction of the principal susceptibilities 122
Discussion 130
a) Zonation of the velocity field 130
b) Flow direction 130
CONCLUSIONS 132

CHAPTER 6: MODE OF FORMATION OF LARGE VESICLES FROM XITLE VOLCANO LAVAS 133
INTRODUCTION 133
SITE DESCRIPTION 135
RESULTS 135
Active ascent 135
Belljar vesicles 144
DISCUSSION 144

CHAPTER 7: FLOW DIRECTION OF THE BIRKETT FLOW, COLUMBIA RIVER BASALT, INFERRED FROM AMS MEASUREMENTS 149
INTRODUCTION 149
SITE DESCRIPTION 149

RESULTS 152
Implications for the mode of emplacement 153

CHAPTER 8: GEOLOGICAL APPLICATIONS OF AMS IN IGNEOUS ROCKS - A CRITICAL REVIEW 157
INTRODUCTION 157
ORIENTATION OF THE PRINCIPAL SUSCEPTIBILITIES 157
Pyroclastic deposits 158
Lava flows 160
Intrusives 162
CONSEQUENCES FOR THE INTERPRETATION OF RESULTS 162
POST-EMPLACEMENT DISRUPTION OF AMS FABRIC 164
SUMMARY 164

APPENDIX 1: SINGLE GRAIN VS. DISTRIBUTION ANISOTROPY - A SIMPLE 3D MODEL 166
INTRODUCTION 166
MAGNETIC INTERACTION: 3D MODEL 166
MAGNETIC INTERACTION: LINEATION 170
MAGNETIC INTERACTION: FOLIATION 171
MAGNETIC INTERACTION: 3D DISTRIBUTION 174
DISCUSSION 174
CONCLUSIONS 182

APPENDIX 2: CODE OF ORIGINAL MATLAB FUNCTIONS 183

APPENDIX 3: TABLES 199

REFERENCES 227

LIST OF TABLES

Table		Page
2.1	Mean susceptibility and density of common rock forming minerals	6
2.2	Saturation magnetization, demagnetization factors, demagnetization fields and crystalline energy barriers for three Ti-magnetites	13
3.1	Degree of anisotropy of various lava flows	28
3.2	Magnetic fabric of various lava flows	31
4.1	Principal susceptibilities of all specimens of near vent a'a (Xitle unit)	47
4.2	Principal susceptibilities of all specimens of near vent a'a (Mauna Kea unit)	50
5.1	General information of hawaiian pahoehoe, toothpaste lava and a'a units	74
5.2	Statistical parameters of distributions of magnetic variables of hawaiian pahoehoe, toothpaste lava and a'a units	76
5.3	Mean principal susceptibilities and regions of confidence of hawaiian lava	119
6.1	Principal susceptibilities of all specimens near large vesicles in Xitle lava	140
A3.1	Data of Xitle pahoehoe lava used in Chapter 3	199
A3.2	Data of S-type pahoehoe lava used in Chapter 5	202
A3.3	Data of P-type pahoehoe lava used in Chapter 5	209
A3.4	Data of a'a lava used in Chapter 5	213
A3.5	Data of toothpaste lava used in Chapter 5	220
A3.6	Data of Birket flow lava used in Chapter 7	223

LIST OF FIGURES

Figure	Page
2.1 Mineral contributions to rock susceptibility	7
2.2 Magnetic domains and grain size	14
2.3 Closure domains	16
3.1 Xitle lava flow field map	23
3.2 Profiles of Xitle pahoehoe lava	24
3.3 Variation of bulk susceptibility in Xitle pahoehoe	26
3.4 Variation of degree of anisotropy in Xitle pahoehoe	27
3.5 Variation of magnetic fabric in Xitle pahoehoe	30
3.6 Equal area projection of principal susceptibilities of Xitle pahoehoe (all specimens)	33
3.7 Plunges of principal susceptibilities closer to geologically inferred flow direction in Xitle pahoehoe	34
3.8 Flow of lava from steeper to shallower slope.	37
3.9 Equal area projection of principal susceptibilities of Xitle pahoehoe (selected specimens)	39
4.1 Photographs of two near vent a'a flows	42
4.2 Foliation patterns and sample location of two near vent a'a units	49
4.3 Equal area projections of principal susceptibilities of two near vent a'a units (all specimens)	53
4.4 Relationship between the plane of magnetic foliation and vesicle foliation in two near vent a'a units	55
4.5 Dependence of orientation of shear plane on relative values of shear stresses	64
4.6 Temporal evolution of adjacent fluid elements under constant stress (2-D)	65
4.7 Velocity profiles of two near vent a'a units	68
4.8 Evolution of the susceptibility tensor under the influence of gravitational forces	71
5.1 Variation of volume and mass susceptibility in hawaiian lava	79
5.2 Variation of volume and mass susceptibility with thickness of hawaiian lava	87
5.3 Frequency histograms of volume and mass susceptibility in hawaiian lava.	88
5.4 Variation of degree of anisotropy in hawaiian lava	92
5.5 Frequency histograms of degree of anisotropy in hawaiian lava	96
5.6 Variation of degree of anisotropy with thickness of hawaiian lava	97
5.7 Temporal evolution of adjacent fluid elements under constant stress (3-D)	99
5.8 Variation of magnetic fabric in hawaiian lava	102
5.9 Frequency histograms of magnetic fabric in hawaiian lava	110
5.10 Variation of magnetic fabric with thickness of hawaiian lava.	111

5.11 Equal area projection of principal susceptibilities of hawaiian lava (selected specimens) . 114
5.12 Density contour plots of selected units of hawaiian lava 124
6.1 Modes of bubble ascent 134
6.2 Photographs of three globular vesicles 136
6.3 Photographs of two belljar vesicles 138
6.4 Relationship between principal susceptibilities and contour of three goblular vesicles in Xitle lava 146
6.5 Relationship between principal susceptibilities and contour of ttwo belljar vesicles in Xitle lava 147
7.1 Map of the zone near Sentinel Gap 150
7.2 Structural features, and sample location in Birkett flow. 151
7.3 Equal area projection of principal susceptibilities of Birkett flow (selected specimens) 154
7.4 Mode of endogenous growth fro the Birkett flow. 156
A1.1 Model used to investigate the relative importance of interactive and non-interactive hypothesis for the origin of magnetic susceptibility in igneous rocks 167
A1.2 Ratios of principal susceptibilities against particle separation (linear example) 172
A1.3 Evolution of magnetic fabric with changing particle separation (linear example) 173
A1.4 Ratios of principal susceptibilities against particle separation (2D example) 175
A1.5 Evolution of magnetic fabric with changing particle separation (2D example) 176
A1.6 Ratios of principal susceptibilities against particle separation (3D example) 177
A1.7 Evolution of magnetic fabric with changing particle separation (3D example) 178
A1.8 Effects of remanence in the measurement of magnetic susceptibility 181

CHAPTER 1: INTRODUCTION

Lava flows are commonly the products of effusive volcanic activity, although in some instances they may originate by the coalescence of explosively generated fragments falling from fire fountains. Irrespective of their origins, all lava flows are complex systems formed of a suspension of solid crystals and gas bubbles in a liquid phase. Both crystals and gas are, for the most part, the result of a decrease in temperature and confining pressure of the parent magma and consequently their abundance and external characteristics are a function not only of the bulk chemical composition of the magma, but also of the way in which the surrounding temperature and pressure conditions change with time. Actually, as the occurrence of lava flows is restricted to its surface, by definition, the most important changes in the pressure conditions of the system have already occurred during the ascent of magma from the interior of the planet, and therefore, the most important changes during the life-time of an active lava flow are those related to cooling. Nevertheless, the internal evolution of a lava flow remains still a complex phenomena, the details of which are only beginning to be barely understood.

From the perspective of an outside observer, lava flows behave as a single coherent phase with some rather peculiar characteristics. The rheological behavior of lavas may be approximated at different times by either Newtonian or Binghamian models, and many of their internal characteristics can be explained, at least in general terms, without the need of really sophisticated techniques. However, as recently pointed out "... despite the wealth of observational data gathered over the last decades, they (active lavas) remain poorly understood in anything but general terms..." (Kilburn and Luongo, 1993).

The original purpose of this dissertation was to increase our understanding of the dynamics of lava flows by studying some of their internal features through magnetic measurements. However, it was necessary to limit its content to the development of a physical model linking the fluid behavior of lava with the anisotropy of magnetic susceptibility (AMS) measured in rock specimens, leaving open the door for the completion of the original goals. Various reasons contributed to this change of emphasis, including time and economical factors, but the main reason is that the methodology commonly

employed to "read" the information gathered by AMS measurements of rock specimens ignores the most essential aspects of the problem, and therefore a number of prior conceptions needed to be modified to fit the empirical evidence. This process of modification of the underlying theory behind AMS measurements required several steps in which the first results served as the supporting point for the following phase by questioning some older conceptions, while only partially suggesting the correct answers that would be resolved after new evidence was gathered. Because each of these steps contained interesting results from the perspective of the particular geological problem, they were conceived as independent studies, and mainly due to time constrains, they are now compiled in this dissertation essentially in their original form. Thus, the organization of the work follows a line traced in time rather than a retrospective view in which part of the first results may well deserve a re-examination to the light of the latter discoveries in order to convey the idea of unalterability commonly associated with scientific knowledge (at least by most outsiders to the field). Rather, let this work be used to illustrate the point that advances in science usually are not the result of overnight revolutions, but of a continuous labor that needs to look back critically every now and then.

In Chapter 2 some basic definitions and concepts are introduced together with a presentation of the model commonly employed to interpret AMS measurements prior to this work. Also, note is made of the most important assumptions made by that model, and of the problems or inconsistencies resulting from it. Chapter 3 is the first attempt to interpret AMS measurements taking into account all the information contained in the measurements. Results of this chapter, thought to be essentially correct, would no doubt suffer the most modification when subject to the final model as developed later. Chapters 4 and 5 contain the bulk of the empirical evidence on which the proposed model is based. Actually, the general lines of that model are outlined in Chapter 4, and details are later refined in Chapter 5. Chapters 6 and 7 are examples of the application of the new approach in the study of the internal structure of lavas, that although limited in scope are nonetheless illustrative of the potential offered by magnetic methods. Finally, in Chapter 8 a survey of the applicability of AMS in igneous rocks is carried out by critically reviewing the literature in the field. Usually, a literature survey of this type is the introductory chapter of any dissertation, but it is considered that, in view of the sometimes

antagonistic conclusions reached by previous works, the discussion is more fruitful by acknowledging the model proposed in this dissertation. The last part of Chapter 8 also includes some indications for future work. Chapters 3 to 7 will be (had been) submitted for publication as separate papers coautored with members of my committee that actively collaborated in their conception. The bulk of their content, as they appear here, is my own responsabilty.

Appendix 1 is devoted to some theoretical aspects of the model that were conceived at about the same time as Chapter 4, and that most certainly lead to the modifications introduced in Chapter 5. Appendix 2 contains a list of most of the software developed for its use at different stages of the work, especially in the latter stages; the code used is that of MATLAB, which enormously simplifies the text of the programs due to the inherent tensorial aspects of the magnetic susceptibility. Finally, Appendix 3 contains the results of the measurements made on all specimens used in the various chapters, if these had not been included already in the main text.

CHAPTER 2: WHAT IS AMS?

MAGNETIC SUSCEPTIBILITY

The general subject of magnetism is intimately related with the atomic structure of matter. Movement of electrons around the nucleus, as well as a spinning motion upon their own axis, result in the magnetic properties of any material. The interaction of electrons with an externally applied magnetic field results in the departure of the equilibrium conditions attained in the absence of the field. This is called "induced magnetization". In particular, crystalline solids are characterized for the possession of an ordered atomic structure in which definite atoms occupy fixed positions. The interaction among electrons of neighbor atoms determines the physical properties of the crystal, including those controlling the details of the magnetization process. These latter define what has been named "magnetic susceptibility".

From a mathematical point of view, both the magnetic field (H) and the magnetization (M) are vectors. In general H and M are not parallel, therefore requiring the magnetic susceptibility (K) to be defined as a second order rank tensor to ensure a linear relationship between H and M. Symbolically, this is represented by the equation

$$\underline{M} = \mu_0 \, \underline{\underline{\kappa}} \, \underline{H} \qquad (2.1)$$

where μ_0 is the permeability of vacuum, a escalar constant equal to $4 \pi \times 10^{-7}$ Henrys / meter. In the SI of units, M and μ_0 H have the same units (Ampere / meter) and therefore K is a dimensionless entity (note that since M is referred to unit volume, although dimensionless K is sometimes called the volume susceptibility, Nye (1960)).

Equation (2.1) is valid in general, except for the cases where the intensity of H is very high, and therefore K is most correctly referred to as low-field volume magnetic susceptibility. In this work, we always will be concerned with this type of susceptibility eliminating the need for the repetition of the

complete name. In a very few instances when the low-field mass susceptibility, χ (defined as $\underline{K}$ / weight) is used, this will be explicitly indicated.

Three different types of susceptibility: diamagnetic, paramagnetic and ferromagnetic, can be distinguished (e.g., Brailsford, 1966). Rock minerals displaying any of these three types exist in nature, the most abundant volumetrically being either paramagnetic or diamagnetic. Certainly, all the mineral grains as well as any non-crystalline material contribute to the total susceptibility of a rock, although their individual influence depends on both their concentration and their individual susceptibility. The higher values of ferromagnetic susceptibility relative to the other two types may produce that the susceptibility of the whole rock is dominated by even a very small fraction of ferromagnetic minerals. For example, Borradaile (1988) estimated that as little as 1 vol % of magnetite would be enough to control the susceptibility of the rock (Figure 2.1). Typical values of the susceptibility of various common rock forming minerals are listed in Table 2.1.

From figure 2.1, it can be observed that in rocks yielding susceptibility values larger than 8×10^{-4} the main contributions will most probably arise from the ferromagnetic fraction, therefore allowing us to interpret the results only in terms of these minerals. Clearly, the higher the measured value of the whole-rock susceptibility the better this approximation. As common values of the susceptibility measured in igneous rocks in general, and most specifically in lavas, are higher than 10^{-3}, we will only be concerned with the susceptibility arising from the ferromagnetic fraction.

ANISOTROPY OF MAGNETIC SUSCEPTIBILITY

Equation (2.1) has been proposed to express the general case of a linear relation between $\underline{H}$ and $\underline{M}$. This includes cases where $\underline{H}$ and $\underline{M}$ are not parallel, as well as cases in which the susceptibility is dia-, para-, or ferromagnetic. If $\underline{M}$ is always parallel to $\underline{H}$, irrespective of the direction in which $\underline{H}$ is applied, $\underline{K}$ is said to be isotropic. Magnetic susceptibility will be anisotropic in any other case.

Ferromagnetic minerals are characterized, among other things, by the possession of a special type of magnetization even in the absence of an externally applied magnetic field. This will be called "spontaneous" or "remanent" magnetization depending on the size and chemical composition of a

TABLE 2.1. Mean susceptibility of some common rock-forming minerals (after Tarling and Hrouda, 1993; Carmichael, 1984)).

	Mineral	Mean Susceptibility x 10^{-6}	Density Kg/m^3
Paramagnetic	Hornblende	8920	3080
	Chlorite	70 - 1550	2800
	Biotite	998 - 1290	2900
	Muscovite	122 - 165	2831
Diamagnetic	Quartz	-14	2648
	Calcite	-14	2710
	Dolomite	-38	2866
Ferromagnetic	Magnetite	30056	5200
	Hematite	1325	5300
	Maghemite	24000	4800
	Pyrhotite	5 - 92	4600

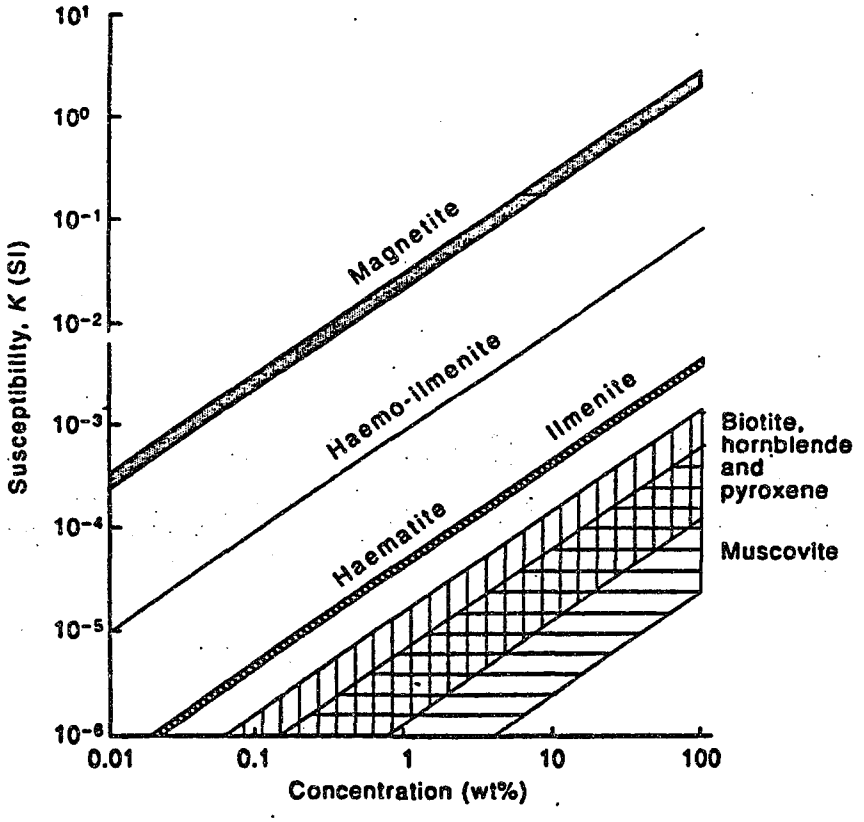

FIGURE 2.1. Contribution to the susceptibility of a rock from various minerals (from Tarling and Hrouda, 1993).

particular grain. In any case, this magnetization is independent of the external magnetic field, and therefore it should be clear that the term $\underline{M}$ in eq. (2.1) does not apply to this type of magnetization exclusive of ferromagnetic minerals. Unfortunately, this limitation of eq. (2.1) is very often overlooked, resulting in some misconceptions regarding magnetic fabric, as will be discussed in the following paragraphs, together with the factors determining whether the measured $\underline{\underline{K}}$ is iso- or anisotropic. The relative importance of the contribution of each of the various sources of anisotropy, that range from crystalline to specimen-size scales, is discussed later in this Chapter.

Crystalline Anisotropy

In Fe - Ti oxides, the outer electrons of their Fe or Ti atoms strongly interact with each other using the intermediate oxygen atoms as "spin-bridges". This coupling of atomic magnetic moments, known as super-exchange (e.g., Stacey and Banerjee, 1974), is in fact responsible for the peculiar magnetic properties of all the ferromagnetic minerals, of which the Fe - Ti oxides are the most common.

The spin structures are directed so as to minimize the magnetic energy of the crystal; the directions for which this is accomplished are called "easy" directions. On the contrary, those directions in which the energy of the crystal is a maximum are called "hard" directions, giving place to what is called magneto-crystalline anisotropy.

In cubic structures, the easy directions correspond to any of the crystallographic directions [100] (the edges of the cube), [110] (the diagonals along the faces), or [111] (the diagonals across the cube), depending on the particular atoms involved and on the temperature of measurement. At room temperature most Ti-magnetites have [111] easy directions and [100] hard directions (O'Really, 1984).

For crystals with hexagonal symmetry, the easy direction may be either parallel or perpendicular to the c-crystallographic axis, depending also on the temperature and exact chemical composition of the mineral. Hematite at low temperatures (below 260 K) has an easy direction parallel to the c-axis, but at higher temperatures the easy direction lies in the basal plane.

The net alignment of atomic magnetic moments in ferromagnetic minerals, due to the super-exchange forces, may give place to a spontaneous magnetization which exists even in the absence of

an externally applied magnetic field. The magnitude of this spontaneous magnetization is characteristic of the particular chemical composition and the dimensions of the unit cell of a given mineral; its direction will coincide, in principle, with any of the easy directions of the crystal. Disregarding the effects of the free surfaces of the crystal (which will be introduced later), the only effect that an externally applied magnetic field may have in a small enough ferromagnetic grain is to rotate its spontaneous magnetization away from the easy direction to make it parallel to the field, provided that the intensity of the field is large enough to overcome the energy barriers that confine the spontaneous magnetization to the easy direction in its absence. If this is the case, the induced magnetization of the mineral is not only a function of the external magnetic field, but also depends on the position of the spontaneous magnetization before the external magnetic field is applied. Further, if the external field was closer to an easy direction that originally did not contain the spontaneous magnetization of the grain (there is always at least one such direction, 180° from the original position), after the field is removed the spontaneous magnetization will not return to its original position but rather will be shifted to the new easy direction. This effect of flipping the direction of spontaneous magnetization has ocasionally been used as a measure of the magnetic susceptibility of the grain. However, due to the dependence on the initial conditions a second measurement of susceptibility may yield exactly the opposite results than those obtained in the first measurement, clearly leading to an internal inconsistency in the quantification of magnetic susceptibility. At present, there are not experimental results available that could be used to solve this problem mainly due to the extremely small grain sizes involved and to the need for avoiding the effects of magnetic interaction between neighboring grains. The inherent technical difficulties associated with these features make uncertain whether such results will be available in the near future. In any case, because this effect involves magnetic fields of relatively high intensity, it is not important in the characterization of the magnetic fabric as concerned in this work, where magnetic fields do not exceed 800 A/m.

If field intensity is not strong enough to rotate the spontaneous magnetization away from the easy direction, or in other words, if $\underline{M}$ remains constant regardless of the orientation of $\underline{H}$, a different situation takes place. In this case, the induced magnetization is zero for every position of the external field, and

therefore, according to eq. (2.1), so will be the magnetic susceptibility. Clearly, this is of little use in the characterization of the magnetic susceptibility of any material, but fortunately the inclusion of the effects of the free surface of the grain modify the situation to our advantage.

Shape Anisotropy

The free surfaces of a crystal result in the presence of uncompensated poles which act as the source for a magnetic field called the "demagnetizing field" ($\underline{H}_d$). The strong dependence of the demagnetizing field on the geometry of the distribution of unpaired poles in the surface of the grain has granted the name of "shape anisotropy" to the effects arising from the action of $\underline{H}_d$.

The demagnetizing field can be obtained from any distribution of unpaired poles (i.e., from any body with an arbitrary shape) by using the same methods commonly employed in the potential theory, although the only possible shapes for which an analytical approach is permissible are ellipsoids (Maxwell, 1904). Inside any ellipsoid, the components of $\underline{H}_d$ along its principal axes are related to the components of $\underline{M}$, in the absence of any other field, by

$$H_{di} = - N_i M_i \qquad (2.2)$$

where i = x, y, z are the directions of the principal axes of the ellipsoid, and N_i are constants determined by the axial ratios of the ellipsoid. Values of N_i for ellipsoids of revolution have been given by Stoner (1945) and for the general ellipsoid by Osborn (1945).

The demagnetizing field is directed opposite to the polarization of the grain-surface that generates it, although according with eq. (2.2) it is not necessarily antiparallel to the spontaneous magnetization (in general, $Nx \neq Ny \neq Nz$; they are equal only in the case of a sphere). Therefore, the demagnetizing field exerts a torque on the spontaneous magnetization to rotate it away from the easy direction in a way completely analogous to the manner in which an externally applied magnetic field would do it (it is very important to remark, however, that the demagnetizing field in small enough grains and their spontaneous magnetization are inseparable). In larger grains the polarization of their free-surfaces results in the division of the grain into separate magnetic domains, and therefore the physical situation

becomes slightly more complex. Examination of this case will therefore be postponed until the following section, and here we will limit the discussion to the cases of small enough grains.

In some instances $\underline{H}_d$ may be strong enough to overcome the energy barriers associated with the magnetocrystalline anisotropy, therefore rotating away the spontaneous magnetization from an easy direction, but in other cases $\underline{H}_d$ is not strong enough to rotate the spontaneous magnetization from an easy direction and will only reduce the energy barriers of the structure. In any case, the magnetic energy of the grain would be a function with several local minima, the position of which depends on the exact chemical composition and shape of the grain, An external magnetic field will change the position of those minima while acting on the grain, so that the magnetization of the grain is rotated from its position of equilibrium. In general, it is assumed that for weak fields the changes in the energy function of the grain are reversible, so that the spontaneous magnetization will return to its original position after the field is not longer present, and therefore, that the induced magnetization can now be described through eq. (2.1). Clearly, the stronger the demagnetizing field (the more elongated or flattened the shape of the grain), the more likely this assumption will be valid even for small grains.

It is possible to evaluate the relative importance of the shape anisotropy for different mineral compositions by comparing values of $\underline{H}_d$ for different grain shapes with the values of the energy barriers (E) required to rotate the spontaneous magnetization away from an easy direction. Shape anisotropy will be dominant if $H_d > E$, and the magnetization will be parallel to the direction of the grain for which H_d is minimized. If, however, the minimum value of $H_d \approx E$, the orientation of the spontaneous magnetization will be controlled to a large extent by the crystalline easy directions. In Table 2.2, values of the energy barriers and of $\underline{H}_d$ for several shapes and compositions within the Ti-magnetites have been calculated using eq. (2.2). Values for the demagnetizing factors were taken from Stoner (1945), of saturation magnetization from O'Really (1984) and of the energy barriers from Stacey and Banerjee (1974). From the Table it can be seen that although shape anisotropy will be dominant for almost any mineral within the Ti-magnetite group, there are some instances in which crystalline anisotropy cannot be neglected. This is especially clear for minerals with larger Ti content, where the energy barrier is more than half the largest value of $\underline{H}_d$ in all but one (the most oblate) case. Crystalline anisotropy is

on the contrary the dominant term for all the minerals of the ilmeno-hematite group (Stacey and Banerjee, 1974).

Magnetic-Domain Anisotropy

It was mentioned in the previous section that free surfaces of larger grains produce different effects than those described for small grains. In effect, because the presence of unpaired magnetic poles is restricted, ideally, to the surface of the grain, an increase in size will tend to leave unaffected the internal parts of the mineral while the atomic moments closer to the free-surface will be subject to the polarization effects more strongly. This asymmetry in the forces acting on the atomic moments deep inside and near the surface of the grain results in the splitting of its magnetic structure. Those atomic moments closer to the surface are more likely to occupy an easy direction closer to the tangent of the free surface so to minimize the polarization by reducing the density of "free" poles. This, in turn, produces that the atomic moments in the internal parts of the grain occupy different easy direction in order to eliminate any internal polarization. Therefore, not all the atomic moments in the internal parts of the grain can lie along the same easy direction (as was the case for small grains), but in adjacent regions they should lie along different (sometimes opposite) easy directions depending on the changes imposed by the alignment of atomic moments near the surface (Fig. 2.2). In a narrow zone at the borders between two regions, each having its atomic moments directed along a different easy direction, the atomic moments will be forced to occupy intermediate, transitional directions. Each of the zones with an uniform direction of magnetization (an easy crystallographic direction) is called a "magnetic domain", and the intermediate zones are called "domain walls".

The details of the creation of a grain possessing several magnetic domains (called multidomain, MD, as opposed to the small grains previously discussed that had only one single domain, or SD-grains), are not well understood, in part because the MD configuration is not unique for a given grain. Two examples of observed, very different arrangements of magnetic domains near the free surfaces of grains are shown in Fig. 2.3.

TABLE 2.2. Values of Saturation magnetization (Ms), Demagnetization factors (Np, Neq), Demagnetizing field($H_{d\,p}$ and $H_{d\,eq}$) and energy barriers (E) for various grain shapes with polar / equatorial ratios as indicated, and three different chemical compositions.

	p/eq	Ms x 10^5 (A/m)	Np	Neq	$H_{d\,p}$ x10^5 (A/m)	$H_{d\,eq}$ x10^5 (A/m)	E x 10^4 (A/m)
	0.4		.588154	.205923	2.82	0.99	
	0.9		.361822	.319089	1.74	1.53	
Fe_3O_4	1.0	4.8	.333333	.333333	1.60	1.60	2.98
	1.1		.308285	.345057	1.48	1.66	
	2.5		.135146	.432427	0.65	2.08	
	0.4		.588154	.205923	2.53	0.88	
	0.9		.361822	.319089	1.56	1.37	
$Fe_{2.9}Ti_{0.1}O_4$	1.0	4.3	.333333	.333333	1.43	1.43	6.22
	1.1		.308285	.345057	1.33	1.49	
	2.5		.135146	.432427	0.58	1.86	
	0.4		.588154	.205923	0.71	0.25	
	0.9		.361822	.319089	0.43	0.38	
$Fe_{2.4}Ti_{0.6}O_4$	1.0	1.2	.333333	.333333	0.40	0.40	2.65
	1.1		.308285	.345057	0.37	0.41	
	2.5		.135146	.432427	0.16	0.52	

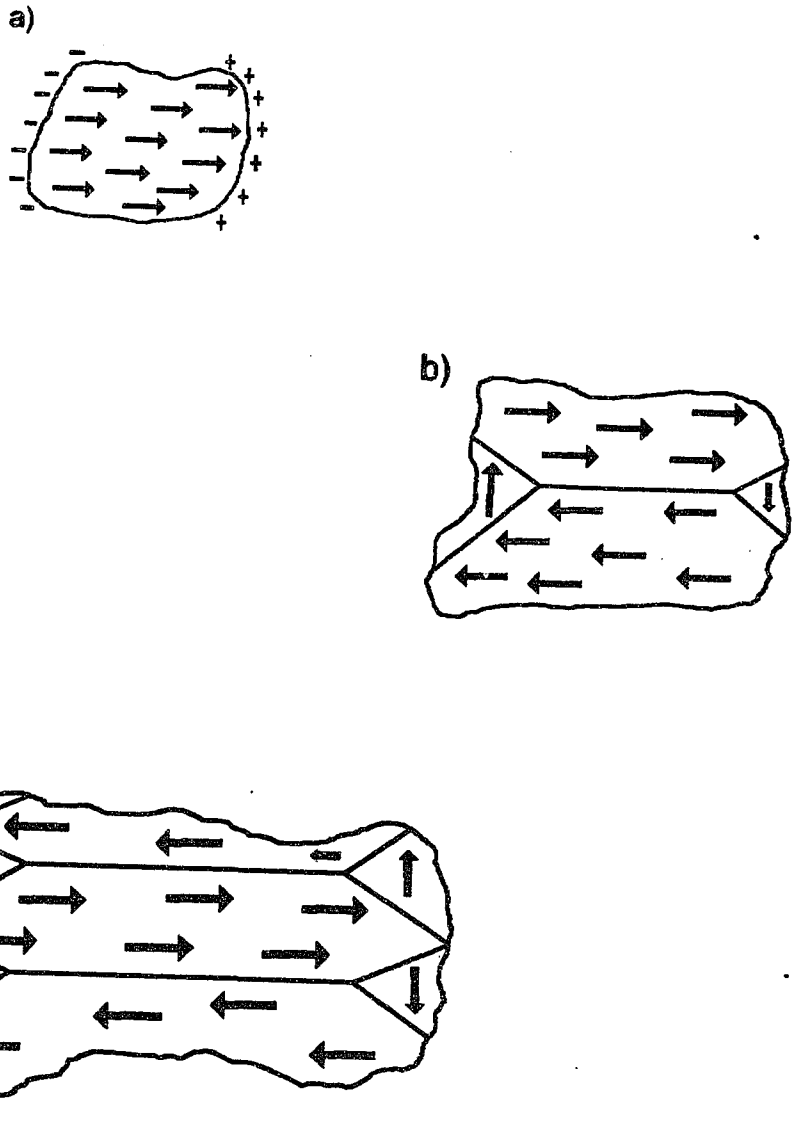

FIGURE 2.2. Magnetic domains and their relation to the size of the grain.

Splitting of a grain in various magnetic domains will in general reduce the strength of the associated demagnetizing field, although only in very few, if any, occasions will the demagnetizing field be reduced to zero. However, as opposed to the SD case, MD grains can have any value of magnetization from zero up to saturation depending on the balance between mutually antiparallel domains. Changing the equilibrium conditions through an external magnetic field results in the displacement of the domain walls, which increases the volume of some domains while decreasing the volume of others. The energy associated with domain-wall displacement is generally small, and if the displacement is not very large it is a reversible process. Depending on the pre-existing domain configuration, as well as on the location of any crystalline defects, not all the directions will require the same amount of energy to induce the same amount of magnetization, and therefore an asymmetry in the magnetic susceptibility is defined. The effective importance of the demagnetizing field as a factor controlling the AMS, is therefore reduced because of the very weak values of the net magnetization commonly encountered in MD grains, although the external shape will be important in determining the orientation of the easy directions of magnetization of a MD grain to the extent that it may have influenced the pre-existing domain configuration, or to the point that it may facilitate the displacement of domain walls along any particular direction. Despite all these differences from the previous case, eq. (2.1) still remains valid.

Textural Anisotropy

So far we have discussed the effects of an externally applied magnetic field over an isolated ferromagnetic grain. In rocks in general, however, ferromagnetic grains are not isolated, but they are surrounded by a large number of other mineral grains with which they interact in different ways. In the present context, the magnetic interaction between neighbor ferromagnetic grains is the most important.

The magnetization of any ferromagnetic grain within a rock produces a magnetic field that affects neighbor particles, especially those at short distances. This field that originated from the magnetization of individual particles will be referred here as the "interactive field". On application of a magnetic field with sources external to the rock, the magnetization induced in any individual ferromagnetic grain will be the resultant of both the external field and the interactive field. Therefore, not only the AMS of the

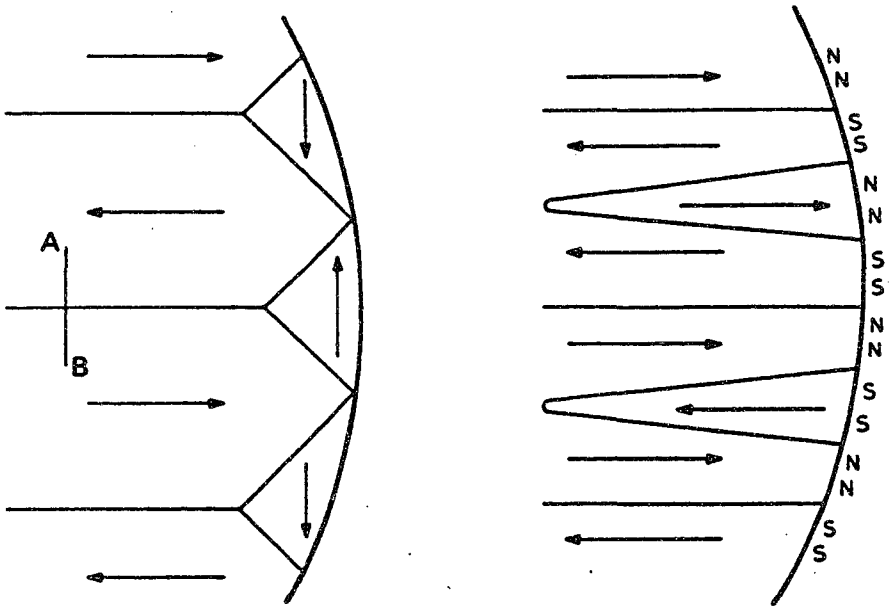

FIGURE 2.3. Two different configurations of closure domains (from O'Reilly, 1984).

individual particles is measured, but the resulting AMS includes a contribution from the magnetic interaction of ferromagnetic particles. The anisotropy resulting from the unequal distribution of ferromagnetic grains within a rock has been called "textural anisotropy" by Grabovsky (1956, as cited in Grabovsky and Brodskaya, 1958), and more recently "distribution anisotropy" by Hargraves et al. (1991). This source of AMS has been usually neglected, although in the model proposed in this work for the AMS of igneous rocks, it becomes the single most important source.

Specimen-Shape Anisotropy

In complete analogy with the demagnetizing field resulting from the unpaired poles on the surface of any ferromagnetic grain, a demagnetizing field associated with the shape of a rock-specimen can be defined. The net magnetization of the rock will be, in general, extremely weak relative to the saturation magnetization of ferromagnetic minerals and therefore, the relative importance of the demagnetizing field associated with the shape of the specimen will be negligible (Collinson, 1983). Ellwood (1979), however, presented experimental evidence showing that the influence of the length/ diameter ratio of specimens with cylindrical shape should not be disregarded. Clearly, in the measurement of the AMS of a rock any anisotropy arising from the shape of the rock specimen used to make the measurements should be completely eliminated. Based in theoretical grounds, Noltimier (1971) showed that a ratio equal to 0.865 allows any cylindrical specimen to be approximated by an uniformly magnetized sphere, therefore possessing zero shape anisotropy. A similar ratio had been previously suggested by Porath et al. (1966) based on experimental results.

Relative Importance Of The Various AMS Sources

Use of the adequate length/diameter ratio, as explained above, will minimize the effects of the specimen shape in the measured AMS. The relative importance that the other factors have in such measurements is difficult to assess in more than general terms due to the large number of parameters involved. For example, each mineral grain may have a characteristic orientation of its individual magnetic anisotropy determined by the relative importance that crystalline and shape anisotropies have

on each particular grain depending on factors such as the particular chemical composition, the shape and size of the grain and the pre-existing domain configuration for the cases of MD grains. Additionally, to estimate the degree of interaction existing among ferromagnetic grains within a specimen it is necessary to know the exact position (in 3D) of every grain, the distance between any two of them, and the intensity of the remanent magnetization of each individual grain.

In nature, clusters of grains will be places where magnetic interaction is certainly important, while large, definite non-equant particles may be practically isolated in magnetic terms. As an example of the difficulties that would be faced in any attempt to create a more realistic source model, in the Appendix 1 the effects of individual shape anisotropies are included in a simplistic array of particles. The resulting orientations of the principal susceptibilities prove to be a complex function of the particle separation along the three directions of reference, and of the orientation and shape of the particles despite all the simplifications made. Nevertheless, it can be concluded from those results that whenever magnetic interaction occurs, this will be the dominant source of AMS.

FIELD AND LABORATORY METHODS

Each of the subsequent chapters is based on the results obtained from the measurement of the AMS of rock specimens collected from several lava flows. In every case, field and experimental methods remained the same, and results were always expressed in terms of a few basic quantities. Definitions of this type are given next with the purpose of avoiding unnecessary repetitions.

Collection of specimens and instrument for AMS measurement

Rock specimens were collected with the help of a gasoline powered drill. Cylindrical cores having a diameter of 2.5 cm were oriented using a magnetic compass and clinometer before removing them from the flows. At least one specimen from each core, having an approximate volume of 10 cm^3, was subsequently cut at the Laboratory of Paleomagnetism of the University of Hawai'i. Measurement of the AMS of the specimens was made using a Kappabridge KYL-2 instrument at this Laboratory.

Bulk (volume) susceptibility

Magnetic susceptibility is the property of matter that determines its internal response to an external magnetic field; it is a dimensionless quantity in the SI. If the applied field has a low intensity (< 800 A/m), the magnetic susceptibility displays a directional variability that is well represented by a second rank symmetric tensor (Tarling and Hrouda, 1993). The principal directions and values of the susceptibility tensor correspond to the directions and magnitudes of the three principal susceptibilities, denoted by kmax, kint and kmin. Bulk susceptibility (km) is defined as the arithmetic mean of the three principal susceptibilities.

Degree of anisotropy

The three principal susceptibilities have been combined in several ways leading to the definition of anisotropy parameters in an attempt to characterize the measured susceptibility tensor. Parameters quantifying the departure from the isotropic case (when all three principal susceptibilities are equal) are usually referred to as "degree of anisotropy" parameters. As shown by Cañón-Tapia (1994), most degree of anisotropy parameters yield qualitatively equivalent results differing only in their range of numerical values. In this work, I used the A parameter ($A = 100\ \{1 - ((kmin + kint) / 2\ kmax)\}$), ranging from 0% (isotropic) to 100%, and in Chapter 2 also the P parameter (Jelinek, 1981) with comparative purposes ($P = \exp\{2((p_1)^2 + (p_2)^2 + (p_3)^2)\}$).

Magnetic fabric

A different type of susceptibility parameter, presumably characterizing the development of magnetic foliation and/or lineation, has also been widely used in AMS studies. Two main classes of the so called shape parameters were identified by Cañón-Tapia (1994) based on their geometrical behavior within the field of the susceptibility tensors. Parameters in the first group are defined in such a way that their range remains constant between two fixed values irrespective of the degree of anisotropy of the corresponding susceptibility tensor, whereas parameters of the second group have a range that is a function of the degree of anisotropy. Because there are not at present any physical bases to prefer any

one group in particular, one parameter from each was used in each chapter. From the first type of parameters I used either U = (2kint - kmax - kmin)/(kmax - kmin) with fixed range between -1 and +1 (Jelinek, 1981), or $V = \sin^{-1}\{ (kint - kmin) / (kmax - kmin) \}^{1/2}$ with fixed range between 0° and 90° (Graham, 1966). From the second type I used B = 100 { (kmin - 2 kint) / kmax + 1} with maximum range within the limits -100 and 100.

Mean directions and regions of confidence around them

I calculated the mean principal susceptibilities using the tensorial approach of Hext (1963). Regions of confidence around the directions of the mean principal susceptibilities were calculated with two different methods: Linear approximation (Jelinek, 1978; Lienert, 1991) and Bootstrapping (Constable and Tauxe, 1990). Graphically, only the former are displayed for clarity, but the lengths of the two semiaxes of each region were always reported numerically for both methods to allow a direct comparison. The size of these regions was classified based on the scheme proposed by Cañón-Tapia et al. (1994).

CHAPTER 3: MAGNETIC FABRIC AND FLOW DIRECTION IN BASALTIC PAHOEHOE LAVA OF XITLE VOLCANO, MEXICO

INTRODUCTION

Xitle is the youngest (2400 BP; Libby, 1951) and only basaltic volcano in the Chichinautzin monogenetic volcanic field (Gunn and Mooser, 1970; Martin del Pozzo, 1982); it is located on the southern edge of Mexico City and human settlements now cover large parts of the flow field. Extensive quarrying of this rock, however, has produced many excellent outcrops which provide easily accessible cross sections of the lava flows.

The Xitle lava preserved in and near the National University of Mexico (UNAM) campus is a compound pahoehoe flow made of a great number of lava flow units that range in thickness from 0.2 to 13.0 m. We sampled two flow units in 1992 as part of a pilot study of the variation of magnetic properties, including magnetic fabric, and due to the encouraging results (Cañón-Tapia et al., 1993), sampled three more units in 1993.

In this chapter I discuss the results of the measurements of anisotropy of magnetic susceptibility (AMS) and its correlation with structural features (e.g., thickness and vesicle-deformation fabric) of the flow units as well as the application of this rock-magnetic technique to determining the flow direction.

SAMPLING LOCATIONS

The locations of the sampling sites are shown in Figure 3.1. In all cases, we collected samples from the topmost unit so as to avoid possible effects of reheating by overlying lava. Moreover, at site 9 the sampled unit rests on a paleosol and is the only unit present.

Of the five sampled profiles, three (profiles 2, 9 and 6) extend from top to bottom of flow units 8.2 m, 4.7 m and 1.6 m thick, respectively; one (profile 22) includes only the lower 1.1 m of a 6.0 m thick unit; and one other (profile 1) embraces the top 5.5 m of the flow and consists of the tilted crust of a tumulus on a unit of unknown thickness (Fig. 3.2). The angle of rotation of different parts of the last profile was inferred from the flat top crust and the vesicle foliation that are clearly observed in the field;

the axis of rotation was assumed to coincide with the geologically-inferred flow direction, and in the following only the structurally corrected results are discussed.

All flow units are highly vesicular in their upper third and almost non-vesicular in their lower two thirds apart from a vesicular layer containing pipe vesicles in the basal 0.5 to 1.0 m (Walker, 1995a). The plunge direction of these pipe vesicles, the orientation of ropy structure on the surface crust of the units, the elongation direction of the flow lobes, and the slope of the terrain were combined to infer the overall flow direction of each unit. This direction is referred to as the geologically inferred flow direction. Minor segregation veins up to 5 cm thick, slightly coarser and more vesicular than the lava they cut, occur near the median plane of each unit and some were sampled. The segregation veins indicate lava that remained liquid after solidification of most parts of the unit; the bulk chemical composition of this late liquid may be slightly more differentiated than that of the flow as a whole (c.f. Kuno, 1965).

RESULTS

Bulk susceptibility

Values for the bulk susceptibility (k_m) calculated as the mean of the three principal susceptibilities from the Xitle lavas average about $6x10^{-3}$. This is slightly lower than the value obtained from lava flows of O'ahu (~$2x10^{-2}$, E. Herrero-Bervera, unpub. data) and from the Azufre volcano in Argentina (~$2x10^{-2}$, Cañón-Tapia et al., 1994). Profiles 2, 1 and 22 give the highest values (between $8x10^{-3}$ and $7x10^{-3}$) and profiles 9 and 6 give the lowest (between $5x10^{-3}$ and $4x10^{-3}$). The difference between the largest and smallest values is very small when compared with the large variations (of several orders of magnitude) found in rocks containing very different amounts of ferromagnetic minerals, as for example some granites or metamorphic rocks (Tarling and Hrouda, 1993).

Variations of k_m within flow units are shown in Figure 3.3. The peak values in the middle of profiles 9 and 2 (Figs. 3 a and b) are given by samples collected from segregation veins. Excluding these, k_m tends to increase toward the upper margin from the central parts of these units, although in a narrow zone at the top a sudden decrease takes place. In profile 6 the reverse relationship is observed.

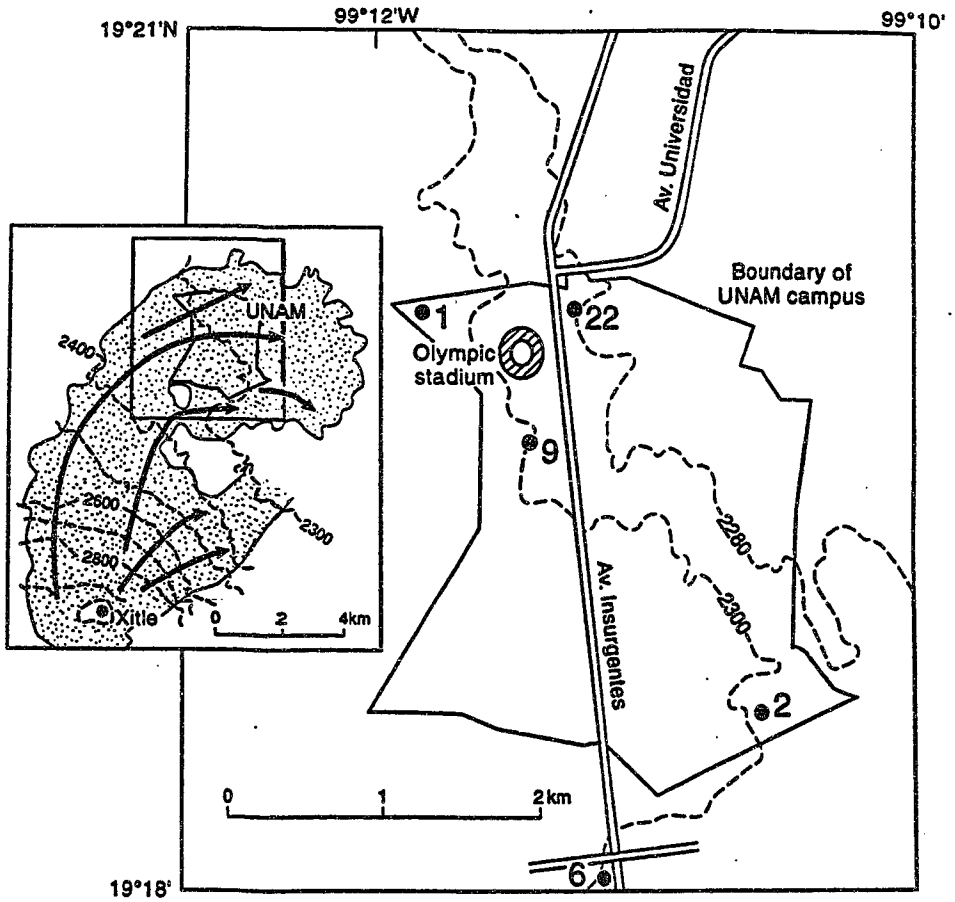

FIGURE 3.1. Location of the sampled profiles in the Universidad Nacional Autonoma de México (UNAM) campus and its vicinity. Dashed lines-contours, elevation in meters. Inset: UNAM campus in relation to Xitle lava flow field. Arrows give the lava flow direction inferred from geological features.

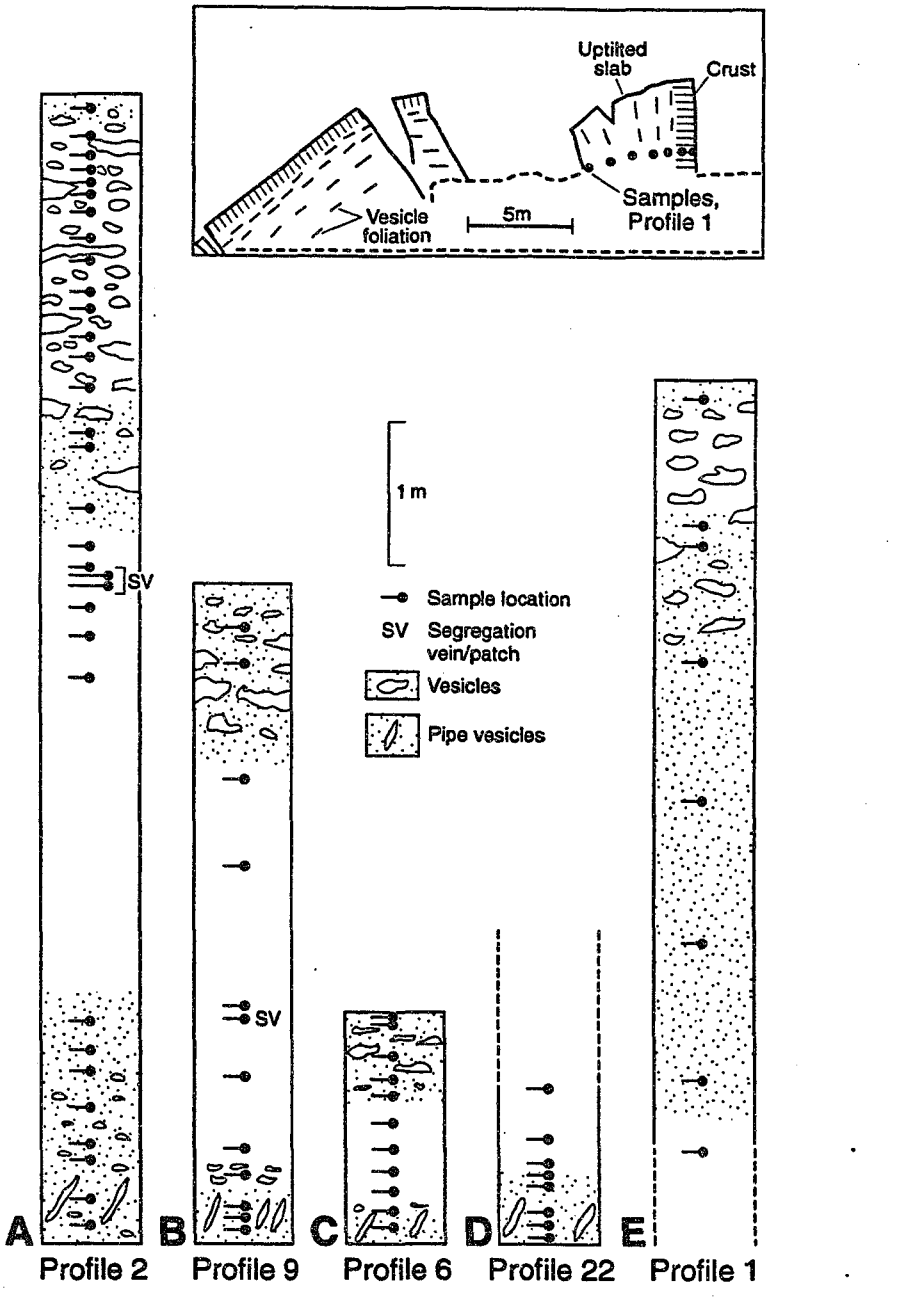

FIGURE 3.2. Profiles of the five lava flow units sampled, showing sample locations in relation to vesicle zonation and other features. Inset - cross section of the tilted block (tumulus) from which the profile 1 samples were collected.

Centeno-García et al. (1986) found similar variations in the magnetic susceptibility across the boundaries of superimposed flow units in the Xitle lavas, suggesting its possible connection with the observed degree of oxidation of the rock. Petersen (1976) pointed out that, in general, the degree of oxidation in thin flows will tend to be higher towards their upper parts, while in flows exceeding 6 m thick preferential escape of hydrogen from their central parts may produce inner zones of high oxidation. In the present case, the observed variations of k_m are compatible with the general picture given by Petersen (1976).

Degree of Anisotropy

Internal variations of the degree of anisotropy within single units are shown in Fig. 3.4. Apparently, the degree of anisotropy increases with depth in the unit, although the differences between top and bottom are rather small and may not be significant. Typical values of anisotropy are between 1% and 2%, except in the middle parts of profile 9 and the lower part of profile 1 (Figs. 3.4 b and e) where values of . 5% were obtained.

When we compare the values obtained in these flows with those from different types of lavas (Table 3.1) we find that andesite lavas from Azufre give much higher values than those from Xitle or Ko'olau suggesting a possible relationship with the silica content (following Tormey et al., 1989; Gunn and Mooser, 1970; Verma and Armienta, 1985; MacDonald and Katsura, 1964), and therefore the viscosity of the lava. General differences in flow thickness (in decreasing order Azufre-Xitle-Ko'olau) seem consistent with this interpretation. Also, from the data in Table 3.1 (a and b) it would appear that a'a flows on average tend to yield higher values of the degree of anisotropy than pahoehoe, although further work is needed before it is possible to draw any definitive conclusion.

Magnetic Fabrics

The two parameters used in this chapter to measure the magnetic fabric yield equivalent results for the two partial profiles and for profile 6, but in profiles 2 and 9 some quantitative differences are observed (Fig. 3.5). In profile 2, the V parameter indicates the presence of a unique zone with a slightly

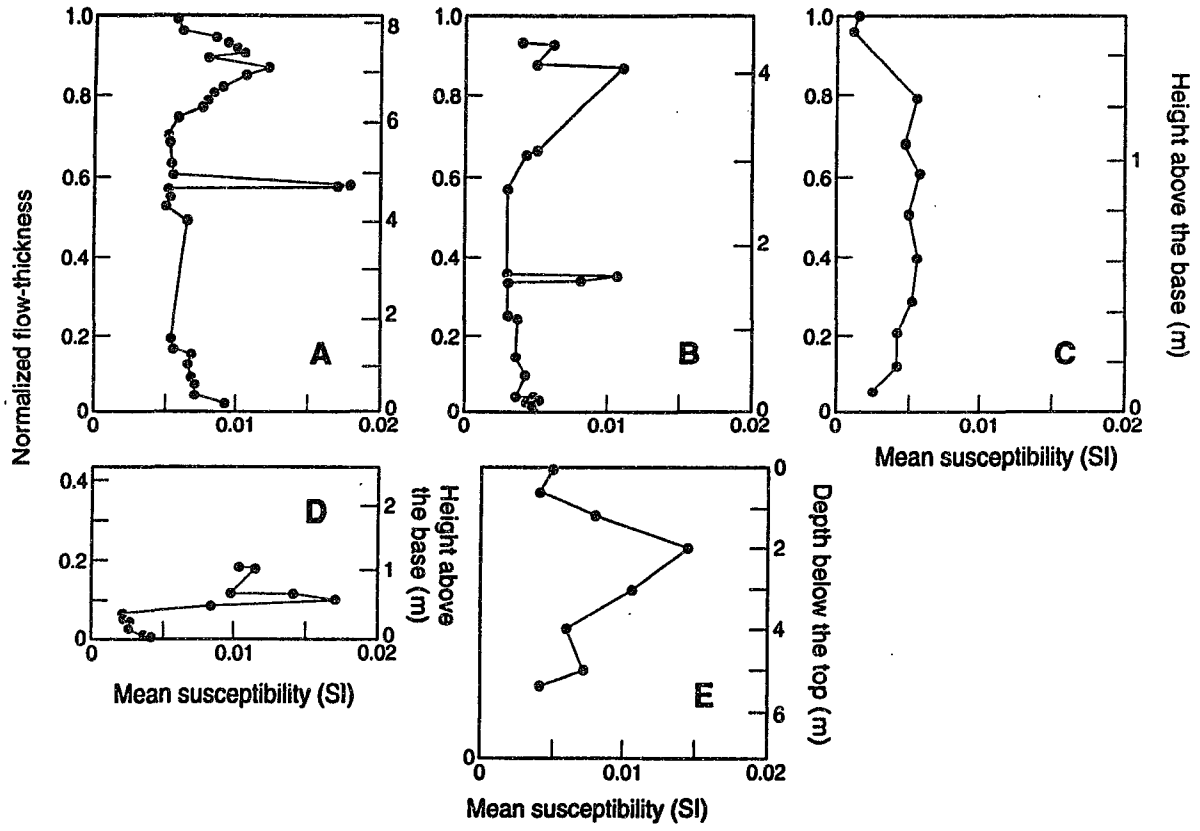

FIGURE 3.3. Variation of bulk susceptibility within the five profiles of Xitle lavas. Total thickness of the flow used to normalize the heights shown (except in profile 1 whose total thickness is not known) is given in the right scale of each profile.

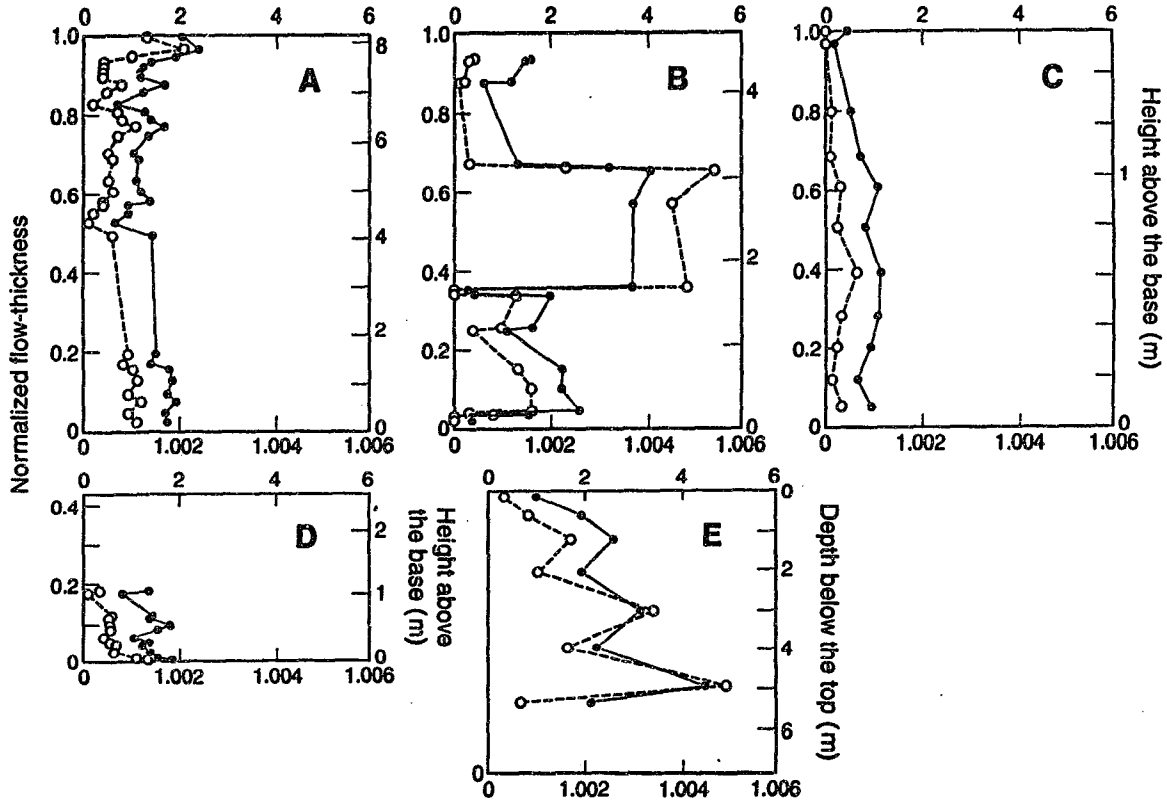

FIGURE 3.4. Variation of the degree of anisotropy within the five profiles of Xitle lavas. See text for details. Dashed lines - P' parameter, solid lines - A parameter.

TABLE 3.1. a) Average values of the degree of anisotropy of the five Xitle units studied. The two figures listed correspond to the A parameter of Cañón-Tapia (1992) and the P' parameter of Jelinek (1981) where $A = 100\ (1-(k_3+k_2)/2k_1))$ and $P' = (\exp\{2(p_1^2 + p_2^2 + p_3^2)\}$, $p_i = \ln(k_i/k_m')$ for i=1,2,3 and k_m'= geometric mean of the principal susceptibilities. b) Average values from different types of lavas, as indicated.

a)

PROFILE	A(%)	P'	
1	2.4	1.0018	Thick unit on moderate slope
9	1.7	1.0013	Moderate unit on shallow slope
2	1.4	1.0007	Thick unit on shallow slope
22	1.4	1.0006	Moderate unit on shallow slope
6	0.7	1.0002	Thin unit on shallow slope
MEAN	1.54	1.0009	

b)

SITE	A(%)	P'	
AZUFRE	3.0	1.0040	8 aa flows on steep slope
XITLE	2.1	1.0013	1 aa flow on steep slope
OAHU	1.0	1.0003	3 aa flows on steep slope
OAHU	0.3	1.0000	1 pahoehoe on shallow slope

higher degree of magnetic foliation at a height fraction of between 0.8 and 0.6, while the B parameter indicates a relatively uniform magnetic foliation through the whole thickness of the unit. In profile 9 the B parameter identifies a zone of higher foliation between 0.35 and 0.65 height fraction that is not shown by the V parameter. The physical relevance of these differences is not clear at present, although by using the B parameter it was possible to design a consistent criterion that allowed the size reduction of the regions of confidence around the mean susceptibilities as explained in the next section.

On average, magnetic foliation is a little more developed in profiles 2 and 1 than in profiles 9, 22 and 6 (Table 2a, B parameter). Assuming that the exposed section of profile 1 is less than half of the total thickness of the flow (which is a reasonable assumption in view of the mechanism of formation of this type of tumulus as discussed by Walker, 1991, 1995b), the degree of development of the magnetic foliation would be directly related to the total thickness of the unit, which may be of great importance in the study of the internal emplacement mechanism of lava flows. For instance, it is known from a structural study (Walker, 1995b) that most of the Xitle flow units continued to thicken by endogenous growth by the "lava rise" mechanism of Walker (1991) after they were emplaced, and therefore it would follow that the thicker units are more likely to be subject to larger degrees of internal deformation or shearing. This internal deformation would conceivably affect the development of the magnetic foliation; the larger the amount of internal shearing, the better developed the magnetic foliation. Clearly, the previous assumption is valid only for the B parameter and not for the V parameter and therefore, as there is yet no physical basis to prefer any one parameter, the conclusions drawn should be taken as a reasonable inference deserving further investigation.

Comparison of the magnetic fabric of the pahoehoe Xitle lavas with that of lavas from other settings (Table 3. 2b, parameter B; data sources as in Table 3. 1b) would seem to indicate that larger degrees of internal deformation occur, on average, in a'a than in pahoehoe units of similar composition. The average magnetic fabric of the Azufre lavas (8 flow units), defines a strong magnetic lineation, which may be the consequence of their higher viscosity as indicated in the preceding section, for such lavas would move more like a plug presenting limited internal deformation therefore preserving a strong vesicle lineation. The data base is, however, meager.

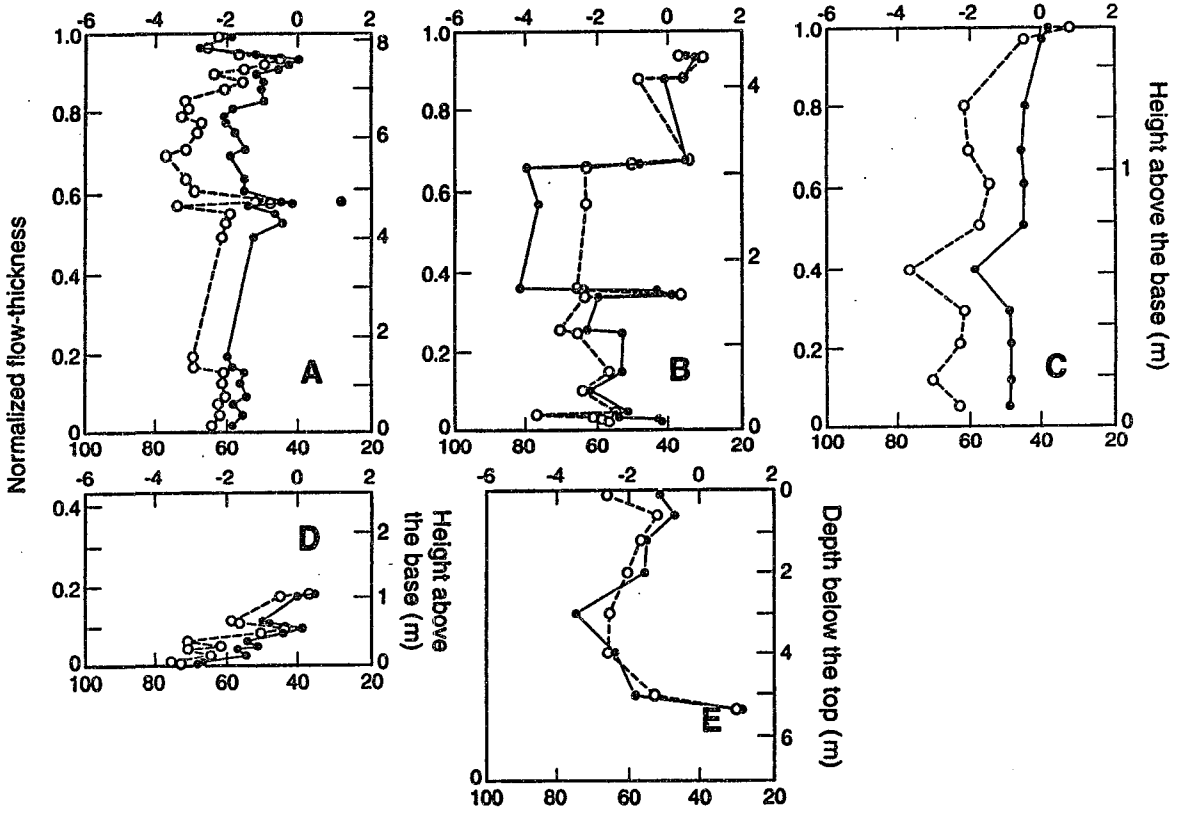

FIGURE 3.5. Variation of the magnetic fabric in the five profiles of Xitle lavas. B parameter (solid lines), V parameter of Graham (dashed lines). Magnetic foliation increases to the left for both parameters.

TABLE 3.2 a) Average values of the magnetic fabric of the five Xitle units contained in this work. The two parameters used were the B parameter of Cañón-Tapia (1992) and the V parameter of Graham (1966) where $B = 100 ((k_3-2k_2)/k_1 +1))$ and $V = \sin^{-1} \{(k_2-k_3)/(k_1-k_3)\}^{1/2}$. See text for details. b) Average magnetic fabric of other types of lavas as in Table 3.1.

a)

PROFILE	B(%)	V(°)	Flow thickness (m)
2	-1.42	64	8.2
1	-1.39	56	> 5.5
9	-1.12	55	4.7
22	-1.10	59	6.0
6	-0.64	58	1.6
MEAN	-1.13	58	

b)

SITE	B(%)	V(°)
XITLE (aa)	-1.43	59
OAHU (aa)	-0.41	57
OAHU (ph)	-0.04	48
AZUFRE (aa)	+1.35	42

Directions of the Principal Susceptibilities

Figure 3.6 consists of lower hemisphere equal-area plots of the principal susceptibility axes for the five Xitle profiles. The apparent large scatter is similar to that found by previous studies of AMS in lava flows (Khan, 1962; Symons, 1975). By using the statistical tools provided by Hext (1963), however, and criteria proposed by Cañón-Tapia et al. (1995) to classify the size of the regions of confidence, the groupings of the principal directions (Fig.3. 6) range from moderate to very good in most cases. An exception is profile 6 where all the three principal susceptibilities are poorly clustered around their mean. In the other four profiles, the minimum susceptibilities are much better grouped than either maximum or intermediate susceptibilities, which usually define a girdle-like arrangement around the mean minimum. The mean direction of the minimum susceptibilities lies within 10° to 20° of the vertical. The direction of the mean maximum susceptibility of profiles 9, 22 and 1 agrees quite well with the geologically-inferred flow direction, but in profiles 2 and 6 it is the mean intermediate instead. In the former cases (Figs. 3.7b, 3.7d and 3.7e), most of the maximum susceptibility axes are contained within ± 22.5° of the flow direction, and have an upflow plunge in the basal parts of the unit. In profiles 2 and 6, on the contrary, all the three principal susceptibilities are within 22.5° of the flow direction (Figs. 3.7a and 3.7c) almost irrespective of the position of the sample in the unit, although in profile 2 (Fig. 3.7a) four distinctive groupings of samples can be identified (see discussion below).

The plunge of the principal susceptibilities in profile 6 (Fig. 3.7c) seems to be rather random, whereas on profile 2 (Fig. 3.7a) an upflow plunge is clear in the upper parts of that flow-unit.

DISCUSSION

AMS and Flow Direction

AMS measurements have proved to be reliable indicators of flow directions in pyroclastic flows (e.g., Ellwood, 1982; Knight et al., 1986) and dikes (e.g., Knight and Walker, 1988; Ernst and Baragar, 1992; Staudigel et al., 1992, Puranen et al., 1992) but some doubt has existed about their utility in lava

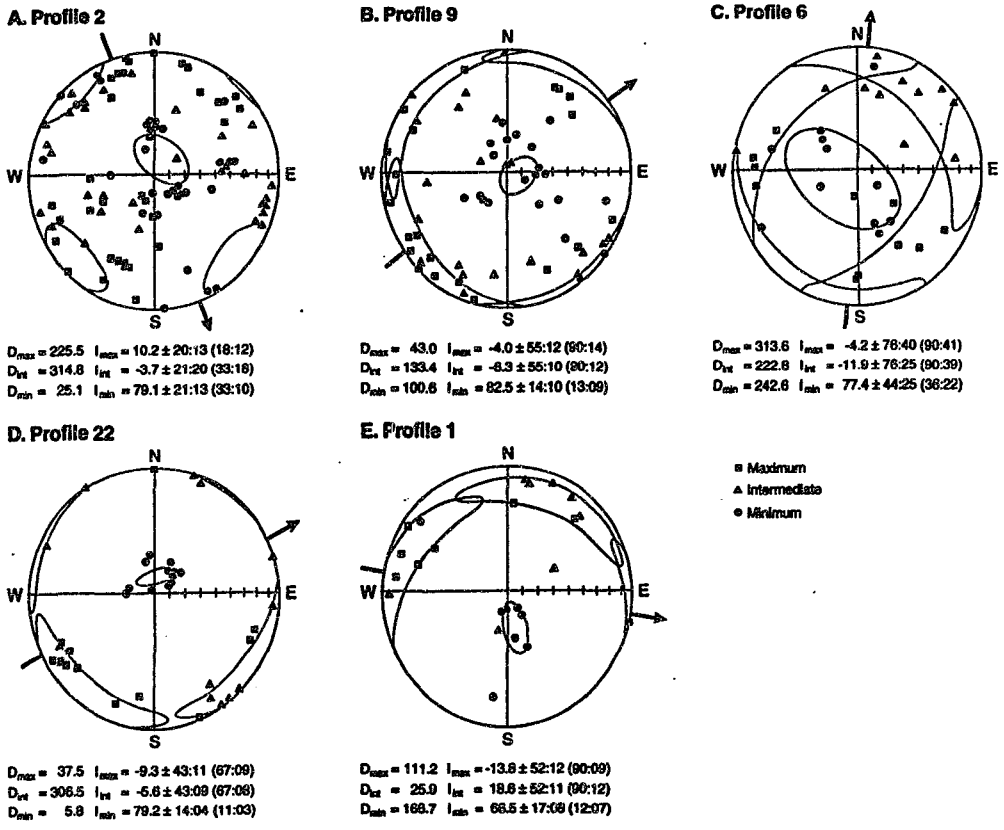

FIGURE 3.6. Equal area projection (lower hemisphere) of the directions of the principal susceptibilities measured on the five profiles. Geologically inferred flow direction is given by the arrows. The regions of confidence shown are those calculated with the linear approximation of Jelinek (1978). Numbers in parentheses allow comparison with the regions of confidence obtained with the bootstrap method of Constable and Tauxe (1990).

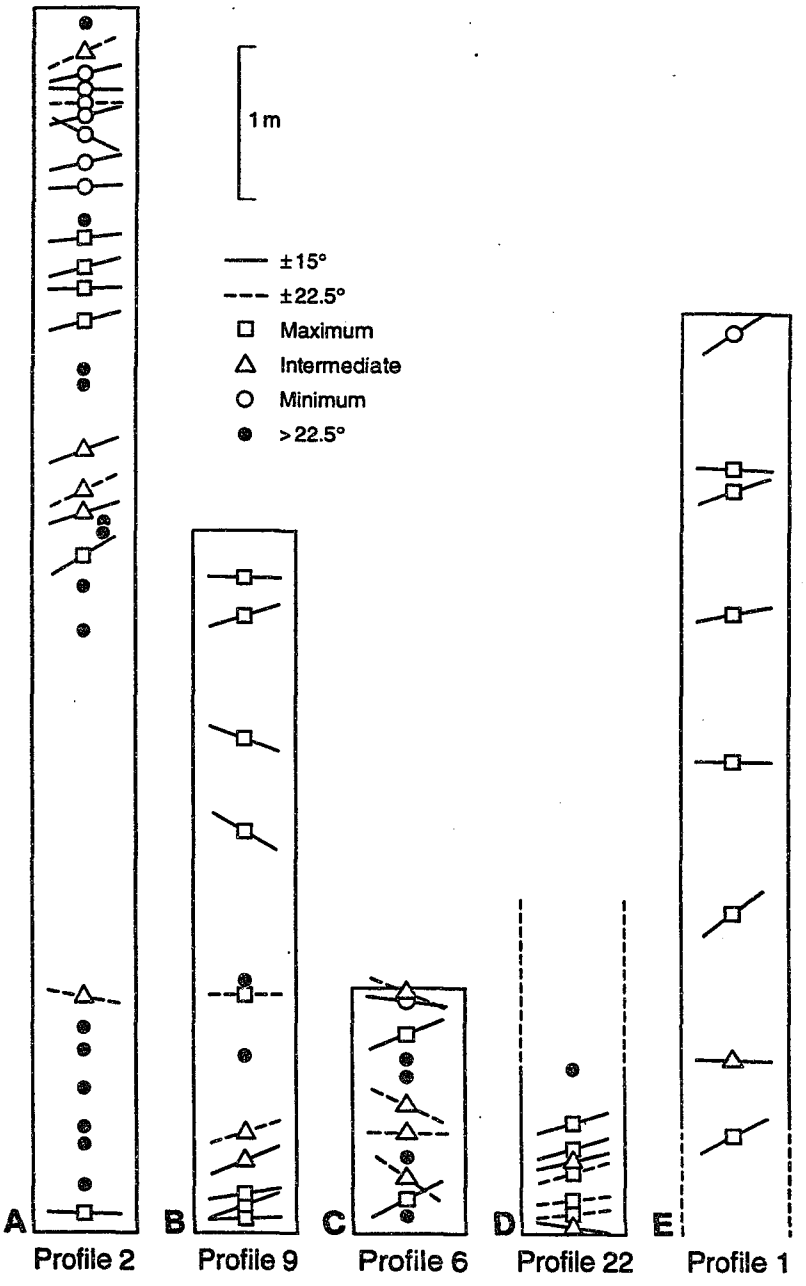

FIGURE 3. 7. Plunges of the mean principal susceptibility lying within ± 22.5° of the geologically inferred flow direction (dashed line) or ± 15° of it (solid line). The central symbol indicates whether it is the maximum (square), intermediate (triangle) or minimum (circle) mean. Solid circles are samples for which no principal susceptibility lies within 22.5° of the flow direction.

flows. For example, Symons (1975) could not find any significant relationship between the geologically inferred flow direction of the Aiyansh flow and the mean direction of the principal susceptibilities. This may be because samples were collected only from the surface of the flow where rotation of blocks during emplacement may occur, or cooling effects could modify to some extent the original directions of AMS. Moreover, the statistical methods available at that time to calculate the mean directions of the principal susceptibilities were largely inappropriate.

More positive results were obtained by Khan (1962), who found that the mean intermediate susceptibility was roughly parallel to the flow direction of lava flows although the scatter of the main susceptibilities was large, and by Kolofikova (1976; reported by Hrouda, 1982) who found a good agreement between the direction of the maximum axis of susceptibility and the flow direction, but only in the intermediate and not in the frontal parts of the flow. MacDonald et al. (1992) also found a parallelism between the principal maximum susceptibility and lineations assumed to be produced by laminar flow of lava.

In the case of the Xitle lavas, I found that either the mean maximum or the mean intermediate susceptibilities point in the same direction as the geologically-inferred flow direction. These apparently contradictory results can be reconciled, however, by considering the way lava flows move.

The dimensions, especially the width and thickness, of lava flows are strongly controlled by the rheological properties and the slope of the preexisting terrain (e.g. Gauthier, 1973; Hulme, 1974; Baloga and Pieri, 1986; Naranjo et al., 1992). Assuming constant rheological properties along a flow, a decrease in slope results in both a widening and a thickening of the lava, to reach the new equilibrium configuration. In widening, the lava will thus be forced to change its direction of movement locally except, perhaps, close to the axis of the flow, as schematically shown in Figure 3.8. Thus, in those regions away from the flow axis, the local flow direction may be nearly perpendicular to the direction of advance of the front of the lava lobe. Moreover, small variations in direction and amount of the groundslope, as well as the resistance that may be encountered by the flow at the front of the lobe due to the formation of a rigid crust or the accumulation of debris, may cause subsidiary lobes to form in directions at an angle of up to 90° with the main lobe.

In our case, the present day slope of the terrain in the locations of profiles 9, 1 and 22, where the mean maximum susceptibility and the geological information were in agreement, is steeper (, 4°) than that of profiles 2 and 6 (< 1°). The first three units form rather narrow lobes, and this can be interpreted as resulting from flow down a moderate paleoslope. Also, profile 9 unit rests on a paleosol, which eliminates the possible effects of the underlying flows on the topography.

I conclude that the mean maximum susceptibility points in the direction of the local movement in every case; the local movement coincides with the direction of advance of the unit as a whole only in the cases where the slope is steeper.

Internal Variation Within Single Units

As described above, the axes of minimum susceptibility are usually better clustered than the other two principal susceptibilities. The degree of clustering of the maximum susceptibilities was improved, however, by filtering out selected specimens from the profile. The criteria that proved to be the most useful to reduce the confidence regions around the mean maximum susceptibility were 1) to eliminate specimens having a degree of anisotropy lower than an arbitrary threshold value (different for each unit) and 2) to take out from the calculations those specimens with a particularly large degree of foliation. These criteria resulted in the removal of 25% - 58% of the specimens in each profile. The remaining specimens yield the distributions shown in Fig. 3.9. The regions of confidence around the mean maximum and intermediate susceptibilities were most clearly reduced after filtering on profiles 9, 22, and 1 (compare figs. 3.6b, 3.6d, and 3.6e with 3.9b, 3.9d and 3.9e).

Groups of specimens at very specific positions within the flow units defining well clustered axes of maximum susceptibility were delineated through filtering. For example, in profile 6 specimens from the upper and lower parts of the unit define two clusters that reflect a 15°- 20° imbrication in opposite directions of k_1; the effects of a rotation around an axis trending in a NW-SE direction are also indicated by these two clusters, and seem to be responsible for the large dimensions of the regions of confidence around the mean values. The opposite imbrication of the k_1 axis of specimens from the upper and lower parts of the unit is most clearly observed in profile 9. Additionally, in unit 9 a third

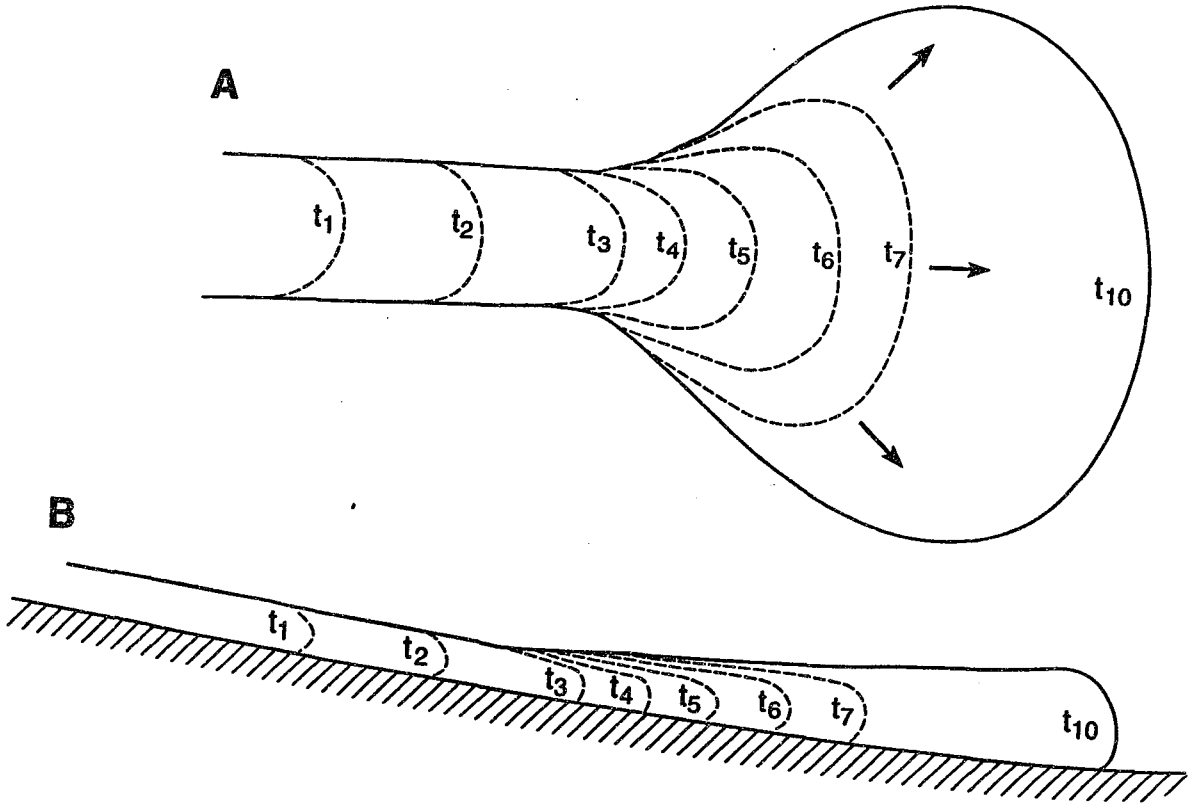

FIGURE 3.8. Flow of lava that passes from a steeper to a shallower slope a) in plan view and b) in cross section. t1...t10 indicate the position of the front at approximately equal time intervals. Note that lava reaching the shallower slope will have significant vertical and lateral components of flow as widening and thickening occur.

group of specimens, in which the directions of maximum susceptibilities are nearly normal to these found near the top and bottom, is defined by specimens from its central parts, namely those showing the higher degrees of development of the magnetic foliation as indicated in a previous section.

In the profile of unit 2, three groups of specimens, roughly corresponding to the upper, middle and basal parts of the unit, were identified. The k_1 directions in the upper and lower parts of the unit do not show the imbrication relationship found in the other two complete profiles, although this could be due to the high vesicularity observed in the upper section. All of the specimens from the upper part of this unit have the k_3 axis parallel to the geologically inferred flow direction. It is not clear why this should occur, although possible explanations may include 1) the exclusive presence of single domain magnetite in this region of the flow leading to an inverse magnetic fabric (Rochette, 1988), 2) distortion of the flow patterns due to turbulence or to the effect of rising bubbles, 3) deviation of flow direction in late-injected lava from the original flow direction during endogenous growth and, 4) the rotation of a rigid crustal block of lava during movement of the flow. The last possibility was suggested by the resemblance of the distribution of the AMS measurements of this group (Fig. 3.9b) to the results for profile 1 before introducing the structural correction (not shown). Detailed study of other magnetic properties is needed to validate the first possibility, while the other three are more difficult to evaluate.

Yet a fourth group of only four specimens located between the upper and middle parts of the flow can be identified in this unit. These specimens have a better degree of definition of the magnetic foliation than the rest of the specimens from the unit. For this reason, they are not included in Figure 3.9a, although their k_1 directions are nearly parallel to the geologically inferred flow direction. Usually, a better development of a magnetic foliation may be associated with a stronger influence of shearing stresses of some sort, and therefore the presence of this fourth group of specimens may be indicating the location of a region within the unit in which internal shearing was stronger during emplacement. The possible rotation of the upper block of the unit is compatible with this interpretation.

SUMMARY

Main conclusions of this chapter are:

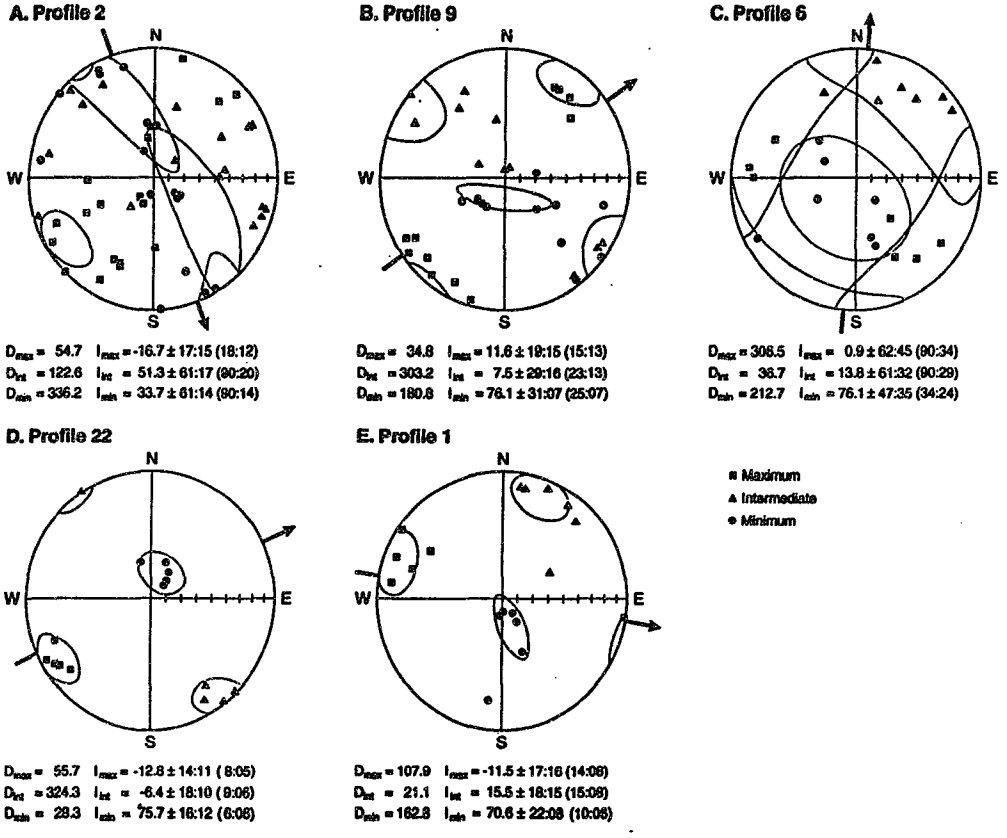

FIGURE 3. 9. Equal area projection of the directions of the principal susceptibilities of selected samples of the five units. Symbols as in Fig. 3.6.

1) It is possible to infer the flow direction of lava flows from AMS measurements.

2) An imbrication of the maximum axis of susceptibility in opposed directions at top and bottom may be observed very clearly in some profiles, which may constrain the azimuth of motion of lava flows, although certainly some complications may distort this behavior.

3) Among the possible complications that may exist in the interpretation of AMS measurements the most important are a) the principal maximum susceptibility is more likely to be directed parallel to the direction of the local movement, which may be different from the direction of advance of a lava flow, b) the presence of large vesicles and the possibility of significant crustal rotations may disturb the AMS initially related with the flow of lava and c) in very thick units it may be possible to obtain different directions of movement from different parts of the unit, especially from its central parts, which may be reflecting a change in the direction of movement of lava with time. In particular, the endogenous growth of lava flow units, by continued injection of lava under a surface crust, and jacking up of that crust, may produce significant deviations from the initial flow direction. Xitle flow units show particularly clear evidence for this type of endogenous growth.

4) In order to obtain significant results from lava flows, it seems necessary to collect as many samples as possible from the same unit and these should be uniformly distributed along a vertical profile that must include the base of the unit, especially in the case of thick lava flows. It also may be necessary to filter the resulting measurements.

Finally, relationships suggested by this study that require further research include:

1) The degree of anisotropy is directly related to either the viscosity of the lava, the morphology of the flow, or both and,

2) The magnetic fabric indicated by the susceptibility ellipsoid is directly related to the state of internal deformation suffered by lava flows during movement. Clearly, should these relationships be confirmed, AMS would offer a unique opportunity to study the details of the formation of flow fields.

CHAPTER 4: NEAR VENT A'A

INTRODUCTION

Many of the details of the movement of lavas are recorded in the solidified rock as foliations and lineations, defined by the ordered orientation of crystals and/or vesicles that range in size from macroscopic to microscopic (and perhaps submicroscopic) scale. Usually, the quantification of these indicators of flow behaviour is tedious and time consuming. Nevertheless, much information has been obtained from such studies (e.g., Waters, 1960; Smith and Rhodes, 1972; Komar, 1976; Coward, 1980; Rowland and Walker, 1987; Baer and Reches, 1987; Husch, 1990; Smith et al., 1993).

A different technique relies on the measurement of the magnetic susceptibility of rock specimens in various orientations relative to an applied magnetic field. The directional dependence of the magnetic susceptibility on a weak field (< 800 A/m) is commonly referred to as anisotropy of magnetic susceptibility, or AMS (Tarling and Hrouda, 1993). The AMS of rock specimens has proved to yield useful results even in cases when no other petrofabric indicators seemed to be present (valuable reviews of this type of study can be found in Hrouda, 1982; Jackson and Tauxe, 1991; Rochette et al., 1992; Tarling and Hrouda, 1993), although the potential applications of this method have still not been fully explored. Several aspects that deserve closer attention have been pointed out in the previous chapter, including the possible relationship of the intensity and type of magnetic fabric with the state of internal deformation of lava flows.

In this chapter, I include the results of measurement of the AMS of specimens from two lava flows displaying a very conspicuous concentric foliation pattern in transverse section (Fig.4.1), and show that there is an almost perfect match between the macroscopically observed vesicle foliation and the instrumentally inferred magnetic foliation. The orientation of these foliations can be explained as resulting from changes in the relative magnitudes of shear stresses within the flows, leading to a model for the origin of AMS in igneous rocks that incorporates some elements of the fluid behaviour of molten rock. Extension of this model to other morphologies (pahoehoe and toothpaste lava), together with a

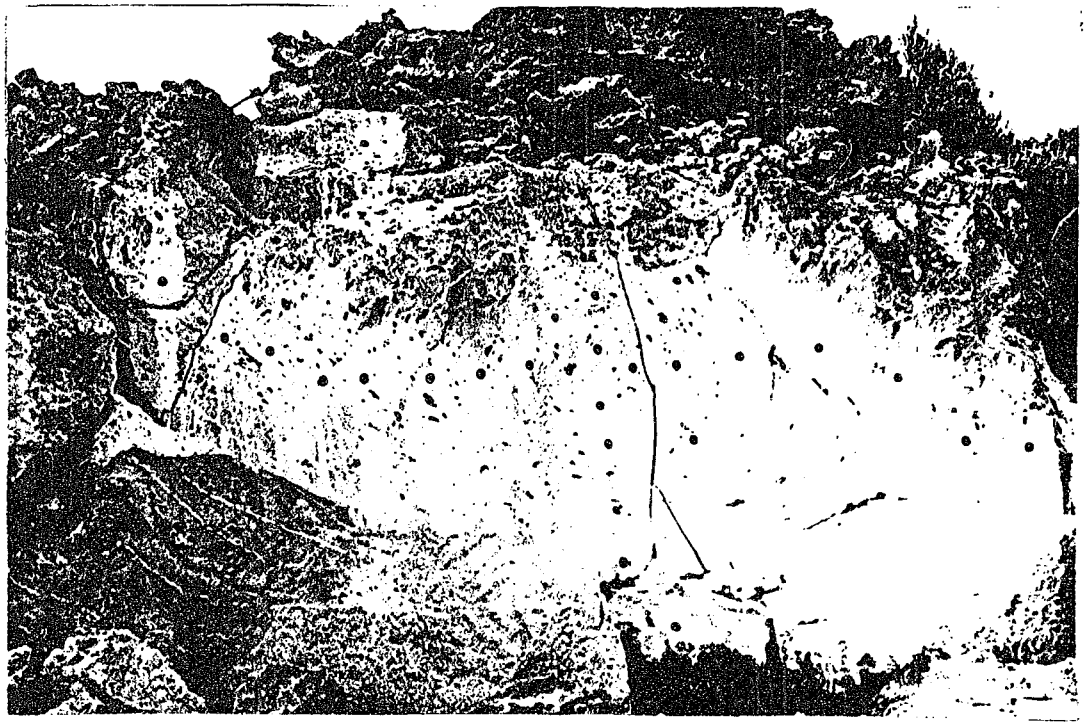

FIGURE 4.1. Photographs of the cross sections showing vesicle foliation patterns. a) Mauna Kea flow unit.

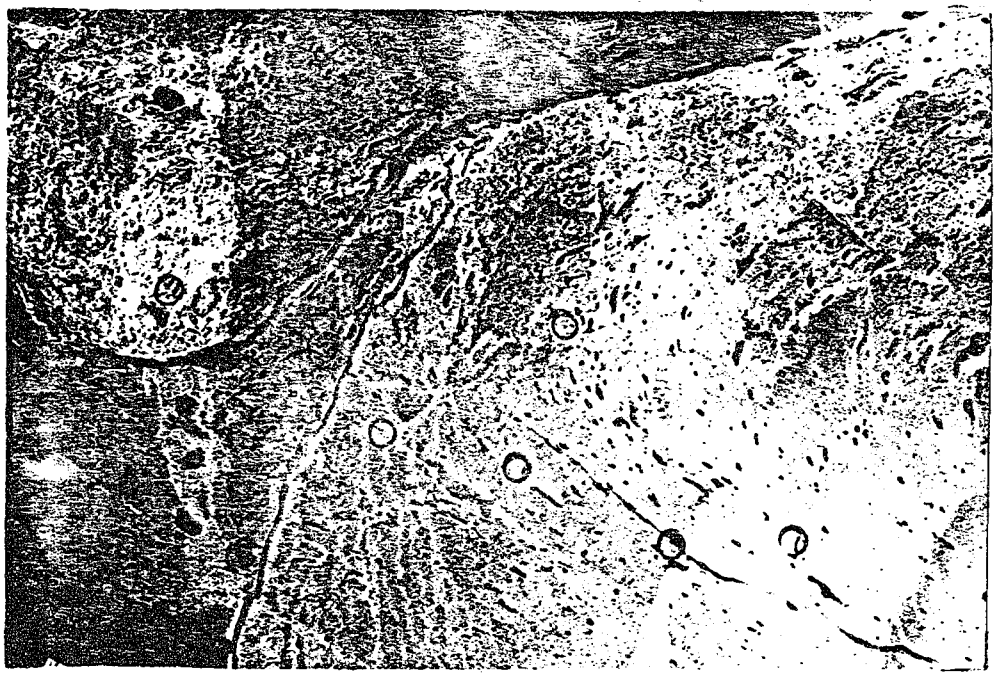

FIGURE 4.1. (CONTINUED) b) detail of the left side of the Mauna Kea unit, c) central part of same unit

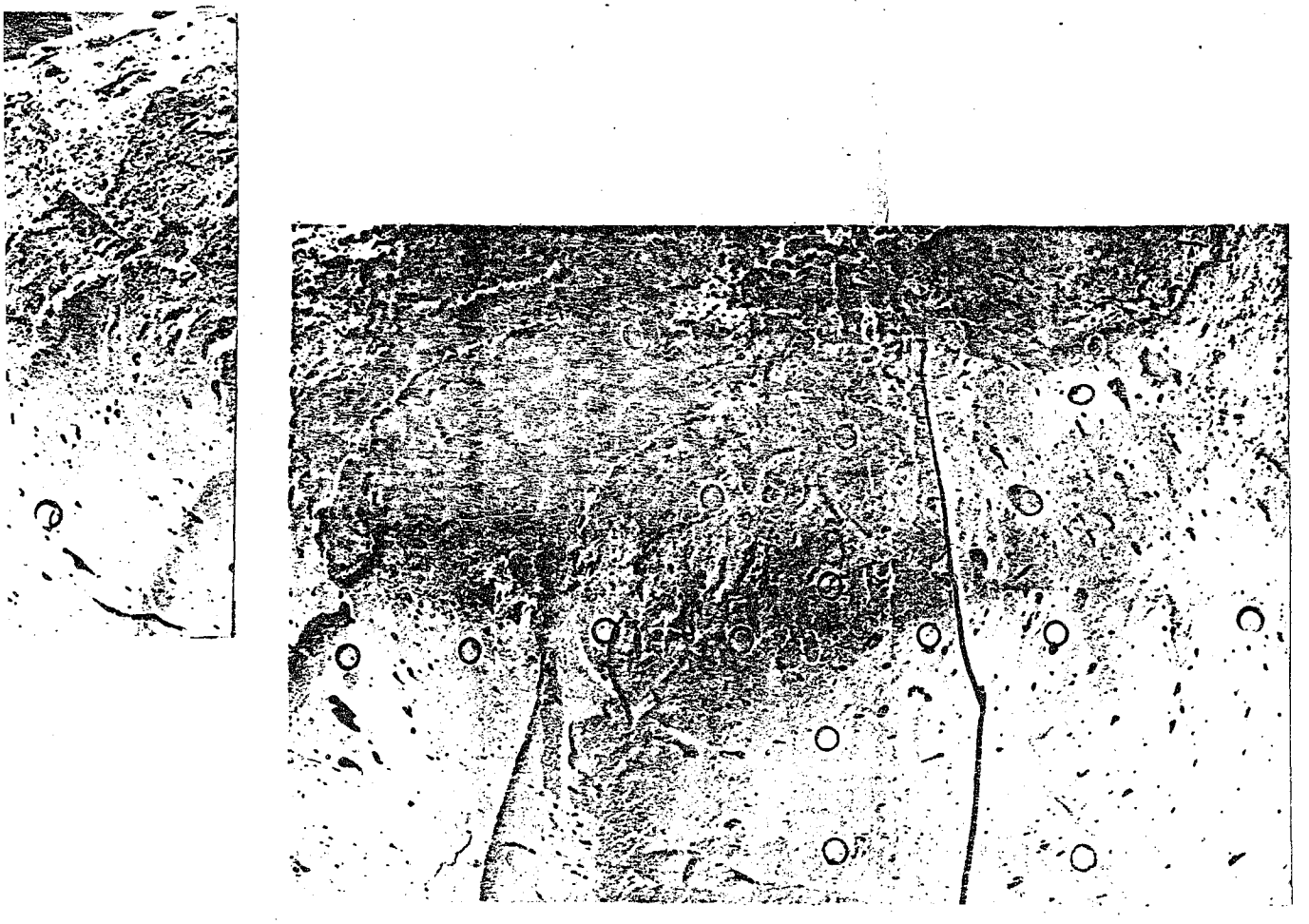

nit, c) central part of same unit

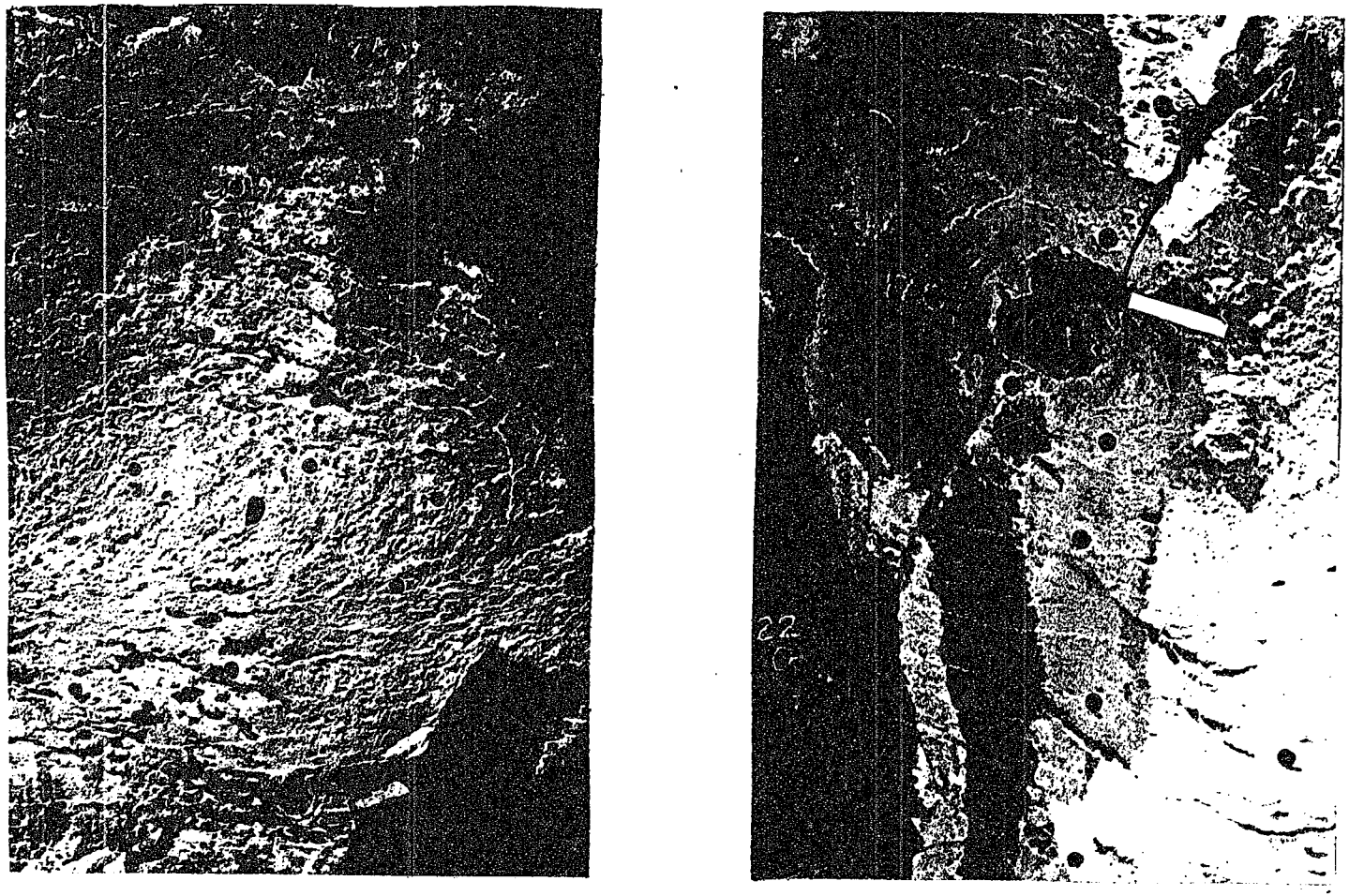

FIGURE 4.1. (CONTINUED) d) Right side of the Xitle unit, e) central part of the Xitle unit displaying large megavesicle. White chalked lines follow the vesicle foliation. Scale is 15 cm long.

fuller discussion of the effects of post-emplacement disruption of the original magnetic fabric is made in the next chapter.

GEOLOGY OF THE LAVA FLOWS

The two lava flows studied here are rather narrow lobes (4.5 and 3.9 m wide) of a'a type that flowed down fairly steep (≈ 10°) slopes. In transverse cross sections both show a concentric foliation marked by a parallelism of strongly flattened vesicles. This foliation is parallel with the direction of flow, as deduced from the slope of the terrain and the elongation of the lobes. It is presumed that the similarities in the vesicle-marked fabrics of both flows may reflect a physical process common to these flows, rather than a peculiarity of the lava from these two particular sites.

One of the flows was erupted from Xitle volcano, which is a small monogenetic basaltic lava shield of the scutulum type (Noe-Nygaard, 1968) located in the southern end of Mexico City. It is exposed in an abandoned quarry approximately 1 km from the scenic road to San Miguel Ajusco town at UTM coordinates (479300 m E, 2129600 m N). The second flow came from a vent high on the south side of Mauna Kea, a large oceanic volcano on the island of Hawai'i. It is exposed in a road cut on the road to the summit of Mauna Kea, at an altitude 10 600 ft above sea level, on a bend 1.6 km northeast of Hale Pohaku.

Differences in the chemical composition of the lavas are presumed to be of secondary importance in determining the mineral fabrics. Xitle products are olivine basalts of high-alumina type while the Mauna Kea flow belongs to the late stage alkali-basalt lavas that cap this volcano.

The Xitle flow (Fig. 4.2a) has two foliation nodes, and could be regarded as being formed by two contiguous lobes each showing the characteristic concentric foliation, the two concentric patterns coalescing and departing from a simple arrangement in the middle parts of the unit. An interesting characteristic of this unit is that it displays some megavesicles in the cross section, one near each node of the observed foliations.

The flow from Mauna Kea (Fig. 4.2b) has a simpler pattern in which the foliation encircles a single node above the middle of the unit. The observed foliation is somewhat asymmetric and departures from the concentric pattern occur near the top of this unit. Megavesicles are absent.

RESULTS

Bulk susceptibility and direction of the principal susceptibilities

a) Xitle flow

The magnitudes and directions of the three principal susceptibilities of all 22 samples from the Xitle flow are listed in Table 4.1 and shown in Figure 4.3a. Values of the bulk susceptibility range from 5.75 x 10^{-3} to 9.84 x 10^{-3} (mean value 7.44 x 10^{-3}) which is roughly the same range found in several pahoehoe units from Xitle volcano (Chapter 3).

The directions of the principal susceptibilities of all the samples (Fig. 4.3a) appear somewhat scattered, but the regions of confidence around the mean maximum susceptibility are indicative of a fairly significant mean direction (Cañón-Tapia et al., 1994). The mean of the maximum susceptibilities is within 20° of the flow direction inferred from the geology (due east), which is a good agreement given the apparent scatter of the data.

b) Mauna Kea flow

The magnitudes and directions of the 44 samples collected from the Mauna Kea flow are listed in Table 4.2 and shown in Fig. 4.3b.

Bulk susceptibility of these samples is an order of magnitude higher than for the Xitle flow, ranging from 3.08 x 10^{-2} to 6.98 x 10^{-2} (mean value of 5.67 x 10^{-2}), in agreement with other flows from the Hawaiian islands (Chapter 5 and Herrero-Bervera, unpub. data). The difference between the bulk susceptibility of Xitle and Mauna Kea flows may be related either to a larger amount of titanomagnetites or to a larger degree of oxidation (hence compositions closer to pure magnetite) of an initially similar amount of titanomagnetites in the Mauna Kea flow.

TABLE 4.1. Values (K) and directions (D -declination, I - inclination) of the principal susceptibilities of samples from the Xitle unit. Last two columns show degree of anisotropy (A=100 (1- (k3 + k2) / 2k1), range: 0 ,100) and magnetic fabric (B=100 (1 + (k3 -2k2) / k1), range: -100 , 100).

Sample #	K_{max} x10^{-3}	D_{max}	I_{max}	K_{int} x10^{-3}	D_{int}	I_{int}	K_{min} x10^{-3}	D_{min}	I_{min}	K_{mean} x10^{-3}	A (%)	B(%)
01	5.788	098	06	5.760	008	06	5.705	229	82	5.751	0.96	-0.47
02	6.934	103	15	6.857	008	15	6.768	237	68	6.853	1.75	-0.17
03	8.542	301	08	8.333	039	45	8.182	204	44	8.352	3.33	0.68
04	6.515	318	32	6.415	079	39	6.333	202	34	6.421	2.16	0.28
05	7.040	319	06	6.929	065	68	6.808	226	21	6.926	2.44	-0.14
06	7.425	298	42	7.417	201	07	7.215	103	47	7.352	1.47	-2.61
07	6.959	277	20	6.925	008	03	6.689	106	70	6.858	2.18	-2.90
08	7.106	233	20	7.048	325	05	6.959	068	69	7.038	1.44	-0.44
09	6.796	343	07	6.762	250	24	6.658	089	65	6.739	1.27	-1.03
10	7.466	261	28	7.411	167	07	7.136	063	61	7.338	2.58	-2.95
11	7.058	228	14	7.004	134	16	6.815	357	69	6.959	2.10	-1.91
12	9.056	220	25	8.988	116	27	8.659	346	52	8.901	2.57	-2.88
13	9.996	085	23	9.864	245	66	9.644	352	08	9.835	2.42	-0.88
14	7.551	086	27	7.515	287	61	7.285	181	09	7.450	2.00	-2.57
15	7.562	040	50	7.543	298	09	7.265	201	38	7.457	2.09	-3.43
16	7.420	064	50	7.359	315	15	7.103	214	36	7.294	2.55	-2.63
17	8.541	159	68	8.370	017	18	8.187	283	13	8.366	3.07	-0.14

TABLE 4.1. (CONTINUED) Values and directions of principal susceptibilities from Xitle unit.

Sample #	K_{max} $x10^{-3}$	D_{max}	I_{max}	K_{int} $x10^{-3}$	D_{int}	I_{int}	K_{min} $x10^{-3}$	D_{min}	I_{min}	K_{mean} $x10^{-3}$	A (%)	B(%)
18	9.024	045	25	8.942	138	06	8.661	240	65	8.876	2.47	-2.21
19	5.964	070	18	5.935	338	04	5.900	237	71	5.933	0.78	-0.10
20	7.369	188	10	7.361	098	04	7.250	345	79	7.327	0.86	-1.40
21	7.174	092	52	7.113	319	28	6.907	215	23	7.065	2.29	-2.02
22	8.758	273	08	8.628	182	05	8.362	061	81	8.583	3.00	-1.55

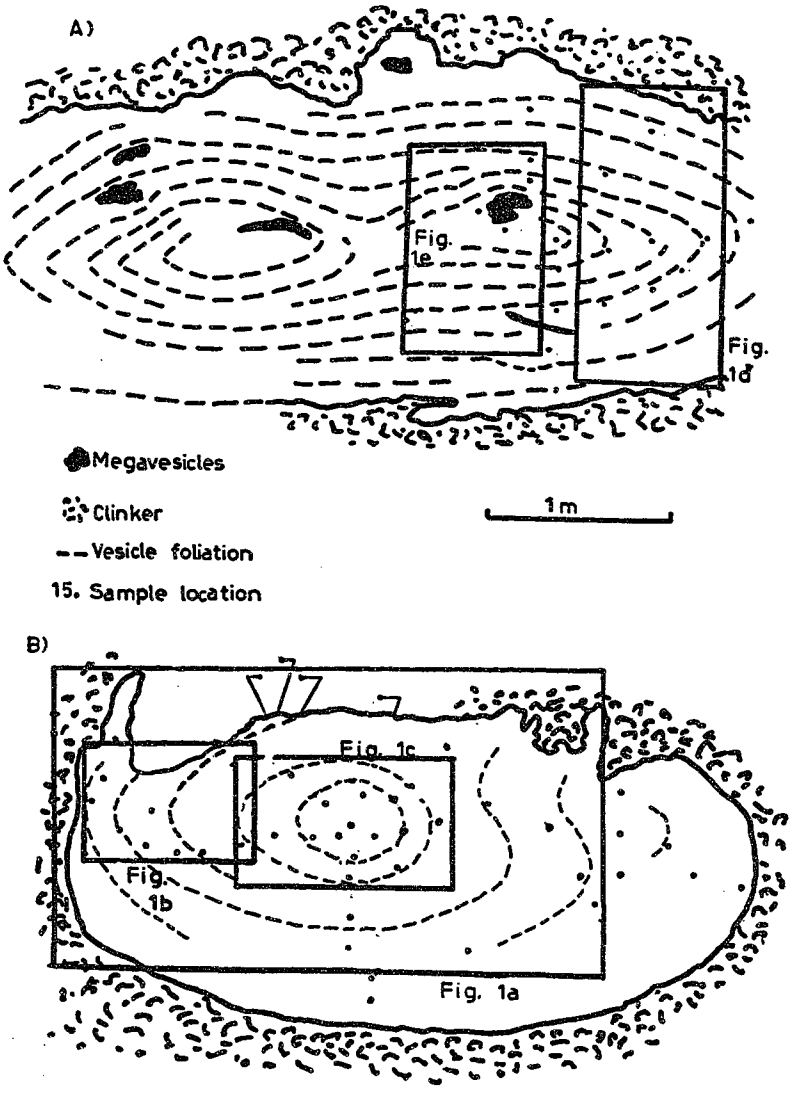

FIGURE 4.2. Diagrams showing the foliation patterns (dashed lines corresponding to the white lines in Fig. 4.1) and sample locations in a) Xitle flow and b) Mauna Kea flow. Rectangles indicate the fields of Fig. 4.1.

TABLE 4.2. Values (K) and directions (D - declination, I - inclination) of the three principal susceptibilities of all samples from the Mauna Kea unit. Last two columns show values of the A (degree of anisotropy) and B (magnetic fabric) parameters as defined in Table 4.1.

Sample #	K_{max} $x10^{-2}$	D_{max}	I_{max}	K_{int} $x10^{-2}$	D_{int}	I_{int}	K_{min} $x10^{-2}$	D_{min}	I_{min}	K_{mean} $x10^{-3}$	A (%)	B(%)
01	5.718	220	24	5.688	126	08	5.604	019	64	4.04	1.26	-0.94
02	5.205	210	24	5.102	303	06	5.064	046	66	4.04	2.34	1.25
03	5.594	201	07	5.503	292	07	5.453	070	80	6.47	2.07	0.73
04	4.756	218	52	4.643	355	29	4.612	098	21	6.23	2.70	1.72
05	4.324	155	46	4.308	327	44	4.224	061	04	4.23	1.34	-1.57
06	4.097	203	58	4.047	015	31	3.988	107	03	6.18	1.94	-0.22
07	6.229	160	39	6.189	047	25	6.051	294	40	6.83	1.75	-1.57
08	6.539	191	18	6.516	066	61	6.348	289	22	6.98	1.64	-2.22
09	6.312	171	28	6.276	353	62	6.102	262	01	6.18	1.95	-2.19
10	4.301	353	62	4.282	201	25	4.107	105	11	4.34	2.48	-3.63
11	6.263	090	38	6.229	182	02	6.034	275	52	5.69	2.10	-2.57
12	6.908	055	37	6.885	153	10	6.697	255	51	5.83	1.69	-2.39
13	7.062	347	04	7.004	083	51	6.871	254	38	6.58	1.76	-1.06
14	6.267	328	46	6.192	126	42	6.084	227	11	6.03	2.06	-0.53
15	4.421	192	26	4.319	099	07	4.271	355	63	6.41	2.85	1.22
16	5.758	169	69	5.697	270	04	5.608	002	20	6.44	1.83	-0.49

TABLE 4.2. (CONTINUED) Values and directions of principal susceptibilities from the Mauna Kea unit.

Sample #	K_{max} $x10^{-3}$	D_{max}	I_{max}	K_{int} $x10^{-3}$	D_{int}	I_{int}	K_{min} $x10^{-3}$	D_{min}	I_{min}	K_{mean} $x10^{-3}$	A (%)	B(%)
17	5.926	171	25	5.82	264	7	5.747	9	63	5.83	2.4	0.56
18	6.685	201	43	6.59	93	18	6.455	347	41	6.58	2.43	-0.6
19	6.124	20	76	6.032	266	6	5.937	174	13	6.03	2.28	-0.05
20	6.488	5	68	6.407	100	2	6.333	191	22	6.41	1.82	0.11
21	6.514	0	21	6.453	267	8	6.341	156	68	6.44	1.8	-0.78
22	6.006	312	0	5.982	42	3	5.889	218	87	5.96	1.17	-1.15
23	6.959	183	7	6.893	92	6	6.79	319	81	6.88	1.69	-0.53
24	4.589	186	1	4.559	96	1	4.487	330	89	4.55	1.44	-0..91
25	6.939	6	6	6.844	97	4	6.74	216	83	6.84	2.12	-0.13
26	4.942	12	12	4.906	102	0	4.827	194	78	4.89	1.53	-0.87
27	3.965	215	35	3.921	49	54	3.874	310	6	3.92	1.7	-0.08
28	5.618	203	33	5.509	89	32	5.447	326	40	5.52	2.49	0.84
29	6.23	192	48	6.183	65	29	6.063	318	28	6.16	1.72	-1.17
30	6.417	11	61	6.346	242	19	6.258	145	21	6.34	1.79	-0.26
31	6.491	243	70	6.459	27	17	6.301	121	11	6.42	1.71	-1.94
32	4.643	4	6	4.594	269	42	4.56	100	48	4.6	1.42	0.32
33	5.24	82	52	5.217	205	23	5.092	308	28	5.18	1.63	-1.95

TABLE 4.2. (CONTINUED) Values and directions of principal susceptibilities from the Mauna Kea unit.

Sample #	K_{max} $x10^{-3}$	D_{max}	I_{max}	K_{int} $x10^{-3}$	D_{int}	I_{int}	K_{min} $x10^{-3}$	D_{min}	I_{min}	K_{mean} $x10^{-3}$	A (%)	B(%)
34	6.86	232	45	6.809	100	34	6.685	351	26	6.78	1.65	-1.06
35	6.38	178	1	6.289	269	18	6.183	84	72	6.28	2.26	-0.24
36	5.814	194	16	5.761	74	60	5.671	291	25	5.75	1.69	-0.64
37	5.608	202	13	5.547	343	74	5.435	110	10	5.53	2.09	-0.91
38	6.287	217	3	6.211	314	66	6.125	125	24	6.21	1.89	-0.16
39	4.486	214	34	4.446	77	47	4.408	321	22	4.45	1.31	0.04
40	6.573	224	14	6.474	99	66	6.396	319	19	6.48	2.1	0.32
41	6.207	206	23	6.08	60	63	6.024	302	14	6.1	2.5	1.14
42	3.16	186	31	3.102	286	16	2.991	41	54	3.08	3.59	-1.68
43	6.428	312	11	6.347	215	31	6.236	59	57	6.34	2.12	-0.47
44	5.254	187	12	5.217	317	71	5.113	94	14	5.19	1.69	-1.28

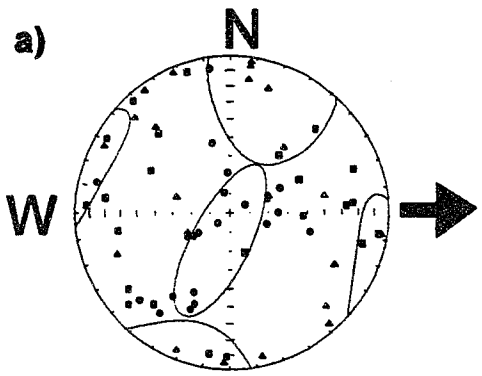

D_{max} = 288 I_{max} = 00 ± 28:16 (29:17)
D_{int} = 18 I_{int} = 16 ± 45:27 (48:28)
D_{min} = 197 I_{min} = 74 ± 45:15 (47:16)

■ Maximum

▼ Intermediate

● Minimum

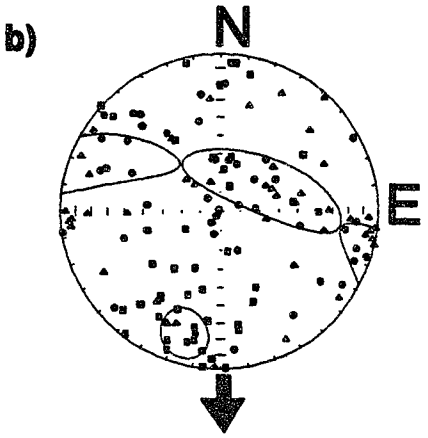

D_{max} = 196 I_{max} = 20 ± 15:10 (15:10)
D_{int} = 61 I_{int} = 63 ± 45:14 (80:16)
D_{min} = 293 I_{min} = 18 ± 45:12 (79:12)

FIGURE 4.3. Directions and regions of confidence of all specimens from a) Xitle flow, and b) Mauna Kea flow. The regions of confidence shown were calculated with the multivariate analysis technique (Lienert, 1991); the dimensions of the regions of confidence obtained with the resampling method (Constable and Tauxe, 1990) are given numerically in parenthesis. Geologically inferred flow direction is shown by the arrows.

The directions of the principal susceptibilities of all samples from this flow also appear scattered, but the regions of confidence around the mean maximum susceptibility are smaller than in the Xitle flow (Fig. 4.3b). The mean of the maximum susceptibilities lies within 20° of the flow direction inferred from the geology (nearly due south), similarly to the results obtained in the Xitle flow.

Two interesting relations can be established from the AMS results. 1) By plotting the principal susceptibilities of each sample in a plane normal to the geologically inferred flow direction assuming an underlying slope of 10° (Fig. 4.4), it becomes clear that the plane containing the maximum and intermediate principal susceptibilities, or plane of magnetic foliation, is systematically oblique to the flow margins and flow axis (Figs. 4.4a, 4.4c, 4.4d) so as to lie on a family of nested cones, the axis of which coincides with the flow axis and the apices of which point down-flow. 2) Using the same plane of projection, it is clear that there is an almost perfect match between the plane of magnetic foliation and the macroscopic vesicle foliation (Fig. 4.4e, 4.4f).

The obliquity of the plane of magnetic foliation is interpreted to constitute an imbrication, as previously observed in the dikes of the Ko'olau volcano (Knight and Walker, 1988) and in Xitle pahoehoe units (Chapter 3). The imbrication angle averages 25° in the Mauna Kea unit, and 20° in the Xitle unit; the larger angles occur near the foliation node in both flows. The inward increase in the imbrication angle is consistent with the down-flow curvature of vesicle foliations observed in places where the plane of the outcrop is parallel to the flow direction, as schematically illustrated in Fig. 4.4b, where the plane of projection of Figure 4.4a has been hypothetically displaced along the flow direction several times.

Magnetic fabrics and degree of anisotropy

The magnetic fabric of this lobe is preferentially foliated, with an average value of the degree of anisotropy of ≈2 %. Larger values of the A parameter are found near the node of foliation, while specimens closer to the borders yield smaller values of A. Two samples with the highest degree of anisotropy, and the only two samples showing a slightly lineated fabric, are located in the vicinity of the central megavesicle.

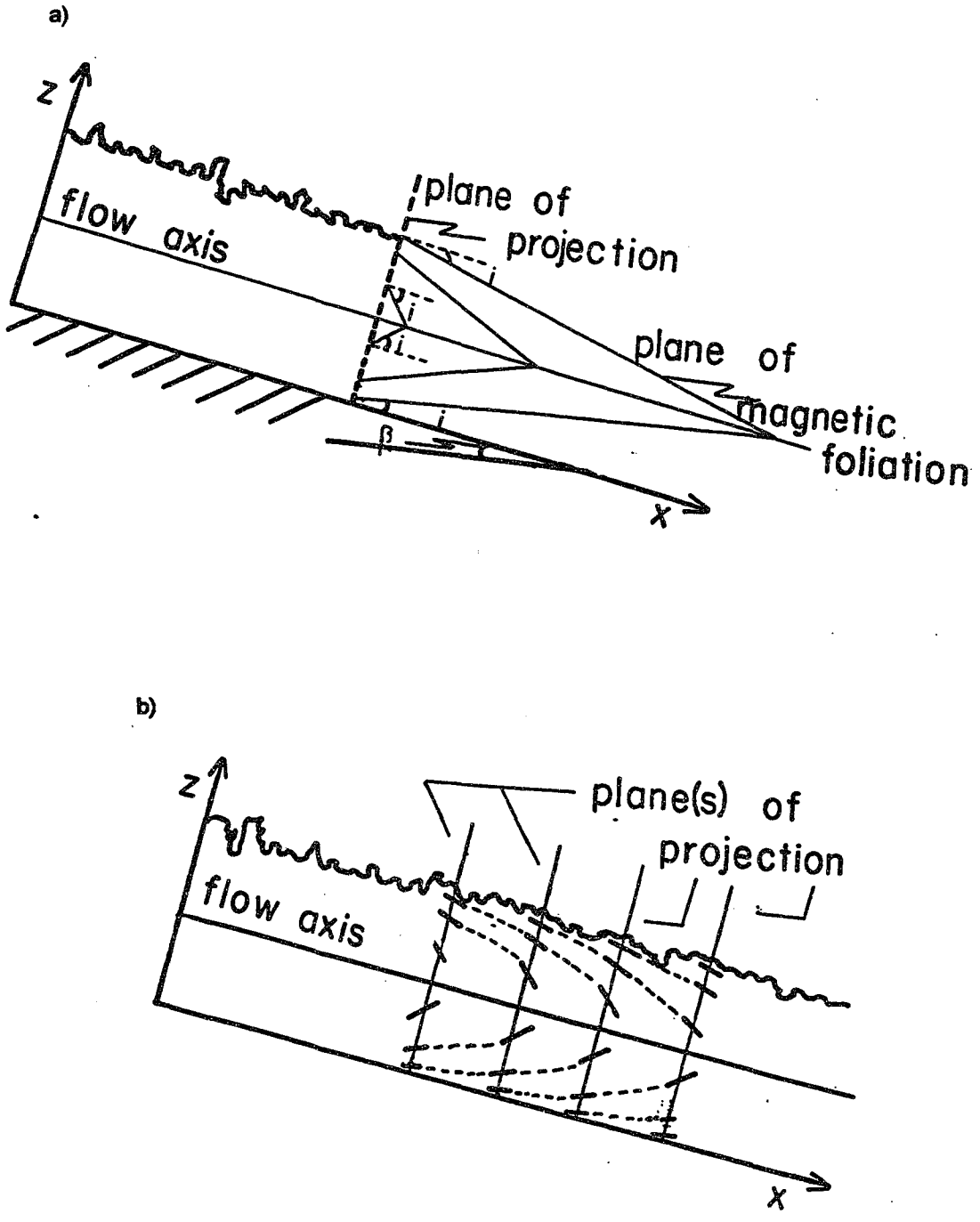

FIGURE 4.4. a) Side view showing the nested cones and the imbrication angles (i) mentioned in the text (B is the angle of the underlying slope taken as 10° in both units of this work). b) Relation of the imbrication angle to the curvature of a foliation in an outcrop parallel to the flow direction.

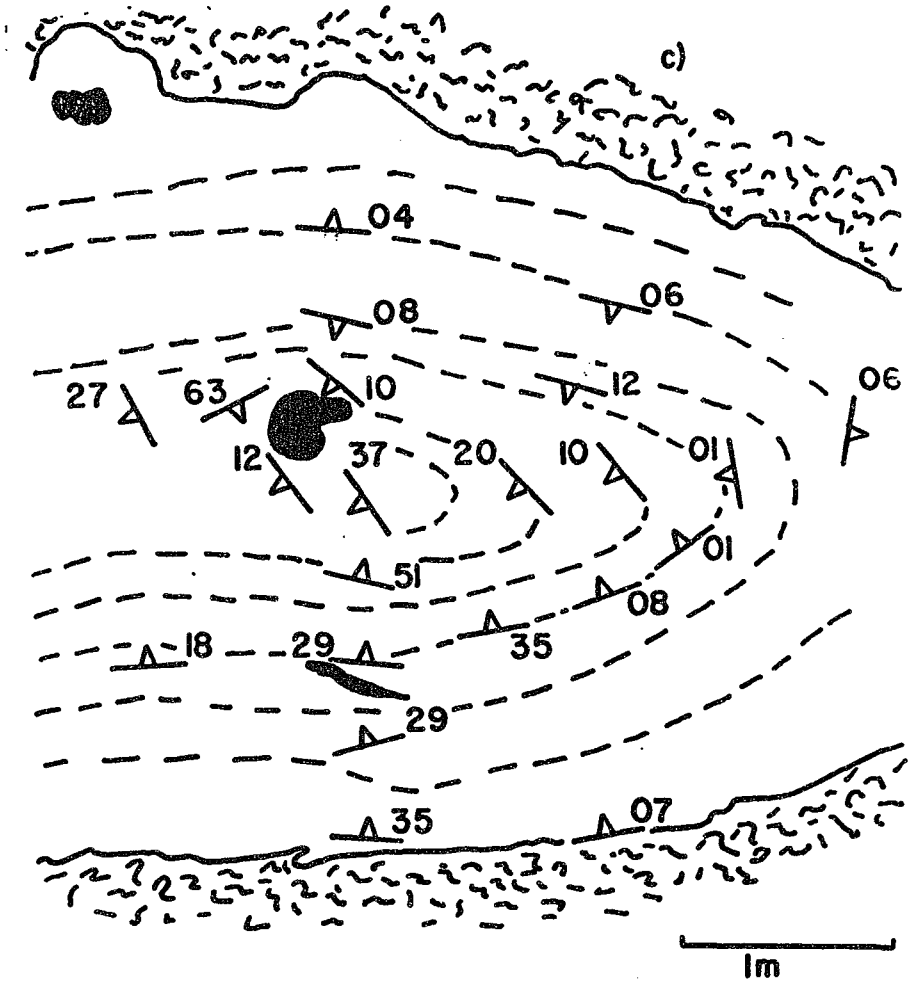

FIGURE 4.4. (CONTINUED) c) Orientation of the magnetic foliation relative to the flow direction for all specimens from the Xitle unit. The angle between the flow direction and the plane of magnetic foliation is indicated numerically for each sample. Note the parallelism between the plane of magnetic foliation and the trend of the vesicle foliation (dashed lines).

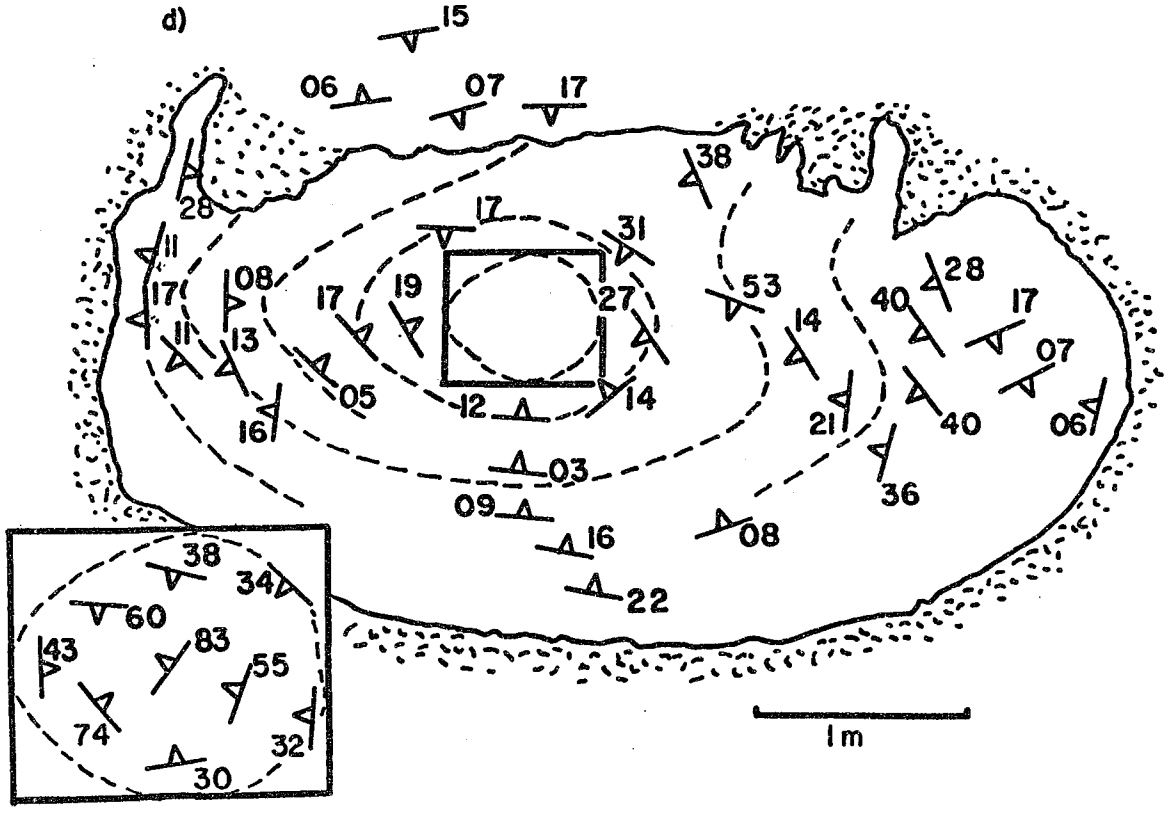

FIGURE 4.4. (CONTINUED) d) Orientation of the magnetic foliation relative to the flow direction for all specimens from the Mauna Kea unit. Symbols as in fig. 4.4 c).

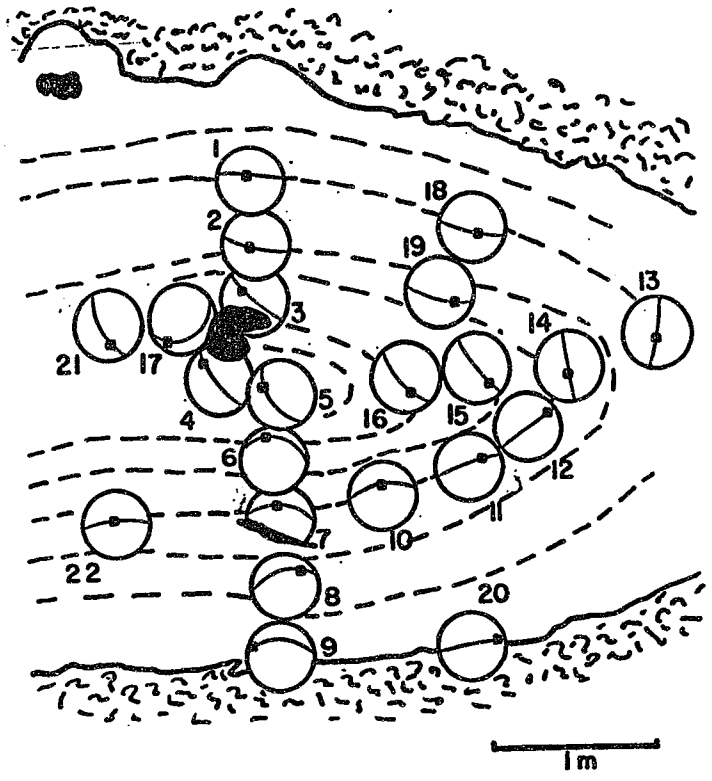

FIGURE 4.4. (CONTINUED) e) Equal area projections of the plane of magnetic foliation (Xitle unit) and the maximum susceptibility indicated by the squares. Numerical values are the sample number as given in Table 4.1. Geologically inferred flow direction is normal to the plane of the projections; the hemisphere towards the observer was used in all cases (observer looking up-flow).

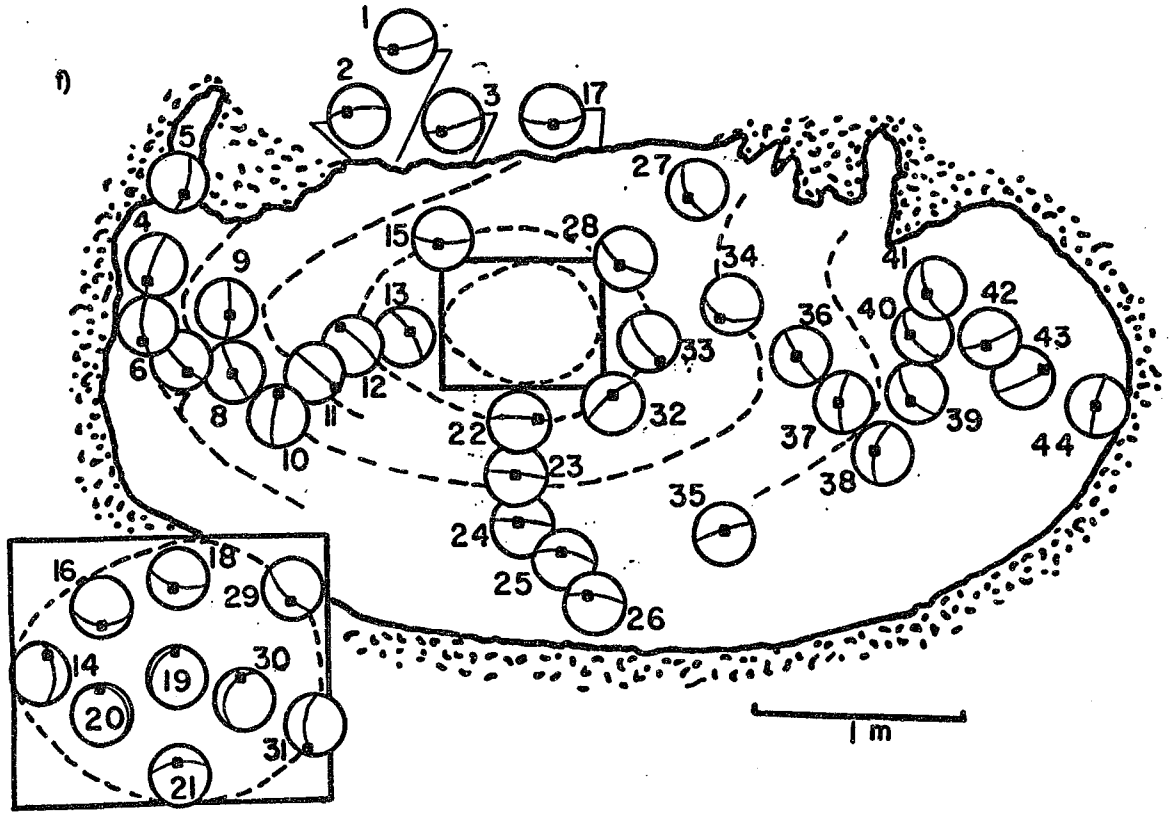

FIGURE 4.4. (CONTINUED) f) Equal area projections of the plane of magnetic foliation (Mauna Kea unit) and the maximum susceptibility indicated by the squares. Symbols as in fig. 4.4 e).

The magnetic fabric of this unit is also preferentially foliated, with an average value of the degree of anisotropy of ≈ 2 %. The magnetic fabric seems to be slightly more foliated in its left side perhaps reflecting the asymmetry in the foliation.

ORIGIN OF THE FOLIATION PATTERNS

The origin of AMS

It has been customary to interpret AMS measurements in terms of the preferred orientation of elongate ferromagnetic grains that move in flowing magma. This interpretation is based on two basic assumptions: 1) the shape of titanomagnetite grains is the dominant factor controlling their magnetic anisotropy, and 2) the AMS of a rock specimen is determined by the individual anisotropies of non-interacting titanomagnetite grains (see the reviews by Hrouda, 1982; Jackson and Tauxe, 1991; Rochette et al., 1992; Tarling and Hrouda, 1993). Most grains of magnetite observable in thin sections of unaltered igneous rocks, however, are not elongated but tend to be irregularly shaped, and the textures of ferromagnetic grains usually suggest that their crystallization occurs after movement of the melted rock or pyroclastic material has already ended (Wolff et al., 1989; Hargraves et al., 1991). Regarding the second assumption, Stephenson (1994) has shown that magnetic interaction of neighbor grains may indeed produce a large degree of anisotropy even in the case of intrinsically isotropic grains (see also Appendix 1). As even a small amount (≈ 1 vol %) of ferromagnetic minerals may result in inter-grain magnetic interactions (Borradaile, 1988; Sprowl, 1990), it is doubtful whether the non-interaction assumption is valid for most igneous rocks.

Hargraves et al. (1991) suggested that the early crystallizing silicates form a sort of template that controls the distribution of small ferromagnetic grains, and to some extent the shape and orientation of larger grains. Magnetic interaction between ferromagnetic grains would in turn determine the susceptibility measured in the specimen and, therefore, the magnetic fabric would mimic the fabric of other crystals more likely to be already present in the flowing magma. The same basic idea was previously proposed by Stacey (1963) although he did not sustain it with any direct observation, and by Wolff et al. (1989) in the context of pyroclastic deposits. Both models (Wolff et al., 1989 and

Hargraves et al., 1991) shift the relative importance from the (magnetically) isolated-particle origin of AMS to an interactive model, but neither investigate the details of the mechanism controlling the distribution of grains, nor its relation with the internal structure of the rock.

To bridge this gap, a model linking the velocity field of a moving fluid to the distribution of minute particles immersed in it and the observed vesicle foliation is proposed in the next section.

Foliations due to fluid motion

In any fluid, it is possible to relate the stress tensor with the Eulerian strain rate, which involves the spatial variations of the velocity field of the fluid through its constitutive equation. For an incompressible Newtonian fluid, the constitutive law takes the form:

$$\tau_{ij} = 2\,\mu\, e_{ij} = \mu\,(v_{i,j} + v_{j,i}) \qquad (4.1)$$

where i and j may each be equal to x, y and z, the components of a Cartesian system of reference, τ_{ij} is the component of the stress tensor applied on a face of the fluid element normal to the i direction and pointing in the j direction, e_{ij} is the Eulerian strain rate tensor, μ the viscosity of the fluid, v_i the component of the velocity in the i direction, and $v_{i,j}$ indicates the rate of change of v_i following a change in position of the observation point in a direction parallel to the j direction (Menke and Abbott, 1981).

The components of the stress tensor given by (4.1) can be easily evaluated if we take the case of a fluid moving with a velocity in one direction, say x, and assume that the velocity remains constant along that particular direction. Kilburn and Lopes (1991) have shown that these assumptions are reasonable for near vent lavas, based on the observation that lava flow lobes do not increase appreciably in width or length except in a small region at their front. Thus, the components of the stress tensor defined by (4.1) become:

$$\tau_{xx} = \tau_{yy} = \tau_{zz} = \tau_{yz} = \tau_{zy} = 0,$$

$$\tau_{xy} = \tau_{yx} = \mu\, v_{x,y} \qquad \text{and,}$$

$$\tau_{xz} = \tau_{zx} = \mu\, v_{x,z} \qquad (4.2)$$

Knowing all the components of the stress tensor, it is easy to estimate the orientation of its principal (all normal) stresses and from these the orientation of the shear plane in any element of fluid (e.g., Hatcher, 1990).

If τ_{xy} in eqs. (4.2) is made infinitesimally small while keeping τ_{zx} finite, the shear plane will tend to be a horizontal plane. If instead τ_{zx} is made infinitesimally small while keeping τ_{xy} finite, the shear plane will be a vertical plane. Different orientations of the shear plane between these two extremes are obtained depending on the relative magnitudes and signs of the four non-zero shear stresses in eqs. (4.2) (Fig. 4.5).

The shear plane can be related with the observed foliations in a very simple way. If we take as a reference any cubic element of fluid, the action of the local stresses will deform it so that after some time it becomes a rectangular box with its shorter dimension normal to the shear plane. Any bubble contained in the fluid element will undergo the same type of deformation, therefore explaining the formation of the flattened vesicles observed in both lava flows.

The magnetic fabric is also related to the shear plane although in a somewhat less direct form. Particles contained in two originally adjacent cubic fluid elements (likely to suffer very similar deformations as long as the elements of reference are small enough and the stresses are continuous, smooth functions of position within the fluid) will be distributed along two non-adjacent rectangular fluid elements after some time, as illustrated in Fig. 4.6. Magnetic interaction between particles along the direction of compression in the figure will thus be enhanced, while interaction between particles along the direction of extension will be reduced. Similarly, magnetic interaction between particles along the direction normal to the plane of the figure can be enhanced or reduced, depending on the sign of the stress in this direction. In any case, particles can be envisaged as distributed over distinct parallel planes that correspond to the respective shear planes of the original cubic elements of reference.

The distribution of particles will not only influence the orientation of the three principal susceptibilities, but also the type of magnetic fabric measured. Stephenson (1994) showed that identical spherical particles homogeneously distributed along parallel, non-interacting planes will have a minimum susceptibility normal to the planes and two larger susceptibilities of approximately equal

values parallel to them; the larger the separation between planes, the smaller the relative size of the minimum susceptibility. At the other extreme, if the distances between particles over a plane are larger than along the normal to it, magnetic interaction along that normal will dominate, and the magnetic fabric will be preferentially foliated (Appendix 1). In the case of Figure 4.6, if it is assumed that the stress normal to the page is equal to that along the vertical direction, the shear plane would be vertical and magnetic interaction along the direction of extension will be negligible, therefore resulting in a preferentially foliated magnetic fabric (indicated by negative values of the B parameter) with its minimum susceptibility parallel to the direction of extension (normal to the shear plane). If on the contrary, the stress normal to the page is equal to the extension shown in the figure, the shear plane will be horizontal and the resulting fabric would be preferentially lineated (positive values of the B parameter) with its maximum susceptibility parallel to the direction of compression (normal to the shear plane).

Thus, it is proposed that whenever a well defined shear plane is created by the local stresses due to lava movement, the principal susceptibilities will be closely related to it. If the magnetic fabric is preferentially foliated, the minimum susceptibility will be close to the normal to the shear plane while if the magnetic fabric is preferentially lineated the maximum susceptibility will be normal to it. The larger the absolute value of the shear the better defined the magnetic fabric (which would be marked by values of the B parameter closer to -1 or +1, respectively).

VELOCITY PROFILES

Flow conditions and rheology

From figure 4.5, it is clear that the pattern of vesicle and magnetic foliations observed in both Mauna Kea and Xitle units can be reproduced by adjusting the relative values of the four non-zero stresses (cf. eqs. 4.2) across the surface of the outcrop. The orientation of the magnetic fabric in three dimensions, however, allows us to infer more regarding the velocity field of moving lava.

If the orientation of the plane of magnetic foliation does indeed parallel the local shear plane as explained in the previous section, its imbrication implies that the approximations made by eqs. (4.2) are

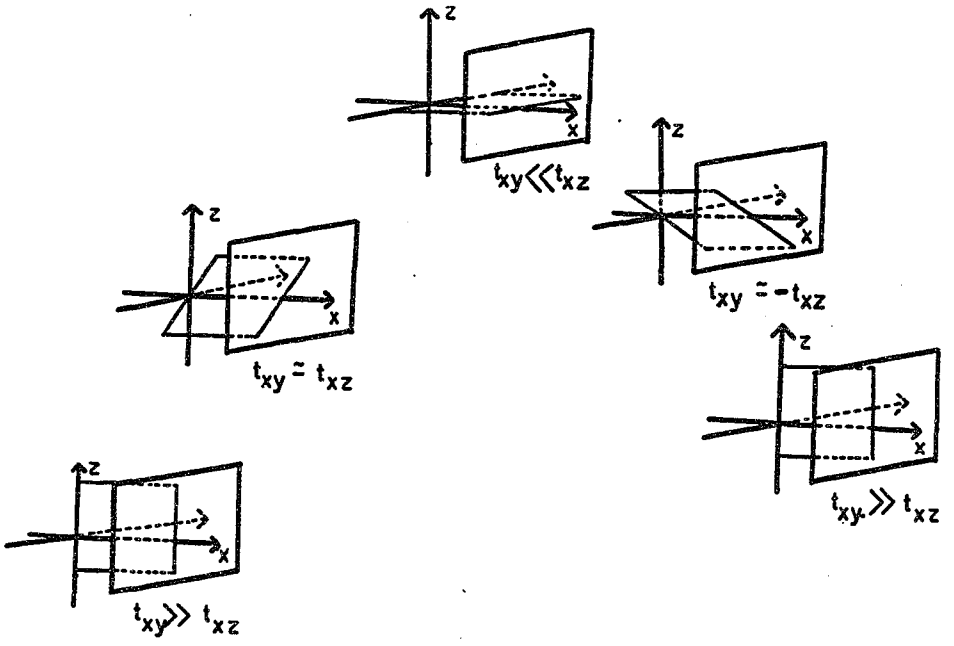

FIGURE 4.5. Different orientation of the shear plane depending on the relative values of shear stresses. The frontal plane is normal to the x direction and corresponds to the plane of projection in Fig. 4.4 a). The second plane (partially delineated with dashed lines) represents the shear plane obtained when the relation between the two non-zero shears indicated below each case is satisfied. The intersection of both planes (thin line) marks the trend of the foliation as observed in the outcrop. Positive y direction is indicated by the dashed arrow in all cases.

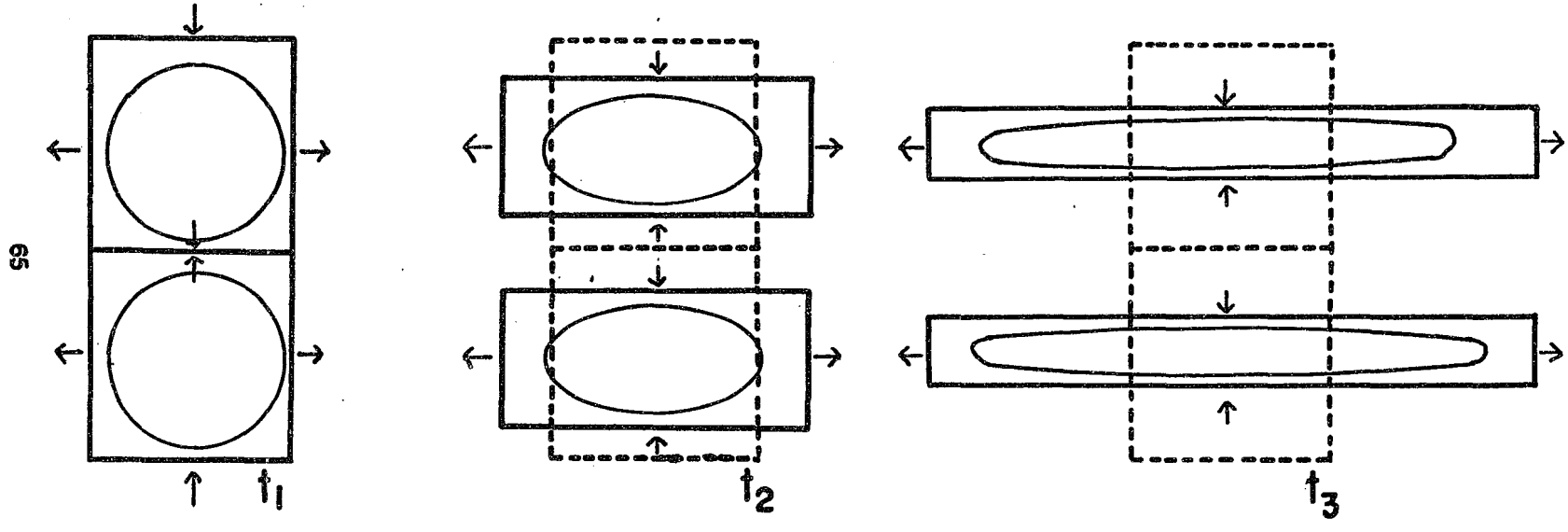

FIGURE 4.6. Temporal evolution (t1 to t3) of two originally adjacent fluid elements each deformed by almost identical stresses (small arrows). See text for details.

not completely valid. In order to reproduce the orientation of the plane of magnetic foliation through the use of the local stress tensor, it is necessary to include at least one extra non-zero term in eqs. (4.2), or in other words, we would need to take into account the contributions of a velocity component in a direction perpendicular to that in which flow is occurring. Alternatively, we can still assume that the velocity remains unidirectional, although it is necessary to allow changes in its magnitude with distance from the vent (i.e., τ_{xx} is no longer zero in eqs. 4.2). This, together with the coordinate system of Figure 4.4a, and according to the orientation of the magnetic foliation shown in Figs. 4.4c - 4.4f, allowed us to infer the velocity profiles shown in Figs. 4.7a and 4.7b.

To construct the velocity profiles, I first located the points in which there is a change in the orientation of the direction of the imbrication assigning to these points the maxima or minima in the velocity values (small arrows in Figs. 4.7a and 4.7b). To estimate the slope of the curve in the profiles two characteristics of the magnetic foliation were used in conjunction, 1) the orientation of the foliation in the plane normal to the flow direction and 2) the angle of imbrication relative to the flow direction. The first factor gives information of whether the changes in the velocity are positive or negative as we move in the positive vertical (z) or horizontal (y) direction, while the second allow us to estimate how different the velocities at two points would be after a displacement along the flow direction has been accomplished. The latter can be used as an indirect estimate of how steep should be the slope of the profile. Certainly, the profiles are only approximations because we only have information about the relative importance of the changes in the velocity along two orthogonal directions at a time, and there is no way to know the absolute value of any of these changes independently (otherwise we would know a priory the velocity profile that we are inferring).

In figures 4.7c (Binghamian) and 4.7d (Newtonian), velocity profiles for the cases of unconfined flow over a stationary surface and between two stationary boundaries are shown for comparison (note that the horizontal profile for each rheology can be represented by the case of flow between two stationary surfaces). It is observed in Fig. 4.7 that the vertical velocity profiles inferred from the foliation patterns in both flows are more closely related to the cases of flow between two stationary boundaries. Therefore it would seem that both flows may have developed a roof that moved slower relative to the

central parts of the flow. The departure of the simple concentric pattern in the foliation in the upper right corner of the Mauna Kea flow can be interpreted as marking the absence of a slow upper layer in this side, so that the roof formation in this flow was only partial.

The maximum velocity along the vertical profiles does not coincide in either unit with its geometrical center, but is slightly above it in the Mauna Kea flow and below it in the unit from Xitle, within the limit of experimental error. In any case, it is likely that changes in the velocity in a small region near the maxima in both units were presumably smaller than nearer to the borders, and therefore could be interpreted to represent a region where plug flow occurred indicating that the rheology of the flows was closer to Binghamian than to Newtonian. The profiles shown in Figs. 4.7a and 4.7b seem to suggest that lava in both flows possessed a small yield strength during its emplacement. The yield strength could not be very large because the region of plug flow is not very clear in the vertical profiles, although it is better defined in the horizontal profile from Mauna Kea unit (it should be noted that only one side of the Xitle flow was sampled, hence explaining the incomplete velocity profile).

DISCUSSION

In the previous sections a model was proposed that explains the orientation of the principal susceptibilities as a result of the different magnitudes of the elements of the local stress tensor, which in turn depend on the changes in the velocity components of fluid elements of a lava flow. Some comments have to be made, however, to better appreciate the advantages and limitations of this model.

First, the proposed model for the origin of the AMS of igneous rocks depends mainly on the grain distribution along the local shear plane. Each mineral grain, however, may have a characteristic shape, and its final orientation may be controlled by factors such as hydraulic forces, grain-grain interactions and / or preferential growth directions. Thus, in general, the anisotropy due to the particular shapes of individual grains will be superimposed on that arising from the distribution of grains in the shear planes, so introducing some deviations from the model proposed. Nevertheless, it is found (Appendix 1) that

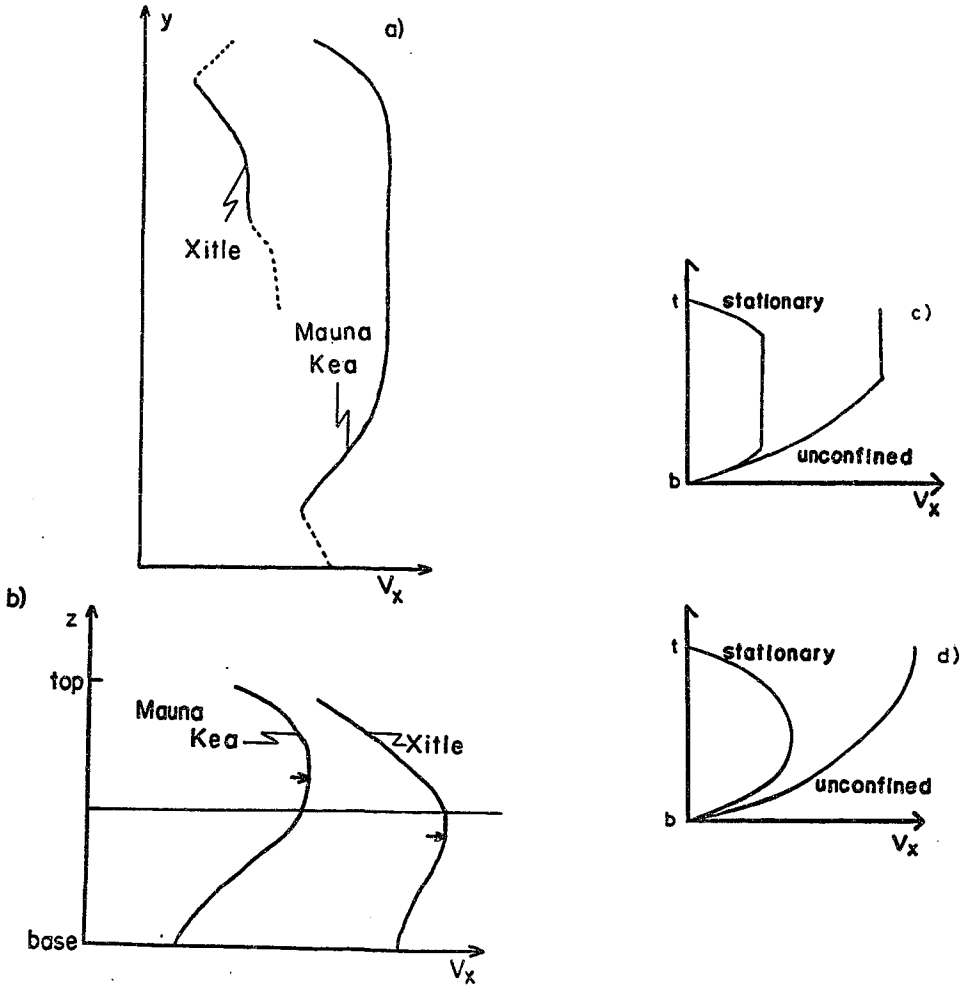

FIGURE 4.7. Velocity profiles (x component) inferred from the orientation of the foliations of Xitle and Mauna Kea flows along a) a horizontal (y) direction and b) a vertical (z) direction. Arrows indicate the position of the foliation nodes shifted relative to the medial plane of the units. Dashed lines indicate changes in the velocity suggested by the orientation of the plane of magnetic foliation that can not be easily explained by a simple rheological model. Profiles of flow unconfined and with stationary boundaries for c) Binghamian and d) Newtonian fluids are given for comparisson.

anisotropy due to shape will usually be dominated by anisotropy arising from magnetic interaction of grains, therefore validating the proposed model in a general context.

Second, it is implicit in the model that the distribution of stresses present during the final stages of movement of the flow was somehow preserved by the minerals or vesicles after solidification of the lava. Although this may be the case in the two units here studied, this is not necessarily true for all lava flows. For instance, in a lava flow that becomes static while still fluid , as when ponded in a depression or in the interior of pahoehoe lobes that are restrained by their chilled crusts, the force of gravity will act in such a way that the effects of the hydraulic forces will have been somewhat distorted in the entrapped lava upon solidification or complicated by convection or vesicle ascent. The amount of distortion will be related to the time elapsed from the moment when movement ceased to the time when the lava reached a yield strength large enough to prevent any further change in the distribution and orientation of grains.

If it is accepted that the measured susceptibilities do indeed have a simple relationship with the average separation of grains as adduced in the previous section, then it is possible to predict how the effects of gravity would disrupt the magnetic fabric associated with movement of lava. For example, taking the case in which kmin is originally vertical and kmax is parallel to the flow direction, we can expect that settling of grains will eventually shorten the inter-grain distances along the vertical leaving more or less unaltered the distances along the horizontal plane. This would result in an increase of kmin that could end in a vertical maximum susceptibility and an intermediate susceptibility parallel to the flow direction. The type of magnetic fabric (whether foliated or lineated) and the degree of anisotropy will be modified in the process following the evolution illustrated in Fig. 4.8. The characteristic AMS of lavas possessing a range of different morphologies seems compatible with this evolutionary process (Chapter 5).

Third, solidification does not occur simultaneously in all points of a flow. A solidification front moves from the boundaries to the central parts of a flow at a velocity that depends on how heat is transported to the bounding surfaces of the flow and on how it is removed from the surfaces by the surroundings (e.g., Fink and Griffiths, 1990; Pinkerton and Wilson, 1994). Thus, the changes in the velocity

preserved by the magnetic foliation do not necessarily represent a single flow regime as assumed in the previous section, but may represent a completely different situation. As the solidification front moves toward the inner parts of the flow it will "freeze" the stress distribution acting just before it passes over a particular point, in which case the imbrication angle would be explained in terms of the shear occurring between a rather solidified layer and a more fluid part of the flow. The presence of a foliation in almost the full width and height of the flow would therefore suggest that movement of the internal parts took place until very late in its history. Furthermore, the location of the places where the maximum imbrication angle is achieved would now be marking the place where the influence of gravity disrupted the most the magnetic fabric related with movement of lava, or in other words, the places where solidification occurred last. In the case of the two units of this work, we could therefore infer that cooling took place at a faster rate from the top in the Xitle flow, but that it was faster from the bottom in the Mauna Kea flow. The first case is what is usually expected because heat transfer to the atmosphere is more effective than to the underlying rock (e.g., Fink and Griffiths, 1990), but the second case is slightly harder to explain. Due to this small complication, I prefer the original interpretation in the sense that a single velocity regimen was preserved in both flows.

Fourth, although the velocity field of the lava flows was extremely simplified in order to arrive at the suggested model, the proposed origin for the AMS of igneous rocks has a more general nature. In other words, there is no reason to suppose that the orientation of the principal susceptibilities can be linked to the velocity field of lavas only in the special circumstances described earlier. In effect, even in the cases of a three dimensional velocity field (when the general expression (4.1) for the stress tensor has to be used) it would be possible to find the orientation of the principal stresses and, therefore, a local shear plane. Unfortunately, this generality results in a multitude of possible configurations of the velocity field each of which could give rise to the observed orientations of the principal susceptibilities. For example, it is possible to obtain a similar orientation of the shear plane and the compressive axis by introducing τ_{yz}, τ_{zy}, τ_{yy} and τ_{zz} as the extra non-zero terms instead of τ_{xx}, implying that the velocity was not really unidirectional, but that it had significant vertical and horizontal components. In any case, due to the fact that a magnetic foliation can be detected even in cases where

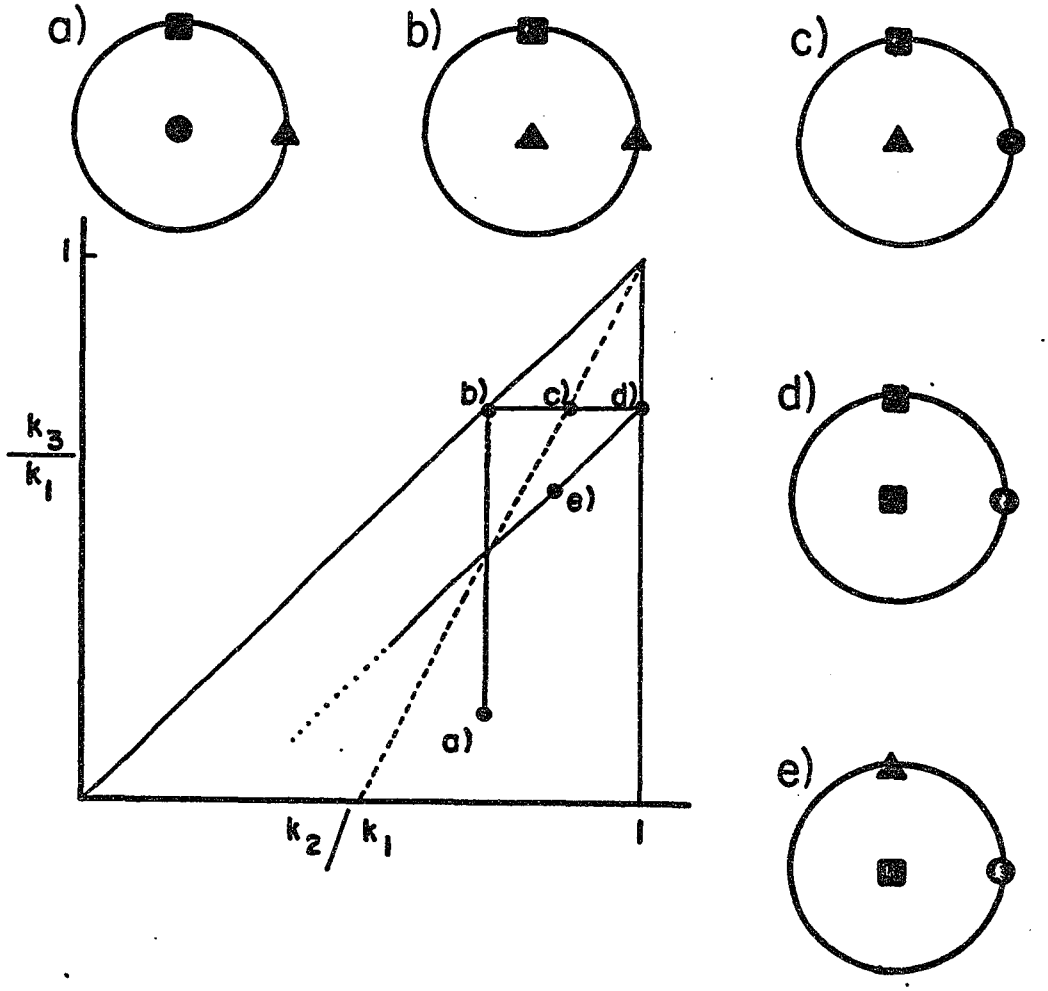

FIGURE 4.8. Diagrammatic evolution of the susceptibility tensor due to the influence of gravitational forces. Projections indicate the position of the principal susceptibilities (squares-maximum, triangles-intermediate, circles-minimum) at different stages during the process. The corresponding magnetic fabric is indicated by the position of the point in the field of the susceptibility tensors (Cañón-Tapia, 1994). Points a, e and d are preferentially foliated, while b is preferentially lineated.

no other mineral foliation is observed, it is suggested that in general it may be possible to obtain some information about the relative magnitudes of shear stresses, and therefore velocity changes, within a lava flow by measuring the AMS of rock specimens.

CONCLUSIONS

The main conclusions of this chapter are:

1) The direction of the mean maximum susceptibility in both flows of this study agrees well with the geologically inferred flow direction despite the apparent large scatter of principal susceptibilities.

2) The general inclination of the magnetic foliation plane to the axis of the flows defines an imbrication indicating the flow direction.

3) There is an excellent agreement between the measured magnetic foliation and the macroscopic vesicle foliation. Both foliations can be explained in terms of the variation of the orientation of a local shear plane.

4) The comprehensive model proposed to explain the origin of the AMS of lava flows incorporates some elements of their fluid behaviour. At variance with previous works (e.g., Khan, 1962; Hargraves et al., 1991) this model offers a systematic approach that opens the possibility of obtaining some information about the dynamic aspects of the movement of lavas through the measurement of the AMS of rock specimens. Results of measurements made on lava flows with other morphologies than the two near-vent a'a flows of this study (Chapter 5) seem to confirm the validity of the proposed model, at least in general terms.

5) Assuming a very simplified situation of unidirectional flow, the orientation of the magnetic plane can be used to obtain approximate velocity profiles of lavas.

6) Based on the velocity profiles inferred from both the vesicle and magnetic foliations, it is suggested that the two units studied here behaved more like Binghamian than Newtonian fluids, and that they developed a roof (perhaps entirely of clinker) that had strength and/or moved slower than the central parts of the flows. The roof development in the unit from Mauna Kea may have been only partial before the end of movement occurred.

CHAPTER 5: HAWAIIAN PAHOEHOE, TOOTHPASTE AND A'A

INTRODUCTION

Distinction between the two main morphological types of basaltic lava, namely pahoehoe and a'a, was originally based on the different appearance of their surfaces (e.g., Dutton, 1884), and ever since their names have been automatically associated with a smooth or rough surface aspect, respectively. Differences between morphologies, however, are not limited to their surface aspect but include their internal structures and their modes of advance (MacDonald, 1953). The relative abundance, distribution patterns and shape of vesicles (e.g., Walker, 1987; 1989; 1995a; Wilmoth and Walker, 1993), the distribution and orientation of mineral grains (e.g., Smith and Rhodes, 1972; Rowland and Walker, 1990), and the deviation from the vertical of columnar jointing (Waters, 1960) are examples of internal features that have been traditionally used to infer some of the characteristics of emplacement of lavas.

Measurement of the anisotropy of magnetic susceptibility (AMS) of rock specimens is another technique that can provide information regarding the dynamics of movement of lava flows (e.g., Cañón-Tapia et al., 1994; Chapter 3; Chapter 4). In this chapter I report the results of the measurement of the AMS of 22 basaltic lava flow-units of various structural types emplaced over different ground slopes in the Hawaiian Islands. I focused my attention on four aspects of AMS, discussing each separately to facilitate the presentation although there is a certain degree of interdependence among them. There are four sections describing and interpreting a) the bulk susceptibility, b) the degree of anisotropy, c) the magnetic fabric and d) the orientations of the principal susceptibilities.

FIELD AND LABORATORY METHODS

Rock specimens were collected with the help of a gasoline powered drill from a total of 22 basaltic flow-units including eight S-type pahoehoe, five P-type pahoehoe, three toothpaste lava, and six a'a (Table 5.1). One of the toothpaste units was sampled at two different outcrops: at the flow frontal part (HTF) and about 25 m behind (HTB). The geologically inferred flow direction was different at each of these sampling sites, and for this reason they are reported as independent profiles in Table 5.1.

TABLE 5.1. General information for all 23 profiles used in this chapter. In the column "# spec. used / collected", the first figure from a unit was used in every other aspect of the study. Flow direction measured directly on the field is marked with an aste flow directions marked with a double asterisk were selected through imbrication patterns. See text for details.

	UNIT NAME	THICKNESS (m)	# SPEC. USED / COLLECTED	SLOPE OF EMPLACEMENT (°)
S-pahoehoe				
	HP02	0.87	9 / 11	<1
	HP06	0.90	25 / 31	> 15
	HP07	0.86	25 / 32	>15
	PO01	0.84	20 / 24	10
	PO02	0.80	20 / 22	10
	PO03	0.68	11 / 13	10
	PU00	0.34	6 / 7	3
	PU01	1.05	9 / 11	3
P-pahoehoe				
	HP01	1.37	10 / 12	<1
	HP03	0.20	5 / 5	5
	HP04	0.30	15 / 17	<1
	HP05	0.72	23 / 29	5
	WA00	3.05	35 / 41	<1

ıpter. In the column "# spec. used / collected", the first figure is exclusive to equal area projections; the total number of specimens irection measured directly on the field is marked with an asterisk, and in this case it is determined within ± 15°. The AMS inferred ırough imbrication patterns. See text for details.

ɜS	# SPEC. USED / COLLECTED	SLOPE OF EMPLACEMENT (°)	EXPECTED FLOW DIRECTION (± 35°)	AMS INFERRED FLOW DIRECTION
	9 / 11	<1	155	40**
	25 / 31	> 15	210	330
	25 / 32	>15	210 *	270
	20 / 24	10	190	220
	20 / 22	10	190	194
	11 / 13	10	190	230
	6 / 7	3	280	270**
	9 / 11	3	280	270
	10 / 12	<1	155	120
	5 / 5	5	155 *	225**
	15 / 17	<1	155	10**
	23 / 29	5	190	151
	35 / 41	<1	160	200

TABLE 5.1. (CONTINUED) General information of all 23 profiles of this chapter.

	UNIT NAME	THICKNESS (m)	# SPEC. USED / COLLECTED	SLOPE OF EMPLACEMENT (°)
TOOTHPASTE				
	HTB	1.00	14 / 16	< 1
	HTF	1.20	11 / 13	< 1
	TP1	0.58	8 / 9	< 1
	TP2	1.15	11 / 15	< 1
A'A				
	HA01	1.30	17 / 22	10
	HA02	0.30	13 / 16	15
	HA03	0.29	11 / 15	15
	HA04	1.71	37 / 42	5
	PO04	1.11	12 / 17	10
	PU02	0.70	6 / 7	3

his chapter.

# SPEC. USED / COLLECTED	SLOPE OF EMPLACEMENT (°)	EXPECTED FLOW DIRECTION (± 35°)	AMS INFERRED FLOW DIRECTION
14 / 16	< 1	70 *	75
11 / 13	< 1	35 *	62
8 / 9	< 1	100 *	110**
11/ 15	< 1	100 *	98
17 / 22	10	270	260
13 / 16	15	270	256
11 / 15	15	270	260
37 / 42	5	240	240
12 / 17	10	190	146
6 / 7	3	280	250**

TABLE 5.2. Estimates of some statistical parameters obtained from the distribution of a) Volume susceptibility (k_m), b) Mas
Magnetic fabric (U and B parameters). Mean and standard deviation (SD) are given for each unit. We additionally calculate the ku
of a particular morphology. Values smaller than 1 x 10^{-4} are not considered significative for magnetic susceptibility.

				k_m				Xm				A	
	UNIT NAME	MEAN x 10^{-3}	SD x 10^{-3}	KURT	SKEW	MEAN x 10^{-4}	SD x 10^{-4}	KURT	SKEW	MEAN	SD	KURT	SK
S-pahoehoe		**9.9**		**3.93**	**0.66**	**6**		**6.41**	**1.08**	**0.5**		**24.77**	**3.6**
	HP02	7.9	1.4			5	4			0.19	0.03		
	HP06	7.7	1.0			5	1			0.36	0.14		
	HP07	6.7	1.9			3	1			0.89	0.28		
	PO01	9.4	0.7			6	1			0.32	0.12		
	PO02	11.6	0.7			7	-			0.41	0.16		
	PO03	15.3	2.4			8	1			1.07	0.70		
	PU00	15.4	2.7			13	2			0.59	0.19		
	PU01	14.8	1.3			7	1			1.16	0.32		
P-pahoehoe		**8.7**		**3.41**	**0.66**	**4**		**3.14**	**0.68**	**0.85**		**3.34**	**1.0**
	HP01	8.8	0.3			4	-			0.43	0.06		
	HP03	1.0	-			-	-			0.20	0.02		
	HP04	2.3	-			1	-			0.32	0.11		
	HP05	5.9	-			3	-			0.48	0.16		
	WA00	14.3	0.1			6	1			1.52	0.29		

ıed from the distribution of a) Volume susceptibility (k_m), b) Mass susceptibility (Xm), c) Degree of anisotropy (A parameter), and d) ation (SD) are given for each unit. We additionally calculate the kurtosis and skewness of the distribution formed by all the specimens not considered significative for magnetic susceptibility.

		Xm				A				U				B	
AN 10^{-4}	SD x 10^{-4}	KURT	SKEW	MEAN	SD	KURT	SKEW	MEAN	SD	KURT	SKEW	MEAN	SD	KURT	SKE
		6.41	**1.08**	**0.5**		**24.77**	**3.65**	**0.16**		**2.64**	**-0.43**	**-0.10**		**11.81**	**-1.3(**
	4			0.19	0.03			0.56	0.14			-0.28	0.19		
	1			0.36	0.14			0.23	0.16			-0.10	0.10		
	1			0.89	0.28			0.23	0.17			-0.28	0.19		
	1			0.32	0.12			-0.18	0.29			0.12	0.14		
	-			0.41	0.16			0.05	0.32			-0.05	0.33		
	1			1.07	0.70			0.13	0.15			-0.03	0.14		
	2			0.59	0.19			0.36	0.12			-0.28	0.09		
	1			1.16	0.32			0.07	0.20			-0.03	0.36		
		3.14	**0.68**	**0.85**		**3.34**	**1.03**	**0.11**		**2.49**	**-0.34**	**-0.23**		**4.67**	**-1.30**
	-			0.43	0.06			0.32	0.15			-0.20	0.10		
	-			0.20	0.02			-0.05	0.28			0.01	0.07		
	-			0.32	0.11			-0.03	0.22			0.02	0.10		
	-			0.48	0.16			0.00	0.16			0.01	0.09		
	1			1.52	0.29			0.14	0.18			-0.52	0.43		

TABLE 5.2. (CONTINUED) Estimates of statistical parameters for all units of this chapter.

				k_m				Xm				A	
	UNIT NAME	MEAN x 10^{-3}	SD x 10^{-3}	KURT	SKEW	MEAN x 10^{-4}	SD x 10^{-4}	KURT	SKEW	MEAN	SD	KURT	SKEW
TOOTHPASTE		11.9		2.59	0.98	5		6.41	1.69	1.32		2.00	0.:
	HTB	10.1	1.6			5	1			1.39	0.31		
	HTF	23.2	1.5			9	2			2.07	0.20		
	TP1	5.9	0.6			3	-			0.57	0.14		
	TP2	7.6	0.7			3	-			1.05	0.22		
A'A		32.0		2.81	0.30	14		3.66	0.75	1.69		4.54	0.:
	HA01	33.2	3.2			14	1			1.85	0.17		
	HA02	27.1	3.1			12	1			1.74	0.24		
	HA03	12.3	5.3			8	3			0.54	0.15		
	HA04	46.8	5.5			19	2			1.87	0.58		
	PO04	23.5	2.9			10	1			2.49	0.36		
	PU02	14.2	0.5			7	-			0.49	0.05		

eters for all units of this chapter.

		Xm				A				U				B	
MEAN x 10^{-4}	SD x 10^{-4}	KURT	SKEW	MEAN	SD	KURT	SKEW	MEAN	SD	KURT	SKEW	MEAN	SD	KURT	SKEW
5		6.41	1.69	1.32		2.00	0.28	0.19		2.11	-0.29	-0.00		3.04	0.17
5	1			1.39	0.31			0.36	0.18			-0.83	0.39		
9	2			2.07	0.20			-0.18	0.15			0.47	0.38		
3	-			0.57	0.14			0.10	0.26			-0.12	0.19		
3	-			1.05	0.22			0.40	0.19			-0.66	0.28		
14		3.66	0.75	1.69		4.54	0.78	-0.02		2.19	0.13	0.00		4.24	0.41
14	1			1.85	0.17			-0.15	0.14			0.35	0.36		
12	1			1.74	0.24			0.05	0.19			-0.25	0.44		
3	3			0.54	0.15			-0.13	0.21			0.08	0.12		
19	2			1.87	0.58			-0.02	0.21			0.23	0.55		
10	1			2.49	0.36			0.07	0.17			-0.13	0.48		
7	-			0.49	0.05			0.30	0.17			-0.26	0.13		

With the exception of the four toothpaste lava profiles, both the top and bottom boundaries of all the studied units were clearly observed in the outcrop. In the case of toothpaste lava, only the uppermost few meters of the unit were exposed and accessible for drilling, and consequently variations with thickness of the AMS of this morphological type could not be completed.

The reported slopes of emplacement (Table 5.1) were usually assumed to be given by the present day slope as determined from the generalized contour lines on topographic maps. In a few instances it was possible to measure the ground slope directly on the field. In any case, the errors associated with the determination of the slope at any particular site are thought to be small.

The uncertainties associated with the estimates of emplacement slope have a more marked effect on the determination of the direction of flow at the sampling locations. Although in some instances it was possible to use other indicators (e.g., the orientation of pipe vesicles, surface structures and/or the elongation direction of lava lobes) to constrain further the local direction of movement, available evidence in general did not allow to estimate it precisely (within a ± 35° interval in most cases, Table 5.1); this will be called the geologically inferred flow direction in the following.

BULK SUSCEPTIBILITY

Variation within units

With the exception of isolated specimens yielding local peak values, most units displayed little variation of k_m across their entire thickness (Fig. 5.1a) except for a weak pattern of decreasing k_m that is observed in most S-type pahoehoe units. The influence of vesicularity (pahoehoe specimens in general possess a larger amount of vesicles than a'a specimens) was investigated by calculating the mass susceptibility (k_m / weight) of each specimen. Variations of mass susceptibility with position (Fig. 5.1b) preserve essentially the same general form as for k_m, although locally smoothing the curves.

Variation between units

S-type pahoehoe and a'a display similar variations of mean magnetic susceptibility, at least in the available common range of unit thickness, whereas P-type pahoehoe yields a distinct trend (Fig. 5.2b).

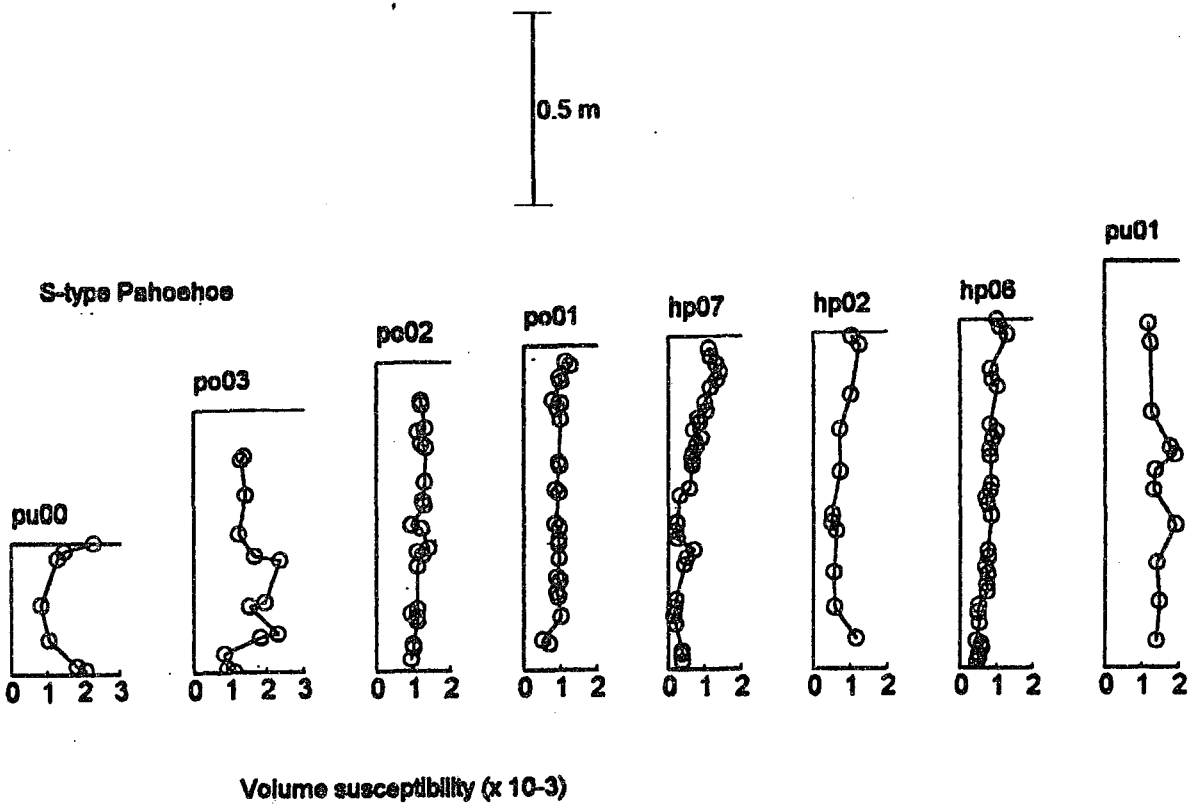

FIGURE 5.1. a) Variation of volume susceptibility across the width of lava flow units (S-type pahoehoe).

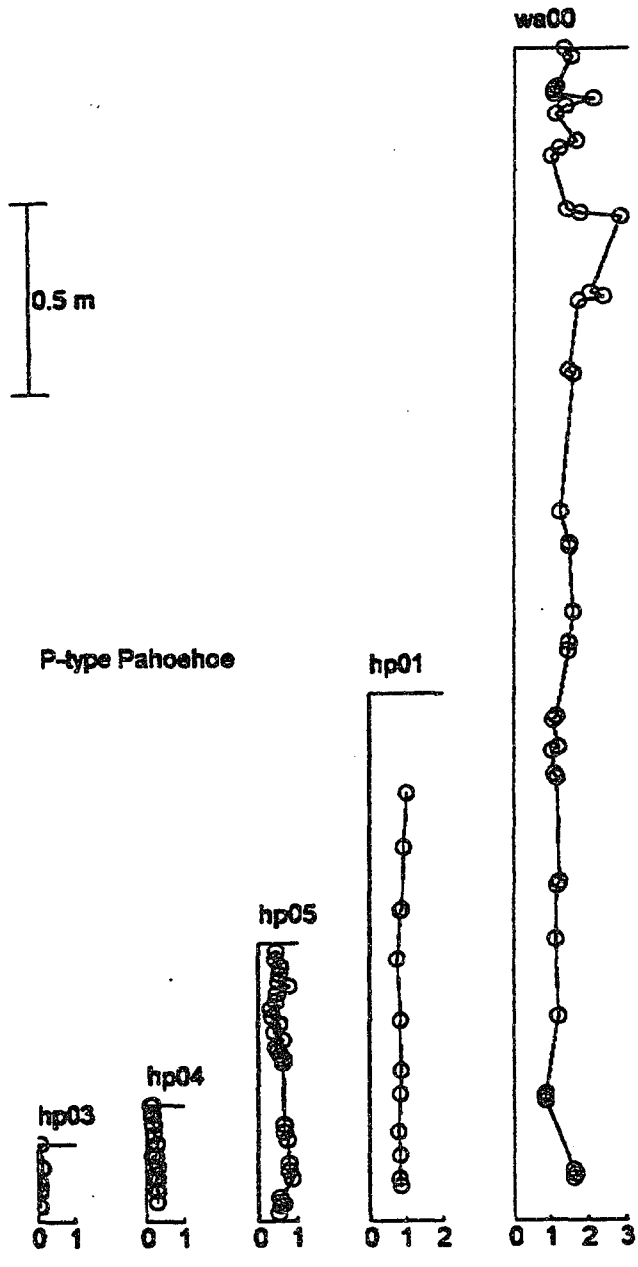

FIGURE 5.1. (CONTINUED) a) Variation of volume susceptibility across the width of lava flow units (P-type pahoehoe).

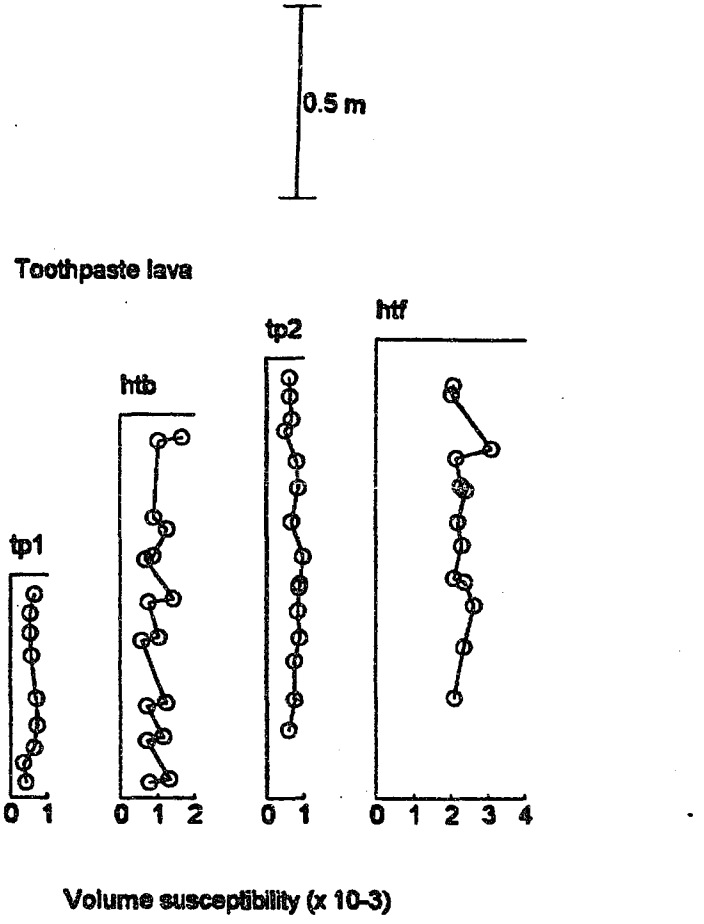

FIGURE 5.1. (CONTINUED) a) Variation of volume susceptibility across the width of lava flow units (Toothpaste lava).

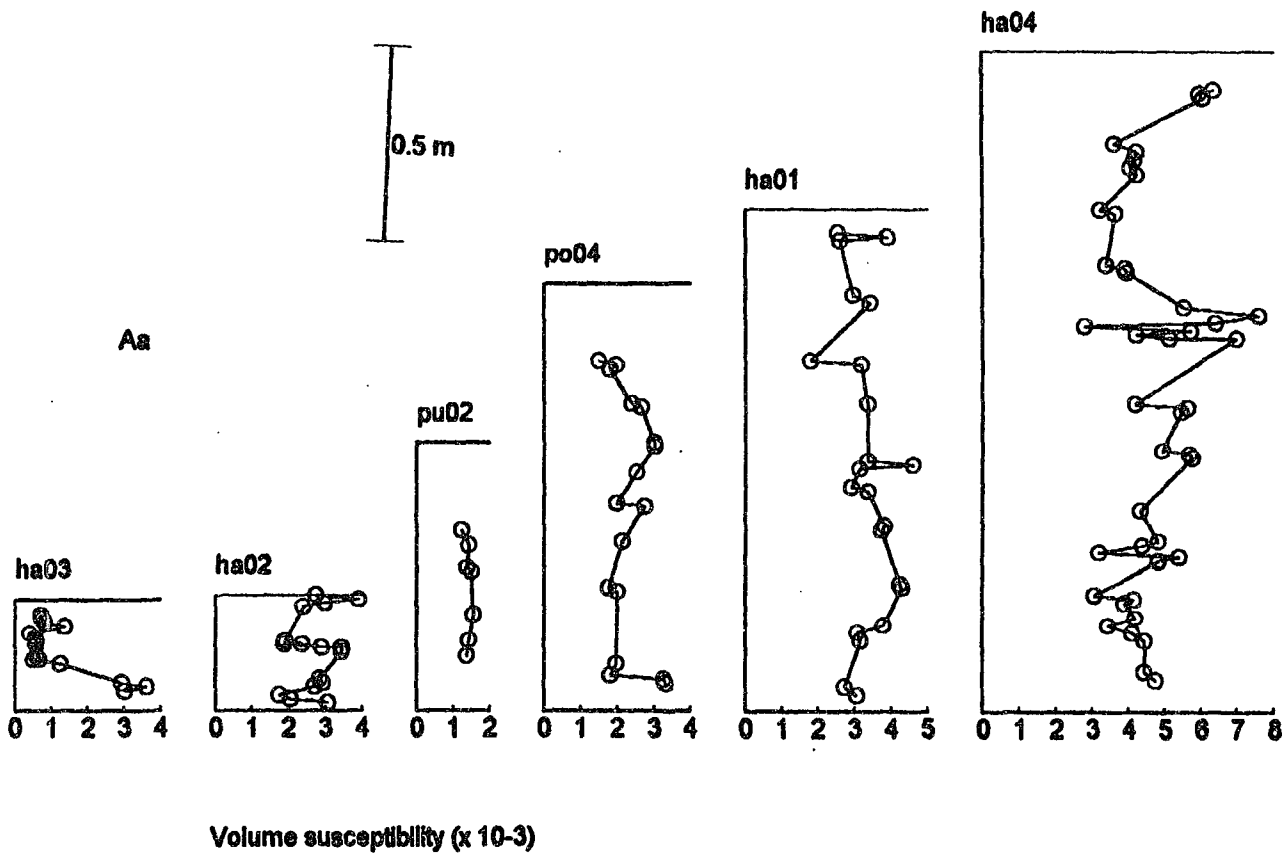

FIGURE 5.1. (CONTINUED) a) Variation of volume susceptibility across the width of lava flow units (A'a).

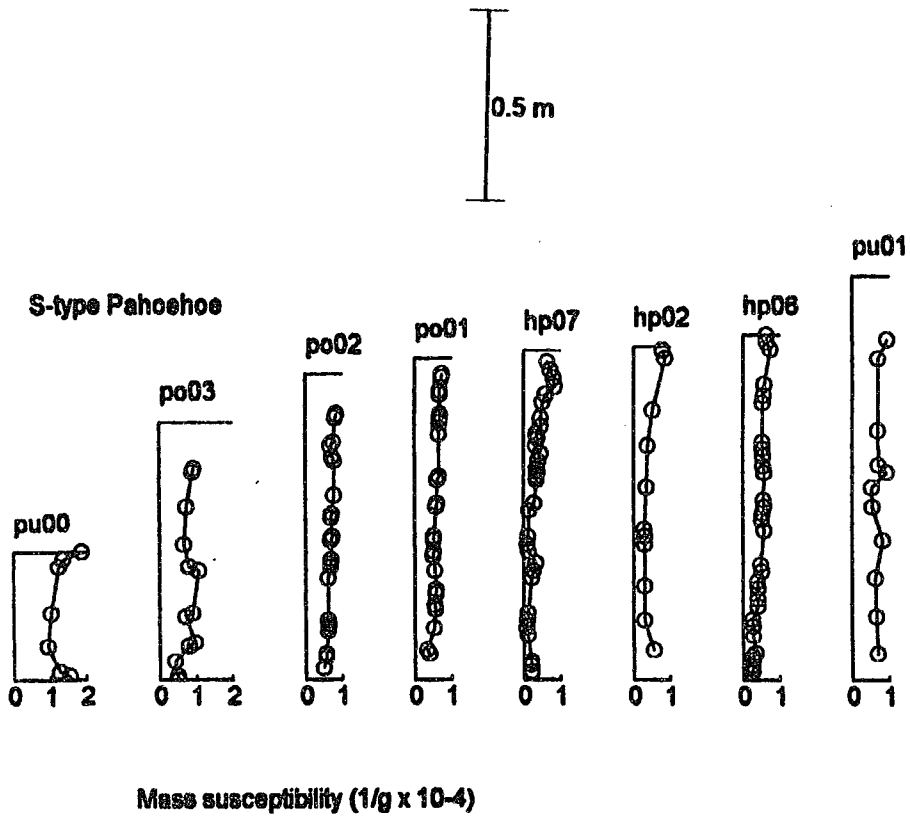

FIGURE 5.1. (CONTINUED) b) Variation of mass susceptibility across the width of lava flow units (S-type pahoehoe).

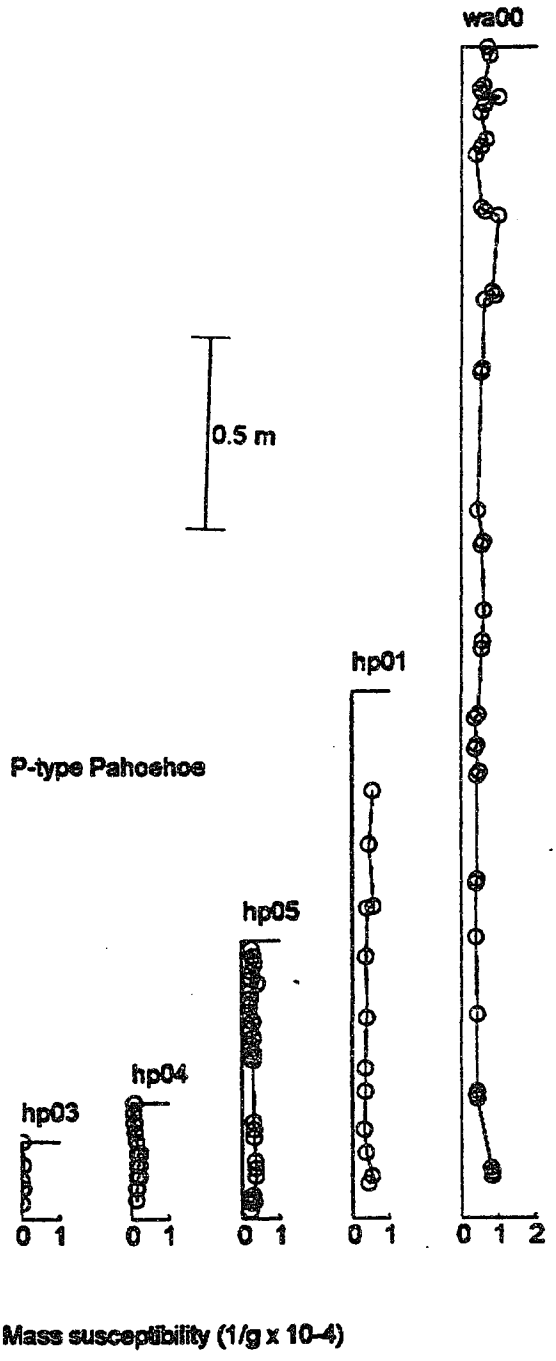

FIGURE 5.1. (CONTINUED) b) Variation of mass susceptibility across the width of lava flow units (P-type pahoehoe).

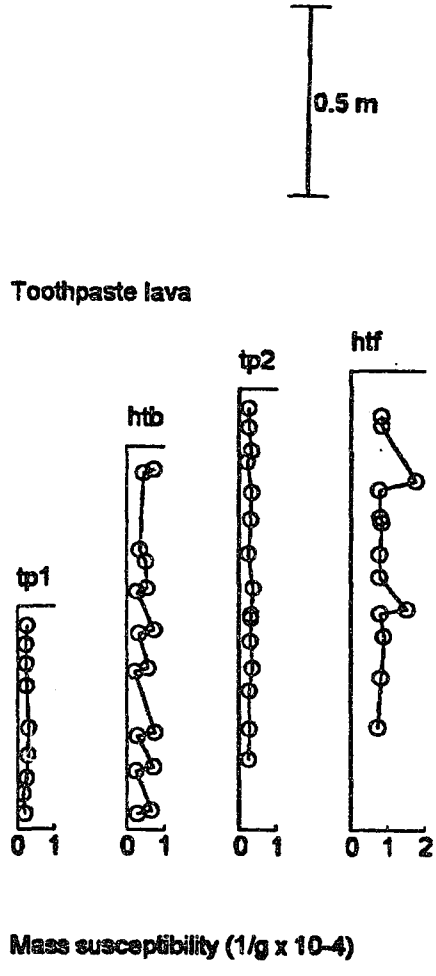

FIGURE 5.1. (CONTINUED) b) Variation of mass susceptibility across the width of lava flow units (Toothpaste lava).

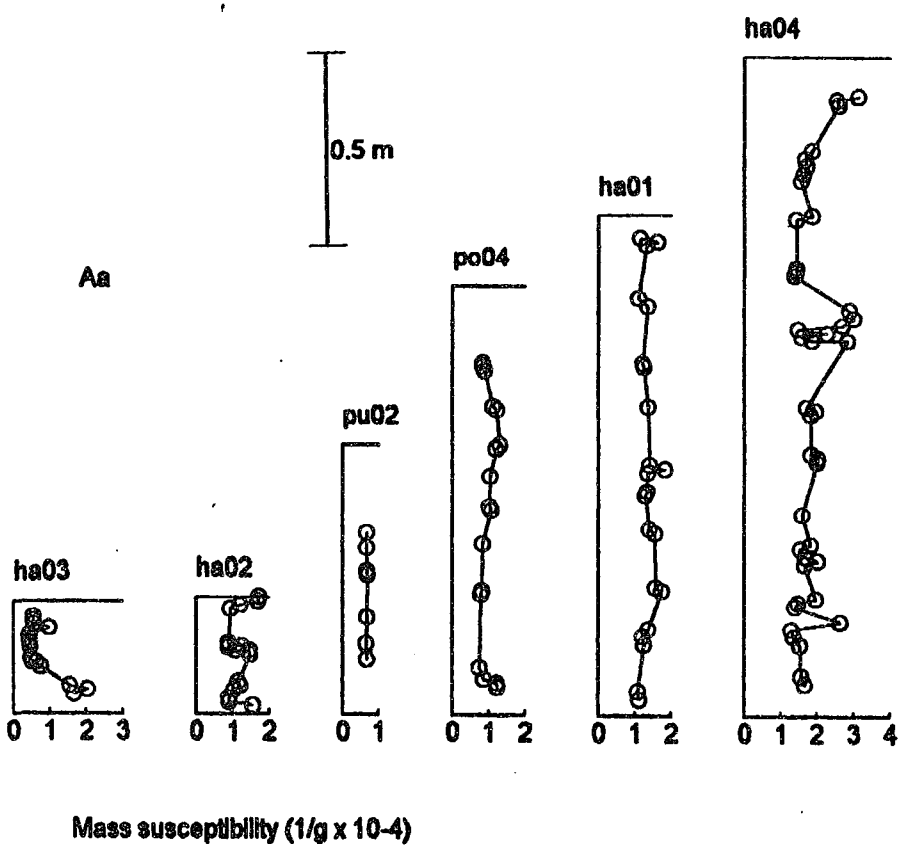

FIGURE 5.1. (CONTINUED) b) Variation of mass susceptibility across the width of lava flow units (A'a).

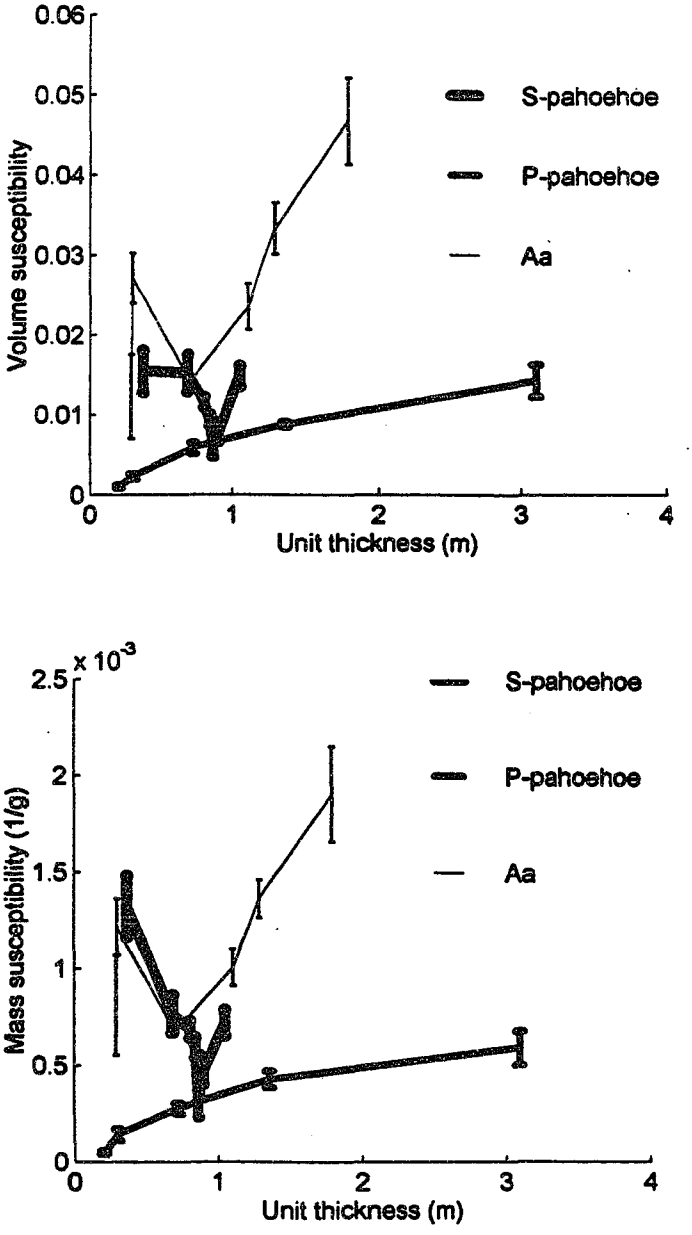

FIGURE 5.2. Variation of volume susceptibility (a) and mass susceptibility (b) with thickness of lava flow units. Bars are centered in the mean value of each unit and have a length equal to 2 standard deviations.

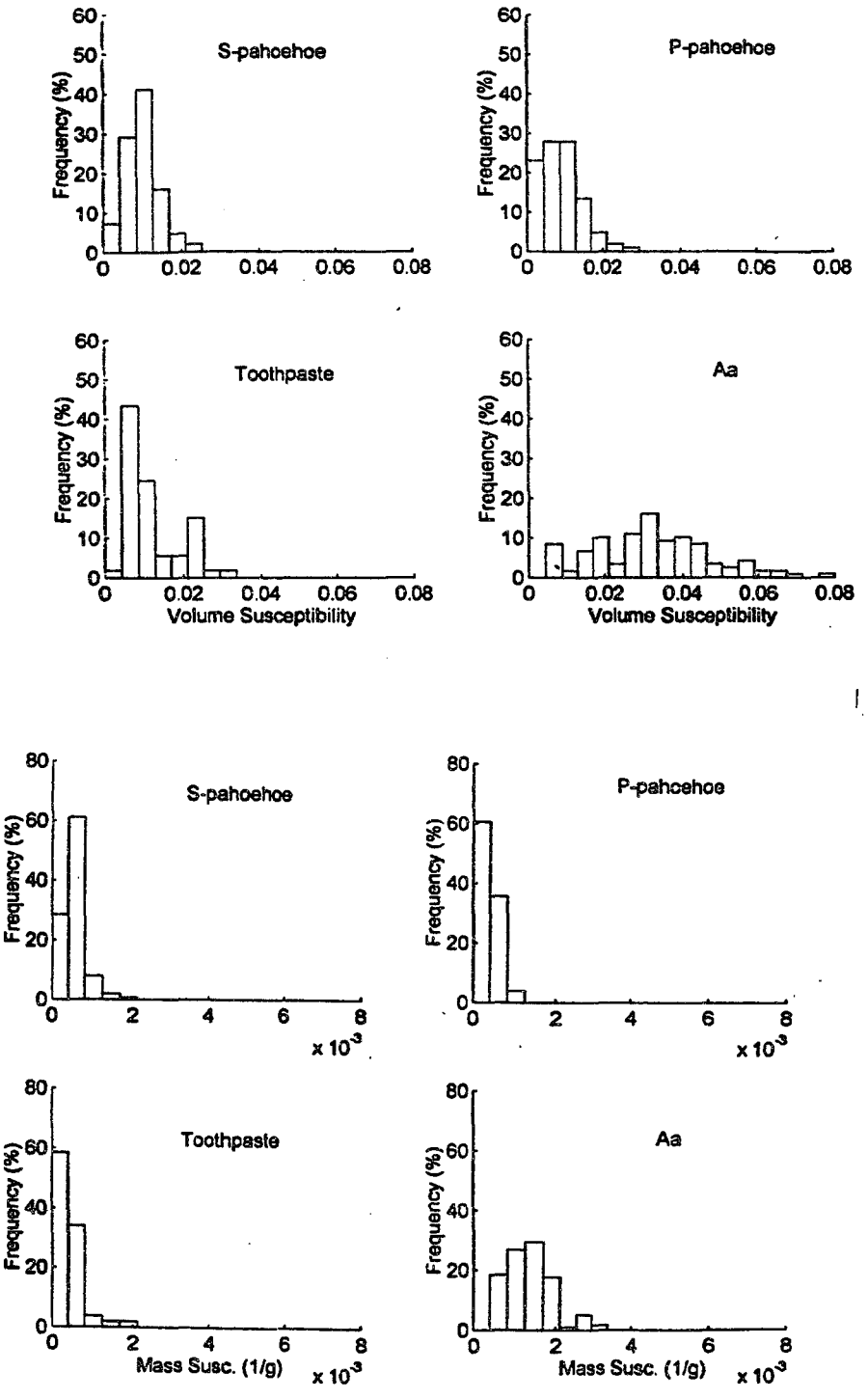

FIGURE 5.3. Relative frequency histograms of volume (a) and mass (b) susceptibility of all specimens collected from each of the four lava flow morphologies studied.

For all morphologies, there is an increase of average magnetic susceptibility with increasing thickness for flow units > 1 m thick. S-type pahoehoe and a'a units with thicknesses < 1 m reverse the trend so that average magnetic susceptibility now increases with decreasing thickness. This change is not observed in P-type pahoehoe units, which are also characterized by a weaker average magnetic susceptibility than both a'a and S-type pahoehoe for a given thickness.

The histograms of figure 5.3a illustrate the frequency distribution of k_m of all the specimens grouped by morphological type, and some statistical parameters are listed in Table 5.2. It is apparent from this information that k_m is to some extent related with the lava morphology: a'a flows yield larger values than either pahoehoe or toothpaste lava. Histograms of mass susceptibility (Fig. 5.3b) show the same trend, which therefore cannot be attributed to the different vesicularity of the specimens.

Discussion

The observed variation of magnetic susceptibility is most certainly the result of a complex interplay of several parameters including bulk chemical composition of the erupted material, rate of cooling, oxygen fugacity conditions prevalent during initial cooling, degree of post-emplacement alteration suffered by the flow and the distribution of magnetic grains. Due to the wide geographic distribution of sampling sites, and because whenever possible both a'a and pahoehoe units were sampled at the same locality, it is unlikely that chemical composition or post-emplacement alteration played an important role in defining the observed trends.

In general, thicker units will cool at a slower rate than thin units and therefore are likely to have larger amounts of crystallized magnetic phases. Also, preferential escape of hydrogen leading to higher oxygen fugacities during cooling of thicker lavas can result in the deuteric oxidation of titanomagnetite, producing the exsolution of phases with compositions closer to pure magnetite (Petersen, 1976). Both of these factors lead to a stronger magnetic susceptibility, and therefore can explain the trend observed for units thicker than 1 m. The trend displayed by thinner a'a and S-type pahoehoe units, or the weaker magnetic susceptibility of P-type pahoehoe and stronger values of a'a regardless of thickness, are, however, not explained by these factors.

To account for the systematic variation of magnetic susceptibility with morphology it is therefore necessary to adopt a different perspective. For example, it is possible that pahoehoe units have a more efficient cooling mechanism than a'a, so that their crystal content is smaller even in units with comparable thicknesses. Although at present it is not known whether the incandescent surface displayed by a'a flows relative to pahoehoe is larger per m^3 of lava, the larger surface observed in a'a flows makes this possibility somewhat unlikely. A more reasonable explanation is that a'a flows promote the development of higher oxygen fugacities across the unit, perhaps through a more efficient mechanism for injestion of air/atmospheric water than pahoehoe.

Yet a third possibility is that units formed under certain conditions allow a larger degree of magnetic interaction between ferromagnetic particles than others. Although it is true that the effects of magnetic interaction are still not well understood, it is becoming clear that they play a very important role in the determination of the magnetic properties of rocks (e.g. Shcherbakov et al. 1995). In particular, magnetic interaction between neighboring particles can increase the measured value of magnetic susceptibility by as much as 40% (Appendix 1). Distribution of magnetic grains promoting magnetic interaction can be related to the internal fluid dynamics of each particular morphology (Chapter 4), and therefore differs from rate of cooling or degree of oxidation in that it explicitly relates magnetic susceptibility with morphological type.

The apparent inverse relationship between magnetic susceptibility and unit thickness observed in thin a'a and S-type pahoehoe units (unlikely to have been formed by endogenous growth) may therefore result from a combination of all these variables. For instance, thin units formed at the frontal parts of a flow are more likely to be buried rapidly by the advancing lava, and therefore their cooling rates are likely to be slower than would be expected from their actual thickness, resulting in an increase of magnetic susceptibility of thinner units relative to thicker ones. This effect is not observed in P-type pahoehoe because this type of lava emerges from the vent with a smaller volatile content (Wilmoth and Walker, 1993) and is therefore more likely to cool down in an environment with a lower oxygen fugacity. Additionally, formation of grain clusters is favored in S-type pahoehoe because crystalization is restricted to those regions that contain liquid squeezed between adjacent vesicles. In cases where

the number of grains per unit volume of liquid is small, magnetic interaction will be favored only if clusters are formed, so that magnetic susceptibility is slightly increased in very thin S-pahoehoe units relative to a'a of comparable thicknesses. If the number of grains per unit volume is large, however, magnetic interaction does not depend so strongly on the formation of clusters, but rather on average separation between grains. In these cases, although clusters will still be formed locally in S-pahoehoe, vesicles have the overall effect of increasing average grain separation, and consequently magnetic susceptibility of thick S-type pahoehoe units is weaker than on a'a of comparable thicknesses.

In summary, although the range of possible values within a single unit is wide in general, it allows the identification of systematic changes among different lava flow morphologies. Rate of cooling, oxygen fugacity and distribution of magnetic phases, all of which are interrelated, are all seemingly important parameters. The specific conditions of emplacement of a particular lava flow may result in departure from the general lines discussed here; the occurrence of endogenous growth is presumed to be especially important in this regard.

DEGREE OF ANISOTROPY

Variation within units

Variation of A within each unit is shown in Figure 5.4. It is observed that A essentially remains constant with depth, although in a few instances the value of A in the lower half is larger than in the upper half of the unit. The difference in values of A between samples near the top and samples near the base is usually small in most pahoehoe units, however, and tends to be obscured by the presence of intermediate specimens with peak values of A. Zonation of A is more clearly observed in a'a units.

Variations between units

Specimens from the same morphological type have been grouped together to form the histograms shown in Fig. 5.5; the corresponding statistical parameters are listed in Table 5.2. A clear trend of increasing value of A from S-type pahoehoe and P-type pahoehoe to toothpaste lava and a'a is

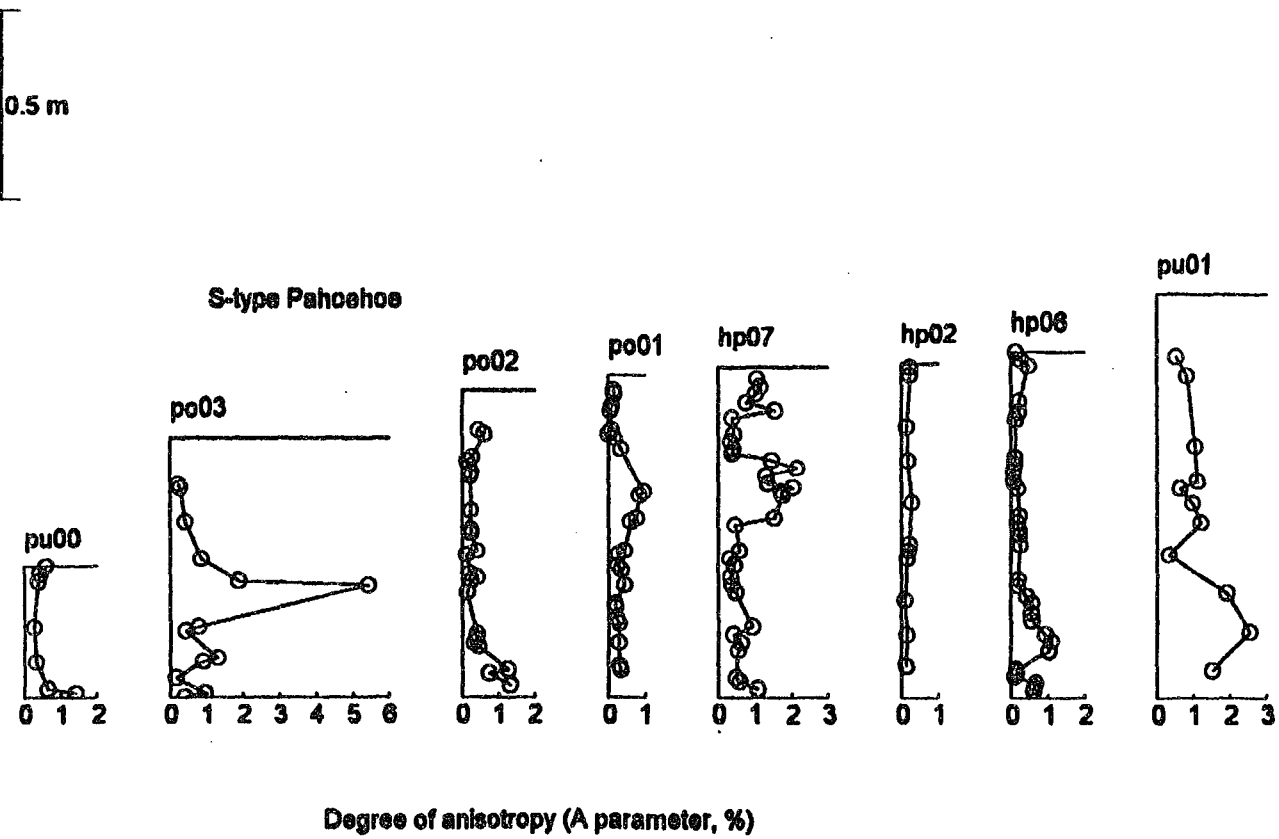

FIGURE 5.4. Variation of the degree of anisotropy (A parameter) across the width of lava flow units (S-type pahoehoe).

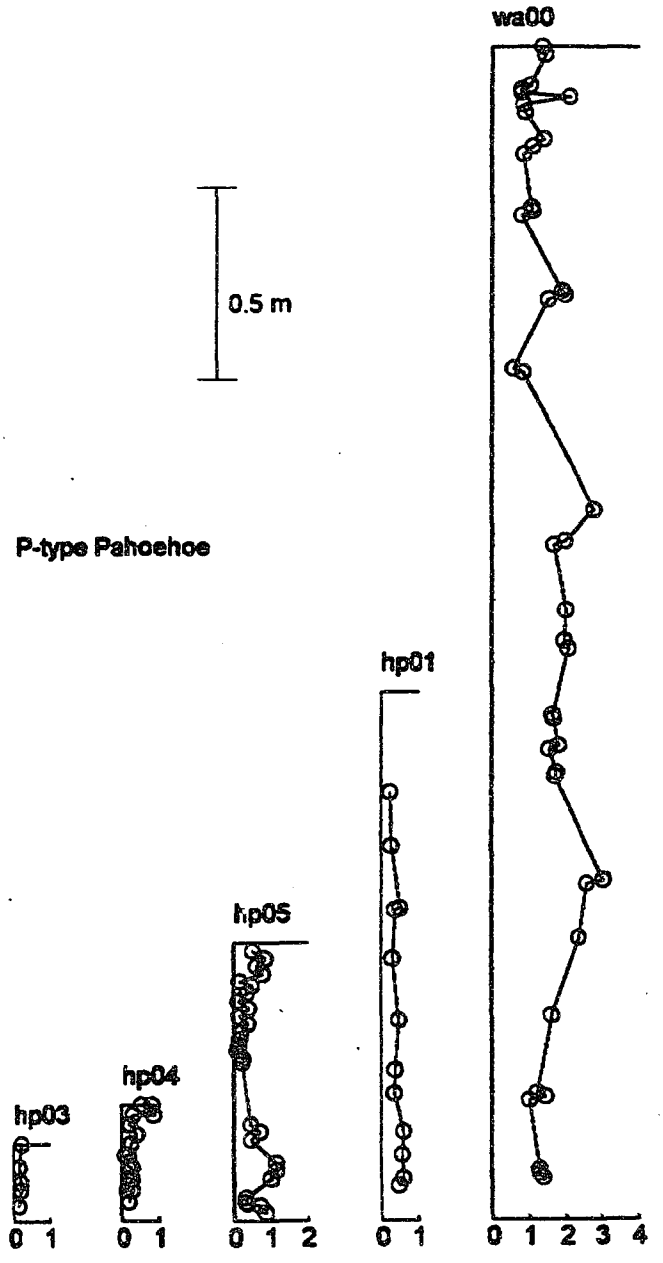

FIGURE 5.4. (CONTINUED) Variation of the degree of anisotropy (A parameter) across the width of lava flow units (P-type pahoehoe).

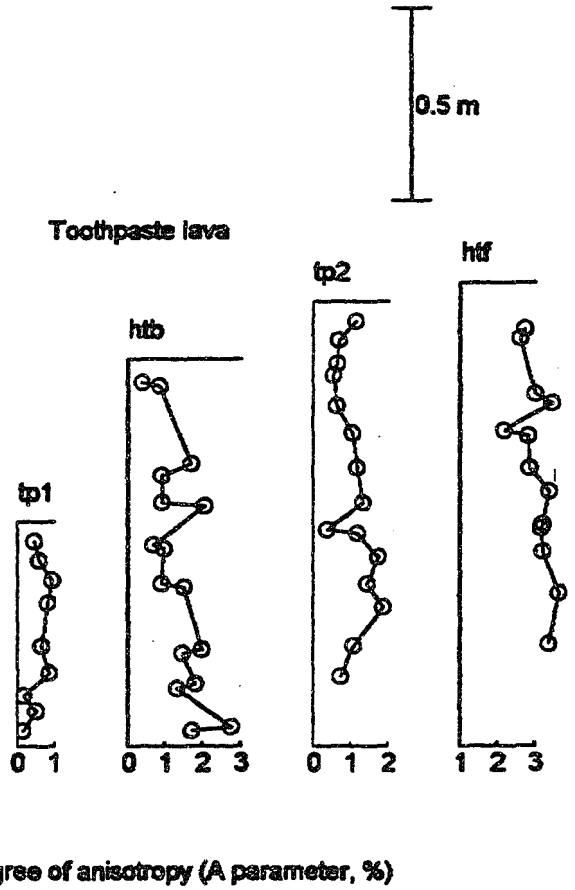

FIGURE 5.4. (CONTINUED) Variation of the degree of anisotropy (A parameter) across the width of lava flow units (Toothpaste lava).

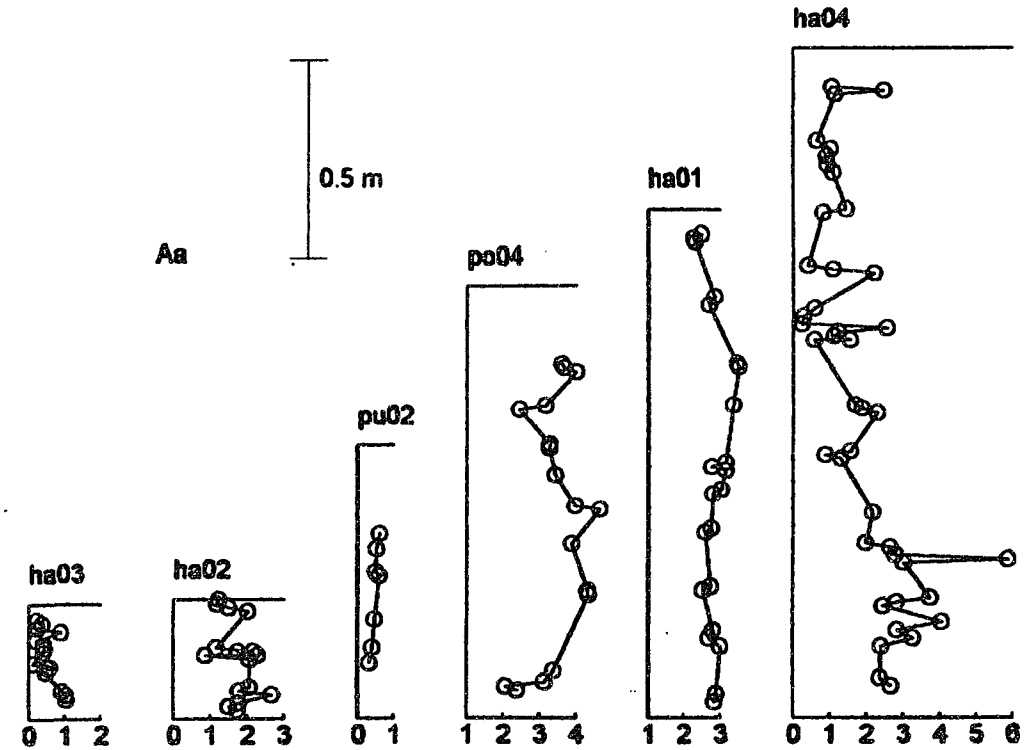

FIGURE 5.4. (CONTINUED) Variation of the degree of anisotropy (A parameter) across the width of lava flow units (A'a).

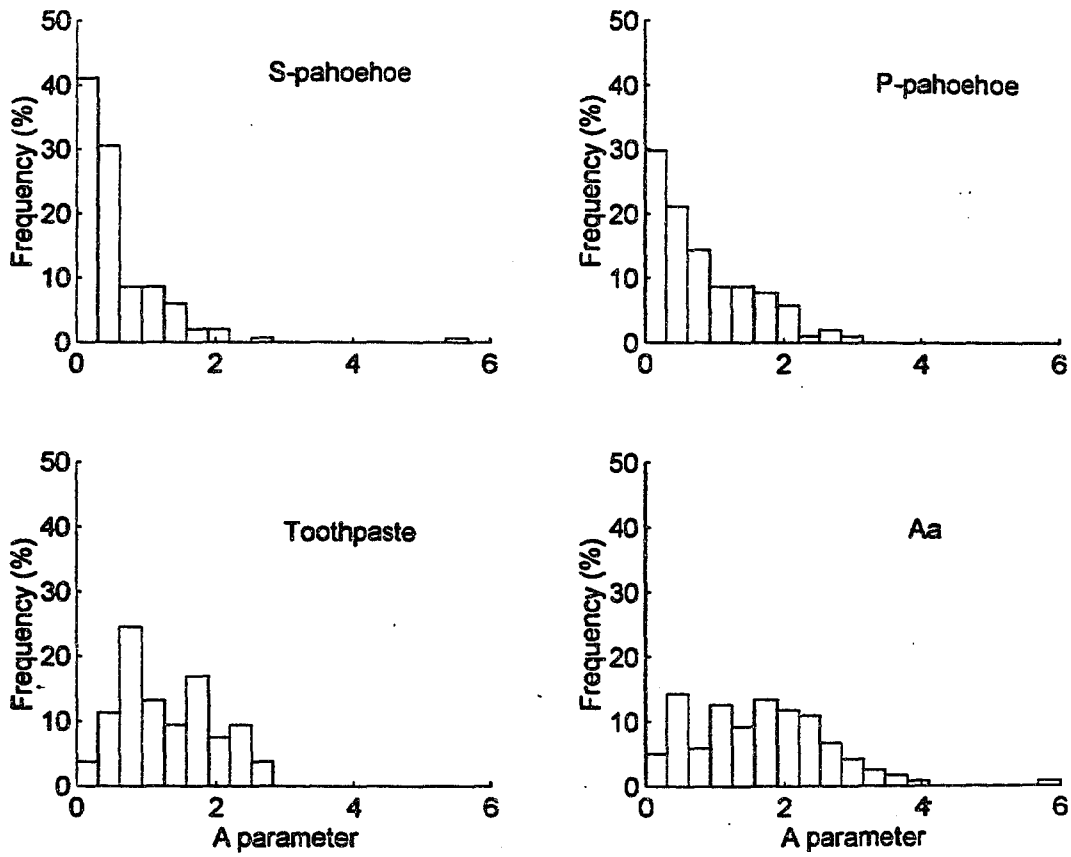

FIGURE 5.5. Relative frequency histograms of the degree of anisotropy of all specimens collected from each of the four lava flow morphologies studied in this chapter.

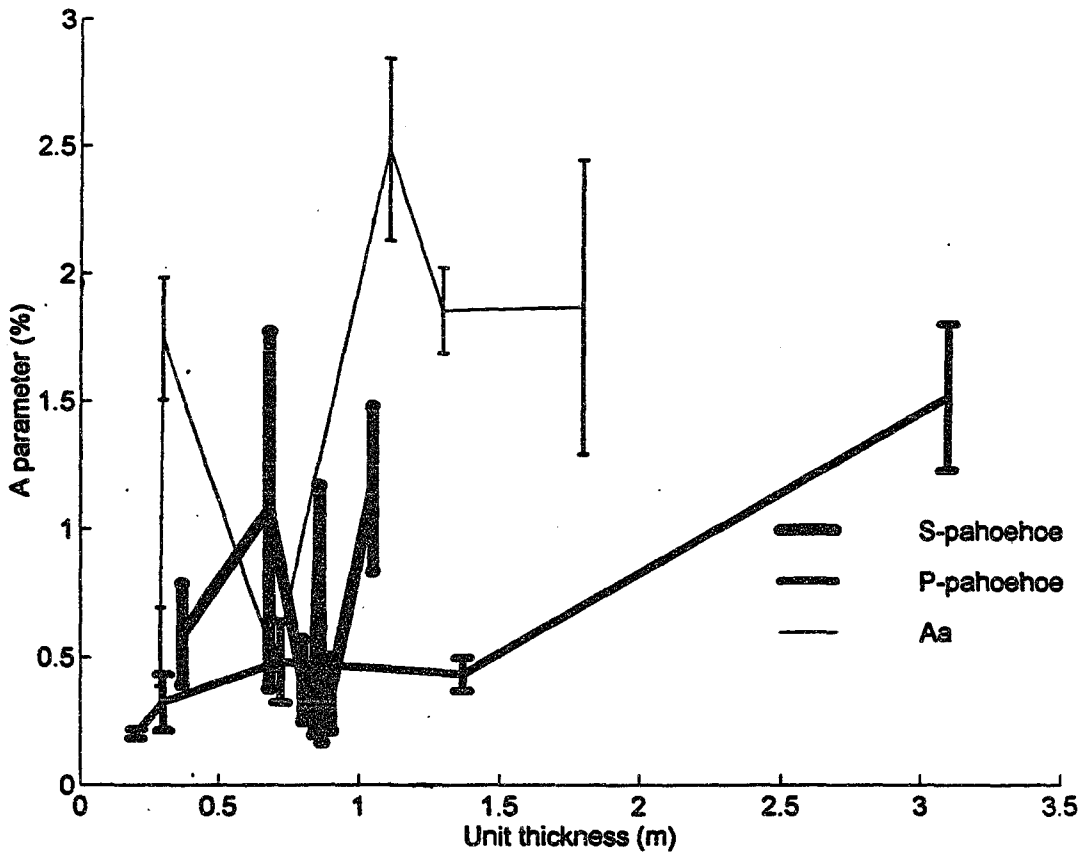

FIGURE 5.6. Variation of the degree of anisotropy with thickness of lava flow units. Symbols as in Fig. 5.2.

observed from the distributions. This trend is similar to that observed in the distribution of magnetic susceptibility, although in the case of A there is no systematic variation with unit thickness (Fig. 5.6).

Discussion

Peterson and Tilling (1980) and Kilburn (1981) showed that the transition from pahoehoe to a'a is intimately related to changes in both (apparent) viscosity and strain rate. From two flows with the same viscosity, that suffering the stronger strain rate is more likely to have the characteristics of a'a, whereas that with the weaker strain rate will resemble pahoehoe; intermediate values of strain rate are associated with toothpaste lava (Rowland and Walker, 1987). The observed progression of values of A from small in pahoehoe to large in a'a are consistent with such difference in the shear rates suggesting that the degree of anisotropy is controlled, at least to some extent, by the local rate of shear (see also Chapter 3).

The model proposed in Chapter 4 can be used as a framework to explain the mechanism through which this dependence is established. The main assumption of the model is that AMS of igneous rocks is controlled by grain distributions resulting from the action of hydraulic forces; magnetic interaction among neighboring ferromagnetic grains finally defines the orientation and magnitude of the measured susceptibility tensor. According to the model in its original form, grain distributions are controlled by the orientation of the local shear plane of individual fluid elements, although it is more convenient to use instead the hypothesis of coaxiality between stress and strain expressed by the constitutive law of an incompressible Newtonian fluid (c.f., eqs. 4.2 and fig. 4.5); this hypothesis, thought of a more general character, also satisfies the required changes in orientation that originally lead to the proposed model. Consequently, I will focus my attention in the deformation suffered by fluid elements over which a particular (fixed) stress tensor is applied.

The deformation of a group of neighboring fluid elements, initially defined as spherical at the arbitrary initial time t_0 can produce distinct planes (lines) depending on the relative sizes of the three principal stresses acting on each element, as illustrated in Fig. 5.7. The stress acting on each element in the figure is approximately the same than that acting on its neighbors, and in both of the cases

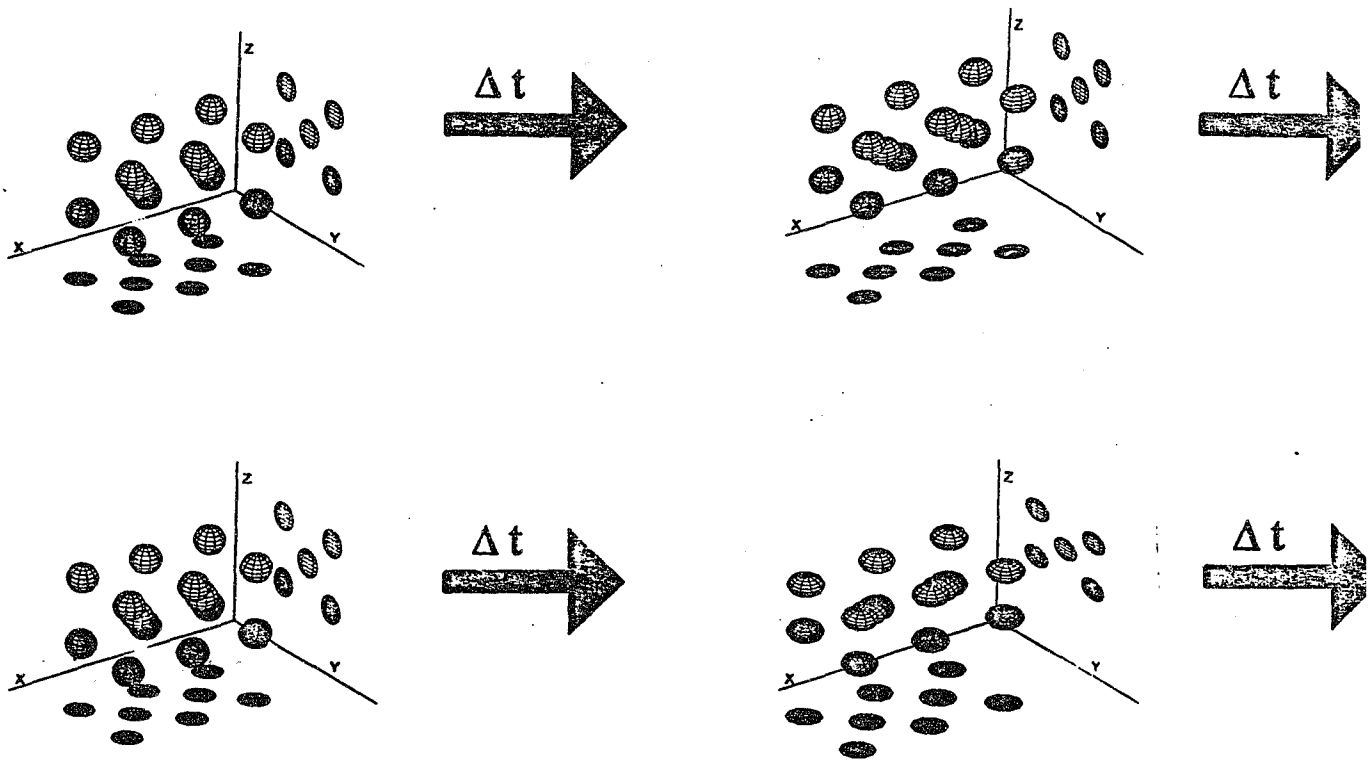

FIGURE 5.7. Two examples of the gradual deformation of adjacent fluid elements originally spherical at the arbitrary time t_0. Proje formation of lines/planes under deformation. The applied stress is assumed constant and equal for each of the fluid elements in each the coordinate system, but in the upper row the y and z strains correspond to shortening (equal to each other) whereas in the lower row constant to indicate mass conservation during deformation.

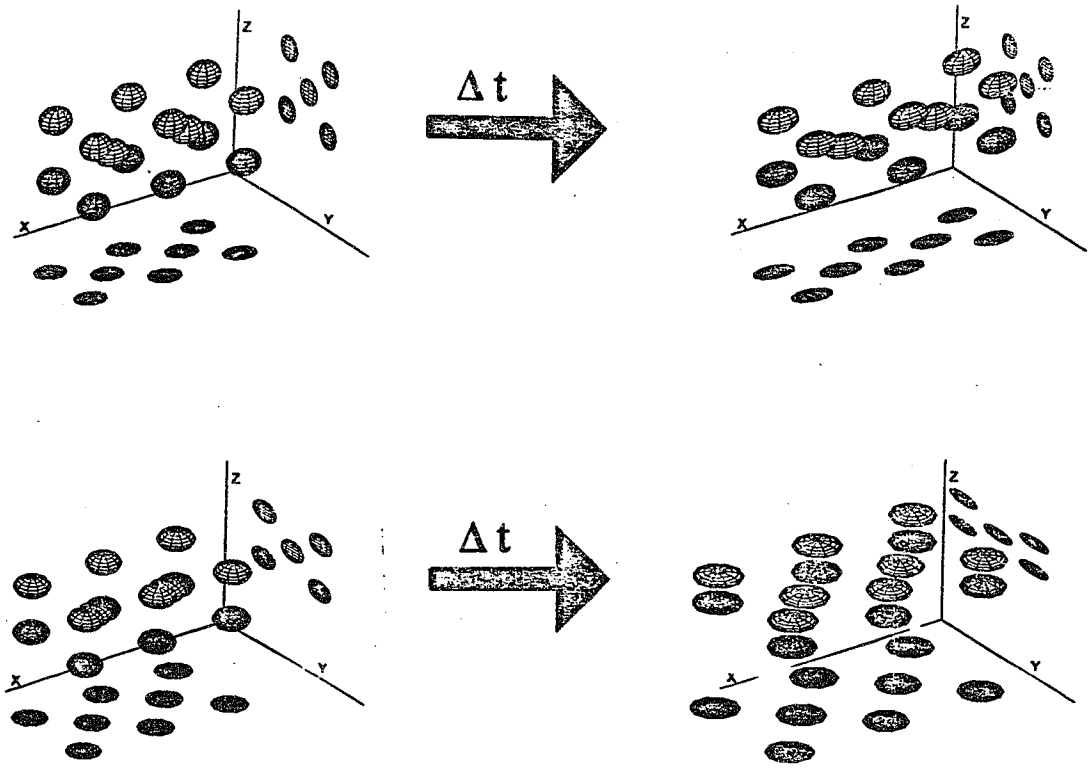

d elements originally spherical at the arbitrary time t_0. Projections over the xy and yz planes are shown as an aid to visualize the d constant and equal for each of the fluid elements in each figure. Principal strains on the upper and lower rows are coaxial with ɔ shortening (equal to each other) whereas in the lower row only z represents a shortening. The volume of each element remains

shown the principal directions of stress are directed parallel to the system of x, y z axes of the figure. After a time interval (dt) has elapsed, ferromagnetic particles contained in one of the original spherical fluid elements will be more likely to interact magnetically with particles on the neighboring fluid element that is closer after deformation, whereas magnetic interaction with elements that are farther is proportionally diminished. The longer the time interval the stronger the deformation of the original elements, and therefore the larger the difference in the magnetic interaction along two perpendicular directions. The changes in the intensity of interaction along different directions just described will result in an increase of the degree of anisotropy associated with a set of fluid elements (Appendix 1), which would explain why the more deformed states possess the larger degrees of anisotropy.

Two aspects of the process of gradual deformation of fluid elements shown in Figure 5.7 deserve further comment. First, it should be clear that the figure is used only to illustrate how deformation of fluid elements may enhance magnetic interaction along one direction while diminishing it along another direction, and does not pretend to portray the actual process that occurs in a moving fluid. Orientation of the principal stresses in a moving fluid in general will not coincide with the direction of movement of a particular point because the local relative velocity is in effect the resultant of the superposition of a pure straining motion and a rigid body rotation (e.g., Batchelor, 1991), and therefore the direction of elongation/flattening should not be associated with the direction of local movement. Inclusion of the rotational motion modifies the orientation of the deformed elements depending on the particular velocity field, although the process of progressive deformation of fluid elements will be preserved. Second, because magnetic interaction is likely to be enhanced when particles are closer and diminished when they are farther, in the case of elongation the maximum susceptibility is more likely to be parallel to the z axis whereas the minimum susceptibility will be parallel to the x axis. It is therefore clear that the final shape of the deformed fluid elements should not be associated with the shape of the susceptibility tensor, even under these schematic conditions.

In summary, even when it is not yet possible to establish a quantitative relationship between degree of anisotropy and lava shear rate, there seems to be a physical relationship between these two parameters that can be used to study the internal kinematics of lava flows. For instance, the observed

variation of degree of anisotropy with height suggests that shear rate was more intense in the lower part of about half of the studied units regardless of morphology. The more deformed basal layer (provided one has been inferred), however, seems to be proportionally thinner in S-type pahoehoe than in P-type pahoehoe or a'a. Therefore, based on magnetic measurements it can be concluded that not only a'a flows are more sheared than pahoehoe, but also that there seems to be an internal zonation of shear that is related to lava flow morphology.

MAGNETIC FABRIC

Variation within units

Variation of magnetic fabrics within a single unit is illustrated in Fig. 5.8a using the U parameter, and in Fig. 5.8b for the B parameter. Despite the lack of a general correlation of magnetic fabric with vertical position, it is possible to identify zones with a distinctive magnetic fabric in some instances, although their identification is commonly hampered by the presence of isolated specimens with "peak" values. The relative importance of these peaks depends on the parameter used, and therefore, zonation of the magnetic fabric within a unit is to some extent parameter-dependent, although detailed examination of both parameters usually lead to the identification of the same regions.

I examined in detail 34 specimens in which clearly deformed vesicles define either a foliation or a combination of both lineation and foliation apparently pervading the entire specimen. The vesicle foliation is of two types: 1) relatively large (diameter > 0.005 m), clearly flattened vesicles, all with a common orientation, and 2) smaller vesicles of an apparently spherical shape, but distributed so that layers containing large numbers of vesicles alternating with layers practically devoid of vesicles are clearly identifiable on the surface of the specimen. Vesicle lineation is more difficult to identify, and I only included specimens containing large vesicles apparently more elongated than flattened; distribution of smaller vesicles in some specimens give the appearance of the above mentioned additional vesicle foliation. The magnetic fabric of all but two of the 17 specimens with an exclusive

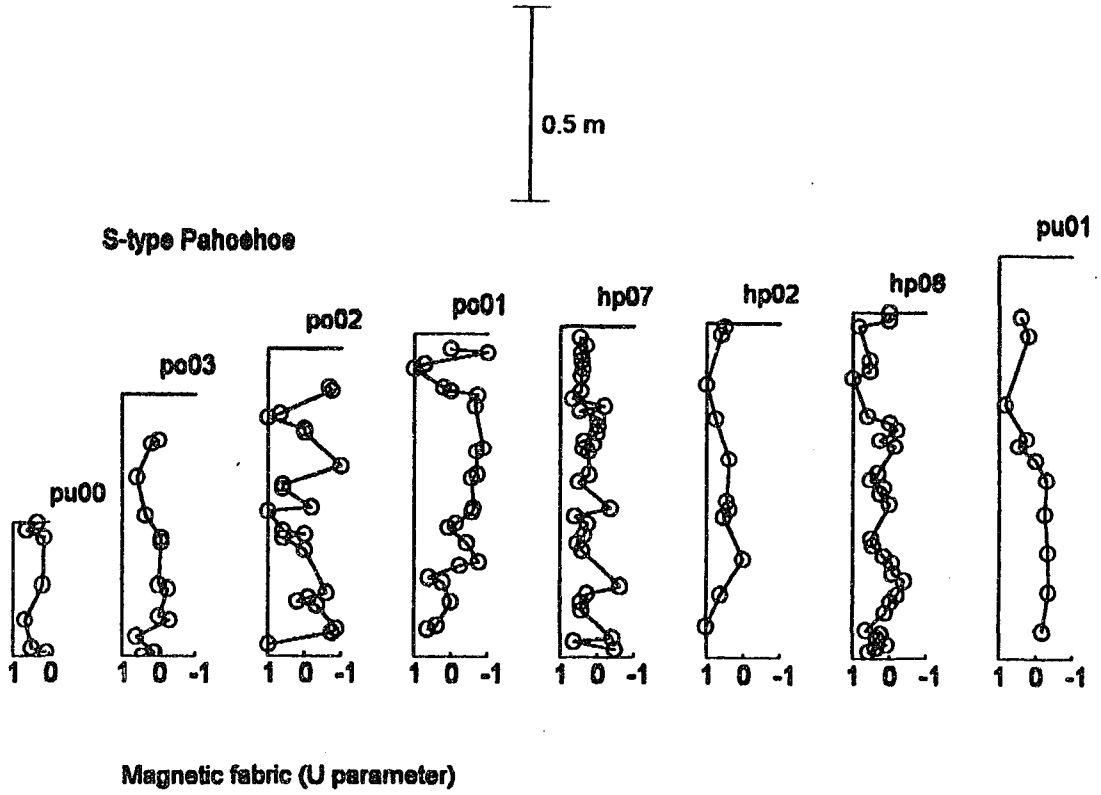

FIGURE 5.8. a) Variation of magnetic fabric (U parameter) across the width of lava flow units (S-type pahoehoe). Note that the scale of the U parameter has been reversed so that magnetic foliation increases to the left for both parameters.

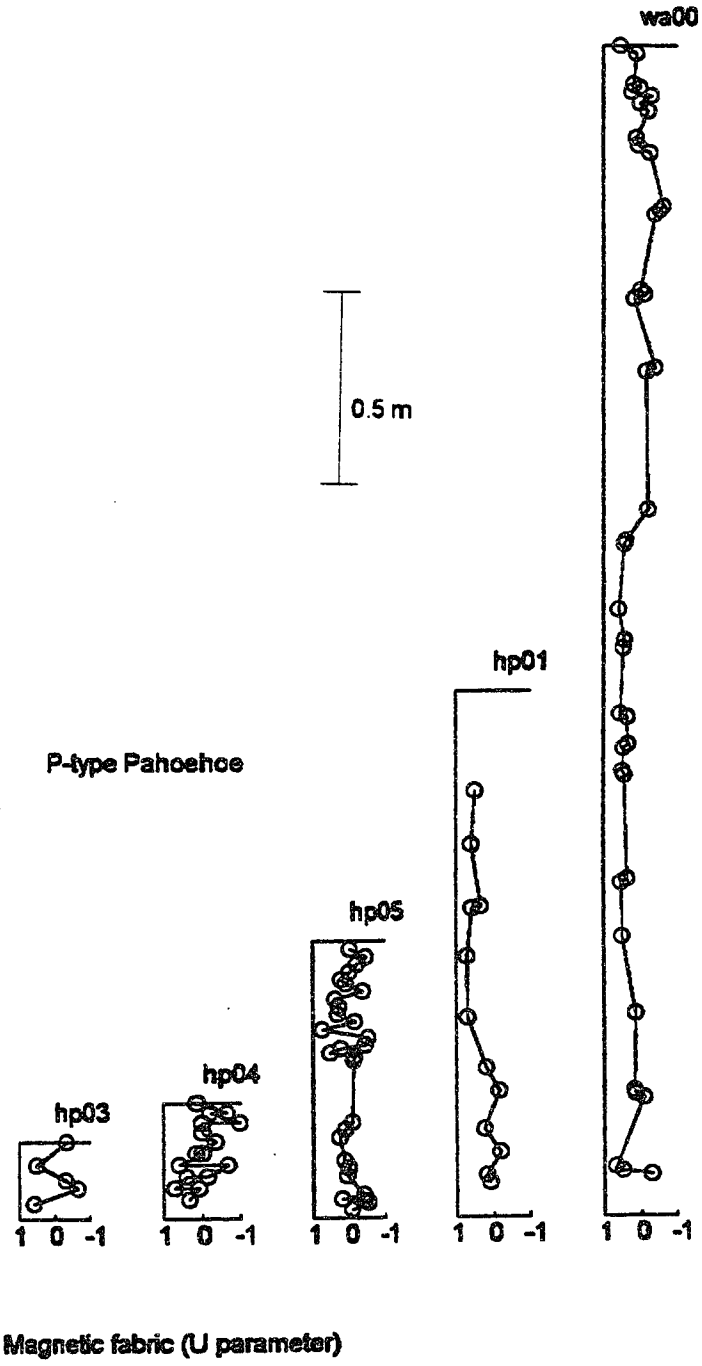

FIGURE 5.8. (CONTINUED) a) Variation of magnetic fabric (U parameter) across the width of lava flow units (P-type pahoehoe).

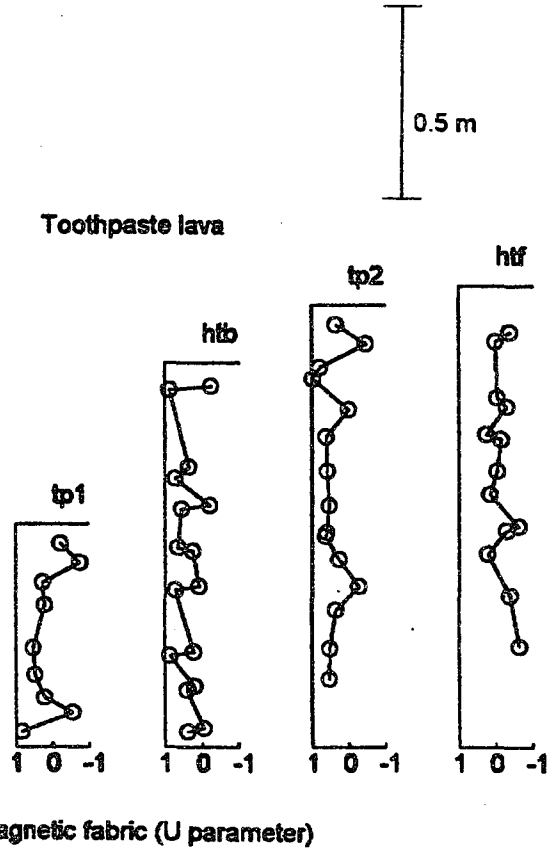

FIGURE 5.8. (CONTINUED) a) Variation of magnetic fabric (U parameter) across the width of lava flow units (Toothpaste lava).

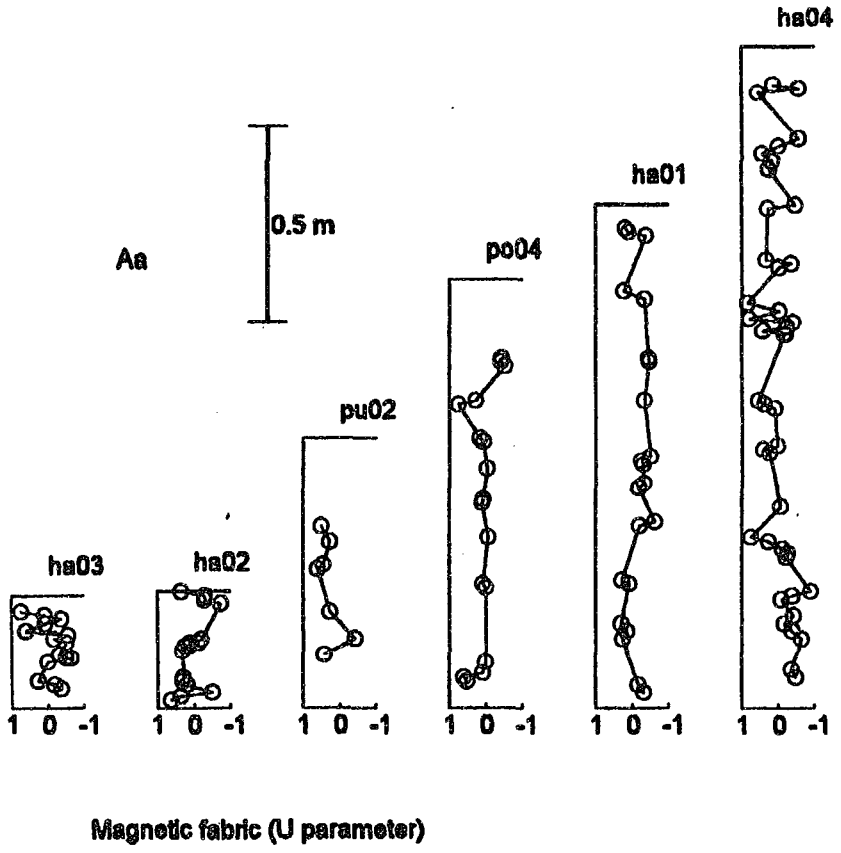

FIGURE 5.8. (CONTINUED) a) Variation of magnetic fabric (U parameter) across the width of lava flow units (A'a).

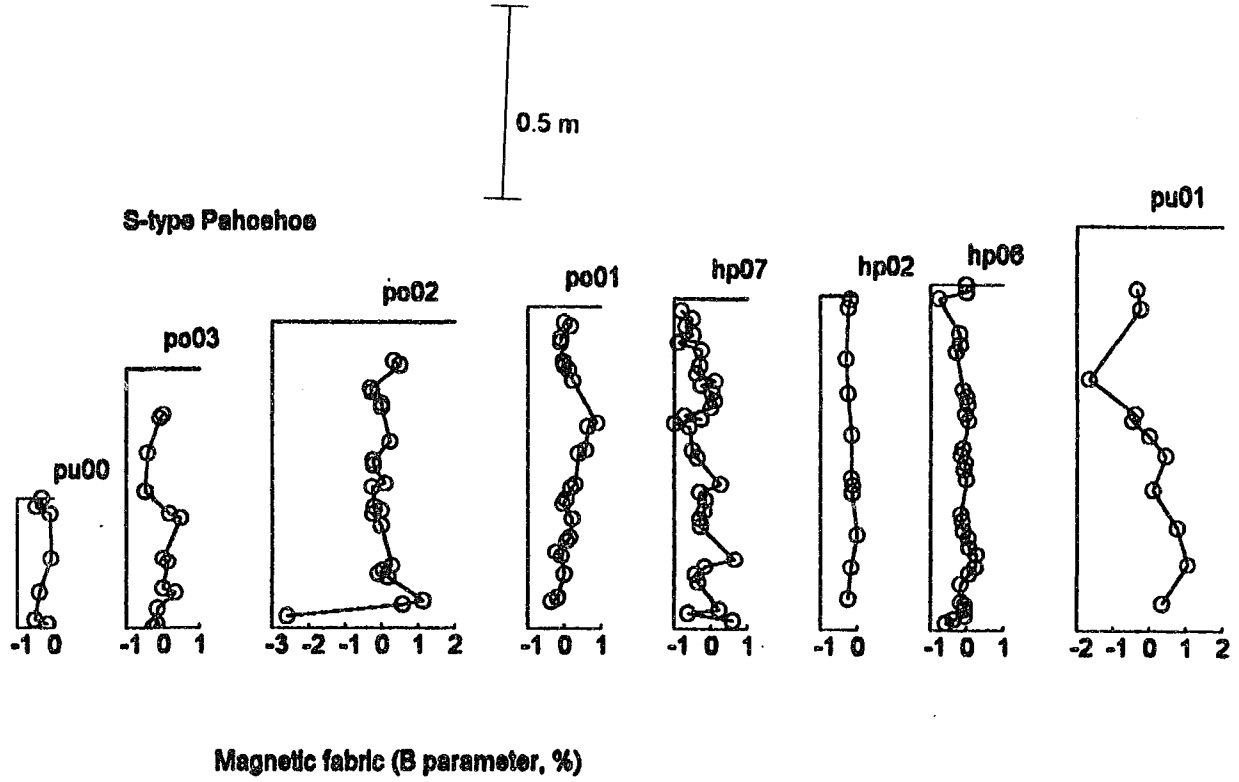

FIGURE 5.8. (CONTINUED) b) Variation of magnetic fabric (B parameter) across the width of lava flow units (S-type pahoehoe).

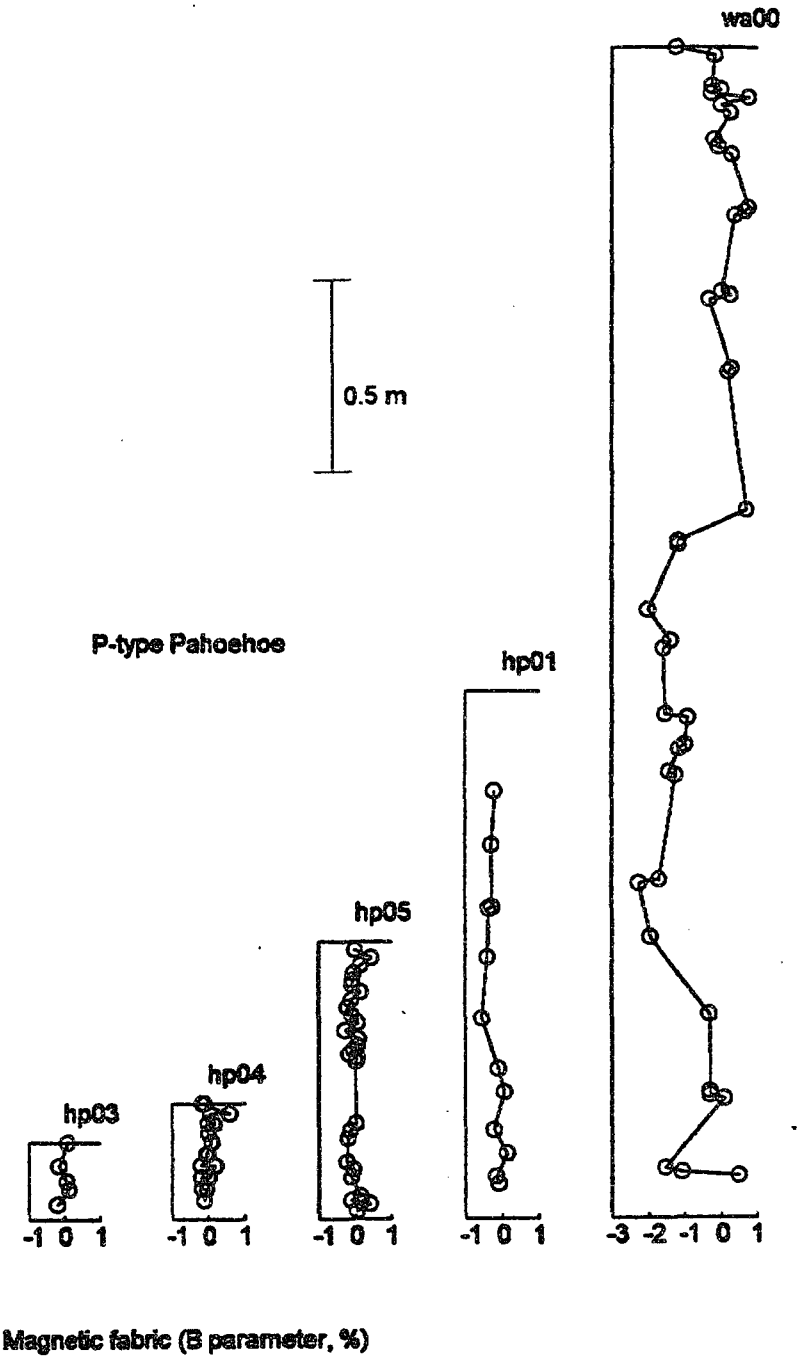

FIGURE 5.8. (CONTINUED) b) Variation of magnetic fabric (B parameter) across the width of lava flow units (P-type pahoehoe).

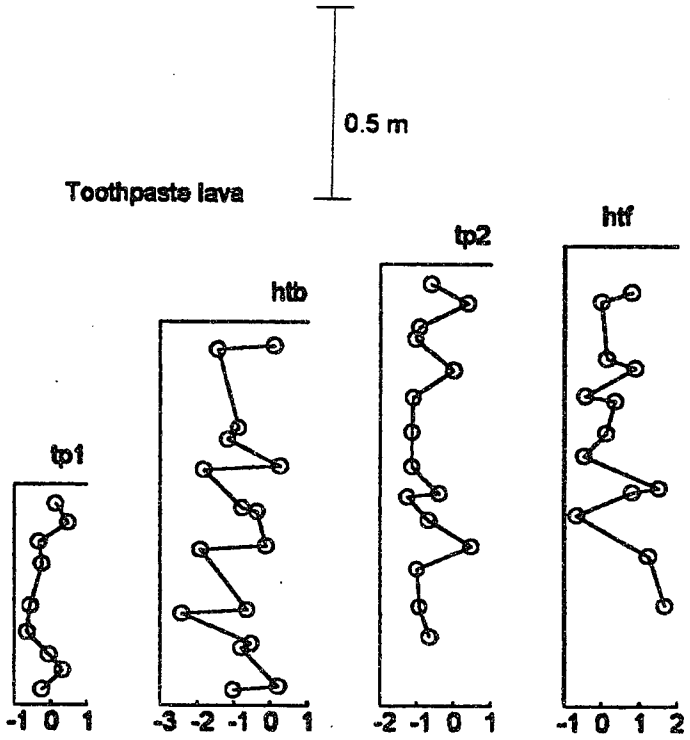

FIGURE 5.8. (CONTINUED) b) Variation of magnetic fabric (B parameter) across the width of lava flow units (Toothpaste lava).

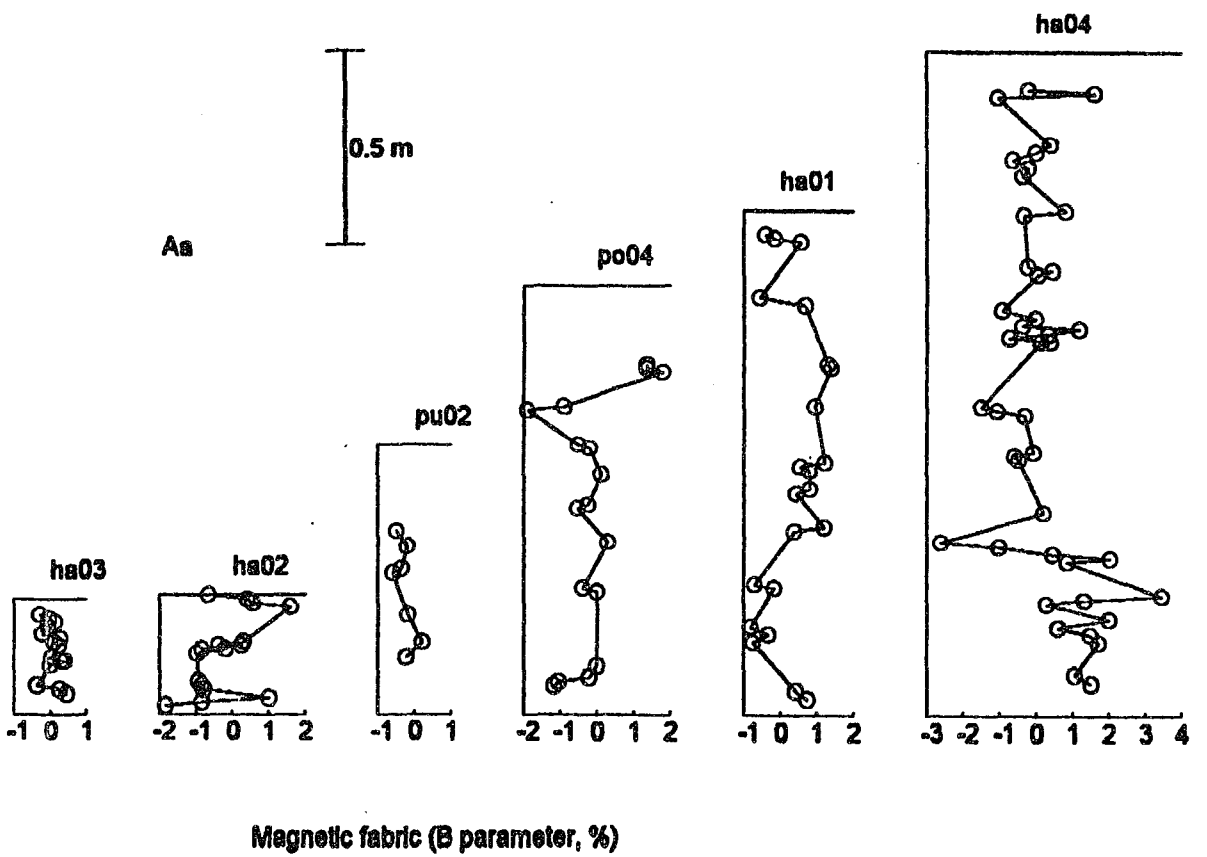

FIGURE 5.8. (CONTINUED) b) Variation of magnetic fabric (B parameter) across the width of lava flow units (A'a).

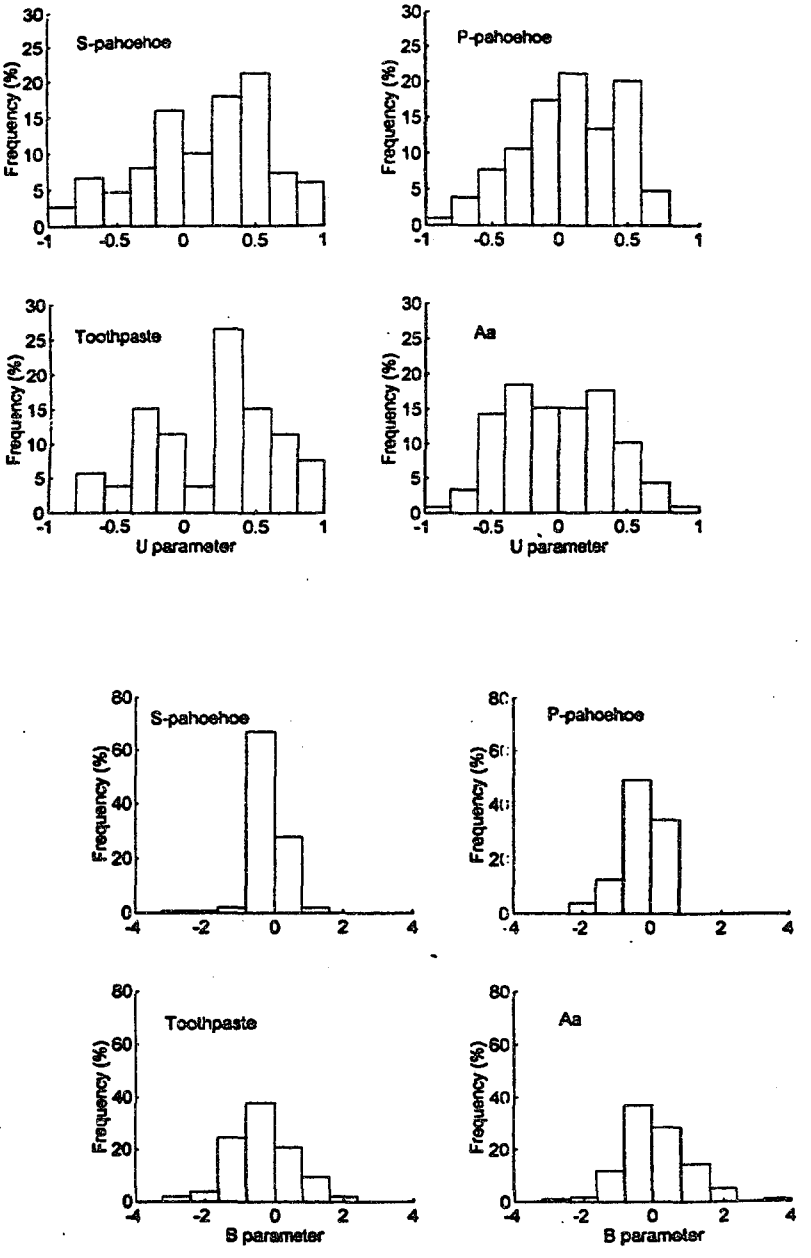

FIGURE 5.9. Relative frequency histograms of magnetic fabric of all specimens collected from each of the four lava flow morphologies studied. a) U parameter, b) B parameter.

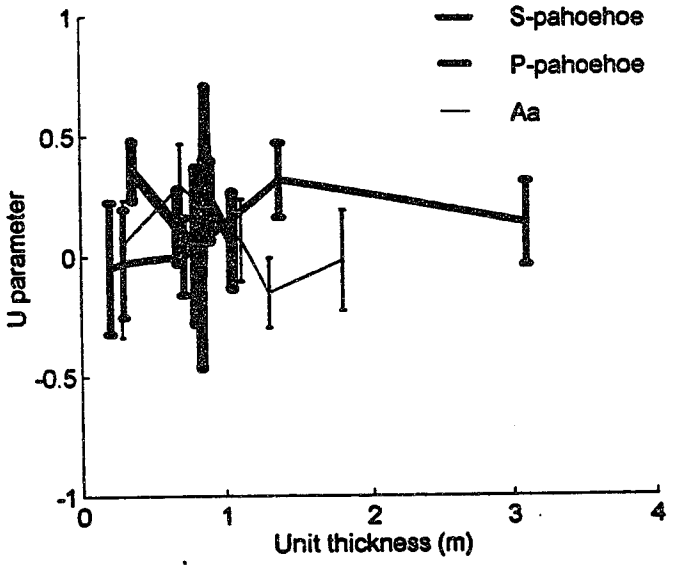

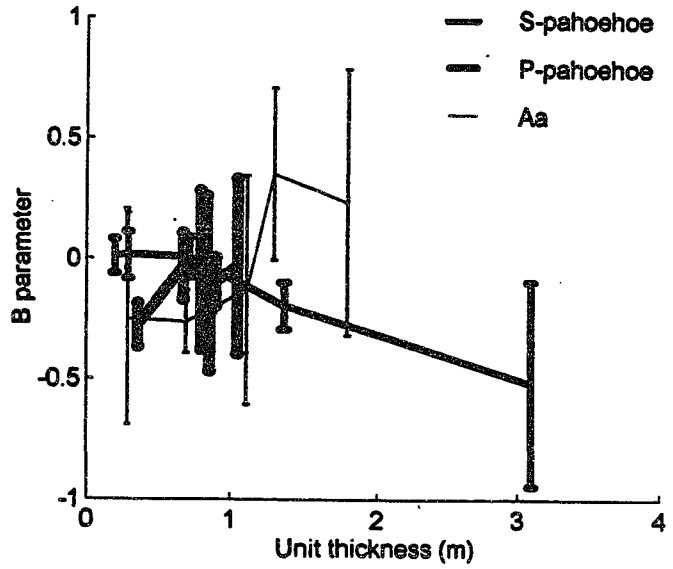

FIGURE 5.10. Variation of magnetic fabric with thickness of lava flow units. a) U parameter, b) B parameter. Symbols as in Figure 5.3

vesicle foliation is foliated (all of them have k_{min} normal to the vesicle foliation) whereas the magnetic fabric of the 17 specimens with an additional vesicle lineation is lineated in 12 specimens (nine with k_{max} parallel to the vesicle lineation) and foliated in the remaining five (all with k_{min} normal to the vesicle foliation). The association of a foliated/lineated magnetic fabric to a particular specimen is independent of the parameter used, but the relative degree of development of either type of fabric is not.

Variations between units

Histograms of U and B for all the specimens, grouped by morphology, are shown in Figures 5.9a and 5.9b, and some statistical estimates are listed in Table 5.2. According to the U parameter (Fig. 5.9a), there is a slight progression from a predominance of foliated fabrics in S-type pahoehoe to an almost symmetrical distribution around a neutral fabric in a'a flows, although the distributions of S-type pahoehoe, P-type pahoehoe and toothpaste lava are very similar to each other in most respects. The B parameter in contrast, suggests a larger proportion of lineated fabrics in toothpaste lava and a'a relative to pahoehoe, and also indicates a clear concentration of specimens with a nearly neutral fabric in S-type pahoehoe that distinguishes this morphology from the other three (Fig. 5.8b and Table 5.2).

Another difference between the two parameters concerns variation of magnetic fabric with flow unit thickness. The B parameter suggests a relative progression toward more lineated fabrics for thicker a'a units, and toward more foliated fabrics for thicker P-type pahoehoe, neither of which is apparent from U (Fig. 5.10).

Discussion

Vertical variation of magnetic fabric within single units, and a better definition of magnetic foliation (as quantified by the B parameter) with increasing thickness, was reported previously for some Xitle lavas (Chapter 3) and may be a common feature of lava flows. Based on this evidence, it was suggested on chapter 3 that there was a possible relationship between internal deformation of the flow and magnetic fabric deserving further examination. It is not clear at this point, however, whether

differences in the quantification of magnetic fabric obtained by the two types of shape parameters are physically relevant, but it is clear that these differences preclude a more detailed interpretation of results. Nevertheless, the close association observed between magnetic fabric and vesicle deformation clearly suggests that both types of fabric are the result of very similar physical processes. The apparent predominance of more lineated fabrics in a'a than in pahoehoe flows may reflect differences in their internal flow mechanism, the details of which remain to be still investigated.

ORIENTATION OF PRINCIPAL SUSCEPTIBILITIES

Directions of mean principal susceptibilities and regions of confidence around them

The relative magnitudes of the principal susceptibilities of individual specimens can influence the regions of confidence (e.g., Ernst and Pearce, 1989), and therefore it is important to eliminate those specimens that otherwise may dominate the results. To this end, we modified the empirical method suggested in chapter 3, and filtered out from the calculations specimens with either a very large degree of anisotropy (a value of the A parameter > three standard deviations in each unit) or a very different magnetic fabric (a value of the B parameter farther than three standard deviations from the mean in each flow). The total number of specimens used in each flow-unit is reported in Table 5.3.

Results show that the regions of confidence calculated with both techniques have the same size from a practical point of view for all the lava flow-units (Fig. 5.11). Nine units yield three non-overlapping regions of confidence with sizes ranging from very small to fairly small, ten have girdle-like regions of confidence around either the mean maximum (3) or the mean minimum (7), and the remaining four units yield regions of confidence that exceed the fair-size threshold value proposed by Cañón-Tapia et al. (1994). Units in the last category were either the thinner units of a given morphology or included less than ten specimens in the calculation of the mean tensor.

Six units yield mean k_{max} nearly vertical, three of which are S-type pahoehoe, and one of each of the other morphologies. One of these units is the front of a toothpaste lava lobe in which vesicle foliation is nearly vertical in the outcrop; a second unit belongs to the category of flows with very large

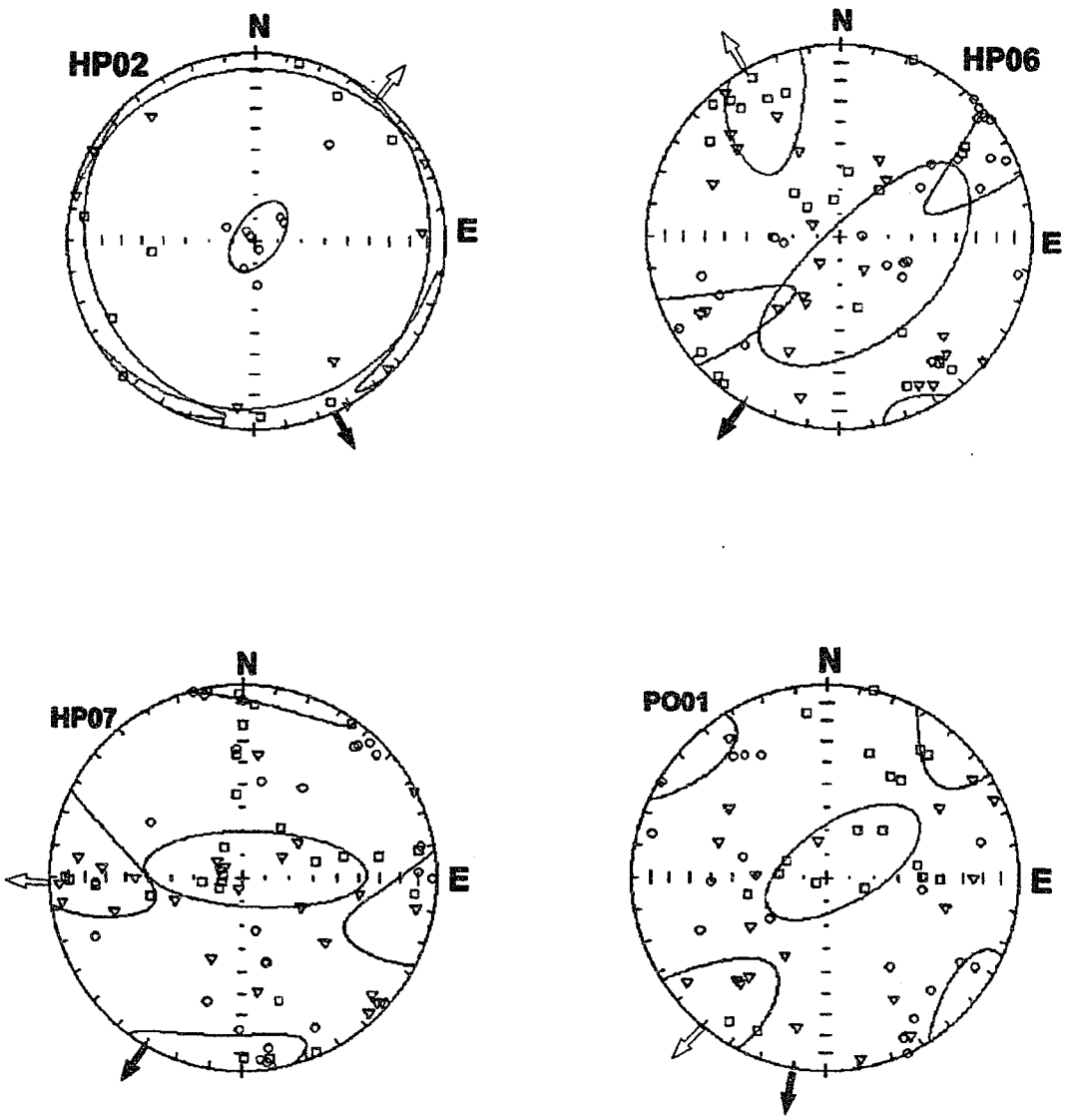

FIGURE 5.11. Equal area projections (lower hemisphere) of the axes of principal susceptibilities of all lava flows studied after filtering of specimens with either a very large degree of anisotropy or a very different magnetic fabric. The sizes of the regions of confidence are given numerically for both the linear and bootstrapping methods in Table 5.3, but only the former are shown for clarity. The solid arrow indicates the trend of the geologically expected flow direction, and the open arrow that of the AMS inferred flow direction. Units with one large arrow are such that AMS and geologically inferred flow directions lie within 5°. S-type pahoehoe.

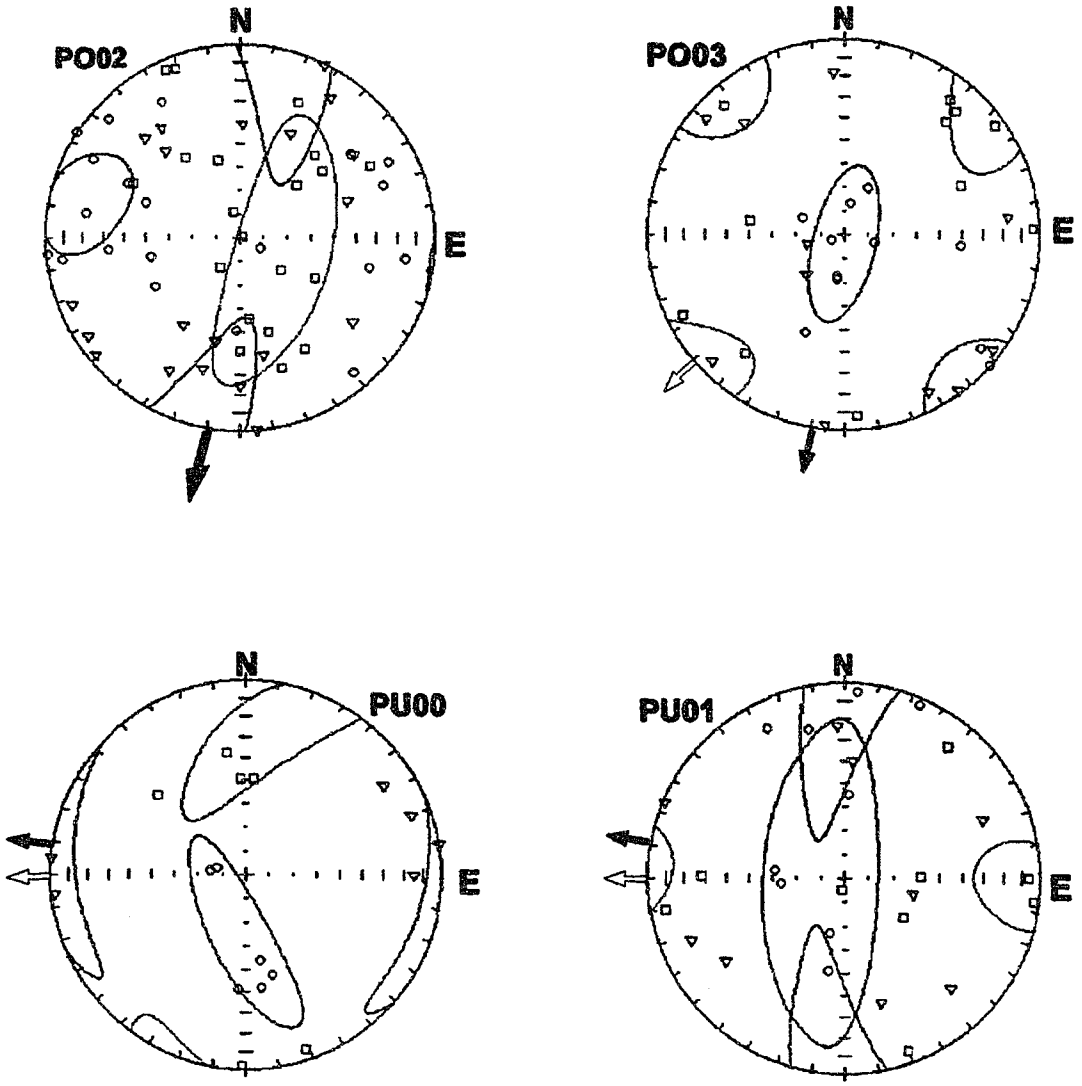

FIGURE 5.11. (CONTINUED) S-type pahoehoe.

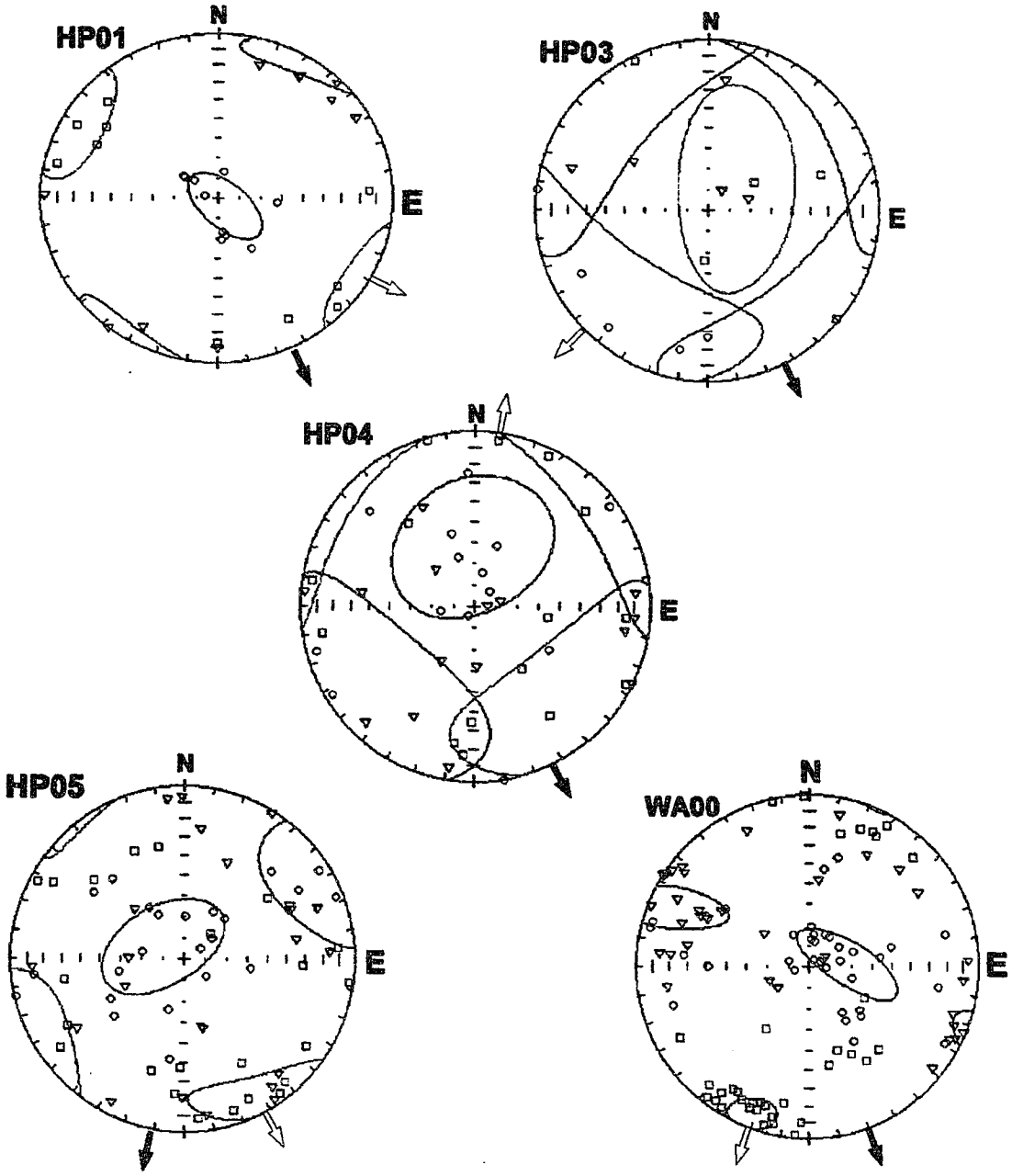

FIGURE 5.11. (CONTINUED) P-type pahoehoe.

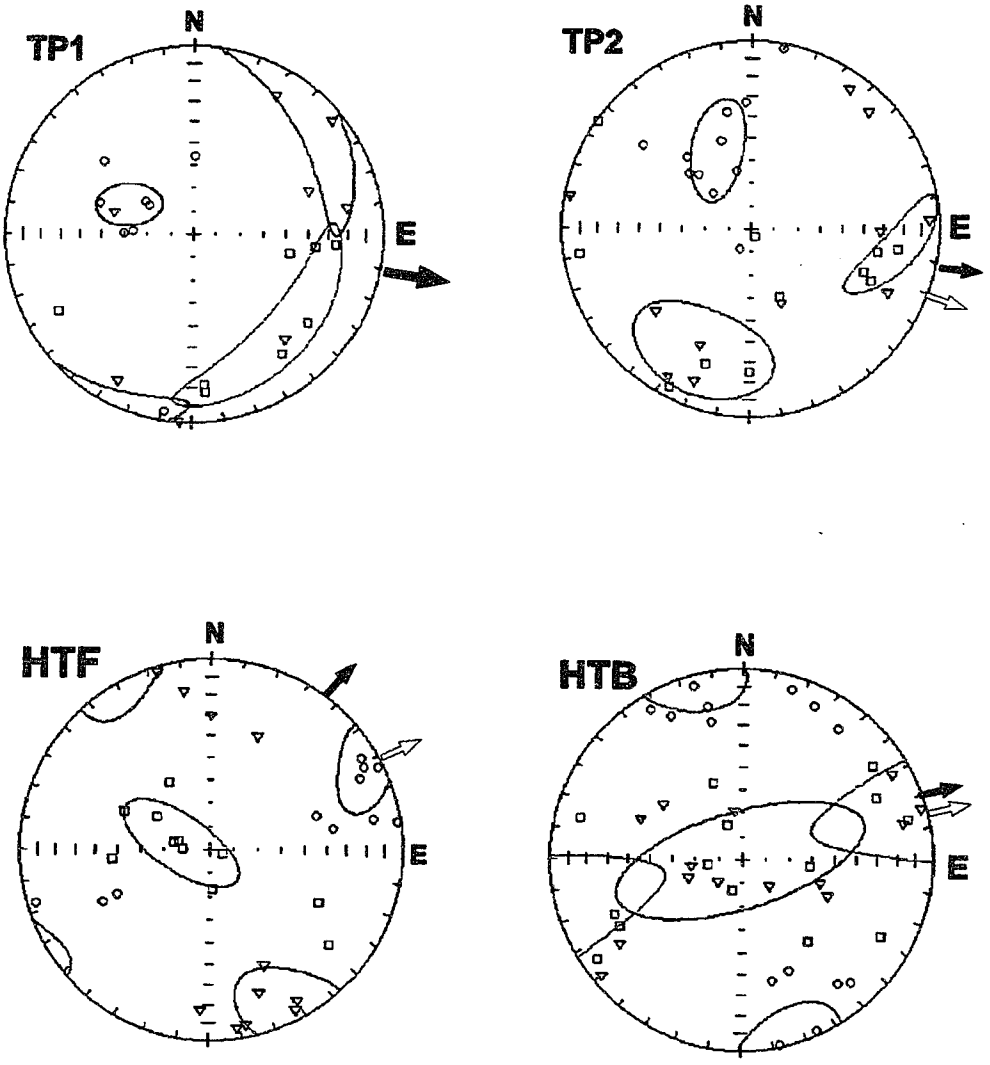

FIGURE 5.11. (CONTINUED) Toothpaste lava.

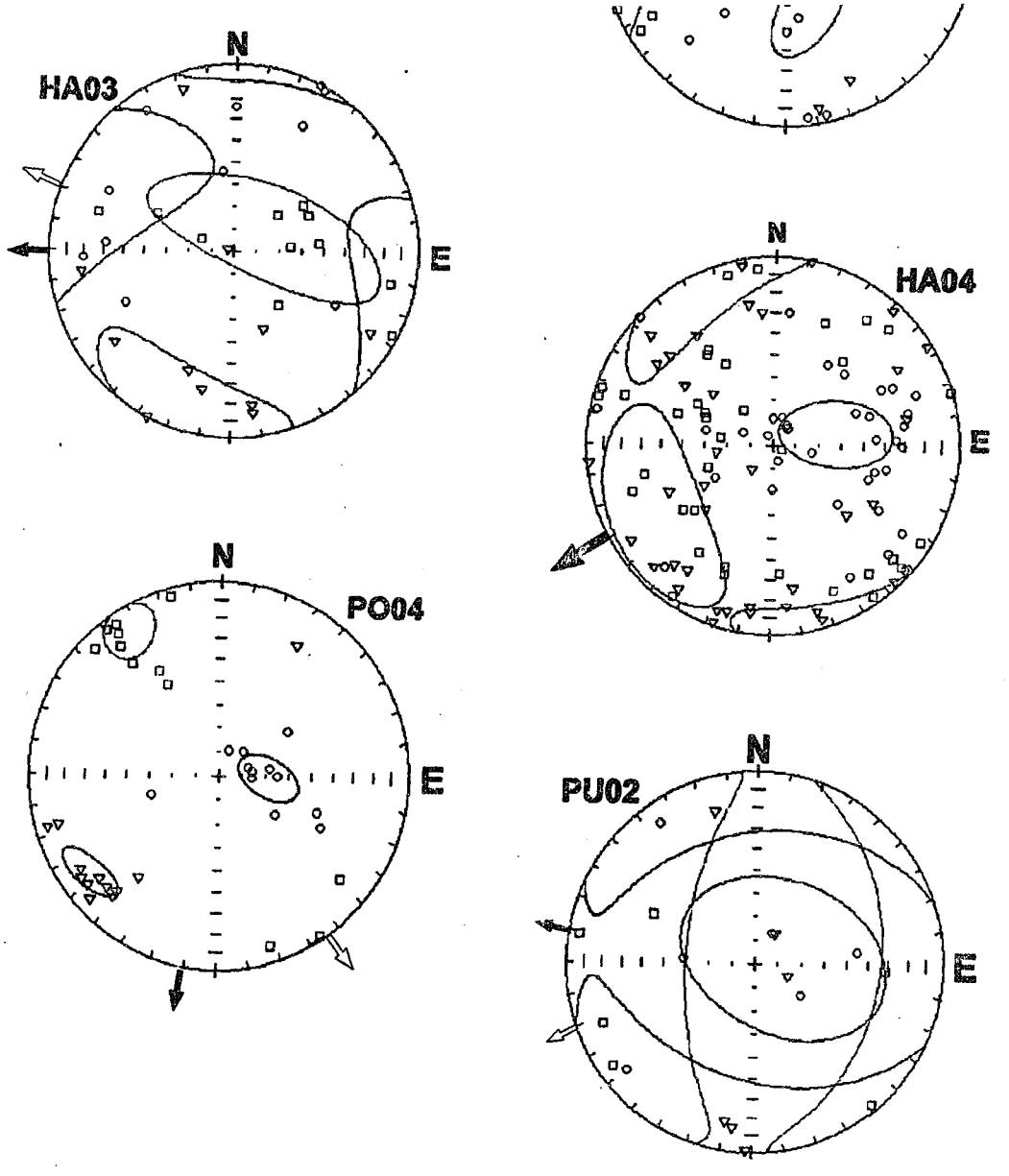

FIGURE 5.11. (CONTINUED) A'a.

N
PO04
N
HA03
E
N
HA01
E
E
HA04
N
E
HA02
N
E

TABLE 5.3. Directions (D-declination, I-inclination) of the mean principal susceptibilities and sizes of the regions of confidenc

	UNIT NAME	# SPEC.	Dmax	Imax	Linear Approx.	Boots.	Dint	Iint	Linear Approx.
S-pahoehoe									
	HP02	9	347.8	-1.6	69:11	90:10	257.9	1.9	69:10
	HP06	25	330.2	20.9	33:15	28:23	137.7	68.6	58:26
	HP07	25	58.4	82.8	48:16	90:18	277.7	5.5	50:17
	PO01	20	46.5	80.3	37:17	50:16	40.9	-9.7	37:15
	PO02	20	113.6	70.6	61:21	90:19	14.1	3.3	61:14
	PO03	11	229.7	-2.8	29:14	21:18	319.6	3	24:16
	PU00	6	7.5	27.2	48:15	72:20	276.8	1.2	43:11
	PU01	9	271.9	-10.4	25:14	20:11	258.4	79.3	72:24
P-pahoehoe									
	HP01	10	299.5	5	23:20	18:12	29.7	1.8	23:11
	HP03	5	51.1	72.1	51:28	90:28	315.4	1.9	63:42
	HP04	15	132.5	21.8	53:32	90:31	50.2	-18.6	53:39
	HP05	23	331.5	-10.1	28:12	25:18	240.4	-6	32:24
	WA00	35	21.2	-8.4	11:08	11:09	293.8	16.9	28:08

an principal susceptibilities and sizes of the regions of confidence around them.

	Linear Approx.	Boots.	Dint	Iint	Linear Approx.	Boots.	Dmin	Imin	Linear Approx.	Boots.
6	69:11	90:10	257.9	1.9	69:10	90:13	38.1	87.5	17:10	13:07
9	33:15	28:23	137.7	68.6	58:26	90:21	239	4.2	58:11	90:32
8	48:16	90:18	277.7	5.5	50:17	90:27	7.3	-4.5	29:14	28:15
3	37:17	50:16	40.9	-9.7	37:15	50:19	311	0.9	21:15	19:16
5	61:21	90:19	14.1	3.3	61:14	90:20	103	-19.1	22:17	20:15
3	29:14	21:18	319.6	3	24:16	20:18	183	85.9	34:13	26:14
2	48:15	72:20	276.8	1.2	43:11	77:14	184	62.8	47:12	25:08
1	25:14	20:11	258.4	79.3	72:24	90:27	1.4	2.4	72:14	90:17
	23:20	18:12	29.7	1.8	23:11	15:08	139	84.7	21:11	16:08
	51:28	90:28	315.4	1.9	63:42	90:67	44.8	-17.7	64:34	52:25
1	53:32	90:31	50.2	-18.6	53:39	90:71	357	60.7	39:32	54:32
	28:12	25:18	240.4	-6	32:24	32:25	300	78.2	32:19	33:18
	11:08	11:09	293.8	16.9	28:08	31:10	85.6	71	28:10	31:09

TABLE 5.3. (CONTINUED). Directions of the principal susceptibilities.

	UNIT NAME	# SPEC.	Dmax	Imax	Linear Approx.	Boots.	Dint	Iint	Linear Appro
Toothpaste lava									
	HTB	14	254.5	-1.1	57:16	90:20	242.5	88.9	57:21
	HTF	11	281.6	76.9	29:12	25:09	333.2	-8.2	27:14
	TP1	8	319.1	-28.6	47:12	36:07	43.1	10.8	47:12
	TP2	11	98.2	22.2	28:08	52:09	21.3	-29.1	28:22
A'a									
	HA01	17	77.3	-14.5	17:09	12:07	348.9	6	39:15
	HA02	13	256.1	3.8	29:16	24:12	348.3	30.5	27:23
	HA03	11	61.8	71.7	57:21	90:17	290.6	12.3	59:29
	HA04	37	334.4	7.9	41:18	90:18	60.2	-27.4	41:24
	PO04	12	326.8	12.8	14:09	11:08	52.9	-16.8	12:07
	PU02	6	275.4	12.9	80:47	90:35	4.5	-3.8	80:34

sceptibilities.

nax	Linear Approx.	Boots.	Dint	lint	Linear Approx.	Boots.	Dmin	Imin	Linear Approx.	Boots.
-1.1	57:16	90:20	242.5	88.9	57:21	90:22	344	0.2	22:16	19:15
76.9	29:12	25:09	333.2	-8.2	27:14	22:12	61.7	10.1	21:11	16:10
-28.6	47:12	36:07	43.1	10.8	47:12	36:12	295	59.1	15:09	11:07
22.2	28:08	52:09	21.3	-29.1	28:22	52:16	337	52	23:11	16:07
-14.5	17:09	12:07	348.9	6	39:15	50:11	101	74.3	39:08	50:08
3.8	29:16	24:12	348.3	30.5	27:23	23:18	160	59.2	27:12	23:11
71.7	57:21	90:17	290.6	12.3	59:29	90:69	17.7	-13.3	39:21	90:26
7.9	41:18	90:18	60.2	-27.4	41:24	90:21	79.1	61.3	26:14	22:15
12.8	14:09	11:08	52.9	-16.8	12:07	11:07	92.2	68.6	14:08	11:07
12.9	80:47	90:35	4.5	-3.8	80:34	90:90	78.2	76.5	47:33	57:38

regions of confidence due, perhaps, to a small number of samples, and all of the remaining four have in common the presence of large amounts of nearly spherical vesicles in the outcrop. The mean k_{int} was closer to the vertical in only three units, two of which are S-type pahoehoe and one is the crustal part of a toothpaste lava lobe. All of these three units yield girdle like regions of confidence around a horizontal mean k_{max}. The remaining 14 units yield a mean k_{min} closer to the vertical.

Directions of the mean susceptibilities and flow direction

The first AMS studies made on lava flows (e.g., Khan, 1962; Symons, 1975; Ellwood, 1978) usually assumed, a priori, that either k_{max} or k_{int} were likely to point along the direction of movement of the lava as a whole. Which of these two principal susceptibilities was preferred depended on whether the model of orientation of isolated ellipsoidal particles moving in a viscous fluid (Jeffery, 1922; Taylor, 1923) was accepted as controlling the measured AMS. Later work (e.g., Cañón-Tapia et al., 1994; Chapter 3; Chapter 4), showed that the hypothesis of mean k_{max} parallel to local flow direction is usually consistent with the geologically inferred flow direction in lavas, although in a few instances this was not immediately evident.

The model proposed in Chapter 4, however, requires a closer examination of the measurements before making a decision of which principal susceptibility is parallel to the flow direction, especially in those cases in which it is suspected that post-emplacement disruption due to the influence of gravity forces has likely occurred. In order to infer flow direction from the AMS measurements I used the following scheme: 1) Two groups of units were formed, one with mean k_{max} horizontal and the other with mean k_{max} vertical, 2) From the first group, the direction of mean k_{max} is selected as flow direction if the region of confidence around k_{max} is at least moderately small, otherwise I relied on the imbrication of either individual k_{max} or k_{min} axes before selecting a flow direction. 3) From the second group (mean k_{max} vertical), I noted that usually not all the specimens had k_{max} vertical, but mainly those from the middle parts of a unit. Following the evolutionary process described in Chapter 4, I attempted to identify imbrication patterns of groups of specimens from the same region of the unit, giving little attention to the particular type of principal susceptibility (i.e., whether it was k_{max}, k_{int} or k_{min}). This procedure usually

yields positive results, and suggests a flow direction that coincides either with the trend of the girdle around the mean k_{min} (if one was defined by the regions of confidence) or with the mean k_{int} (if no girdle was defined). The only exception to this was unit HTF, in which the observed vesicle foliation in the outcrop made me anticipate a horizontal k_{min} pointing along flow direction, so the AMS inferred flow direction in this case was selected as that of the mean k_{min}.

As most units defined an imbrication of axes regardless of what group they were placed in, imbrication was studied independently of the size of the regions of confidence. The results of this procedure (see below) always confirmed the flow direction selected in the base of the regions of confidence alone, and allowed me to infer a flow direction in those cases that it had not been possible with the described scheme.

The flow direction inferred from AMS results from each of the 23 units is compared with the geologically inferred flow direction in Table 5.1. Differences in the azimuth of expected and AMS-inferred flow directions average 38°, and only in 10 units the difference exceeds 35°. Agreement between both flow directions is better in a'a flows than in pahoehoe.

The overall agreement obtained between geologically and AMS-inferred flow directions in most units is similar to that reported in previous studies of the AMS of lava flows in which the tensor averaging method was used to calculate mean direction of principal susceptibilities (e.g., Cañón-Tapia et al., 1994; Chapters 3 and 4).

Vertical variation of the direction of the principal susceptibilities

Despite the relatively small regions of confidence found in some cases, usually the principal susceptibilities of all specimens from one flow unit are scattered all over the equal area projection. In some instances, however, it is possible to identify clusters of principal susceptibilities either consisting of a single type of axis (i.e. k_{max}, k_{int} or k_{min}) or by a combination of two or all three. I further investigated this observation through axial density contour plots (cf., Fisher et al., 1993) of populations of 3n principal susceptibilities, where n is the number of specimens included in each plot; it was varied from no less than 3 up to the total number of specimens collected from each unit. It should be noted that

although each principal direction is now treated as an independent datum (the method identifies clusters of directions irrespective of the type of susceptibility) there are always two data perpendicular to it (and to each other) corresponding to the other two principal directions of the same specimen. Thus, it was anticipated that the contour plots should be the result of the combination of three basic types of distributions: 1) three mutually orthogonal clusters, 2) a girdle distribution with a cluster at the pole of the girdle and 3) a uniform distribution.

Contour plots including all the specimens of all but two a'a and all four toothpaste lava units display a complex combination of the two first basic distributions, and very commonly the general aspect is closer to that of a uniform distribution. However, division of specimens according to their vertical position in the outcrop always leads to isolation of several basic distributions (Fig. 5.12). In the simplest case (Fig. 5.12a), there are two distributions of 3 clusters each, corresponding to samples from the upper and lower levels respectively. This type of structure reveals very clearly the effect of an opposite imbrication of axes of principal susceptibility, unambiguously indicating the absolute direction of flow. A second case, slightly more complex, reveals a relative rotation about a nearly vertical axis of both distributions (Fig. 5.12b), which tends to obscure the direction of flow. A further complication is encountered when one, or both of the basic distributions are instead of a girdle-like type (Fig. 5.12c), although flow direction still can be inferred from these plots with some care.

Some units display not only upper and lower level distributions, but there is an additional zone defined by specimens from the central parts of the flow. The distribution of the central parts in some instances can be identified as a transition zone between those in the upper and lower levels (Fig. 5.12d), but it also can be completely unrelated to them (Fig. 5.12e). In any case, flow direction is not as clearly indicated as in the simplest cases because very often upper and lower levels in units with the additional central zone show the effects of relative rotation as explained above. A final category of structures corresponds to units in which no opposite imbrication is defined. The four toothpaste lava and most a'a units belong to this type (Fig. 5.12f). In the case of toothpaste lava this may reflect the fact that only the upper part of the unit was accessible for sampling.

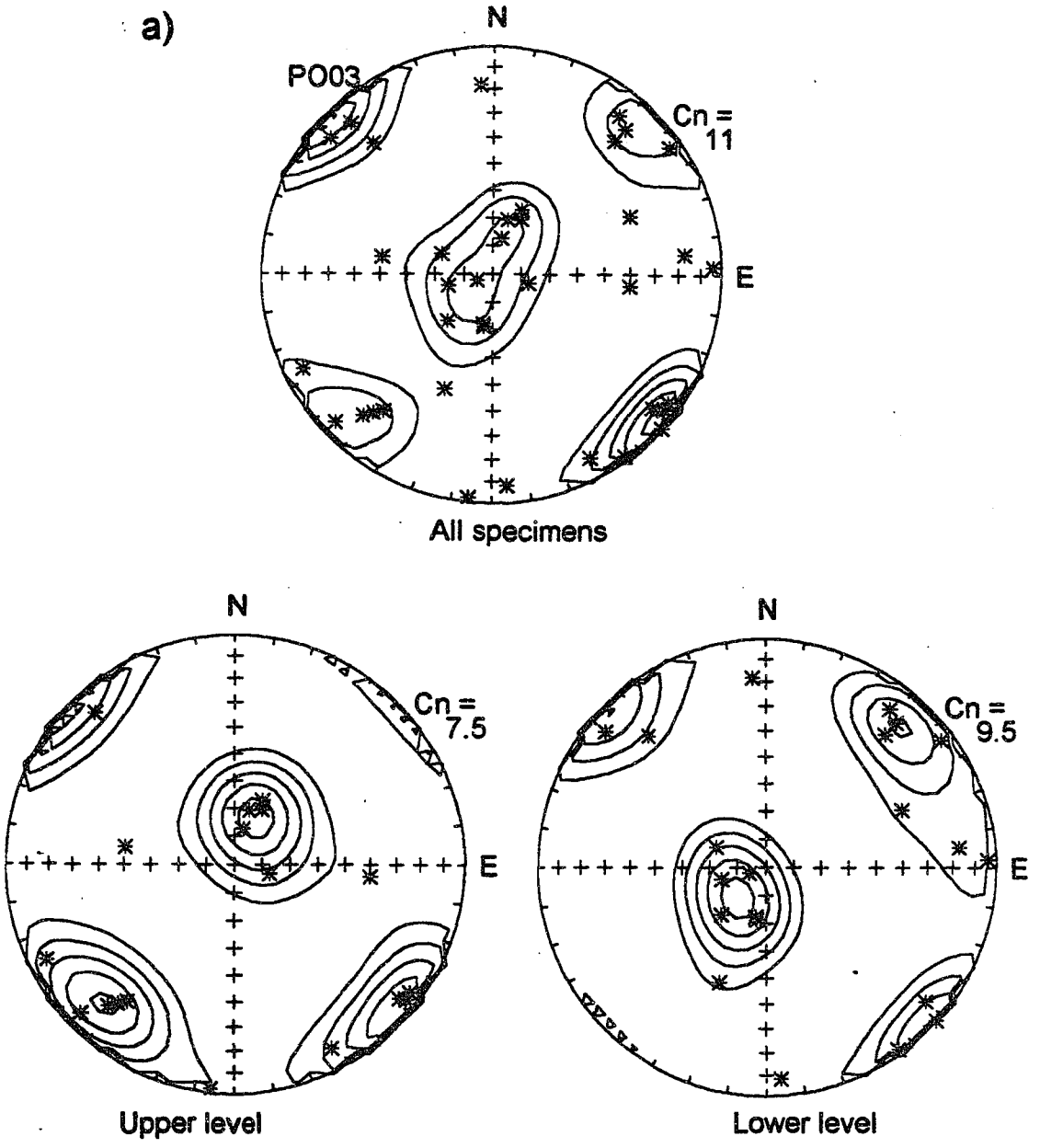

FIGURE 5.12. Examples of the degree of clustering defined by the principal susceptibilities of specimens within a unit. Specimens from different positions in the unit define various simple distributions as discussed in the text.

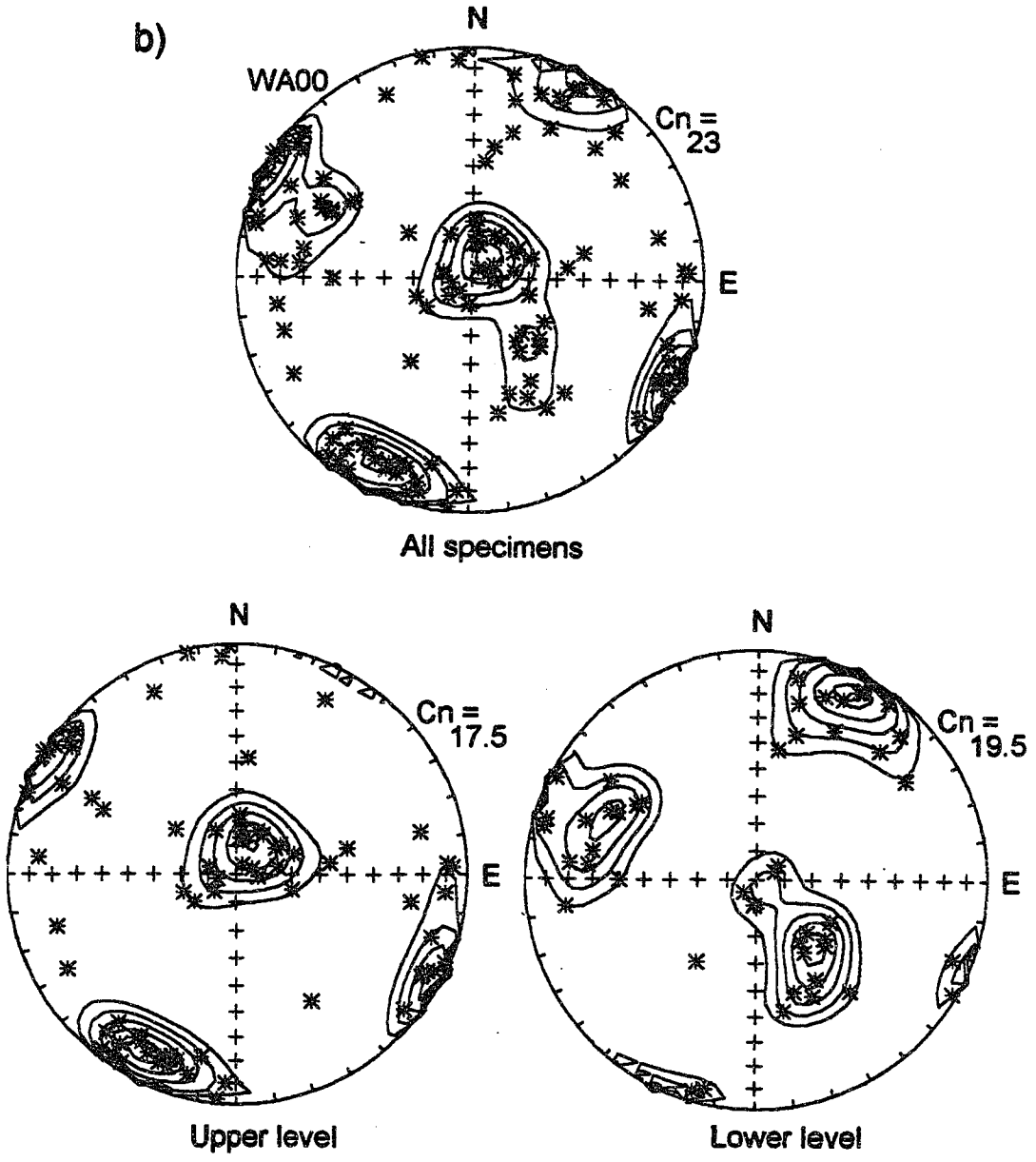

FIGURE 5.12. (CONTINUED) Degree of clustering of principal susceptibilities. See text for details.

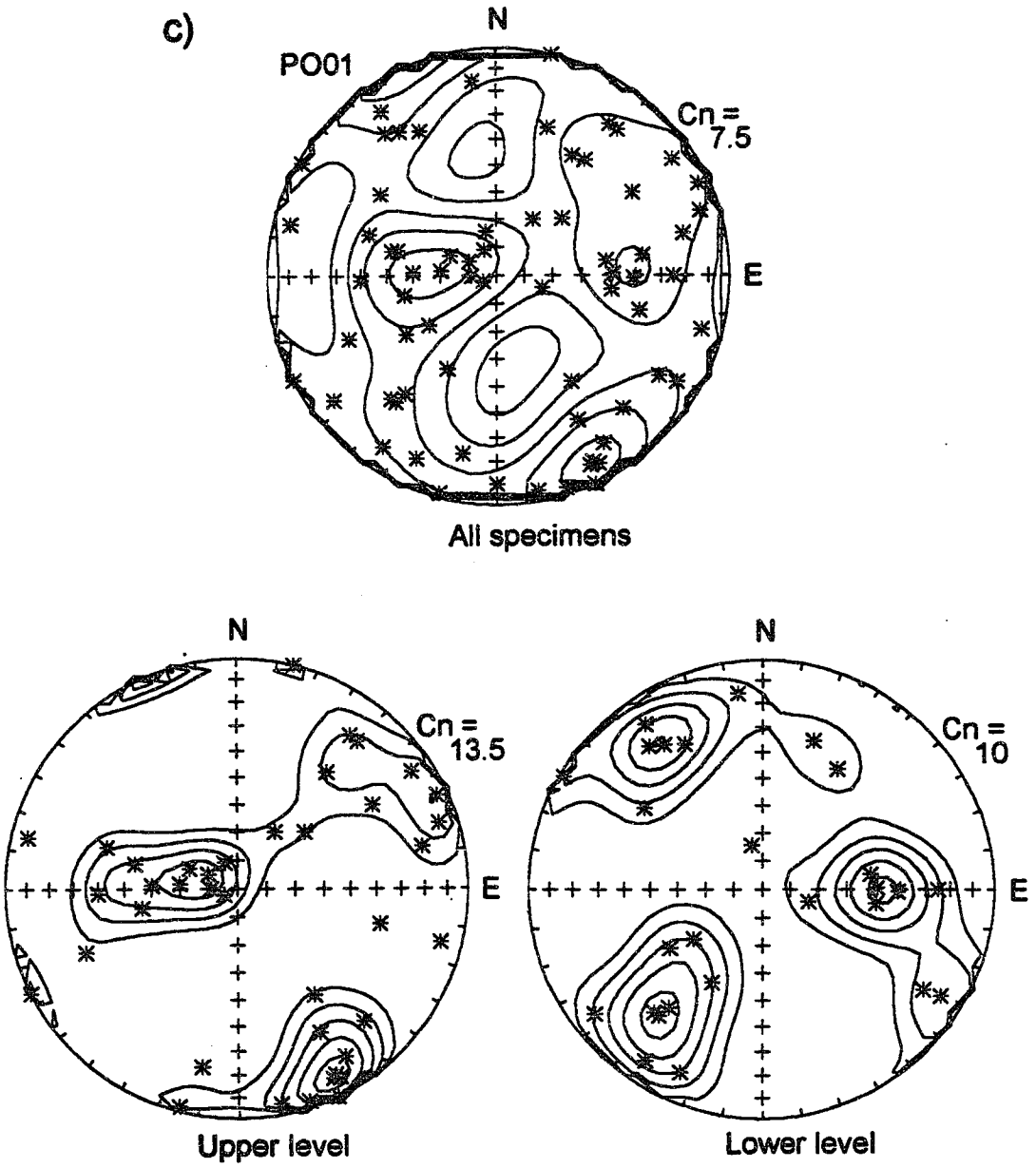

FIGURE 5.12. (CONTINUED) Degree of clustering of principal susceptibilities. See text for details.

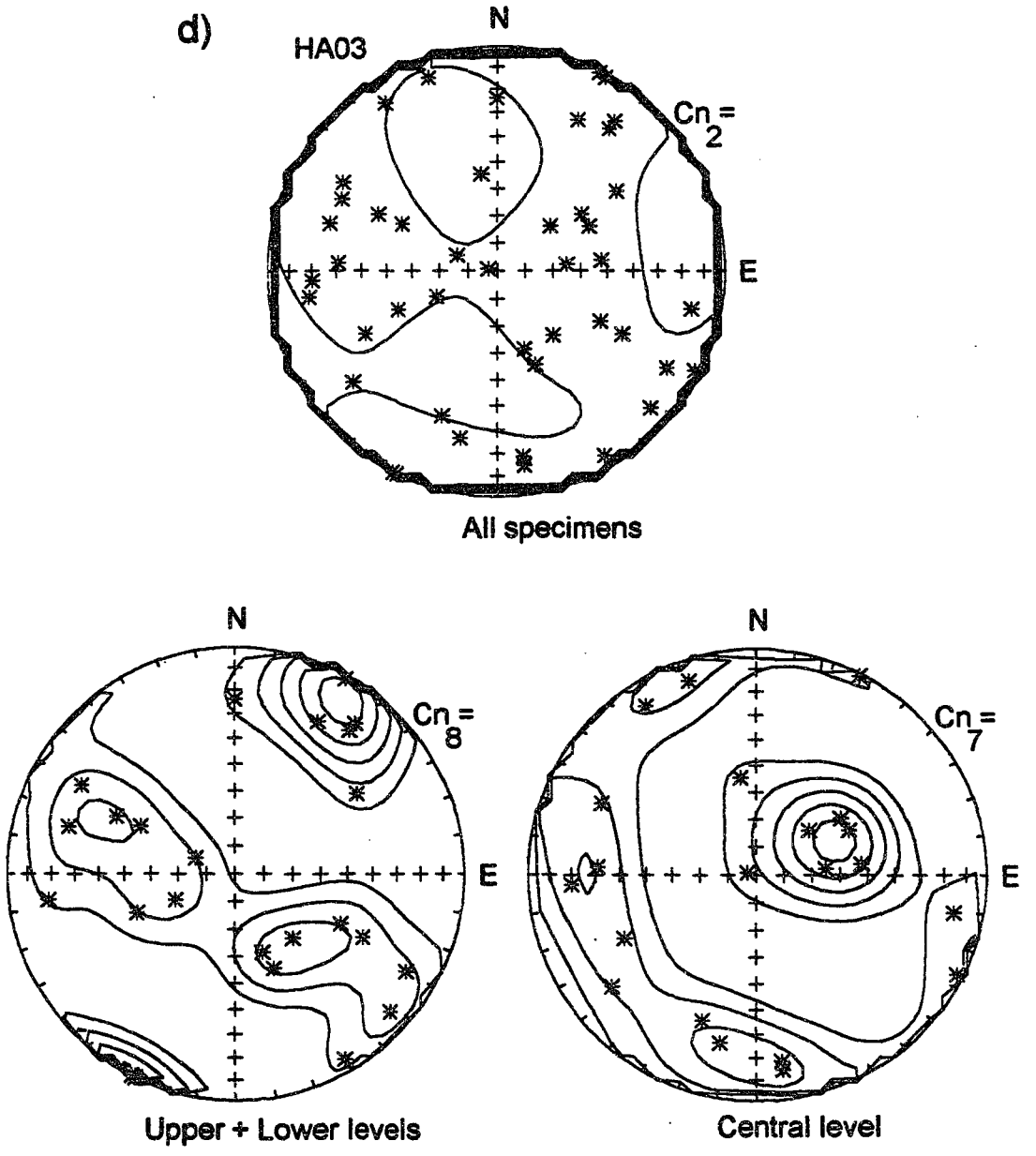

FIGURE 5.12. (CONTINUED) Degree of clustering of principal susceptibilities. See text for details.

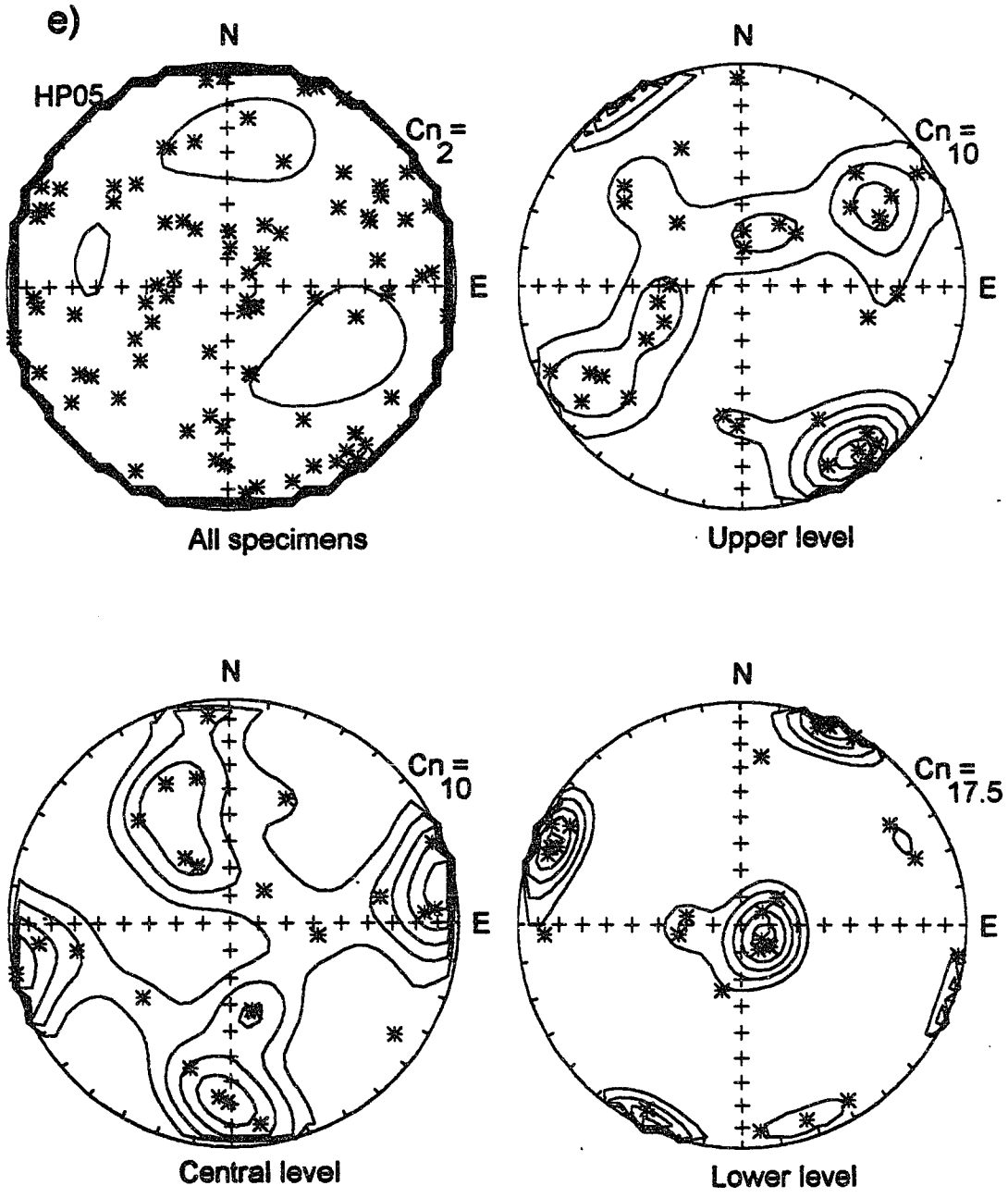

FIGURE 5.12. (CONTINUED) Degree of clustering of principal susceptibilities. See text for details.

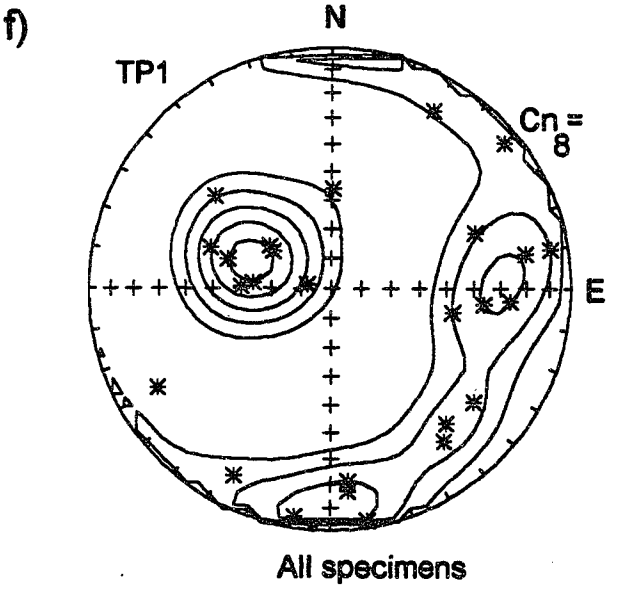

FIGURE 5.12. (CONTINUED) Degree of clustering of principal susceptibilities. See text for details.

Discussion

a) Zonation of the velocity field

There is clear evidence that the directions of the principal susceptibilities bear a close relationship with the local deformation suffered by fluid elements of moving lava (Chapter 4; previous section). Therefore, the formation of clusters of principal susceptibilities by specimens collected from adjacent parts of the same unit indicate that this deformation changes systematically with position. In general, the flow has two main zones displaying opposite imbrications of the susceptibility axes. Such a change in the orientation of the principal susceptibilities is related to a change in the relative magnitude of the velocity component along the direction of movement, and can be used to locate approximately the region where velocity was higher (Chapter 4). This type of structure is common to all studied pahoehoe units and rare in a'a, suggesting that velocity has a maximum in the medial parts of the former, but near the top of the massive part in the latter. Examples of roofed a'a units, however, can also be found through AMS measurements (Chapter 4).

The presence of a central zone with a characteristic orientation of principal susceptibilities is more common in thick S-type pahoehoe than in other morphologies, indicating a change in the conditions of movement in the internal parts of this type of lava. The absence of a clear secondary structure of some of these central parts may be interpreted as cooling under static conditions (absence of deformation), whereas a change in direction of movement, perhaps related to endogenous growth, is recorded as a well defined distribution of principal susceptibilities different from those observed in the upper and lower zones.

b) Flow direction

Imbrication of the axes of principal susceptibility is a very important indicator of the direction of movement . It was shown that this imbrication is to some extent independent of the type of principal susceptibility, therefore suggesting that the mechanism controlling the orientation of the principal susceptibilities is stronger than that controlling their relative magnitudes. The examples of the magnetic fabric of individual specimens discussed in the previous section also lead to the same conclusion. This

type of behavior can be explained in terms of magnetic interaction between neighbor particles as shown in the Appendix 1.

The intimate relationship existing between the rate of strain and the orientation of the principal susceptibilities, together with the weaker control that the former exerts over the relative sizes of the later, introduces an undesirable complication in the study of AMS. The main assumption made to calculate mean directions with the tensorial approach is that every specimen is a random sample of a unique susceptibility tensor which is no longer satisfied if the susceptibility of each specimen follows the systematic changes of the strain rate with position in the flow. This not only questions the validity of the method employed to calculate a mean direction for a given unit, but also obscures the physical significance of the calculated mean. The agreement found between the geologically and the AMS inferred flow directions in this and previous works on lava flows that used the tensorial method to calculate the directions of the mean principal susceptibilities (Cañón-Tapia et al. 1994; Chapter 3; Chapter 4), however, seems to indicate that the tensorial method is not only valid but that the inferred flow direction is reliable.

A common feature of all these works is that samples were collected across the width of a single unit, so that the various zones undergoing distinct deformations are more or less equally represented. As shown above, the deformation suffered in opposite sides of the unit tends to be opposite in direction so that the mean direction from the complete collection of specimens tends to average out the systematic variations related with lava movement. For this reason, the mean direction of principal susceptibilities is therefore physically significant. Filtering out selected specimens that otherwise could bias the calculations also helps to explain the general agreement between geologically and AMS inferred flow directions because in so doing the weaker control on the relative sizes of the principal susceptibilities exerted by the moving lava is also screened. The number of specimens collected is another important factor because fewer specimens are more likely to reflect the effects of the weaker control in the relative sizes of principal susceptibilities. Usually, large regions of confidence around the mean principal susceptibilities are the main consequence of the collection of few specimens.

CONCLUSIONS

Most of the characteristics displayed by the measured AMS of lava flows can be explained quite satisfactorily if magnetic interaction among particles is accepted to be its main source. The distribution of ferromagnetic grains seems to be intimately related to the local shear rate, therefore allowing us to investigate the internal variations of this dynamic parameter through magnetic measurements. Although all aspects of the susceptibility tensor are ultimately controlled by the local shear and post-emplacement crystallization, shear seems to be more important in defining the directions of principal susceptibilities. Each of the other parameters (average susceptibility, degree of anisotropy or magnetic fabric), however, can yield information that can help to characterize the internal processes taking place in moving lava. For example, differences in magnetic susceptibility suggest that the cooling mechanism of a'a flows is different from that of P-type pahoehoe, and these two may be different from that of S-type pahoehoe. Variation in degree of anisotropy between morphologies is consistent with the view that a'a flows are in general more sheared than pahoehoe, and the combined results of magnetic fabric and directions of principal susceptibilities suggest that the internal parts of pahoehoe units are more likely to have suffered a different deformation history than the interior of a'a flows. All of this information suggests that a'a continues to move until lava has a high viscocity; any flow-induced fabric is therefore more likely to survive unaltered. Pahoehoe, on the contrary, becomes static when lava still has a low viscocity so that the flow-induced fabric is more likely to be disrupted. The ocurrence of endogenous growth complicates things still further. Directions of principal susceptibility can also be used to locate zones of maximum velocity in the interior of lavas, as well as to infer the direction of movement of units. Regarding this last point, it is not possible to generalize that flow direction is always parallel to a particular susceptibility axis, but an adequate sampling strategy and detailed examination of the variation in the orientation of axes of principal susceptibility from top and bottom of a single unit will usually give a reliable flow direction. In any case, the study of AMS of lavas can yield important information regarding their internal mechanism of movement, and therefore the method has a wide range of possible applications in volcanology.

CHAPTER 6: MODE OF FORMATION OF LARGE VESICLES FROM XITLE VOLCANO LAVAS

INTRODUCTION

Vesicles are common features that preserve valuable information about the fluid characteristics of lava flows. Several studies have been devoted to investigate the effects of bubble coalescence (Sahagian, 1985; Sahagian et al., 1989: Manga and Stone, 1994), growth and rise of bubbles (Aubele et al., 1983; Walker, 1987; 1989) and gas exsolution due to crystallization of lava (Philpotts and Lewis, 1987; Godinot, 1988). Also, some attempts have been made to explain the shape of vesicles in terms of hydrodynamic forces acting on bubbles in highly viscous media (e.g., McMillan et al., 1987; Stein and Spera, 1992; Chapter 4).

In a recent paper, Walker (1996) identified two different mechanisms of ascent of large bubbles (Fig. 6.1), based in observations made on lavas from Xitle volcano, Mexico. In one of these modes, the bubbles rise actively due to the buoyant forces resulting from their lower density relative to the surrounding liquid producing the so called "globular vesicles", whereas in the second (passive) mode the gas contained in the bubble is forced upwards by the action of a collapsing roof of jelly-like material. Although in both of these modes bubbles rise buoyantly (i.e., gravity is the ultimate control), in the active mode the upward movement of the bubble is likely to disrupt its vicinity while in the passive mode the bubble and the immediately overlying material exchange places leaving undistorted their surroundings producing the so called "belljar vesicles". The mode of ascent of larger bubbles can therefore be inferred in the field from the deformation and orientation of other bubbles in the vicinity.

In this chapter, I report on the anisotropy of magnetic susceptibility (AMS) of rock specimens drilled at different distances from two belljar vesicles, and from a system of three large globular vesicles that clearly ascended actively in an attempt to gain independent evidence regarding the mechanisms of bubble ascent proposed by Walker (1994).

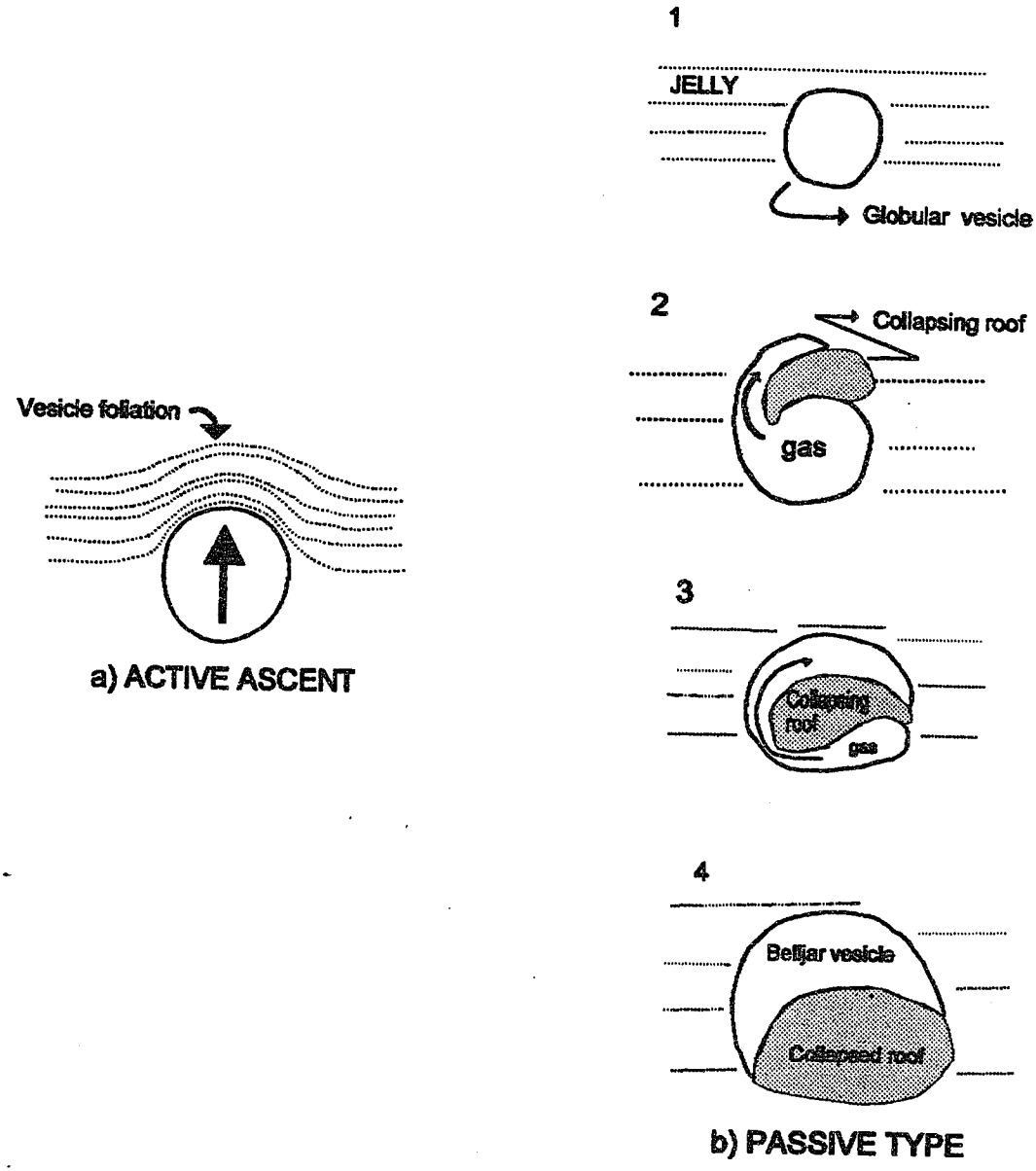

FIGURE 6.1. Two modes of bubble ascent in basaltic flows. a) active due to buoyancy forces, and b) passive due to collapsing of the bubble roof (after Walker, 1996).

SITE DESCRIPTION

All the studied vesicles are exposed in outcrops located in the campus of the National University of Mexico (UNAM). The three globular vesicles are exposed in the lower part of the quarry behind the building of the "Dirección General de Asuntos del Personal Académico", very close to the profile 2 outcrop reported on Chapter 3. They form a system of contiguous globular vesicles, each with an approximate diameter of 0.2 m (Fig. 6.2). The floor of the two upper vesicles is concave upwards, suggesting that it was pushed from below under the influence of the trailing bubbles, although apparently coalescence was never completed. A few deformed, small vesicles surround the three globular vesicles apparently defining a vesicle foliation that follows their contour. The scarcity of small vesicles, however, make uncertain the orientation of the foliation in several places.

The two bellijar vesicles belong to a different unit exposed on an outcrop in front of the "Facultad de Ciencias Polfticas" (Fig. 6.3). One has a concave-upward cavity with a maximum separation of approximately 0.1 m. Its lower left side defines a very thin, almost vertical cylinder-like shape, somewhat reminiscent of the late stages of the passive mechanism of gas-ascent shown in Fig. 6.1b. The second is rather elongated with a lower tip as the only vestige of the gas-ascent process. Smaller vesicles surrounding the two bellijar vesicles are abundant and do not display any signs of deformation.

RESULTS

The measured directions of the three principal susceptibilities of each specimen were individually projected into a vertical plane parallel to the corresponding outcrop. The hemisphere of the projections shown in Figures 6.4 and 6.5 is the hemisphere towards the observer; the projected plane is the plane of magnetic foliation (by definition is the plane containing the k_{max} and k_{int}) and the direction of the maximum susceptibility is indicated by the square. The orientation of the principal susceptibilities, magnetic fabric and degree of anisotropy of each specimen are listed in Table 6.1.

Active ascent

From figure 6.4, it is apparent that the plane of magnetic foliation near the three vesicles follows

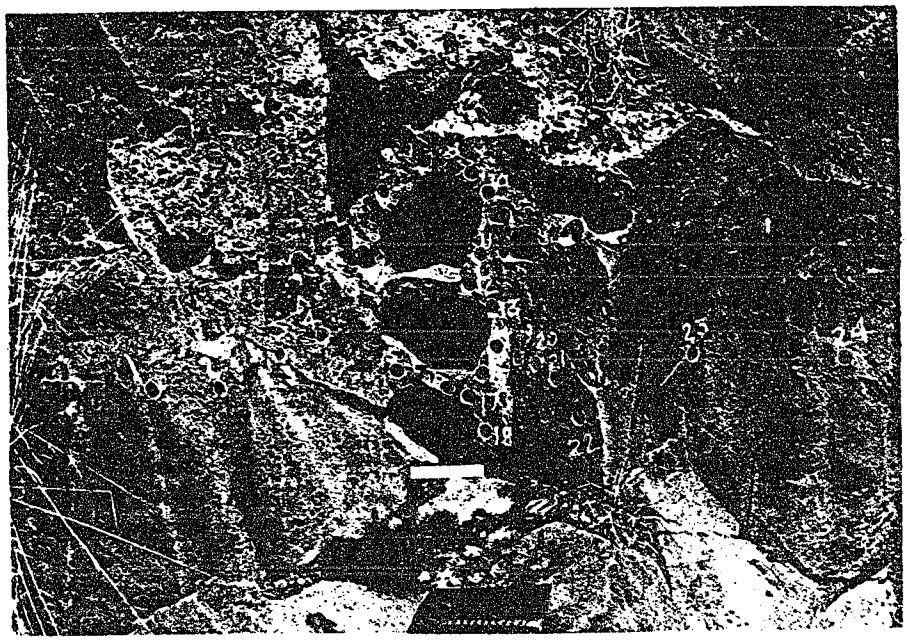

FIGURE 6.2. a) Photograph of the three globular vesicles that ascended actively showing sample locations.

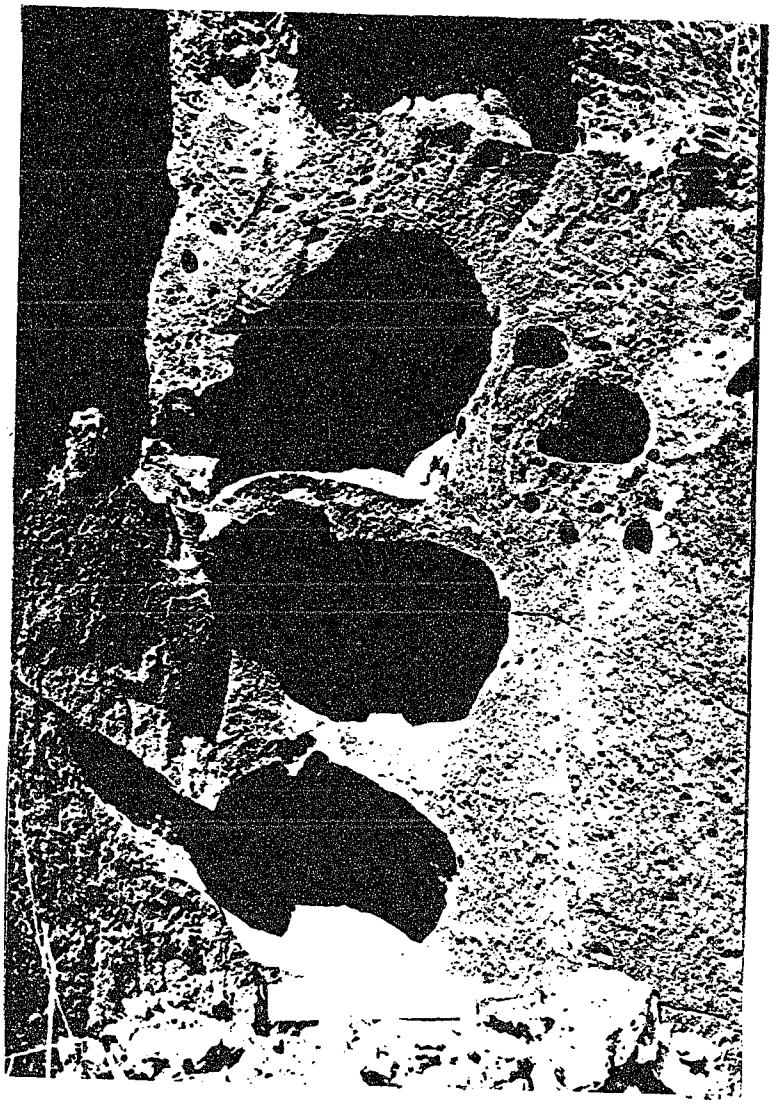

FIGURE 6.2. (CONTINUED) b) Close-up of the three vesicles before collection of samples. Note vesicle foliation chalked on the outcrop. Scale is 15 cm.

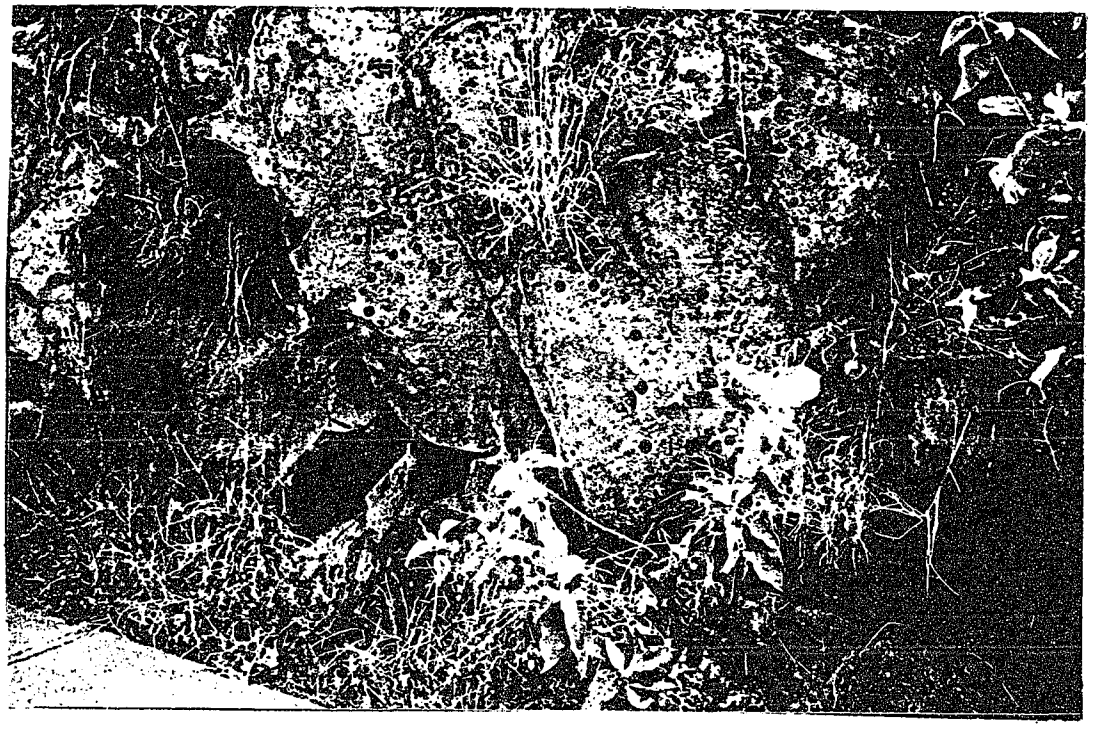

FIGURE 6.3. a)General view of the roadcut where the two belijar vesicles are located. One of the vesicles was covered by vegetation a few months after the samples were collected, when this picture was taken

FIGURE 6.3. (CONTINUED) b) Close-up of the smaller belljar vesicle.

TABLE 6.1. Values (K) and directions (D-declination, I-inclination) of the principal susceptibilities of all specimens used in this chapter. Last two columns show degree of anisotropy (A=100(1 - (k3 + k2) / 2k1), range: 0,100) and magnetic fabric (B=100 (1 + (k3 - 2k2) / k1), range: -100, 100).

Sample #	K_{max} x10^{-3}	D_{max}	I_{max}	K_{int} x10^{-3}	D_{int}	I_{int}	K_{min} x10^{-3}	D_{min}	I_{min}	K_{mean} x10^{-3}	A (%)	B(%)
Globular vesicles												
1	6.261	273	77	6.249	171	03	6.195	81	13	6.235	0.62	-0.67
2	6.784	178	51	6.754	314	30	6.649	58	22	6.729	1.22	-1.11
3	5.385	149	61	5.358	247	04	5.315	339	29	5.353	0.90	-0.30
4	6.121	159	55	6.106	332	34	5.995	64	4	6.074	1.15	-1.57
5	6.78	351	6	6.752	252	58	6.625	85	32	6.719	1.35	-1.46
6	4.55	180	20	4.439	289	42	4.353	71	41	4.447	3.38	0.55
7	5.86	207	57	5.832	315	11	5.714	51	31	5.802	1.48	-1.54
8	5.499	125	43	5.473	242	26	5.339	353	36	5.437	1.69	-1.96
9	6.307	157	65	6.259	50	8	6.138	317	23	6.235	1.72	-1.16
10	6.081	216	47	6.042	11	40	5.941	112	13	6.021	1.47	-1.02
11	6.753	177	59	6.735	21	29	6.591	285	11	6.693	1.33	-1.87
12	6.72	198	34	6.666	90	34	6.609	317	46	6.665	1.23	-0.04
13	7.563	150	56	7.544	35	16	7.363	296	29	7.490	1.45	-2.14
14	6.703	184	49	6.67	49	32	6.543	304	23	6.639	1.44	-1.40
15	7.278	207	9	7.209	112	26	7.144	315	62	7.210	1.39	0.06
16	7.207	116	29	7.202	19	13	6.993	267	58	7.134	1.52	-2.83

TABLE 6.1. (CONTINUED) Values and directions of the principal susceptibilities

Sample #		K_{max} $x10^{-3}$	D_{max}	I_{max}	K_{int} $x10^{-3}$	D_{int}	I_{int}	K_{min} $x10^{-3}$	D_{min}	I_{min}	K_{mean} $x10^{-3}$	A (%)	B(%)
	17	6.807	36	18	6.777	136	27	6.63	277	57	6.738	1.52	-1.72
	18	7.192	73	52	7.164	199	25	6.938	303	26	7.098	1.96	-2.75
	19	6.95	126	66	6.871	29	3	6.761	298	24	6.861	1.93	-0.45
	20	6.636	122	59	6.522	213	1	6.489	303	31	6.549	1.97	1.22
	21	6.833	128	50	6.738	248	23	6.673	352	31	6.748	1.87	0.44
	22	7.035	120	67	6.923	262	18	6.874	356	13	6.944	1.94	0.90
	23	7.277	195	66	7.195	35	23	7.17	302	8	7.214	1.3	0.78
	24	6.935	97	54	6.867	238	29	6.753	339	19	6.858	1.66	-1.24

TABLE 6.1. (CONTINUED) Values and directions of the principal susceptibilities

Sample #	K_{max} x10^{-3}	D_{max}	I_{max}	K_{int} x10^{-3}	D_{int}	I_{int}	K_{min} x10^{-3}	D_{min}	I_{min}	K_{mean} x10^{-3}	A (%)	B(%)
Belljar vesicle 1												
1	6.768	346	1	6.711	76	11	6.69	251	79	6.723	1.00	0.53
2	6.112	336	24	6.085	69	6	6.046	173	65	6.081	0.76	-0.20
3	6.402	8	38	6.391	114	20	6.246	226	46	6.346	1.3	-2.09
4	10.26	359	50	10.25	140	33	10.18	244	20	10.23	0.44	-0.58
5	6.268	109	31	6.255	9	16	6.131	256	54	6.218	1.2	-1.77
6	6.56	25	18	6.536	117	7	6.509	228	70	6.535	0.57	-0.05
7	5.129	359	42	5.118	248	22	5.056	138	40	5.101	0.82	-0.99
8	5.929	330	5	5.917	65	40	5.857	234	50	5.901	0.71	-0.81
9	5.965	342	10	5.939	76	20	5.829	227	67	5.911	1.36	-1.41
10	6.628	4	47	6.595	140	33	6.456	246	24	6.56	1.55	-1.60
11	6.613	26	31	6.558	130	22	6.409	249	51	6.527	1.96	-1.42
12	6.9	2	12	6.863	95	14	6.726	232	72	6.83	1.53	-1.45
13	7.079	5	16	6.979	101	18	6.911	237	65	6.99	1.89	0.45
14	7.186	6	60	7.144	133	19	7.04	232	22	7.123	1.31	-0.86
15	7.1	145	5	7.023	46	59	6.97	238	30	7.031	1.46	0.34
16	7.023	359	38	6.988	111	30	6.877	233	43	6.963	1.29	-1.08
17	7.734	53	8	7.682	315	41	7.522	152	48	7.646	1.71	-1.40

TABLE 6.1. (CONTINUED) Values and directions of the principal susceptibilities

Sample #	K_{max} x10^{-3}	D_{max}	I_{max}	K_{int} x10^{-3}	D_{int}	I_{int}	K_{min} x10^{-3}	D_{min}	I_{min}	K_{mean} x10^{-3}	A (%)	B(%)
Belljar vesicle 2												
18	7.165	342	36	7.154	106	38	7.014	225	32	7.111	1.13	-1.80
19	6.598	71	20	6.564	341	00	6.494	251	70	6.552	1.05	-0.55
20	6.585	330	15	6.538	72	38	6.467	223	48	6.53	1.25	-0.36
21	6.13	321	21	6.108	59	20	6.038	189	60	6.092	0.93	-0.78
22	9.543	311	1	9.531	44	65	9.499	220	25	9.524	0.29	-0.21
23	6.737	342	0	6.731	252	12	6.632	72	78	6.7	0.82	-1.38
24	6.844	344	20	6.839	83	23	6.725	217	59	6.803	0.91	-1.59
25	9.831	320	16	9.825	51	2	9.819	148	73	9.825	0.09	0.00
26	7.399	344	17	7.392	78	12	7.346	202	69	7.379	0.41	-0.53
27	6.625	63	40	6.617	329	5	6.504	233	50	6.582	0.97	-1.58
28	6.715	353	21	6.704	105	48	6.591	245	39	6.67	1.01	-1.52
29	7.422	107	42	7.414	2	15	7.25	257	44	7.362	1.21	-2.10

very closely their contour but farther do not show a definite pattern of preferred orientation. Another difference between the 10 farther samples (1 to 4 and 19 to 24) and the 14 samples that are in the near proximity of the vesicles is that those in the first group yield an average maximum susceptibility closer to the vertical (mean inclination: 61° ± 8°), than those in the second group (mean inclination: 39° ± 19°). Distinction between farther and closer samples is not extensive to the values of bulk susceptibility, degree of anisotropy or magnetic fabric.

Belljar vesicles

Contrary to the results obtained from the globular vesicles, the plane of magnetic foliation of those samples closer to both belljar vesicles do not follow their contour but rather display an orientation similar to that observed on the farther samples (Fig. 6.5). The inclination of the axis of maximum susceptibility is independent of the location of the sample relative to the belljar vesicles, and it is shallower than in the outcrop of the globular vesicles (mean of all 29 samples from this unit 23° ± 16°). Values of the degree of anisotropy seem to be related to sample position: samples near the vesicles (samples 1 to 9 and 18 to 24) have, in average, a lower degree of anisotropy (0.91 ± 0.31) than those farther from the vesicles (1.27 ± 0.54). Bulk susceptibility and magnetic fabric are independent of position.

DISCUSSION

It was shown in Chapter 5 that the orientation of the principal susceptibilities may be related to the degree of solidification reached by the lava after motion ended. A vertical maximum susceptibility is associated with lava likely to have crossed the solidification threshold while static, whereas a horizontal maximum susceptibility is more likely associated to lava crossing the same threshold while still moving. According with this interpretation, the orientation of the principal susceptibilities of specimens far from the vesicles can be used to infer the state of lava in each of the two units of this chapter. For instance, the unit containing the globular vesicles was likely to be stagnant liquid lava, but on the unit with the belljar vesicles it likely reached a larger value of viscosity before stopping, although solidification may

have been not complete at the time when movement ceased. The changing orientation of the plane of magnetic foliation around the globular vesicles can therefore be attributed to the deformation of the surrounding liquid lava during the ascent of the bubbles in analogy with the deformation due to lava motion discussed in Chapter 4. In contrast, the nearly constant orientation of the principal susceptibilities of samples near the bellijar vesicles suggests the absence of any systematic deformation of the surrounding lava associated with bubble ascent.

The obtained results therefore yield evidence that confirms the existence of two distinct mechanisms of vesicle formation in Xitle lavas as proposed by Walker (1995a). Further, AMS measurements yield information regarding the conditions of lava that may favor the development of either vesicle type. These conditions are unlikely to be found in the same location simultaneously, which would explain why the two bubble types do not coexist in close proximity in the same flow.

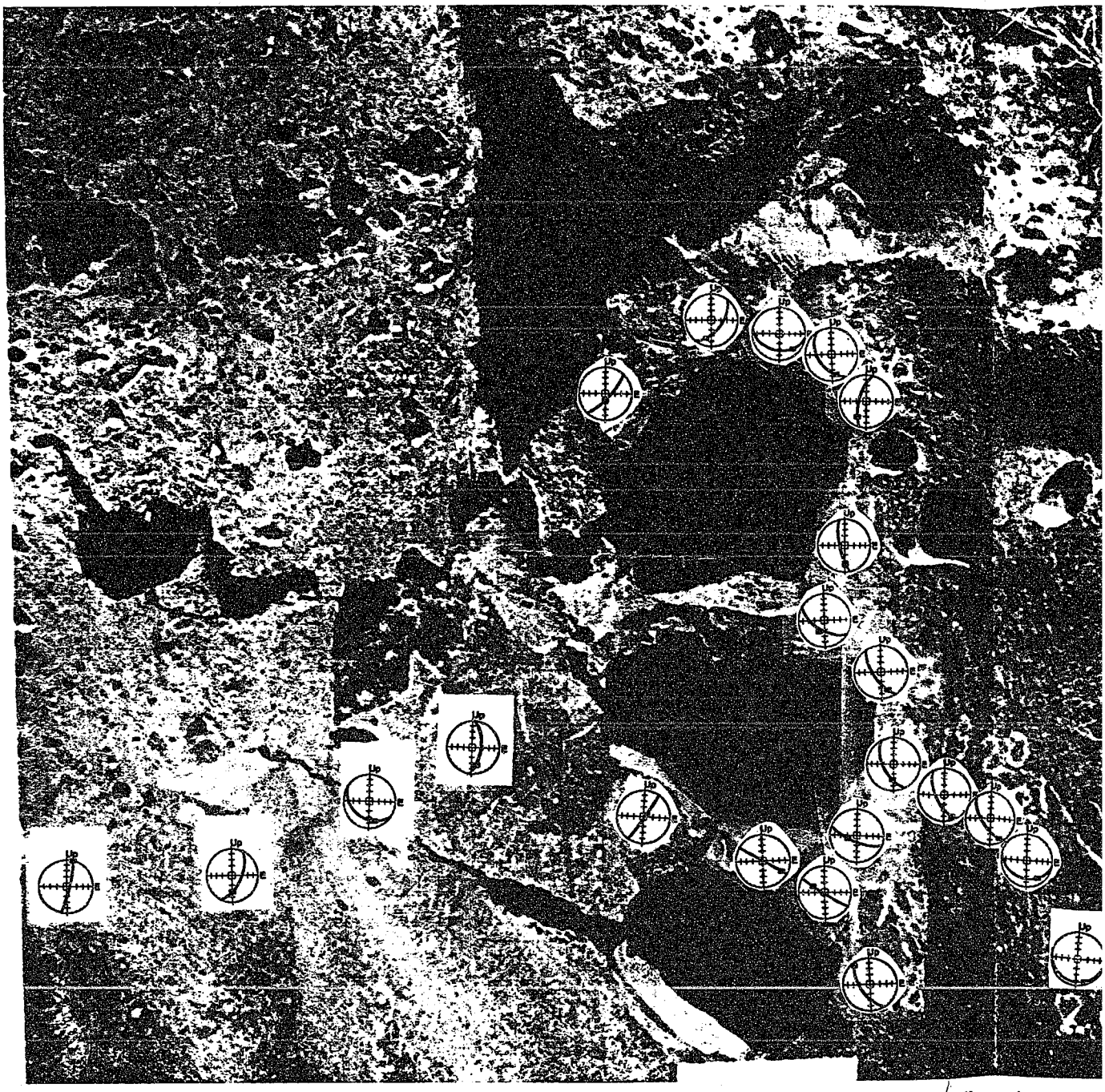

FIGURE 6.4. Projection of the principal susceptibilities of each specimen in a vertical plane nearly parallel to the outcrop of th the observer, the great circle is the plane of magnetic foliation and the square is the maximum susceptibility.

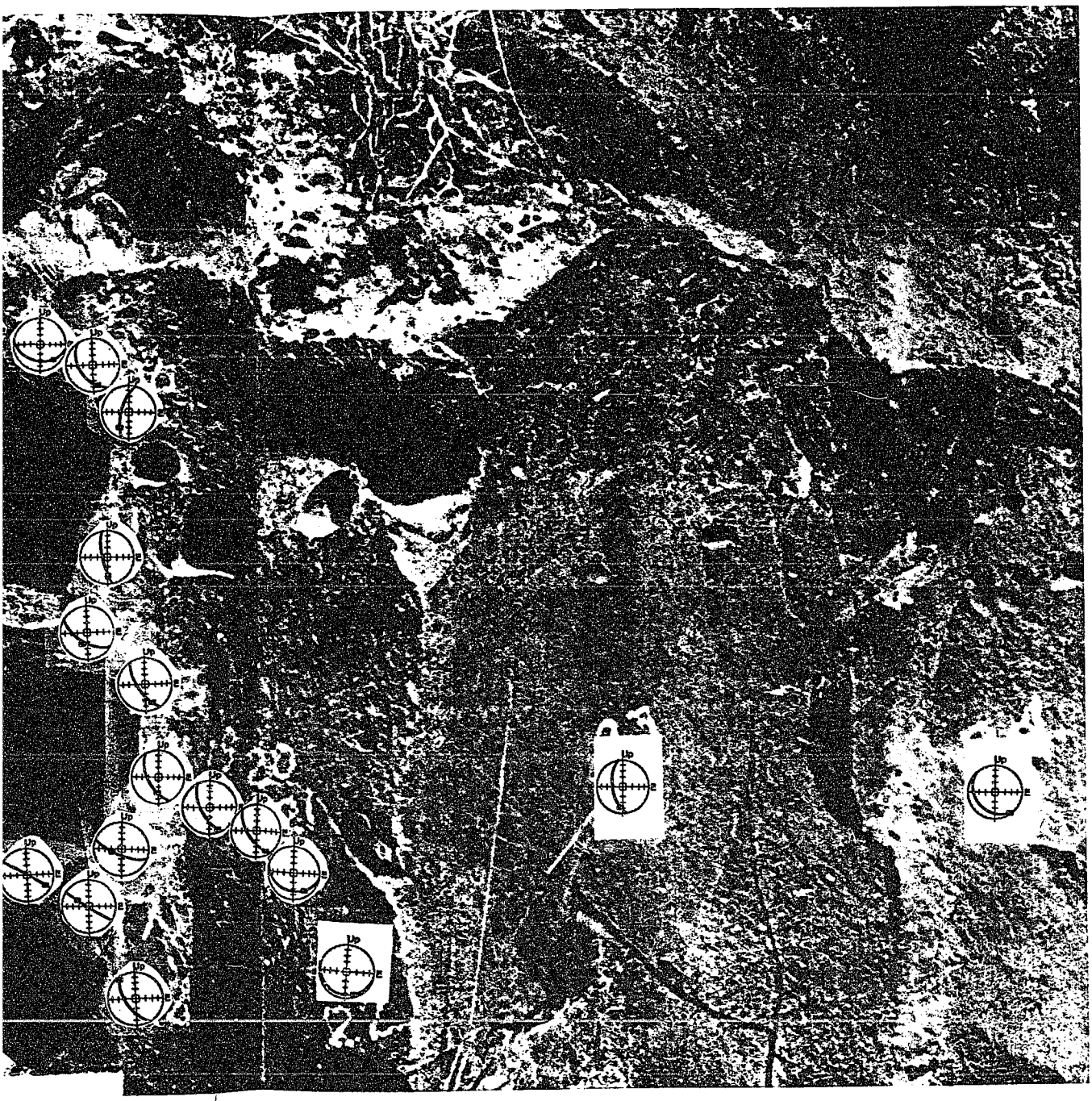

cal plane nearly parallel to the outcrop of the three bubbles shown in Fig. 6.1. The hemisphere projected is towards
is the maximum susceptibility.

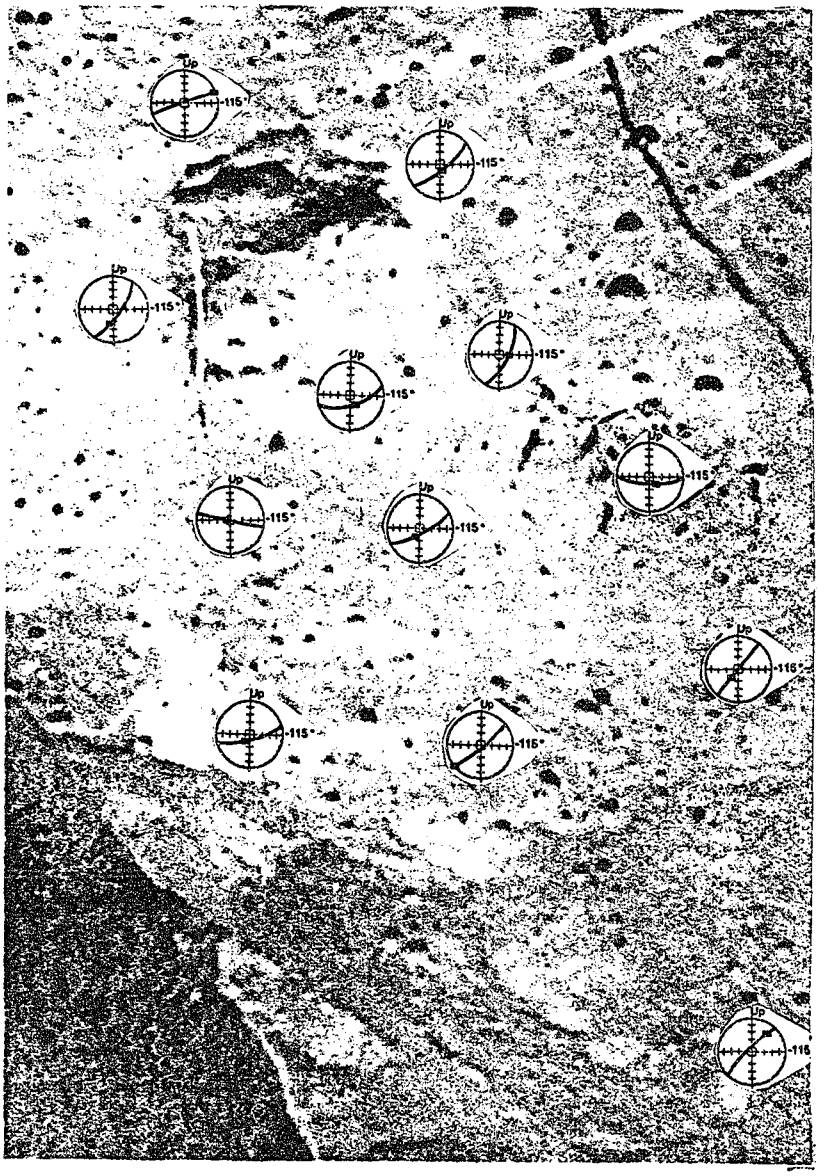

FIGURE 6.5 Projection of the principal susceptibilities of each specimen in a vertical plane nearly parallel to the outcrop of the two bubbles shown in Fig. 6.2. Symbols as in Fig. 6.4

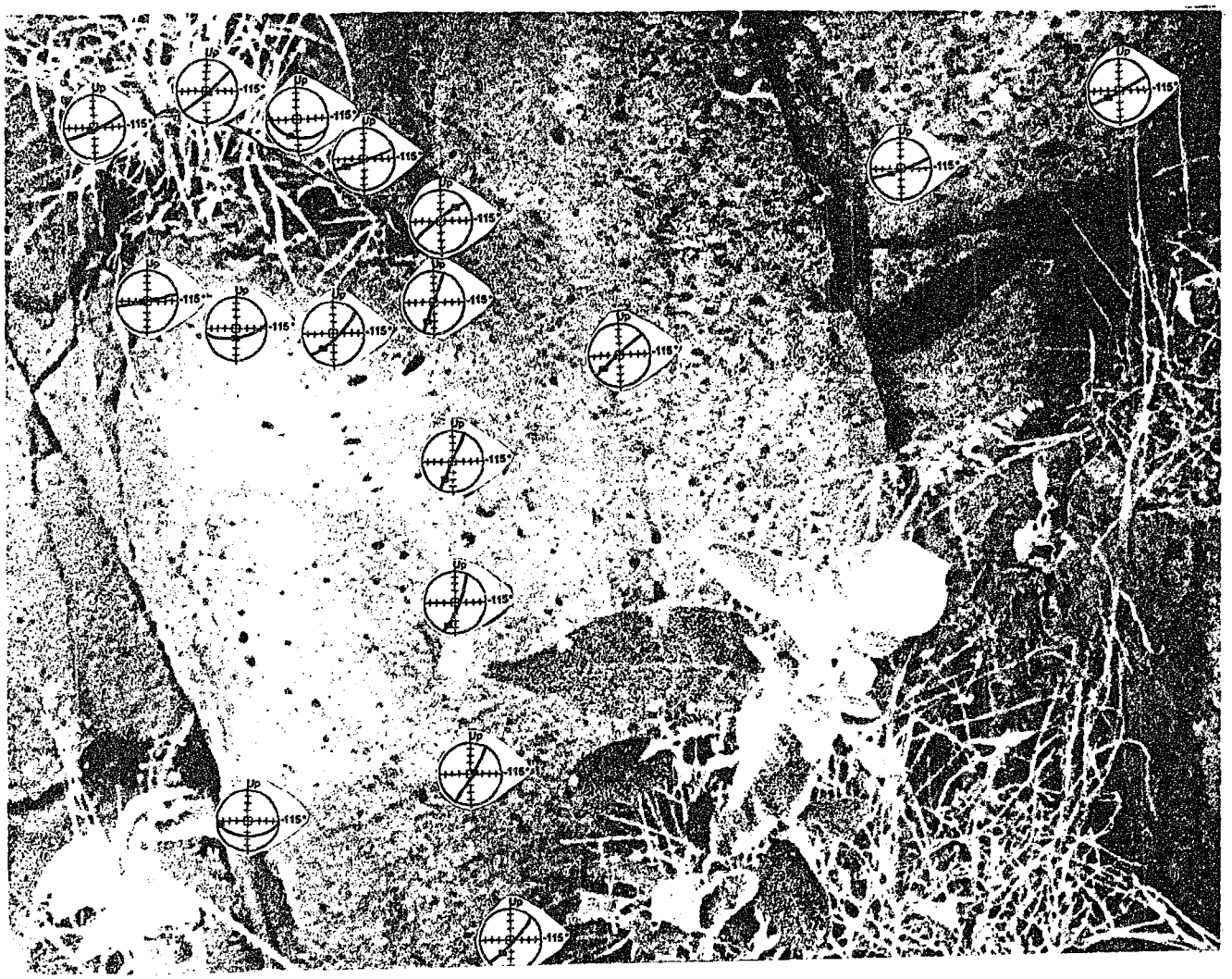

FIGURE 6.5. (CONTINUED) Projection of the principal susceptibilities around belljar vesicles.

CHAPTER 7: FLOW DIRECTION OF THE BIRKETT FLOW, COLUMBIA RIVER BASALT, INFERRED FROM AMS MEASUREMENTS

INTRODUCTION

Paleoflow direction in flood basalts can be determined from the orientation of spiracles or pipe-vesicles found at the base of the flow (Cas and Wright, 1988). Unfortunately, the base of the flow is not always exposed, or the available outcrop may not contain the required number of pipe-vesicles to infer a statistically significant flow direction. An alternative method to infer flow direction of lavas is the examination of the microscopic fluidal texture (e.g., Smith and Rhodes, 1972). The microscopic method, however accurate may be, has as major drawbacks the time and the large effort required for the counting of elongated grains in each thin section. A much faster, and considerably accurate, method is the measurement of the anisotropy of magnetic susceptibility (AMS) of rock specimens. In this chapter, I report the results of the measurement of the AMS of rock specimens collected from the Birkett flow on the Columbia River Basalt Group.

SITE DESCRIPTION

The Birkett flow is part of the Grande Ronde Basalt Formation of the Columbia River Basalt Group in south-central Washington (Landon and Long, 1989). According to the classification of Long and Wood (1986), this flow is a Type III flow in which multiple colonnade-entablature tiers are not prominent. The upper part of the flow exposed at Sentinel Gap exhibits a layered structure of abundant vesicles, similar to that described by McMillan et al. (1987) on the Cohassett flow. The lower part of the flow consists of poorly formed columns and vesicles are almost completely absent. The base of the flow is not exposed.

Cylindrical specimens of 0.025 m diameter were drilled on the exposed surface of the Birkett flow at Sentinel Gap (Fig. 7.1), and oriented with magnetic compass and clinometer before retrieving them. A total of 61 samples were collected, 38 from the lower 23 m and 23 from a layer 2.8 m thick within the vesiculated section of the flow (Fig. 7.2). Average sample separation on the lower, non-vesicular

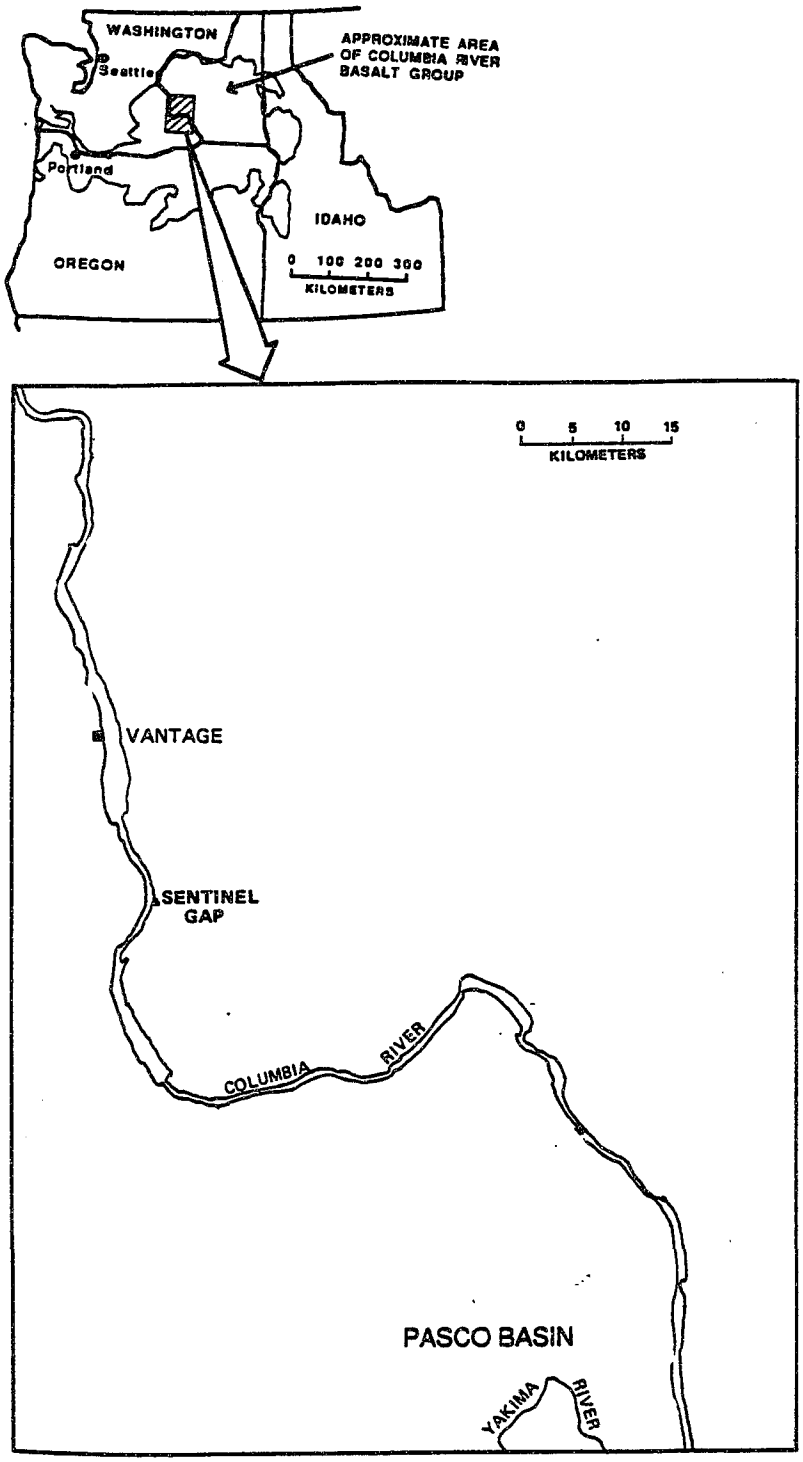

FIGURE 7.1. Location map of the area around Sentinel Gap, where the Birkett flow used in this study is exposed.

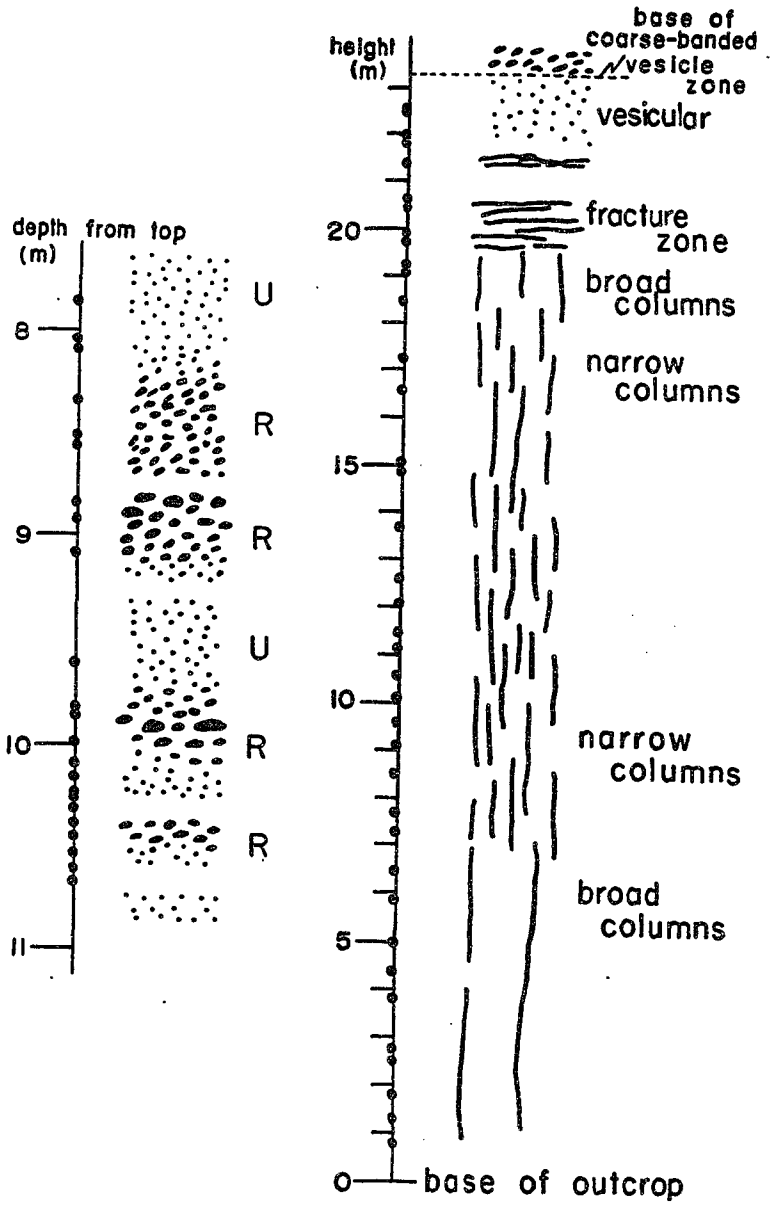

FIGURE 7.2. Diagrams showing some of the most important structural features of the Birkett flow and the location of samples (filled circles on the scale) used in this study. a) Upper part of the flow. R - reverse grading vesicle layer. U - layer with vesicles of uniform size. b) Lower part of the flow.

part of the flow was 0.6 m while on the vesicular section samples were separated by a shorter distance (0.13 m in average). The more detailed sampling in the vesicular zone included six layers of vesicles with distinctive population characteristics (Fig. 7.2a).

RESULTS

When plotted in the lower hemisphere of an equal area projection , the principal susceptibilities of all 68 specimens show a somewhat scattered distribution. Density contour plots (e.g., Fisher et al., 1993; Chapter 5), however, reveal the presence of three mutually orthogonal clusters of directions (Fig. 7.3a). About half of the specimens from the upper part of the flow and 9 specimens from the lower part of the flow yield either almost isotropic or ill-defined susceptibility tensors (as indicated by the failure, at a 95% confidence level, of the anisotropy tests accompanying the output of the Kappabridge), which results in a reduced significance of the directions of the principal susceptibilities of each specimen. Elimination of these specimens from the equal area projection reduces the apparent scatter while preserving the definition of the three clusters of directions (Fig. 7.3b).

In Chapter 6, I explored the magnetic fabric of various lava flow-morphologies from the Hawaiian islands. These results indicate that cases in which lava is likely to have stopped while still liquid are characterized by nearly vertical maximum susceptibility axes (subsequently referred to as "V") and almost uniform distribution of susceptibility axes. Despite the nearly uniform distribution, however, it was common to observe an opposite plunge of the principal susceptibility V on specimens collected from upper and lower parts of the same unit. These contrary plunges were interpreted to constitute a double imbrication similar to that used to infer the absolute flow direction from the AMS measurements of dikes (e.g., Knight and Walker, 1987) and a'a flows (Chapter 4), and allowed me to infer the absolute flow direction of lava flows independently from the orientation of the mean principal susceptibilities. In the present case, most of the maximum susceptibility axes are nearly vertical and the plunge of the V axes is different on specimens from the upper and lower parts of the flow (Fig. 7.3), therefore suggesting that the Birkett flow a) stopped while still liquid in its interior (although subsurface growth continued as explained below), and b) its flow direction at the sampling location was towards the west.

In Chapter 4 it was postulated that the influence of the gravitational force causing vertical movement of gas bubbles and crystals in static, liquid lava would tend to disrupt the orientation of the principal susceptibilities according to a well defined evolutionary scheme that resulted in the exchange of orientation of principal susceptibility axes accompanied by a decrease of the degree of anisotropy of individual specimens. Thus it was anticipated that static-cooling lava should be characterized by a large number of maximum susceptibility axes nearly vertical, and a rather large scatter of directions of the principal susceptibilities leading to almost uniform distributions. These features were later observed in some Hawaiian flows (Chapter 5). In the present case, the orientation of the principal susceptibilities is compatible with a static-cooling lava, although the definition of the three clusters of directions suggests an additional effect not observed previously. This mechanism is also responsible for the formation of the observed vesicle-imbrication, and consists of the successive injection of vesicular lava as explained in the next section.

There are two additional lines of evidence that seem to support the above interpretation of AMS results. First, Landon and Long (1989) pointed out that flows in the Crab Creek flow-package were probably emplaced from the east and southwest of the Pasco Basin based on the decreasing thickness of these flows observed in drill holes from various points in the region. Second, there is a Westward imbrication of elongated vesicles that has been measured in the field by Walker (unpublished data). Thus, measurement of the AMS of rock specimens from the Birkett flow yields a flow direction that is consistent with that inferred from other sources.

Implications For The Mode of Emplacement

In the preceding interpretation of AMS data, post-emplacement disruption, probably related to crystal settling, is assumed to have played an important role. The shape of the vesicles in the upper half of the flow, however, is not consistent with this interpretation. Liquid lava, with such a small viscosity as to allow vertical movement of crystallites would also allow vertical (upwards) displacement of bubbles due to buoyancy. Although in effect, MacMillan et al. (1987) suggested that vertical displacement of bubbles had certainly occurred in some of the CRB flows, ascending bubbles in a

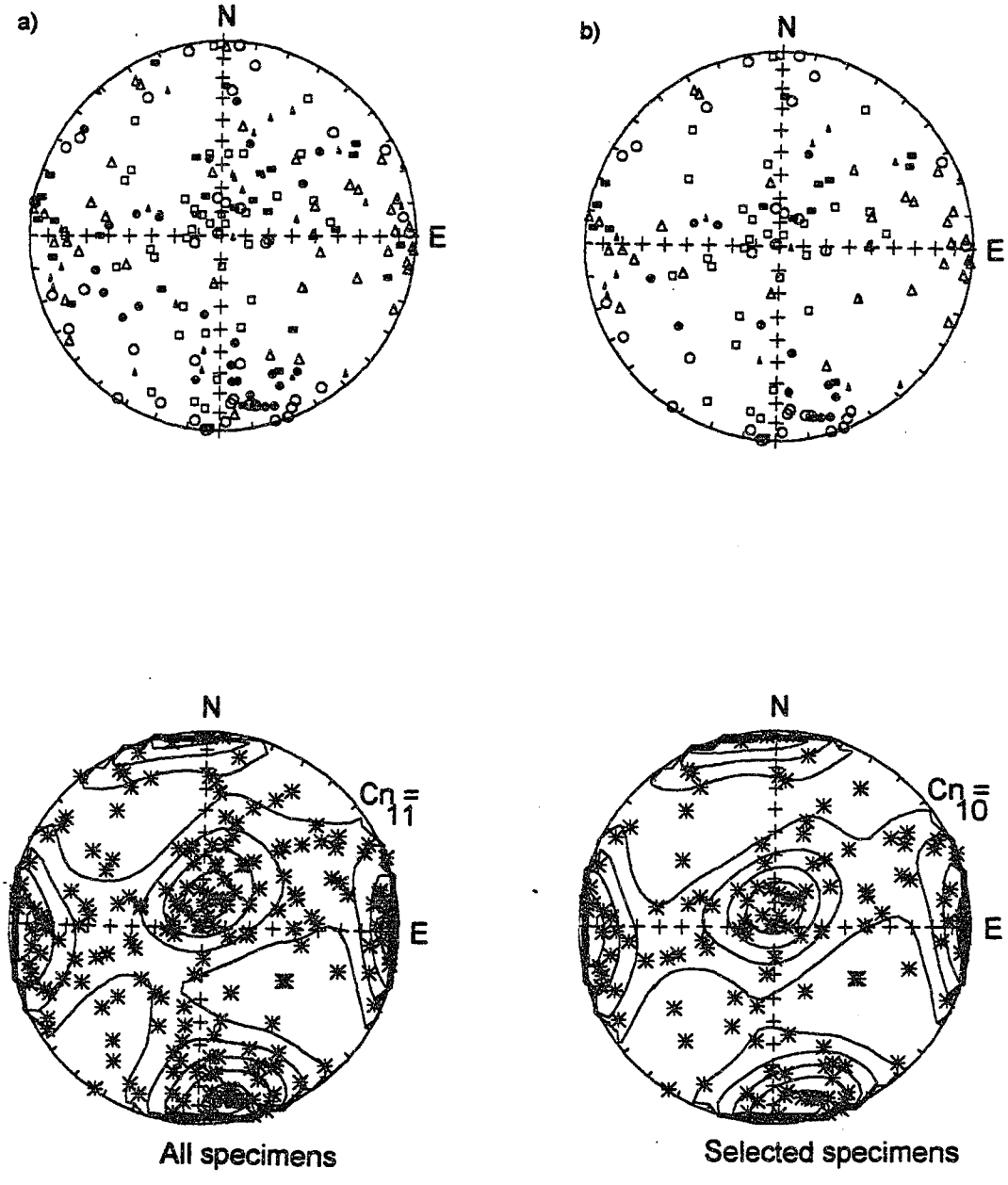

FIGURE 7.3. Equal area projection(above) and density contour plots (below) of the principal susceptibilities. a) All specimens, and b) eliminating specimens with any anisotropy test failed. All directions are in the lower hemisphere; in the two projections on top, solid symbols are samples collected from the upper, vesiculated part of the flow and open symbols are specimens from the lower part of the flow. Squares - kmax, Triangles - kint, Circles - kmin.

viscous fluid are likely to develop either an elongated shape with the elongation directed near the vertical (e.g., Manga and Stoner, 1994), or retain a nearly spherical shape if their velocity of ascent is very small (Clift et al., 1978). The vesicles preserved in the outcrop, however, are flattened with their shorter dimension near the vertical and a preferred elongation plunging towards the East. Preservation of these flattened vesicles in the outcrop indicates that the viscosity of the lava was large enough to prevent surface forces from restoring their spherical shape; lava this viscous would have prevented any vertical displacement of bubbles or crystals.

These apparently contradictory observations can be reconciled by the mechanism of endogenous growth proposed by Walker (1995b). In Fig. 7.4 a sequence of lava pulses is shown, each injected near the medial plane of the preceding pulse. According with this model, the lava of each pulse stopped while still fluid enough to allow a significant vertical displacement of both bubbles and crystals (therefore disrupting the original AMS). When the following pulse was injected, shearing between the new and old lava produced the deformation of the bubbles along a nearly horizontal plane and lead to the measured AMS. This implies that viscosity of the first pulse of lava at the time of shearing would had already reached a value large enough to preserve the deformation of the bubbles and AMS orientation, but viscosity of the second lava pulse was still small enough to begin the cycle for a second time. The whole process would then be repeated several times, at least as many as independent vesicle layers are in the upper vesicular zone of the flow.

A consequence of this model is that the time elapsed between two successive pulses of lava could not be very long because otherwise the whole unit would have not solidified as a single cooling unit, but it had to be long enough to allow some significant vertical displacement of bubbles and crystals to take place. The model also requires a large increase in viscosity in a narrow temperature range, as has been suggested by some workers (cf., Williams and McBirney, 1979).

In summary, AMS measurements not only yield independent evidence supporting previously inferred flow directions for the Birkett flow, but also support the endogenous growth of this thick unit.

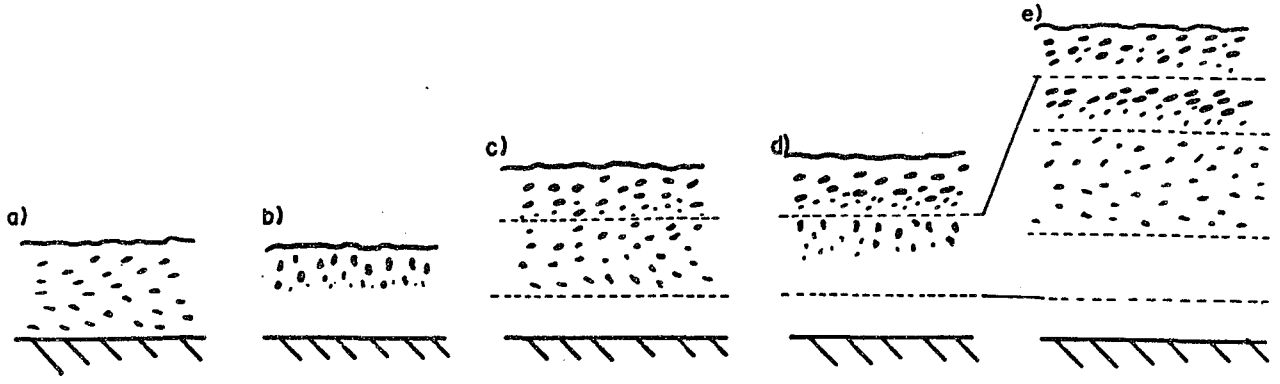

FIGURE 7.4. Model of endogenous growth proposed for the Birkett flow. a) First pulse of lava with sheared bubbles comes to rest while still fluid. b) Ascent of bubbles and settling of crystals (not shown) takes place before c) a second pulse of lava occurs. d) Ascent of bubbles in the second pulse takes place before e) a third pulse arrives.

CHAPTER 8: GEOLOGICAL APPLICATIONS OF AMS IN IGNEOUS ROCKS - A CRITICAL REVIEW

INTRODUCTION

Low-field anisotropy of magnetic susceptibility (AMS) is a unique petrofabric indicator because of its speed and low cost (Tarling and Hrouda, 1993). Its sensitivity to small variations in the amount, type and, perhaps more important, distribution of ferromagnetic grains makes this technique very attractive to study in detail the internal structure of some igneous rocks. In order to interpret the results of AMS measurements, a number of assumptions regarding its origin are usually made, although due to the complexity of natural phenomena the same assumptions may not be applicable to every situation. Rochette et al. (1992) reviewed some of the most common assumptions to the light of magnetic mineralogic considerations, and expressed the need to asses their validity in each case study. In this chapter, the consequences of accepting magnetic interaction between particles instead single shape anisotropy as the main source for the measured AMS in rock specimens are discussed. It is also attempted to show that AMS methods are a powerful, so far mostly unexploited tool that can greatly increase our understanding of the dynamics of movement and emplacement of some igneous rocks.

The proposed model to explain the distribution of particles (cf., Chapter 4) is likely to be valid only in cases in which the source of AMS is the ferromagnetic fraction, and for which the contribution of para- and diamagnetic minerals can be neglected. This clearly limits the scope of this review to AMS studies on igneous rocks in which the bulk susceptibility is usually > 2×10^{-3} SI. A further restriction will be imposed by excluding, rather arbitrarily, large plutons in which the susceptibility value is larger than the above threshold value but for which a complex fluid dynamic history is anticipated. In this regard, the term "intrusive" will in the remainder be restricted to structures like dikes or cone sheets in which laminar flow between parallel boundaries seems to have been the main form of magma transport.

ORIENTATION OF THE PRINCIPAL SUSCEPTIBILITIES

Until now, it has been most commonly accepted that the AMS measured in rock specimens is directly related with the preferred orientation of magnetically non-interacting mineral grains. This is not

unreasonable as a first approximation, because the AMS of large single grains of magnetite is directly related with its shape (cf., Chapter 2). Consequently, in order to explain the orientation of the AMS of a rock specimen, a mechanism capable to produce a preferred orientation of, say, elongated grains needs to be sought for. In the following sections I shall demonstrate that a more detailed examination of the data together with the inclusion of geological considerations indicate that this hypothesis is not the most adequate, and therefore a different model has to be adopted. Textural anisotropy (i.e., AMS resulting from the distribution of ferromagnetic grains in a para- or diamagnetic matrix) as suggested by Wolff et al. (1989) and Hargraves et al. (1991) is perhaps the most likely substitute for the single-grain shape hypothesis, while the fluid model linking this type of anisotropy to the conditions of emplacement of lava in previous chapter seems a plausible physical mechanism.

Pyroclastic deposits

Workers interested in the study of pyroclastic deposits adopted from the first studies, sedimentological models in which grains moving in a concentrated suspension orient themselves with their longest dimension approximately parallel to the direction of motion and their shortest dimension along the direction of maximum gradient (Rees, 1968). Accordingly, it was expected that the maximum susceptibility (kmax) of some pyroclastic deposits pointed along the direction of movement of the flow that produced the deposit, and indeed this was the result found by Ellwood (1982) and MacDonald and Palmer (1990) in natural deposits for which the source region was relatively well constrained geologically. Knight et al. (1986) and Hillhouse and Wells (1991) adopted this model, and used it to successfully establish the previously unknown sources of natural deposits in Sumatra and southwestern United States, respectively.

Although all this evidence could suffice to reasonably conclude that both the assumed source of AMS and the mechanic model of grain orientation were correct, some details deserve a closer examination. For instance, the magnetic fabric of most specimens in all the published studies of AMS

in pyroclastic deposits (Ellwood, 1982; Incoronato et al., 1983; Knight et al., 1986; Wolff et al., 1989; MacDonald and Palmer, 1990; Hillhouse and Wells, 1991; Palmer et al. 1991; Seaman et al., 1991) is preferentially foliated (this term is equivalent to an oblate shape, and a prolate shape is equivalent to a preferentially lineated fabric as shown by Cañón-Tapia 1994), yet the kmax axes are usually well clustered parallel to the direction of flow.

A preferentially oblate fabric requires, always within the single-grain shape hypothesis, either a predominance of flattened grains or a rather uniform distribution over the plane of magnetic foliation (this plane is defined as the plane containing the maximum and intermediate susceptibilities) of the long axes of elongated grains. If the first possibility is correct, the predominance of flattened grains would preclude the definition of a significant cluster of kmax axes, and therefore it would not be possible to infer the flow direction of this type of deposits. Actually, in all of the mentioned studies, with the exception of those by Incoronato et al. (1983) and Seaman et al. (1991), a good grouping of kmax axes is characteristic of the obtained results, and therefore this assumption does not seem justifiable (the two exceptions mentioned can be in part due to the fact that Incoronato et al. (1983) did not used the most adequate statistical method to calculate the mean directions and regions of confidence around it, while the specimens measured by Seaman et al. (1991) all yield a very low value of the bulk susceptibility).

Optical inspection of thin sections made by Knight et al. (1986) revealed that a preferred orientation of elongated particles was clearly observed in most cases, but their results also show that the direction of kmax do not necessarily coincide with the direction of alignment of the elongated particles. This evidence is in clear conflict with the second assumption, automatically invalidating this possibility. Therefore, a somewhat different approach seems to be necessary to explain more satisfactorily the observations. Wolff et al. (1989) had already pointed out other problems faced by the single-grain hypothesis, suggesting that instead, the AMS fabric is controlled by groundmass microlites distributed within the existing tuff fabric (i.e., a textural anisotropy). Unlike the single-grain hypothesis, textural anisotropy strongly depends on the magnetic interaction among ferromagnetic grains, as discussed in previous chapters.

According with the model proposed in Chapters 4 and 5, the orientation of the principal susceptibilities is intimately related to the stresses / deformation suffered by each element of fluid, and in the simplest case of a unidirectional velocity, kmax will be nearly parallel to the flow direction (cf., Chapter 4). The orientation of elongated grains already present in the moving fluid is to some extent independent of the orientation of the magnetic fabric due to the internal deformation of fluid elements. If hydrodynamic orientation of elongated grains is effective, the individual-grain shape anisotropy may reinforce the orientation of the kmax axes, and therefore a coincidence between kmax and the optically observable fabric will be obtained, but if individual grain orientation is not effectively controlled by hydrodynamic forces either because the drag associated with the individual shapes was not strong enough, or because the grains themselves were not present during movement of the fluid (i.e., late growth crystallization of minerals did occur) the individual shape anisotropies will be superimposed in the textural fabric in a rather complex way (cf. Appendix 1). In this last case, it is very likely that the optically observable fabric and the magnetic fabric will not coincide, because the latter will be controlled by magnetic interactions.

A consequence of the adoption of the fluid model is that most of the mentioned AMS studies in pyroclastic deposits imply a relatively simple fluid behavior in the region where deposition was actually occurring, so that kmax is parallel to flow direction. Further, the orientation of the plane of magnetic foliation would suggest a marked difference in the velocity with vertical position in the flow, while horizontal changes are almost negligible.

Lava flows

Similarly to the case of pyroclastic deposits, the AMS of lava flows has been found to be preferentially foliated in most specimens, although unlike the pyroclastic counterpart, the directions of the principal susceptibilities usually yield a rather large scatter within the same cooling unit. This scatter of susceptibility axes precluded, at least in part, the adoption of a single model to explain the orientation of individual grains required by the isolated-grain hypothesis, but instead, two different models have been suggested.

One of the models adopted the results obtained by Jeffery (1922) and Taylor (1923) regarding the movement of isolated ellipsoids immersed in a fluid of very large density. In accordance with this model, Khan (1962) suggested that both kmax and kmin axes should be perpendicular to the direction of movement of lavas (consequently kint is parallel to the flow direction) and presented a few specimens from different lava flows that seemed to support his conclusion. As more recent results proved, however, the orientation of the principal susceptibilities does not follow a simple relationship with the direction of advance of lava flows (e.g., Symons, 1975; Cañón-Tapia et al., 1994; Chapters 3, 4, 5, 6 and 7), and therefore, the evidence presented by Khan (1962) can not be accepted as representative of lava flows in general. In other works in which Khan's approach was adopted (e.g., Brown et al., 1964; Ellwood, 1978), the geological evidence was not clear enough to support the validity of the model, but in fact, the interpretation of results was "forced" to fit it, therefore eliminating these works as valid examples in favor of this approach.

The second model used a reasoning similar to that explained for pyroclastic deposits, therefore predicting that kmax should be parallel to the flow direction of lavas. Although this assumption found slightly more support from the geological evidence, early results were still somewhat controversial. For example, Symons (1975) found that kmax was within 10° of the flow direction of the Ainyash flow in 25% of his sites, while in nearly 13% kmax was making an angle of 80° - 90° from it. Nevertheless, he acknowledged that these results could be due to a sampling biasing towards the crustal parts of the flow. As shown in Chapter 3, there is clear evidence that the crustal parts of thick flows may indeed yield kmax orientations that are very different from those obtained from specimens collected lower in the unit. Nevertheless, the assumption of a kmax parallel to flow direction found more support from the geological evidence presented in later works. For instance, MacDonald et al. (1992) report an 80% agreement between the direction of kmax and field measured lineations, and as shown by Cañón-Tapia et al. (1994) and in Chapter 3, kmax indicates reasonably well the flow direction of lavas, in agreement with the geological evidence (provided that no disruption of the original fabric has occurred).

Both of these models, however, relying in the isolated-grain hypothesis are prone to the same criticism than that made to pyroclastic deposits. Hargraves et al. (1991), for example, used the same

arguments than Wolff et al. (1989) have used in the case of pyroclastic deposits against the isolated-grain hypothesis in lavas and intrusives, suggesting that it was the distribution of grains (i.e., textural anisotropy) the main factor controlling the AMS of these type of rocks. This opened the door for the conception of the fluid model presented in Chapters 4 and 5. An immediate consequence of this model is that AMS measurements suggest that the internal structure of lava flows is more complex than that of a pyroclastic flow. However, unlike the case of pyroclasts, care should be exercised when interpreting the AMS of lavas because of the disruptive effects of gravity forces (see below).

Intrusives

Studies of the AMS of intrusive rocks follow the same trend than that described for lava flows regarding the relationship between the principal susceptibilities and flow direction. Khan (1962) and Ellwood (1978) assumed that magma direction in intrusives was indicated by kint, while Knight and Walker (1988), Park et al. (1988), Rochette et al. (1991), Ernst and Baragar (1992) and Puranen et al. (1992) assumed instead that kmax indicated the magma flow direction. Like in the case of lava flows, geological evidence, whenever available, seemed to favor the latter assumption (see also Abouzakm ,1974; Halvorsen, 1974). The presence of a large proportion of intrusives in which this simple scheme does not seem to apply, however, leads to question the validity of the assumptions made in the interpretation of AMS measurements. In analogy with the evidence from both pyroclastic deposits and lava flows it seems reasonable to adopt the interactive model in this case again.

CONSEQUENCES FOR THE INTERPRETATION OF RESULTS

The various models so far proposed to explain the sources of AMS in igneous rocks lead to very different conclusions based in the same experimental results. To illustrate this point, let us assume that we collect samples across the whole width of a horizontal intrusive, and that the AMS results show two different groups of orientations. Nearer to the walls, the plane of magnetic foliation coincides with the plane of the intrusive, but in its central parts kmax is normal to it. Furthermore, lets say that the orientation of the kint axes changes from N-S near the walls to E-W in the middle of the sheet.

Although this may seem a rather arbitrary and idealized case, there are some examples from intrusives in the island of Skye (E. Herrero-Bervera, unpub. data) that share most of these conditions.

If we adopt the isolated-grain hypothesis, and assume that kmax is parallel to the flow direction, we would conclude that the initial pulse of magma occurred in an E-W direction and that the conditions of movement in the interior of the intrusive were either turbulent or strongly influenced by convective currents, hence explaining the different orientation observed in the middle of the intrusive. Alternatively, we could have inferred that cooling or overloading stresses normal to the walls of the intrusive had reoriented the principal susceptibilities in this region, or that the conditions of movement changed with time in a rather complex way. If we assume instead that kint is parallel to the flow direction (remaining within the isolated-particle hypothesis), the interpretation of the results would be that the direction of magma movement was originally along a N-S trend changing latter to an E-W trend, making unnecessary the occurrence of turbulence, convective currents or the effects of any post-emplacement stresses. The change in orientation of the other two principal susceptibilities could be easily disregarded, or in the best of the cases considered as fortuitous.

A very different interpretation of results would be given if we adopt the textural anisotropy hypothesis together with the dynamic model explained in previous chapters. In this case, our conclusions would be that magma motion took place in an E-W direction originally, coinciding with the first interpretation, although none of the presumed complications would be inferred. Instead, settling of crystals in a stationary still fluid magma would suffice to explain the change in orientation of the susceptibility axes from the walls to the center of the intrusive.

These abundance of interpretations forces us to seek additional information to evaluate which of the described processes of emplacement was more likely to have actually occurred. The first and third cases would be supported by an imbrication of kmax axes from samples collected at opposite sites of the intrusive, whereas the second case would be supported by an imbrication of kint axes. Thus at least one possibility can be eliminated if sampling across the intrusive is completed. Now, a change in the type of magnetic fabric from preferentially foliated to preferentially lineated and back to foliated from one side to the center of the intrusion would be compatible with the interactive hypothesis, but would

be very hard to explain with a single-grain hypothesis. Therefore, in principle, it would be possible to select the most likely scenario based only in data from the AMS measurements alone.

POST-EMPLACEMENT DISRUPTION OF AMS FABRIC

In the previous section, the importance of disruptive processes due to stresses or gravitational settling of minerals has been exemplified. Other types of disruption can be related to mechanical compaction, welding, devitrification and rheomorphism in pyroclastic deposits (MacDonald and Palmer, 1990), and to the ascent of large bubbles in lava flows (Chapter 6) and intrusives. Certainly, any event accompanied by the formation of new mineral species or the transformation or disappearance of primary minerals (e.g. hydrothermalism, extreme weathering or higher degrees of metamorphism) also may affect the AMS of the rock. Therefore, geological indicators of any of such alterations should be well documented in each case.

The extent to which post-emplacement disruption may obscure the significance of AMS results can in some instances be assessed from the measurements of AMS alone, provided that an extensive and systematic sampling strategy has been followed. This is specially valid in the cases of rheomorphic flow or whenever reactivation of viscous flow occurs in a different direction than before because these phenomena are likely to take place over a limited area, and on some specific locations rather than all over the extent of the unit under study. The predicted pattern followed by the disruption process will depend not only on the process itself, but also on the orientation and type of the original fabric and on the model adopted to interpret the AMS results, as shown in the previous example. In any case, it is reasonable to suggest that whenever disruptive processes become dominant, these would almost certainly affected other type of fabric and therefore we would not be concerned any longer with the primary structures of igneous rocks.

SUMMARY

Three different models, including that developed in this dissertation, have been proposed to interpret AMS measurements on igneous rocks. In general, geological evidence has favored those in

which kmax is parallel to the local flow direction, although in some cases, specially in lava flows and intrusives, departures from this general rule are encountered. These departures can be explained in terms of some post-emplacement disruptive effects, the nature of which depends on the model adopted to explain AMS measurements in the first place. In any case, it is extremely important to make an interpretation that incorporates all the available information provided from the AMS measurements (i.e. including both directions and relative magnitudes of the principal susceptibilities of each specimen, regional patterns etc.) as well as any other source of geological evidence. An extensive and systematic sampling strategy would greatly contribute to the successful interpretation of results.

Unfortunately, many studies made in the past have disregarded the importance of one or more of the above mentioned requirements and therefore the potential of AMS methods has still not been fully realized. Hopefully, this situation will change in the near future, this dissertation being one of the first steps in such direction.

APPENDIX 1: SINGLE GRAIN VS. DISTRIBUTION ANISOTROPY - A SIMPLE 3D MODEL

INTRODUCTION

Stephenson (1994) presented two simple models showing that non-uniform distributions of otherwise magnetically isotropic particles can give rise to large degrees of anisotropy of magnetic susceptibility (AMS) due to magnetic interactions between neighboring particles. It is important, however, to estimate the relative contribution of the individual-particle anisotropies to the resulting AMS, because rocks in general will contain particles that are not completely isotropic. In this paper, the same basic approach used by Stephenson (1994) is utilized to study the effects of individual-particle anisotropies in the measured AMS of a three dimensional array of ellipsoidal particles. Following the presentation of a general expression, some specific examples are discussed and the effects of a remanent magnetization are briefly examined. The examples presented are used to draw inferences for a rock specimen in which magnetic interaction can be presumed to be important.

MAGNETIC INTERACTION: 3D MODEL

Individual-particle anisotropy can arise from different sources, but it is convenient to represent it as if it were related only to the shape of the individual grains. Shapes other than ellipsoids will in general require numerical methods to estimate their magnetization, and the field at a point outside the particle resulting from this magnetization will also be a little troublesome to calculate. If ellipsoids of revolution are used instead, not only are the calculations greatly simplified but they are amenable to analytical treatment. Further, the field outside a uniformly magnetized ellipsoid can be approximated by a dipole at the center of the ellipsoid provided that its ratio of largest to shortest semi-axis is close to unity (e.g., Sprowl, 1990).

A three dimensional distribution of particles can be approximated by an arrangement in which six nearest neighbors act upon a central reference particle (Fig. A1.1). Clearly, the principal axes of

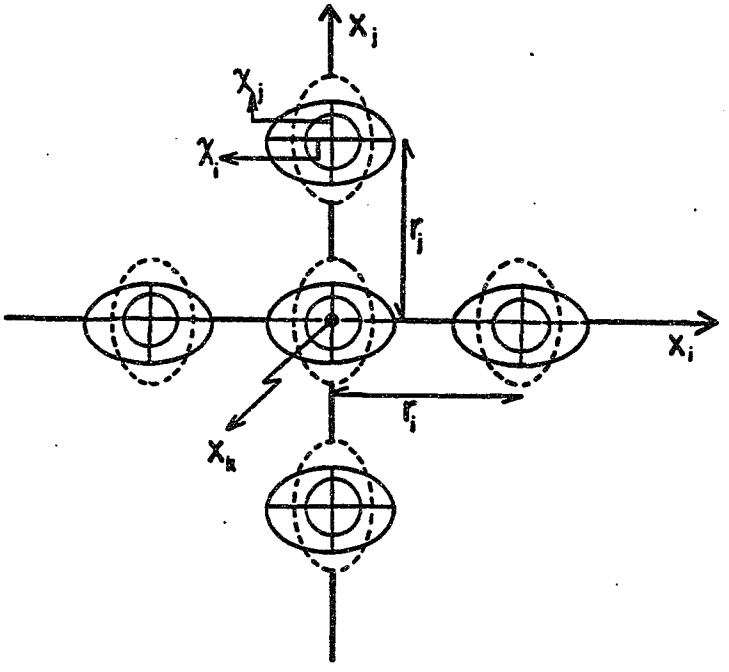

FIGURE A1.1. Diagram showing the relative positions of four nearest neighbors of a reference particle located in the xi - xj plane. Two other particles are symmetrically disposed above and below the reference particle along the xk direction. The circles indicate the contour in the xi - xj plane of particles having their axes parallel to xk (whether oblate or prolate). Dashed ellipses indicate either the projection of prolate particles with axis parallel to xj or oblate particles with axis parallel to xi. Solid ellipses represent the projection of either prolate particles with axis parallel to xi or oblate particles with axis parallel to xj. The corresponding principal susceptibilities are indicated only for the solid line ellipses.

susceptibility of the particles (χi, χj) coincide with the axes of symmetry of the array of particles (xi, xj and xk) as shown in Figure A1.1.

By assuming that all the particles are identical and have the same orientation the effects of their interaction can be estimated. The enhancing field, h, experienced by the central particle due to the induced magnetization of the six nearest neighbors in an external field applied along any of the three axes of reference will be given by:

$$h_i = \frac{2m_i}{2\pi r_i^3} - \frac{2m_i}{4\pi r_j^3} - \frac{2m_i}{4\pi r_k^3}$$

$$= \frac{m_i}{2\pi}\left(\frac{2}{r_i^3} - \frac{1}{r_j^3} - \frac{1}{r_k^3}\right) \qquad \text{... (A1.1)}$$

where ri, rj , rk are the distances to the adjacent particles along the corresponding axis of symmetry (cf. Fig. A1.1), mi = v Mi is the component of the dipolar moment induced by the field in each particle of volume v along the i direction, and Mi is the component of the induced magnetization, also along the i direction. The bulk susceptibility along any of the xi directions is, following Stephenson (1994),

$$\chi_i = \frac{M_i}{H}$$

$$= \frac{\chi_{i\text{-}app}(H + h_i)}{H}$$

$$= \chi_{i\text{-}app}\left(1 + \frac{v}{2\pi}\left(\frac{2}{r_i^3} - \frac{1}{r_j^3} - \frac{1}{r_k^3}\right)\chi_i\right) \qquad \text{... (A1.2)}$$

where $\chi_{i\text{-}app}$ is the apparent susceptibility along the i direction.

From eq. (A1.2), the general expression

$$\chi_i = \frac{\chi_{i\text{-}app}}{1 - \frac{v}{2\pi}\left(\frac{2}{r_i^3} - \frac{1}{r_j^3} - \frac{1}{r_k^3}\right)\chi_{i\text{-}app}}$$

$$= \frac{1}{N_i - \frac{v}{2\pi}\left(\frac{2}{r_i^3} - \frac{1}{r_j^3} - \frac{1}{r_k^3}\right)} \qquad \text{... (A1.3)}$$

is obtained. The approximation of the apparent susceptibility as the inverse of the demagnetization factor, Ni, in eq. (A1.3) is valid for any material possessing a high value of its intrinsic susceptibility (e.g., Stephenson, 1994). Equation (A1.3) can be used to study the arrangement of particles along lines and planes noting that:

a) A line of particles can be formed by letting two of the r_ns tend to infinity. The line can always be taken as parallel to x1, in which case r2 and $r_3 \rightarrow \infty$.

b) A plane of particles can be formed by letting one of the r_ns tend to infinity. The plane can always be taken as the x1 - x2 plane and therefore, $r_3 \rightarrow \infty$.

Values for the demagnetizing factors can be obtained from the tables given by Stoner (1945). Following his nomenclature, if the length of the polar axis of each ellipsoid is *a* and the equatorial axis *b*, the ratio *a/b* > 1 indicates a prolate shape while *a/b* < 1 represents an oblate ellipsoid. In the following sections, the range 0.4 < *a/b* < 2.5 was selected because, as mentioned previously, the smaller the departure from the spherical shape, the more accurate the approximation of the model. Using a ratio = 1, and taking into account the above considerations, the expressions given by Stephenson (1994) for a line and a plane of spheres can be easily obtained from eq. (A1.3).

It should be noted that although the magnetic fabric can be quantified in various ways, the model does not justify the use of any one parameter. However, the qualitative aspects

displayed by most of the so called shape parameters turn out to be very illustrative of how magnetic interaction may affect the measured AMS of rocks. In this regard, the terms lineated and foliated fabrics used in subsequent sections make reference to the corresponding general regions in the field of the susceptibility tensors (Canon-Tapia, 1994) rather than to any specific parameter.

A case of practical interest is the comparison of the calculated susceptibility along the three directions x_1, x_2 and x_3 as a function of inter-particle separation (Figures A1.2, A1.4 and A1.5). The separation between particles in these figures is given as multiples of their equatorial semi-axis (hereafter called b-units) to allow direct comparisons among different shapes. Clearly, particles in contact will be separated by a distance of 2 b-units.

MAGNETIC INTERACTION: LINEATION

Let us first examine the case of ellipsoids having their axis of revolution parallel to x2 while defining a line along x1. As mentioned earlier, in this case r2 and $r_3 \rightarrow \infty$. Thus, from equation (A1.3) we obtain

$$\chi_1 = \frac{1}{N_1 - \frac{v}{2\pi}\left(\frac{2}{r^3_1}\right)}$$

$$\chi_2 = \frac{1}{N_2 + \frac{v}{2\pi}\left(\frac{1}{r^3_1}\right)}$$

$$\chi_3 = \frac{1}{N_3 + \frac{v}{2\pi}\left(\frac{1}{r^3_1}\right)}$$

Figure A1.2 shows the ratios of these susceptibilities as function of the inter-particle separation for particles with various *a/b* values and Figure A1.3 illustrates the sequence followed by the orientation of the principal susceptibilities of the set of particles. From these results, it is apparent that magnetic interactions become important at separations of less than 4 b-units, and dominant at separations less than 2.5 b-units irrespective of the shape of individual particles. Whenever magnetic interaction is dominant the resulting susceptibility anisotropy will be that of a lineated fabric along x_1 for both prolate and oblate particles, although it should be recalled that the long axis of each prolate particle is perpendicular to the direction of the lineation. If magnetic interaction is negligible (r1 > 5 b-units), the resulting magnetic fabric corresponds to that associated with the shape of individual particles (i.e., prolate particles yield a lineated fabric parallel to x_2 while oblate particles yield a foliated fabric with minimum susceptibility along x_2). In the case of prolate particles, a transitional zone in which the magnetic fabric of the array is foliated with maximum susceptibility along x_3 is also defined.

MAGNETIC INTERACTION: FOLIATION

A second example of the effects of magnetic interaction in the resulting magnetic fabrics is obtained by distributing the particles over the x_1 - x_2 plane, orienting their axes of symmetry parallel to x_3 (i.e., normal to the plane of distribution). According to eq. (A1.3), it is now necessary to specify the separation between particles along two directions to get a value of the measured susceptibility. To simplify the discussion, a separation of 2.5 b-units along x_1 (i.e., r1 = 2.5) was used in the construction of Figures A1.4 and A1.5.

In this case, magnetic interaction along x_2 is dominant for values of $r_2 < 2.5$, as suggested by the fact that at this point χ_2 becomes larger than both χ_1 and χ_3 irrespective of the shape of the particles (Fig. A1.4). The resulting magnetic fabric of the array, however, is lineated in a direction parallel to x_2 only if the particles are prolate or weakly oblate (*a/b* > 0.9); particles with a smaller *a/b* ratio will yield a foliated magnetic fabric with minimum susceptibility parallel to x_3 even if they are in contact along x_2 (i.e., r2 = 2). For large values of r_2 the resulting magnetic fabric reflects the stronger interactions along x_1, as in the previous example, although the ratios of the susceptibilities (Fig. A1.4) indicate that

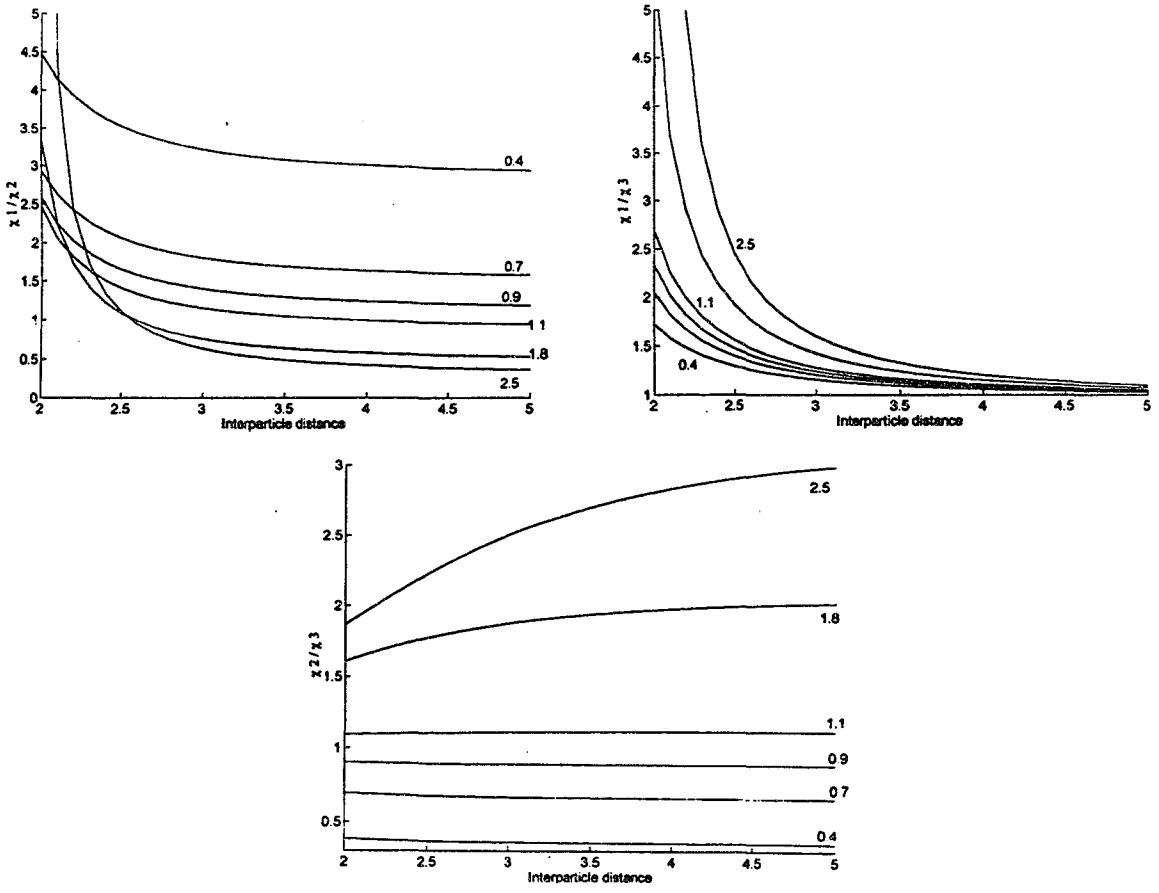

FIGURE A1.2. Plots of the ratios of the three principal susceptibilities for a linear array of particles as a function of the separation of particles along the x1 direction. Figures over the lines indicate the value of the polar to equatorial semi-axes (>0 - prolate particles, <0 - oblate particles).

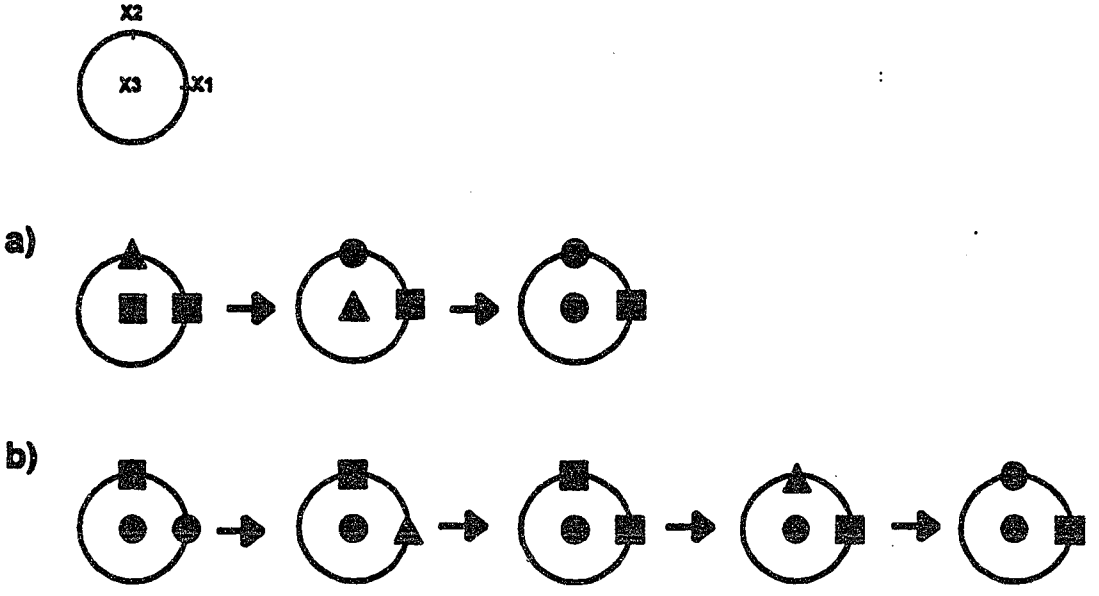

FIGURE A1.3. Schematic evolution of the magnetic fabric of the linear array of particles as a function of the interparticle separation along x1. a) Oblate particles. b) Prolate particles. Squares - maximum susceptibility, Triangles - intermediate susceptibility, Circles - Minimum susceptibility.

magnetic interaction along x_2 takes place even at r_2 values around 5 b-units. For intermediate values of r_2, the magnetic fabric of the array can take several different orientations as shown in Fig. A1.5. The value of r_2 at which a transition from one orientation to another occurs depends on the exact value of the *a/b* ratio.

MAGNETIC INTERACTION: 3D DISTRIBUTION

A 3D arrangement of particles in which all of them have their axes parallel to x_1 and constant separations along x_1 and x_2 equal to 3 and 2.5 b-units, respectively was used to construct Figures A1.6 and A1.7. For particles distributed in this way, the effects of the magnetic interaction may take many different forms depending on the individual particle shape and separation along x_3. Perhaps the most important points to mention are that all particles yield a resulting maximum susceptibility along x_3 and minimum susceptibility along x_1 below a critical value of r_3 ($r3 < 2.5$ b-units for oblate particles and $r_3 < 2.1$ b-units for prolate particles). Also, the evolution of the resulting magnetic fabric with decreasing r_3 is more complex than in the previous examples depending strongly on the axial ratio involved (Fig. A1.7).

DISCUSSION

The most important feature of all the examples examined in previous sections is that there is no unique correspondence between the individual-grain shape and the resulting AMS if magnetic interaction is taken into account. Situations in which prolate grains all have their longest axes along one direction while the measured maximum susceptibility is perpendicular to that direction were presented in all of the previous examples. The most extreme case was encountered in the 3D distribution when longest grain dimensions could correspond to minimum measured susceptibility and shortest grain elongation was parallel to maximum susceptibility. A situation of this type has been often referred to as "inverse fabric", and has been usually ascribed to the predominance of single-domain magnetite (Rochette, 1988). In the model presented here, there was no assumption made about the domain state of the individual particles, which suggests that the non-correspondence of an observed mineral fabric

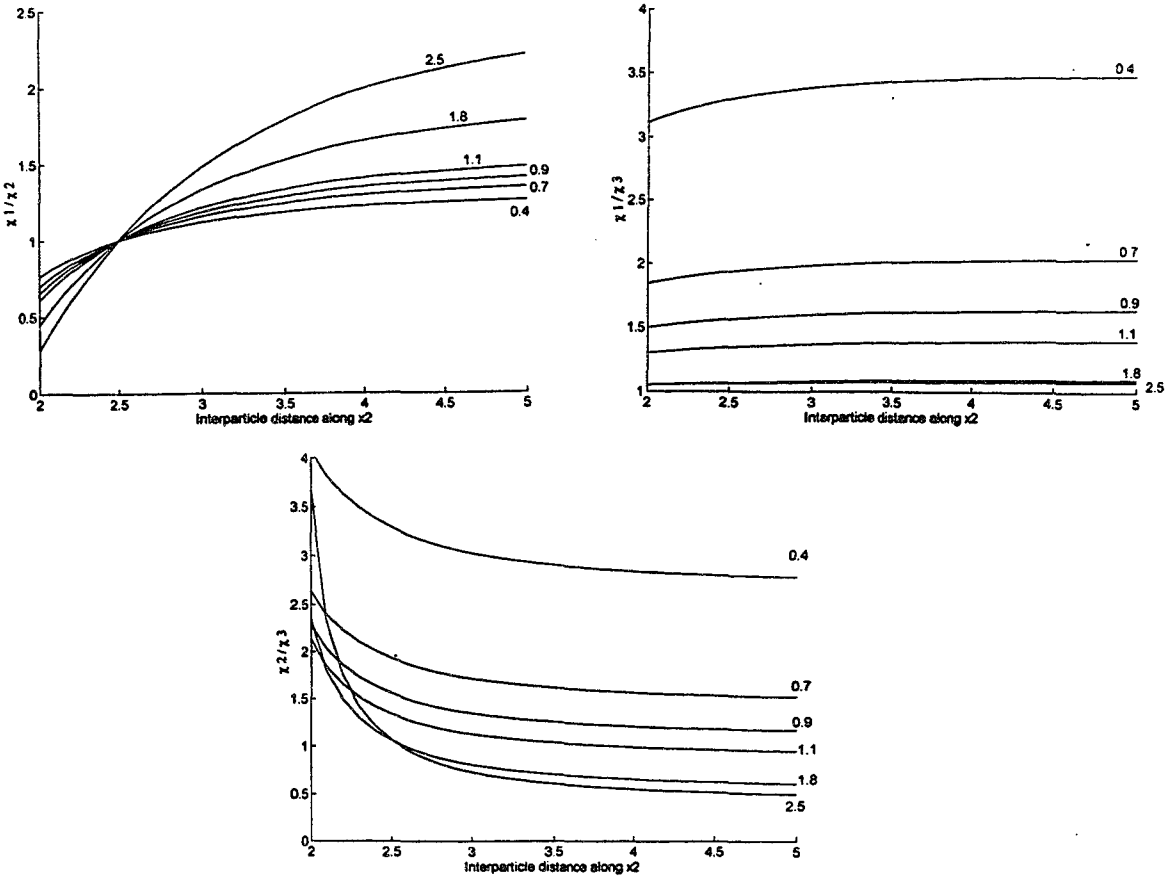

FIGURE A1.4. Plots of the ratios of the three principal susceptibilities for a planar array of particles as a function of the separation of particles along the x_2 direction. The distance of the particles along r_1 was fixed to 2.5 b-units. Numbers as in Figure A1.2.

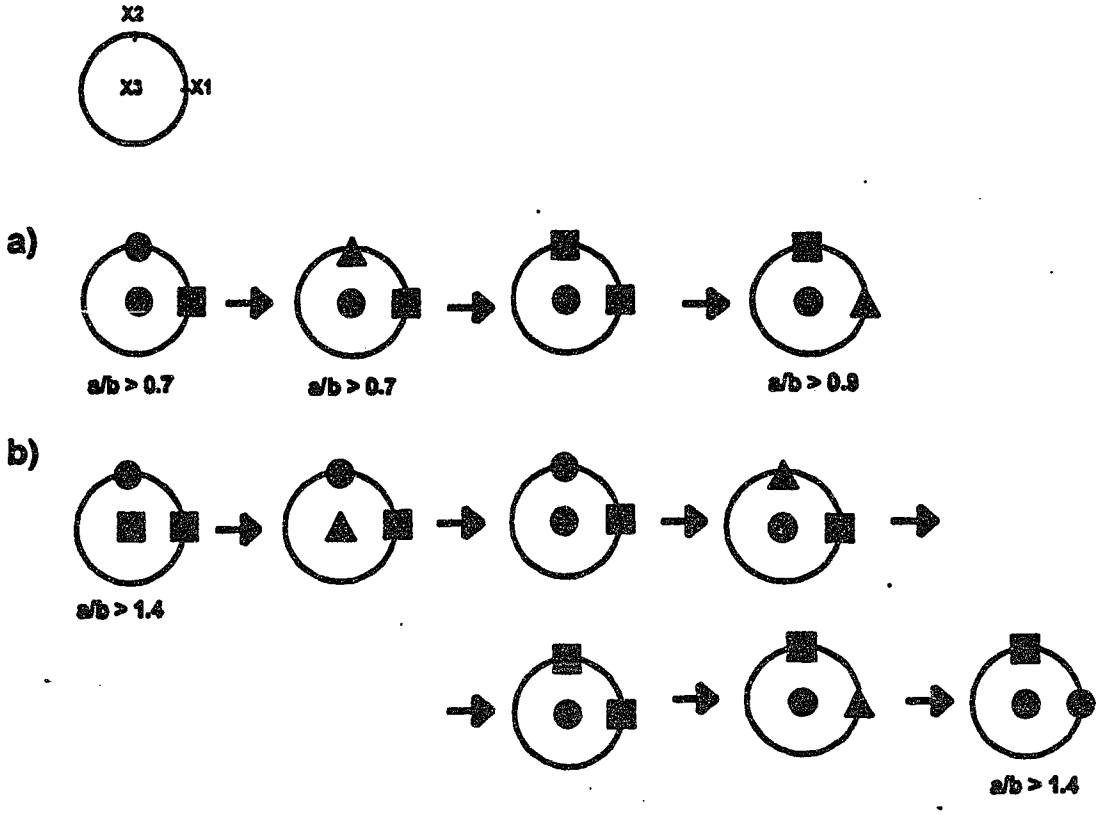

FIGURE A1.5. Schematic evolution of the magnetic fabric of the planar array of particles as a function of the interparticle separation along x_2. a) Oblate particles. b) Prolate particles. Note that certain configurations can only be attained for certain values of the polar/equatorial axial ratio (a/b) of the particles as indicated. a) Oblate particles. b) Prolate particles. Symbols as in Figure A1.3.

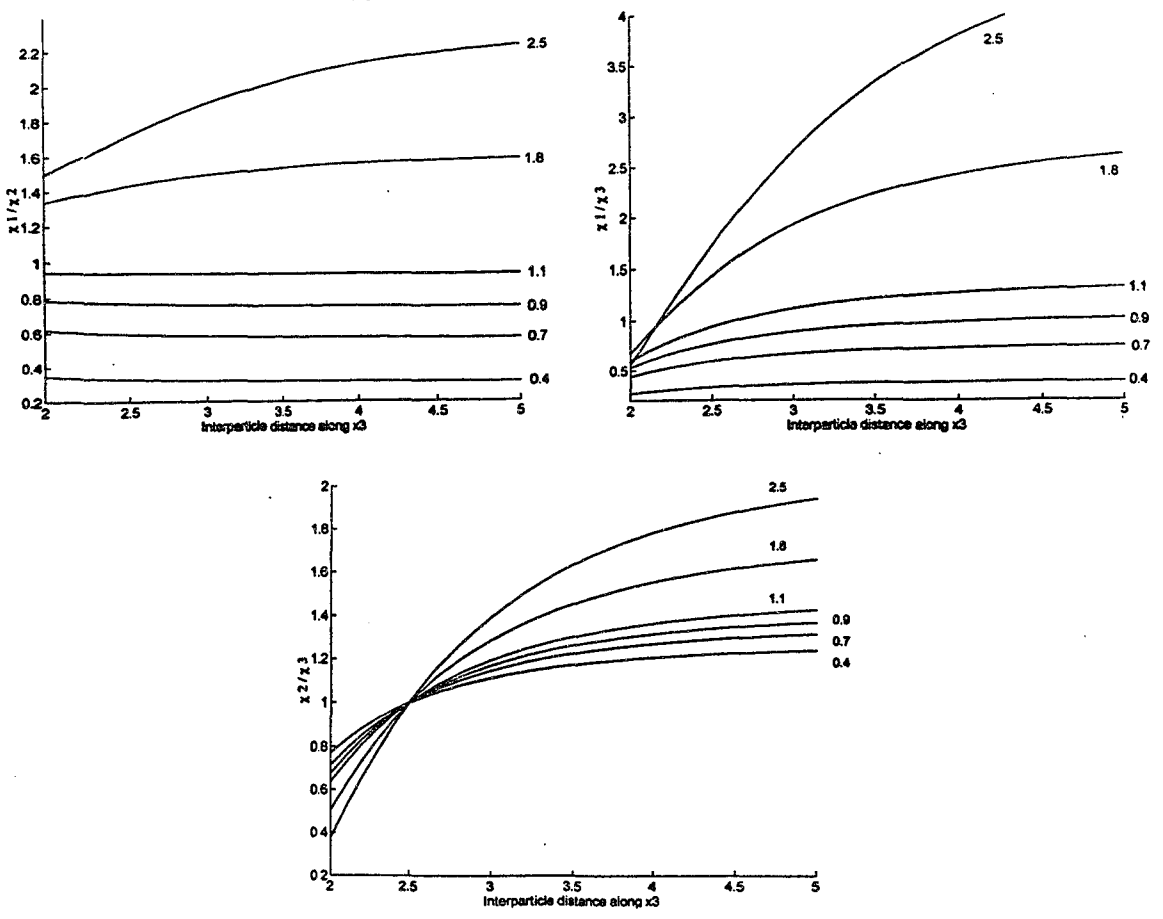

FIGURE A1.6. Plots of the ratios of the three principal susceptibilities for a 3D array of particles as a function of the separation along the x_3 direction. The separations along x_1 and x_2 were fixed at 3 and 2.5 b-units, respectively. Numbers as in Figure A1.2.

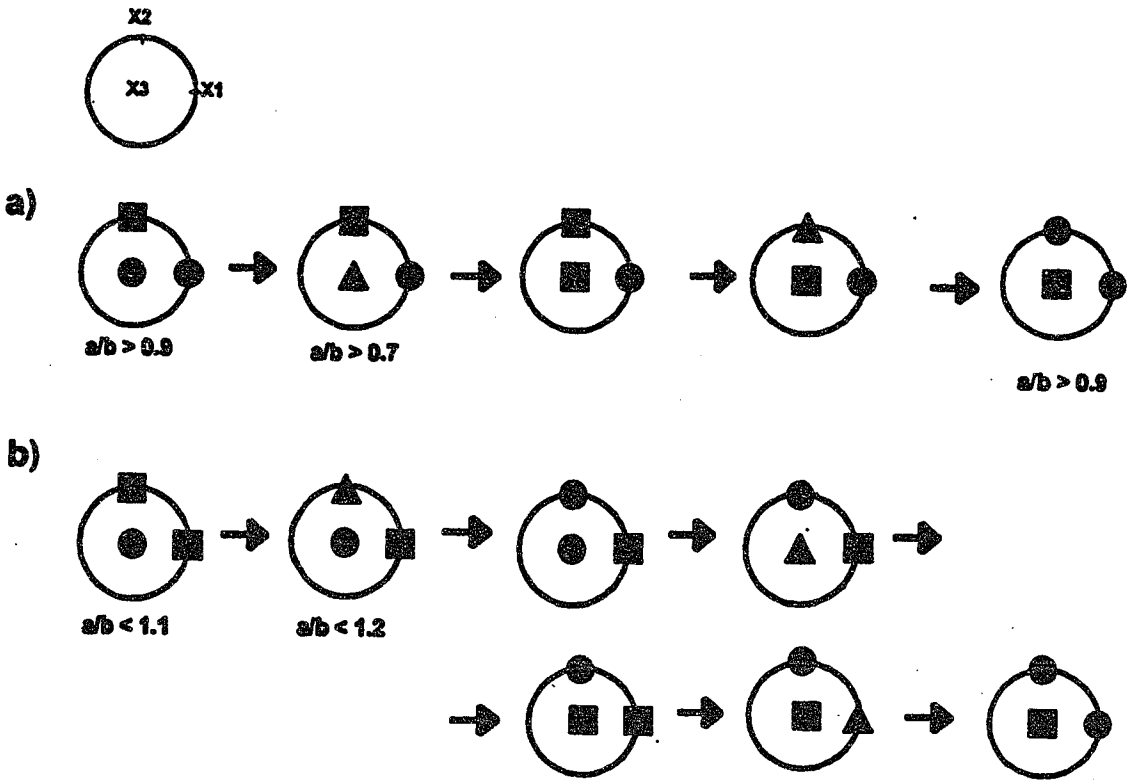

FIGURE A1.7. Schematic evolution of the magnetic fabric of the 3D array of particles as a function of the interparticle separation along x_3. a) Oblate particles. b) Prolate particles. Symbols and numbers as in Figure A1.5.

with that inferred from the measurement of AMS can, at least in principle, be most simply explained in terms of interacting ferromagnetic particles, without the need for making reference to their magnetic-domain state.

It was also shown that the resulting magnetic fabric is a complex function of the shape of individual particles, their orientation and distribution. The complexity of this function will certainly prevent us from firmly establishing a one to one correlation between the observed mineral fabric (as for example in thin sections) and the measured magnetic fabric in at least those cases in which magnetic interaction is likely to occur. According to Hargraves et al. (1991) and Sprowl (1990), the usual content of ferromagnetic grains in most igneous rocks is around 1 vol %, enough to grant magnetic interactions. Therefore, not only the measured AMS in these rocks should be interpreted in terms of grain distributions and not in terms of grain orientations, but also the notion that there is a unique relation between, say, flow direction and principal susceptibilities should be abandoned. Thus, a new model linking the fluid behavior of magma, lava or pyroclastic flows with the measured AMS becomes necessary. The general dynamic aspects of such a model are discussed in Chapters 4 and 5.

Another aspect that deserves attention is the effect of the remanence on the measured AMS. In the development of the model it was made clear that the enhancing field is the result of the magnetization of the particles, and it was assumed that such magnetization was entirely due to the action of the externally applied magnetic field. This is valid if the ratio of the induced to remanent magnetization is much larger than one. If this ratio is near or smaller than one, however, the enhancing field experienced by the central particle will be due to the remanent magnetization of its nearest neighbors. In other words, even in the absence of an external field to the array, the central particle in figure 1 may have an induced magnetization due to the remanences of the other particles. The inclusion of a remanence will in general complicate the situation to the extent that any analytical study would be most impractical, although its effects can be illustrated by the set of five particles shown in Figure A1.8.

Let us assume that all the particles have identical properties, and that for simplicity, they are magnetically isotropic. In Figure A1.8a, the arrows in the outer particles represent their remanent

magnetization while the small arrow in the central particle represents the induced magnetization of this particle due to the effect of the remanences of the other four (the remanence of the central particle is omitted only for clarity in the figure). If a weak enough magnetic field is now applied to the array in a direction perpendicular to the remanence of the particles so that a small induced magnetization is produced in the particles as shown in figure A1.8b, the total induced magnetization of the central particle will not be parallel to the applied field, giving the impression that this particle is not isotropic. The smaller the ratio of the induced (due exclusively to the external field) to the remanent magnetization of the particles, the stronger the apparent deviations from the isotropic case. It is important to remark that it is not suggested that the remanence of a given particle can influence the susceptibility of this same particle, but rather that the remanence of one particle can influence the susceptibility of other neighboring particles due to their magnetic interaction.

A line of evidence that seems to support the above considerations is the process of re-orientation of the measured principal directions of susceptibility described by Park et al. (1988) as well as the "enhancing" effect on the magnetic fabric of specimens subjected to demagnetization by application of alternating magnetic fields mentioned by Tarling and Hrouda (1993). The "cleaning" process results, generally, in the partial reduction of the strength of the remanence of any given particle, and therefore is reasonable to suggest that the changes in magnetic fabric with magnetic demagnetization are a consequence of a modification on the way in which magnetic interaction is taking place within a particular specimen. It is not possible, however, to be sure whether the magnetic cleaning completely eliminates the effects of the interaction therefore revealing the magnetic fabric associated with grain orientations (as for example assumed by Park et al., 1988). At most, if either a stable orientation of the magnetic fabric is reached, or if the magnetic fabric was not affected at during the magnetic cleaning, it would only be possible to assure that the remanence was not important in the definition of the measured AMS. To conclude based in this evidence alone that magnetic interaction between grains is not important may be misleading.

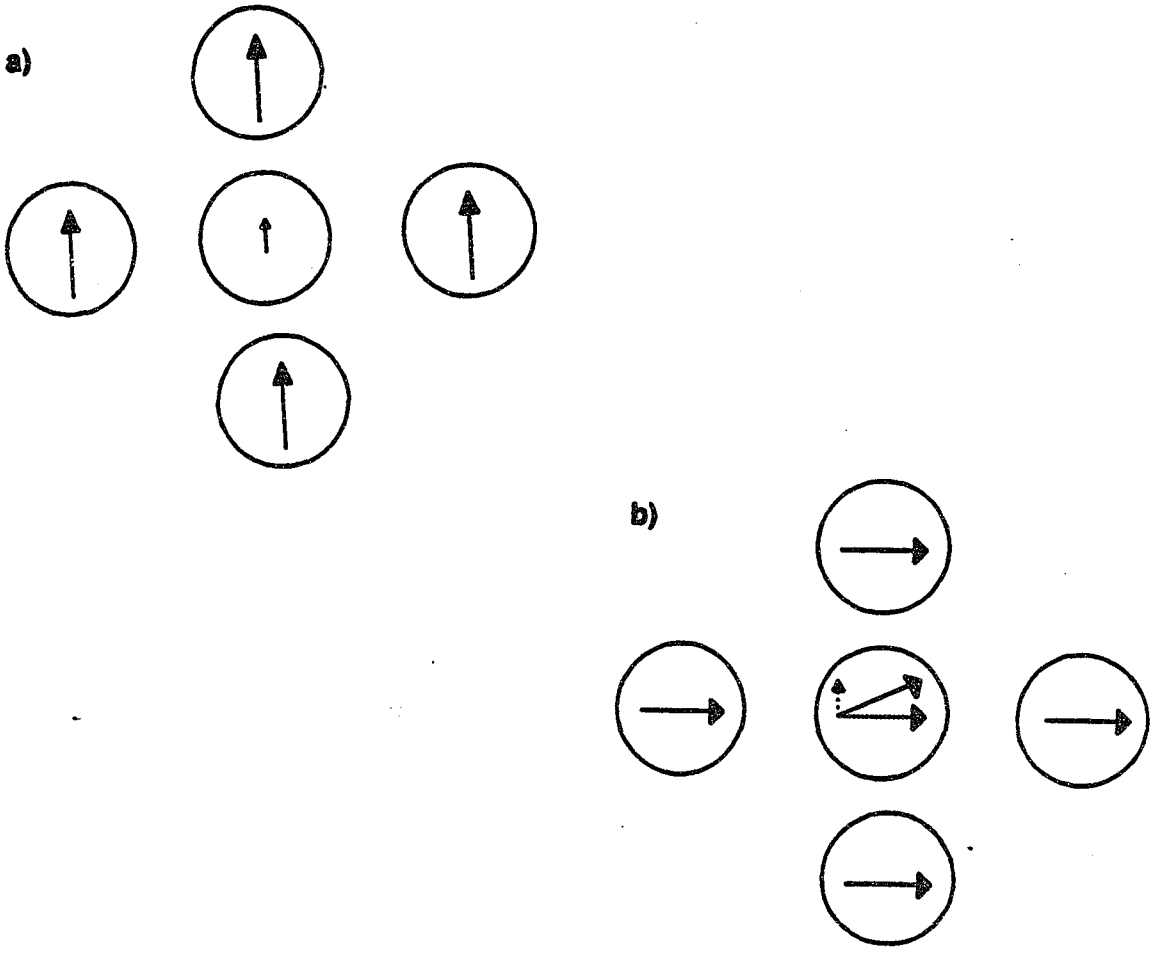

FIGURE A1.8. System of five identical isotropic particles. a) The remanence of the outer particles (large arrows) produce an induced magnetization in the central particle (small arrow). b) An external magnetic field applied in the plane of the figure perpendicular to the remanence of the particles in a) produces an induced magnetization in all the particles as indicated. The net induced magnetization in the central particle therefore has two components and is not parallel to the external field, as it would be if the remanences of the surrounding particles were negligible.

CONCLUSIONS

Despite all the approximations necessary to arrive to the proposed model, it has been shown that whenever magnetic interaction between neighbor particles is present the measured AMS is more likely to be defined by this interaction rather than by single-grain shape anisotropy. In these cases, the inferred magnetic fabric may have a completely different orientation relative to any directly observable mineral fabric, and the source of AMS should be sought for in processes capable of producing (or changing) grain distributions rather than grain orientations. Clearly, if grain orientations are consistent with the textural anisotropy, the measured AMS will be more clearly defined. Magnetic interaction due to a strong remanent magnetization of individual particles can also influence to some extent the measured magnetic fabric. Changes in the measured magnetic fabric during magnetic cleaning will in general reveal whether this type of magnetic interaction is likely to be important in a given specimen, although stability of the measured magnetic fabric should not be interpreted as ruling out the possibility of magnetic interactions related to induced magnetization.

APPENDIX 2: CODE OF ORIGINAL MATLAB FUNCTIONS

The MATLAB code was used to analyze most of the data in this work, and to generate some of the figures, because of its relative simplicity of operation, its flexibility (it allows the inclusion of case-specific requirements very easily), and the good quality of the figures generated requiring a minimal of post-editing work. A total of nine original MATLAB functions are listed in this appendix, all of which were used at several stages during the completion of the present study. Adjustments were necessary to produce some of the figures in their final version depending on the specific circumstances, but these adjustments do not interfere with the general nature of the nine functions listed below. An example is the substitution of the "plot" command by the "fill" command in order to generate a figure with solid symbols. The list of specific commands used to generate a particular figure is not included due to their very restricted interest, but rather the programs included are of a general character and can be used in other contexts than that of AMS. Although all efforts were made to test the correct function of the programs below in a general context, it is not uncommon in software development to overlook very specific situations in which the code may not operate correctly. The identification of these "bugs" is only possible by the continued use of the software on very different situations. In this sense, it may be important to note that the programs below are an XX.1 generation.

```
function reaprj1(datadec,datainc,opdec,opinc,ldec,linc,lnstyle);
%
% REAPRJ1(datadec,datainc,opdec,opinc,ldec,linc,lnstyle)
% DRAWS EQUAL AREA PROJECTIONS IN A PLANE WITH ANY ORIENTATION.
% ALL DATA ARE CONVERTED TO LIE IN ONE HEMISPHERE.
% THE ORIGINAL AXES OF REFERENCE ARE (screen coordinates):
% x=N, y=E and out=+Z(down), BUT THE DEFAULT AXES ARE
% x=E, y=N AND out=-Z(up).
% (hence the default projection is in the upper hemisphere, a lower hemispher projection is
% obtained by setting  he = 1).
% OPDEC AND OPINC ARE THE COORDINATES OF THE OBSERVATION POINT
% (NORMAL TO THE SCREEN, OR "OUT"), WHEREAS
% LDEC AND LINC ARE THE COORDINATES OF A POINT NORMAL TO OP
% (A POINT ON THE SCREEN) ALONG THE "x" AXIS.

if nargin ~= 7
 if nargin ~= 6
  if nargin ~= 3
```

```
  if nargin ~= 2
   error('Wrong number of input arguments')
  end
 end
end
end

if nargin == 6
 lnstyle = 'y*';
elseif nargin == 3
 lnstyle = opdec;
 opdec =  0;
 opinc = -90;
 ldec  = 90;
 linc  =  0;
elseif nargin == 2
 lnstyle = 'y*';
 opdec =  0;
 opinc = -90;
 ldec  = 90;
 linc  =  0;
end
p=180/pi;


 sz=sph2car([opdec,opinc]);
 sz=sz(:);
 sx=sph2car([ldec,linc]);
 sx=sx(:);
 sy=[sz(2)*sx(3)-sz(3)*sx(2);sz(3)*sx(1)-sz(1)*sx(3);sz(1)*sx(2)-sz(2)*sx(1)];
 X=sph2car([datadec,datainc]);

 xz = sx' * sz;              % Check orthogonality of sz and sx
 if abs(xz) >= 0.017         % allows up to one degree non-orthogonality
  error('The pair observation point-east coordinate is not perpendicular')
 end

 a11=[1, 0, 0] * sx;             % rotation matrix
 a12=[0, 1, 0] * sx;
 a13=[0, 0, 1] * sx;
 a21=[1, 0, 0] * sy;
 a22=[0, 1, 0] * sy;
 a23=[0, 0, 1] * sy;
 a31=[1, 0, 0] * sz;
 a32=[0, 1, 0] * sz;
 a33=[0, 0, 1] * sz;

a = [a11, a12, a13; a21, a22, a23; a31, a32, a33];

XP=a*X';                  % actual rotation

xp=XP(1,:);
yp=XP(2,:);
zp=XP(3,:);
```

```
dec=atan2(yp,xp);
inc=asin(zp);

he = 0;                %This should be changed to 1 for lower hemisphere projections

for i=1:length(xp),
 if he == 0
  if inc(1,i) < 0,
  dec(1,i)=dec(1,i)+pi;
   inc(1,i)=-inc(1,i);
  end
 elseif he ==1
  if inc(1,i) > 0,
  dec(1,i)=dec(1,i)+pi;
   inc(1,i)=-inc(1,i);
  end
 end
end

rho = sqrt(2)*sqrt(1-abs(sin(inc)));    % 'Radius' of projected points.

xx  = rho .* cos(dec);                  % Coordinates of projection.
yy  = rho .* sin(dec);

eaprgrid                                % generate grid and

if strcmp(lnstyle,'max')                % make the plot
 [xx, yy] = squares(xx,yy);
 plot(xx,yy,'r-')
elseif strcmp(lnstyle,'int')
 [xx, yy] = triangle(xx,yy);
 plot(xx,yy,'y-')
else
 plot(xx,yy,lnstyle);
end

tex=a*eye(3);                           % generate labels
texdec=atan2(tex(2,:),tex(1,:));
texinc=asin(tex(3,:));
for i=1:length(texdec)
 if texdec(1,i) < 0
  texdec(1,i) = 2*pi + texdec(1,i);
 end
end
if (texdec(1,1) == pi/2) & (abs(texinc(1,1)) < 1e-5)
 text(-.05,1.6,'N')
 if ((texdec(1,2) < 1e-5) | (abs(texdec(1,2) - 2*pi) < 1e-5)) & (abs(texinc(1,2)) < 1e-5)
  text(1.5,0,'E')
 elseif ((texdec(1,3) < 1e-5) | (abs(texdec(1,3) - 2*pi) <1e-5)) & (abs(texinc(1,3)) < 1e-5)
  text(1.5,0,'Down')
 elseif (texdec(1,2) == pi) & (abs(texinc(1,2)) < 1e-5)
  text(1.5,0,'W')
 elseif (texdec(1,3) == pi) & (abs(texinc(1,3)) < 1e-5)
  text(1.5,0,'Up')
```

```
 else
  an=round(10*p*acos([0 1 0]*tex(2,:)'))/10;
  if tex(1,3) > 0
   an=-an;
  end
  text(1.5,0,num2str(an));text(1.7,0,' from E')
 end
elseif (texdec(1,1) == 3*pi/2) & (abs(texinc(1,1)) < 1e-5)
 text(-.05,1.6,'S')
 if ((texdec(1,2) < 1e-5) | (abs(texdec(1,2) - 2*pi) < 1e-5)) & (abs(texinc(1,2)) < 1e-5)
  text(1.5,0,'E')
 elseif (texdec(1,3) == pi) & (abs(texinc(1,3)) < 1e-5)
  text(1.5,0,'Up')
 elseif (texdec(1,2) == pi) & (abs(texinc(1,2)) < 1e-5)
  text(1.5,0,'W')
 elseif ((texinc(1,3) < 1e-5) | (abs(texdec(1,3) - 2*pi) < 1e-5)) & (abs(texinc(1,3)) < 1e-5)
  text(1.5,0,'Down')
 else
  an=round(10*p*acos([0 1 0]*tex(2,:)'))/10;
  if tex(1,3) > 0
   an=-an;
  end
  text(1.5,0,num2str(180-an));text(1.7,0,' from E')
 end
elseif (texdec(1,2) == pi/2) & (abs(texinc(1,2)) < 1e-5)
 text(-.05,1.6,'E')
 if ((texdec(1,1) < 1e-5) | (abs(texdec(1,1) - 2*pi) < 1e-5)) & (abs(texinc(1,1)) < 1e-5)
  text(1.5,0,'N')
 elseif (texdec(1,3) == pi) & (abs(texinc(1,3)) < 1e-5)
  text(1.5,0,'Up')
 elseif (texdec(1,1) == pi) & (abs(texinc(1,1)) < 1e-5)
  text(1.5,0,'S')
 elseif ((texdec(1,3) < 1e-5) | (abs(texdec(1,3) - 2*pi) < 1e-5)) & (abs(texinc(1,3)) < 1e-5)
  text(1.5,0,'Down')
 else
  an=round(10*p*acos([1 0 0]*tex(1,:)'))/10;
  if tex(1,3) > 0
   an=-an;
  end
  text(1.5,0,num2str(an));text(1.9,0,' from N')
 end
elseif (texdec(1,2) == 3*pi/2) & (abs(texinc(1,2)) < 1e-5)
 text(-.05,1.6,'W')
 if ((texdec(1,1) < 1e-5) | (abs(texdec(1,1) - 2*pi) < 1e-5)) & (abs(texinc(1,1)) < 1e-5)
  text(1.5,0,'N')
 elseif ((texdec(1,3) < 1e-5) | (abs(texdec(1,3) - 2*pi) < 1e-5)) & (abs(texinc(1,3)) < 1e-5)
  text(1.5,0,'Down')
 elseif (texdec(1,1) == pi) & (abs(texinc(1,1)) < 1e-5)
  text(1.5,0,'S')
 elseif (texdec(1,3) == pi) & (abs(texinc(1,3)) < 1e-5)
  text(1.5,0,'Up')
 else
  an=round(10*p*acos([1 0 0]*tex(1,:)'))/10;
  if tex(1,3) > 0
```

```
 an=-an;
 end
 text(1.5,0,num2str(180-an));text(1.7,0,' from N')
end
elseif (texdec(1,3) == pi/2) & (abs(texinc(1,3)) < 1e-5)
 text(-.05,1.6,'Down')
 if (texdec(1,2) == pi) & (abs(texinc(1,2)) < 1e-5)
  text(1.5,0,'W')
 elseif (texdec(1,1) == pi) & (abs(texinc(1,1)) < 1e-5)
  text(1.5,0,'S')
 elseif ((texdec(1,2) <1e-5) | (abs(texdec(1,2) - 2*pi) < 1e-5)) & (abs(texinc(1,2)) < 1e-5)
  text(1.5,0,'E')
 elseif ((texdec(1,1) < 1e-5) | (abs(texdec(1,1) - 2*pi) < 1e-5)) & (abs(texinc(1,1)) < 1e-5)
  text(1.5,0,'N')
 else
  an=round(10*p*acos([1 0 0]*tex(1,:)'))/10;
  if tex(1,3) > 0
   an=-an;
  end
  text(1.5,0,num2str(an));text(1.7,0,' from N')
 end
elseif (texdec(1,3) == 3*pi/2) & (abs(texinc(1,3)) < 1e-5)
 text(-.05,1.75,'Up');
 if (texdec(1,2) == pi) & (abs(texinc(1,2)) < 1e-5)
  text(1.5,0,'W')
 elseif (texdec(1,1) == pi) & (abs(texinc(1,1)) < 1e-5)
  text(1.5,0,'S')
 elseif ((texdec(1,2) < 1e-5) | (abs(texdec(1,2) - 2*pi) < 1e-5)) & (abs(texinc(1,2)) < 1e-5)
  h1=text(1.5,0,'E'); set(h1(1),'fontsize',10)
 elseif ((texdec(1,1) < 1e-5) | (abs(2*pi - texdec(1,1))  < 1e-5)) & (abs(texinc(1,1)) < 1e-5)
  text(1.5,0,'N')
 else
    an=round(10*p*acos([1 0 0]*tex(1,:)'))/10;
  if tex(1,3) < 0
   an=-an;
  end
  text(1.5,.10,num2str(an));text(2.5,.10,'');
 end
else
 text(-.15,1.6,'dE = ');text(.15,1.6,num2str(p*texdec(1,2)))
 text(-.15,1.5,'iE = ');text(.15,1.5,num2str(p*texinc(1,2)))
 text(1.5,.1,'dN = ');text(1.8,.1,num2str(p*texdec(1,1)))
 text(1.5,-.1,'iN = ');text(1.8,-.1,num2str(p*texinc(1,1)))
end
axis('equal'); axis('off')
hold off



function Cn=deapw(dec, inc)
%DEAPW Density - equal area projections of points on lower hemisphere
%    using Watson-like kernel (Fisher et al., 1993).
%    It uses weigw to assign a weight to each point in the sphere
% Cn = DEAPW(DEC,INC)
```

```
%   Returns the value of the smoothing parameter finally used in weigw

% Creates grid of points for later plotting, and
% pick up only those inside the area of the projection.

r = sqrt(2);
g = linspace(-r,r,40);
[x, y] = meshgrid(g,g);
[m, n] = size(x);
z = sqrt(r^2 - x .^2 - y .^2);
x = x(:);
y = y(:);
z = z(:);
j = 0;
for i = 1:length(z)
 if imag(z(i,:)) == 0
  j = j + 1;
  xx(j,:) = x(i,:);
  yy(j,:) = y(i,:);
  zz(j,:) = z(i,:);
 end
end
clear g

% Transform points in the projection to points in the unitary sphere

decp = 90 - atan2(yy,xx) * 180/pi;
incp = asin(1 - (xx.^2 + yy.^2)/2) * 180/pi;

% Calls weigw to calculate the density of each point on the projection

p = [dec, inc];
P = [decp, incp];
sf=input('Enter the desired smoothing parameter Cn (0 if unknown)  ');

if sf == 0
 [t1, t2, t3, d] = weigw(p,P);
else
 [t1, t2, t3, d] = weigw(p,P,sf);
end

% Associate the density with the correponding point in the projection

j = 0;
for i = 1:length(z)
 if imag(z(i,:)) == 0
  j = j + 1;
  z(i,:) = d(j,:);
 else
  z(i,:) = 0;
 end
end

mincon=(max(z)-min(z))/4;
```

```
con=linspace(mincon,max(z),11);
for i=11:-2:1
 con(:,i)=[];
end

Cx=num2str(t3);
ax=reshape(x,m,n);
ay=reshape(y,m,n);
ad=reshape(z,m,n);
figure(2)
contour(ax,ay,ad,con);
text(1.1,1,'Cn =');text(1.3,.85,Cx)
text(-.05,1.6,'N');text(1.5,0,'E')
axis('square');axis('off')
hold on
reaproj1(dec,inc,'w*');


function [A, B, C, Wn]=weigw(p,P,CN);
% Weight given to point p when estimating the density at P
% for equal area projection contour plots using WAtson-like kernel.
% Wn = weigw(p,P,CN)
% p can be either a m x 3 or a m x 2 matrix containing the coordinates
% of the points in the array from which the density is to be calculated.
% P can also be n x 3 or n x 2, and it contains the points on the sphere
% (or hemisphere) in which the density is to be estimated.
% In both p and P:
% If m x 3 it is assumed that coordinates are x, y, z
% If m x 2 it is assumed that coordinates are dec, inc (r=1).
% CN is a smoothing factor. If not provided, a suitable value is
% automatically calculated.

% If no region is given (P=[]), the lower hemisphere of a sphere is used

if nargin == 3
 Cn = CN;
else
 Cn=smoothw(p,P);
end

if nargin == 1
 x1 = linspace(-1,1,40);
 [x, y] = meshgrid(x1,x1);
 z = sqrt(1 - x.^2 - y.^2);
 [a, b]=size(z);
 x=x(:);
 y=y(:);
 z=z(:);
 j=0;
 for i=1:length(z)
  if imag(z(i,:)) == 0
   j=j+1;
   xx(j,:)=x(i,:);
   yy(j,:)=y(i,:);
```

```
  zz(j,:)=-z(i,:);
 end
end
P1 = [xx yy zz];
end

% Transform coordinates of the region to Cartesian, if necessary

[g,h]=size(P);
if h == 2
 P1 = sph2car(P);
else
 P1 = P;
end

% Transform coordinates of the collection of points to Cartesian, if needed

[m, n]=size(p);
if n == 2
 p1 = sph2car(p);
else
 p1 = p;
end

% Calculate the weight of each point in the collection (p)
% for each point in the area of interest (P)

u  = 0:.01:1;
u1  = exp(Cn* u.^2);
U  = diff(u);
U1  = (u1(1,1:length(u1)-1) + u1(1,2:length(u1)))/2;
area= sum(U .* U1);
w1 = 1/(4*pi*area);
w2 = (p1 * P1').^2;
w3 = sum(w1 * exp(Cn * w2));
w3=w3(:);

if nargin == 1
 wn = zeros(size(z));
 j=0;
  for i=1:length(z)
   if imag(z(i,:)) == 0
    j=j+1;
    wn(i,:)=w3(j,:);
    z(i,:)=-z(i,:);
   else
    z(i,:)=0;
   end
  end
 if nargout == 0
  Wn = reshape(wn,a,b);
  x = reshape(x,a,b);
  y = reshape(y,a,b);
  z = reshape(z,a,b);
```

```
 surf(x,y,z,Wn)
 colormap(jet)
elseif nargout == 4
 A = x;
 B = y;
 C = z;
 Wn=Wn;
end

elseif nargin == 2
 A  = [];
 B  = [];
 C  = Cn;
 Wn = w3;
elseif nargin == 3
 A  = [];
 B  = [];
 C  = Cn;
 Wn = w3;
 end
end


function Cn = smoothw(p,P)
% Selection of a suitable Smoothing factor, Cn
% for the calculation of density contour lines
% in the exploratory analysis of 3D directional data

% Transform coordinates of the region to Cartesian, if necessary

[g,h]=size(P);
if h == 2
 P1 = sph2car(P);
else
 P1 = P;
end

% Transform coordinates of the collection of points to Cartesian, if needed

[m, n]=size(p);
if n == 2
 p1 = sph2car(p);
else
 p1 = p;
end

CN = 1:.5:50;
d1 = zeros(m,length(CN));
for i = 1:m
 if i == 1
  p2 = p1(2:m,:);
  P2 = p1(i,:);
  for j = 1:length(CN)
   cn(1,1) = CN(:,j);
```

```
 [t1, t2, t3, d2]=weigw(p2,P2,cn);
 d1(i,j)=d2;
 end
elseif i == m
 p2 = p1(1:m-1,:);
 P2 = p1(i,:);
 for j = 1:length(CN)
  cn(1,1) = CN(:,j);
  [t1, t2, t3, d2]=weigw(p2,P2,cn);
  d1(i,j)=d2;
 end
else
 p2 = [p1(1:i-1,:); p1(i+1:m,:)];
 P2 = p1(i,:);
 for j = 1:length(CN)
  cn(1,1) = CN(:,j);
  [t1, t2, t3, d2]=weigw(p2,P2,cn);
  d1(i,j)=d2;
 end
end
end
L = sum(log(d1));
Cn = CN(1,find(L == max(L)));

if Cn == 1
 figure(1)
 plot(CN,L')
 xlabel('Smoothing factor, Cn')
 ylabel('Pseudo log-likelihood, L(Cn)')
 set(gca,'xtick',1:1:50)
 set(gca,'xgrid','on')
 set(gca,'xticklabels',[])
 h=get(gca,'ylim');
 x=0;
 for i=1:10
  x=x+5;
  text(x,h(1,2)+1,int2str(x))
 end
else
 Cn = Cn;
end


function a=sph2car(b)
% Conversion from Spherical (geological) coordinates to Cartesian.
%     A = sph2car(B)
% B can be either a n x 3 matrix, containing dec, inc and r
% or a n x  2 matrix, where r is assumed = 1.
% A is a n x 3 matrix containing n - x,y,z triplets.
% Note that by convention:
%    Declination (0:360; 0=N, 90=E)
%    Inclination (-90:90; += plunge down)
% and
%    x = North; y = East; z = Down.
```

```
[n, m]=size(b);
if m >= 3
 error('Size of B needs to be either n x 3 or n x 2')
elseif m == 3
 r = b(:,3);
elseif m == 2
 r = ones(n,1);
end

p = 180/pi;

x(:,1) = r(:,1) .* cos(b(:,1)/p) .* cos(b(:,2)/p);
y(:,1) = r(:,1) .* sin(b(:,1)/p) .* cos(b(:,2)/p);
z(:,1) = r(:,1) .* sin(b(:,2)/p);

a = [x y z];


function eaprgrid
% Generates the circle and tick marks used in all equal area projections.

r  = sqrt(2);                % equatorial circle and reference points
x  = r * sin(0:pi/100:2*pi);
y  = r * cos(0:pi/100:2*pi);
xtic=[(r-.04)*sin(0:pi/18:2*pi); r*sin(0:pi/18:2*pi)];
ytic=[(r-.04)*cos(0:pi/18:2*pi); r*cos(0:pi/18:2*pi)];
tic = r * sqrt(1-sin(0:pi/9:pi/2));
tic = [-tic tic];
z  = zeros(size(tic));

plot(x,y,'w-',z,tic,'w+',tic,z,'w+')  % create plot-grid
hold on
for i = 1:max(size(xtic))
 plot(xtic(:,i),ytic(:,i),'w-')
end


function [sx, sy]=squares(xx,yy);
% create 'square' symbols to plot in equal area projections

sf = 2.5;        % scale factor

sx = [xx-sf*(.035) xx+sf*(.035) xx+sf*(.035) xx-sf*(.035) xx-sf*(.035)]';
sy = [yy-sf*(.025) yy-sf*(.025) yy+sf*(.025) yy+sf*(.025) yy-sf*(.025)]';


function [tx, ty]=triangle(xx, yy)
% create 'triangle' symbols to be plotted in equal area projections

sf = 2.5;        % scale factor

tx = [xx-sf*(.025) xx+sf*(.025) xx        xx-sf*(.025)]';
ty = [yy-sf*(.045) yy-sf*(.045) yy+sf*(.045) yy-sf*(.045)]';
```

```
function interactive
% Program used to calculate the ratio of two principal susceptibilities
% with distance along a fixed direction, as in the Appendix 1.
% It also calculates the magnetic fabric using the B-parameter.
% Input requires the ratio of the axes of the particle,
% the polar demagnetizing factor (easy to get from Stoner, 1945),
% and to answer a series of questions about the specific array.
% The sections reported in the appendix have fixed limits so that the multiple
% plots there described could be produced.
% The commands used to plot the figures have been updated to use MATLAB 4.2
% therefore caution is necessary if using an earlier version.


a    = input('Enter the ratio polar / equatorial axes of particle,   ');
D_a  = input('and the "polar" demagnetizing factor   ');
geom = input('Do you want a line, a plane or a 3D array (1-3)?   ');

vol = 4 * pi * a / 3;

D_b = 0.5 * (1 - D_a);          % equatorial demag. factor
r = 2:.1:5;                     % interparticle distance as "aligned" axis multiples.
r_o = ones(size(r));

if geom == 1,

geom_a = input('Are the particle-axis parallel to x1, x2 or x3 (1-3)? ');

 if geom_a == 1,
 susc_p = r_o ./ (r_o * D_a - (r_o * vol ./ (pi * r.^3)));
 susc_n = r_o ./ (r_o * D_b + (r_o * vol ./ (2* pi * r.^3)));
 susc_r = susc_p ./ susc_n;
 figure(1)
 plot(r,susc_r,'-')
 xlabel('Interparticle distance (polar-axis units)')
 ylabel('c 1 / c 2')
 set(gca,'YlabelFontname','symbol')
 text(0.2,0,'X1 / X3 plot is identical to this because X2 = X3')

 elseif geom_a == 2,
 susc_1 = r_o ./ (r_o * D_b - (r_o * vol ./ (pi * r.^3)));
 susc_2 = r_o ./ (r_o * D_a + (r_o * vol ./ (2* pi * r.^3)));
 susc_3 = r_o ./ (r_o * D_b + (r_o * vol ./ (2* pi * r.^3)));
for i=1:length(susc_1),
B_1 = sort([susc_1(1,i) susc_2(1,i) susc_3(1,i)]);
B(1,i) = (B_1(1,1) - 2*B_1(1,2))/B_1(1,3) + 1;
end

 elseif geom_a == 3,
 susc_1 = r_o ./ (r_o * D_b - (r_o * vol ./ (pi * r.^3)));
 susc_2 = r_o ./ (r_o * D_b + (r_o * vol ./ (2* pi * r.^3)));
 susc_3 = r_o ./ (r_o * D_a + (r_o * vol ./ (2* pi * r.^3)));
for i=1:length(susc_1),
B_1 = sort([susc_1(1,i) susc_2(1,i) susc_3(1,i)]);
B(1,i) = (B_1(1,1) - 2*B_1(1,2))/B_1(1,3) + 1;
```

```
end

else,
break
end

if geom_a ~= 1,

figure(1)
plot(r,susc_1./susc_2,'b-')
axis([2 5 0 5])
set(gca,'Box','off')
xlabel('Interparticle distance')
ylabel('c 1 / c 2')
set(get(gca,'ylabel'),'fontname','symbol')
hold on

figure(2)
plot(r,susc_1./susc_3,'b-')
axis([2 5 1 5])
set(gca,'Box','off')
xlabel('Interparticle distance')
ylabel('c 1 / c 3')
set(get(gca,'ylabel'),'fontname','symbol')
hold on

figure(3)
plot(r,susc_2./susc_3,'b-')
axis([2 5 0.3 3])
set(gca,'Box','off')
xlabel('Interparticle distance')
ylabel('c 2 / c 3')
set(get(gca,'ylabel'),'fontname','symbol')
hold on

figure(4)
plot(r,B,'b-')
axis([2 5 -.8 .8])
set(gca,'Box','off')
xlabel('Interparticle distance')
ylabel('B parameter')
hold on

end

elseif geom == 2,
geom_a = input('Is the particle-axis parallel or normal to the plane (1-2)? ');
if geom_a == 1,
geom_b = input('Is the particle-axis parallel to x1 or x2 (1-2)? ');
 if geom_b == 1,
  r_1   = input('Enter part.-separation along x1 as multiple of polar axis  ')
  susc_1 = r_o ./ (r_o * D_a - (vol/(2*pi)) * ((2/r_1^3)*r_o - r_o ./ r.^3));
  susc_2 = r_o ./ (r_o * D_b - (vol/(2*pi)) * ( 2*r_o ./ r.^3 - (1/r_1^3)*r_o));
  susc_3 = r_o ./ (r_o * D_b + (vol/(2*pi)) * (r_o ./ r.^3 + (1/r_1^3)*r_o));
```

```
 for i=1:length(susc_1),
  B_1 = sort([susc_1(1,i) susc_2(1,i) susc_3(1,i)]);
  B(1,i) = (B_1(1,1) - 2*B_1(1,2))/B_1(1,3) + 1;
 end

elseif geom_b == 2
 r_1   = input('Enter part.-distance along x1 as multiple of equat.-axis  ')
 susc_1 = r_o ./ (r_o * D_b - (vol/(2*pi)) * ((2/r_1^3)*r_o - r_o ./ r.^3));
 susc_2 = r_o ./ (r_o * D_a - (vol/(2*pi)) * ( 2*r_o ./ r.^3 - (1/r_1^3)*r_o));
 susc_3 = r_o ./ (r_o * D_b + (vol/(2*pi)) * (r_o ./ r.^3 + (1/r_1^3)*r_o));
 for i=1:length(susc_1),
  B_1 = sort([susc_1(1,i) susc_2(1,i) susc_3(1,i)]);
  B(1,i) = (B_1(1,1) - 2*B_1(1,2))/B_1(1,3) + 1;
 end

else,
break
end


elseif geom_a == 2,
 r_1   = input('Enter part.-distance along x1 as multiple of equat.-axis  ');
 susc_1 = r_o ./ (r_o * D_b - (vol/(2*pi)) * ((2/r_1^3)*r_o - r_o ./ r.^3));
 susc_2 = r_o ./ (r_o * D_b - (vol/(2*pi)) * ( 2*r_o ./ r.^3 - (1/r_1^3)*r_o));
 susc_3 = r_o ./ (r_o * D_a + (vol/(2*pi)) * (r_o ./ r.^3 + (1/r_1^3)*r_o));
 for i=1:length(susc_1),
  B_1 = sort([susc_1(1,i) susc_2(1,i) susc_3(1,i)]);
  B(1,i) = (B_1(1,1) - 2*B_1(1,2))/B_1(1,3) + 1;
 end

else,
break
end

figure(1);
plot(r,susc_1./susc_2,'b-');
axis([2 5 0 2.5])
set(gca,'Box','off')
xlabel('Interparticle distance along x2')
ylabel('X1 / X2')
hold on

figure(2);
plot(r,susc_1./susc_3,'b-');
axis([2 5 1 4])
set(gca,'Box','off')
xlabel('Interparticle distance along x2')
ylabel('X1 / X3')
hold on

figure(3);
plot(r,susc_2./susc_3,'b-');
axis([2 5 0 4])
set(gca,'Box','off')
```

```
xlabel('Interparticle distance along x2')
ylabel('X2 / X3')
hold on

figure(4);
plot(r,B,'b-');
axis([2 5 -.8 .8])
set(gca,'Box','off')
xlabel('Interparticle distance along x2')
ylabel('B parameter')
hold on

elseif geom == 3,
geom_a = input('Is the particle axis parallel to x1, x2 or x3 (1-3)?  ');
 if geom_a == 1,
  r_1   = input('Enter part.-distance along x1 as multiple of polar-axis  ');
  r_2   = input('Enter part.-distance along x2 as multiple of equat.-axis  ');
  susc_1 = r_o ./(r_o * D_a - (vol/(2*pi)) * ((2/r_1^3)*r_o - (1/r_2^3)*r_o - r_o ./ r.^3));
  susc_2 = r_o ./(r_o * D_b - (vol/(2*pi)) * ((2/r_2^3)*r_o - (1/r_1^3)*r_o - r_o ./ r.^3));
  susc_3 = r_o ./(r_o * D_b - (vol/(2*pi)) * ( 2*r_o ./  r.^3 - (1/r_1^3)*r_o - (1/r_2^3)*r_o));

   for i=1:length(susc_1),
    B_1 = sort([susc_1(1,i) susc_2(1,i) susc_3(1,i)]);
    B(1,i) = (B_1(1,1) - 2*B_1(1,2))/B_1(1,3) + 1;
   end

 elseif geom_a == 2,
  r_1   = input('Enter part.-distance along x1 as multiple of equat.-axis  ');
  r_2   = input('Enter part.-distance along x2 as multiple of polar-axis  ');
  susc_1 = r_o ./(r_o * D_b - (vol/(2*pi)) * ((2/r_1^3)*r_o - (1/r_2^3)*r_o - r_o ./ r.^3));
  susc_2 = r_o ./(r_o * D_a - (vol/(2*pi)) * ((2/r_2^3)*r_o - (1/r_1^3)*r_o - r_o ./ r.^3));
  susc_3 = r_o ./(r_o * D_b - (vol/(2*pi)) * ( 2*r_o ./  r.^3 - (1/r_1^3)*r_o - (1/r_2^3)*r_o));

   for i=1:length(susc_1),
    B_1 = sort([susc_1(1,i) susc_2(1,i) susc_3(1,i)]);
    B(1,i) = (B_1(1,1) - 2*B_1(1,2))/B_1(1,3) + 1;
   end

 elseif geom_a == 3,
  r_1   = input('Enter part.-distance along x1 as multiple of equat.-axis  ');
  r_2   = input('Enter part.-distance along x2 as multiple of equat.-axis  ');
  susc_1 = r_o ./(r_o * D_b - (vol/(2*pi)) * ((2/r_1^3)*r_o - (1/r_2^3)*r_o - r_o ./ r.^3));
  susc_2 = r_o ./(r_o * D_b - (vol/(2*pi)) * ((2/r_2^3)*r_o - (1/r_1^3)*r_o - r_o ./ r.^3));
  susc_3 = r_o ./(r_o * D_a - (vol/(2*pi)) * ( 2*r_o ./  r.^3 - (1/r_1^3)*r_o - (1/r_2^3)*r_o));

   for i=1:length(susc_1),
    B_1 = sort([susc_1(1,i) susc_2(1,i) susc_3(1,i)]);
    B(1,i) = (B_1(1,1) - 2*B_1(1,2))/B_1(1,3) + 1;
   end

 else,
 break
 end
```

```
figure(1)
plot(r,susc_1./susc_2,'b-')
axis([2 5 .2 2.4])
set(gca,'Box','off')
xlabel('Interparticle distance along x3')
ylabel('X1 / X2')
hold on

figure(2)
plot(r,susc_1./susc_3,'b-')
axis([2 5 .2 4])
set(gca,'Box','off')
xlabel('Interparticle distance along x3')
ylabel('X1 / X3')
hold on

figure(3)
plot(r,susc_2./susc_3,'b-')
axis([2 5 .2 2])
set(gca,'Box','off')
xlabel('Interparticle distance along x3')
ylabel('X2 / X3')
hold on

figure(4)
plot(r,B,'b-')
axis([2 5 -.8 .8])
set(gca,'Box','off')
xlabel('Interparticle distance along x3')
ylabel('B parameter')
hold on

else
break
end
```

APPENDIX 3: TABLES

TABLE A3.1 Directions (D - declination, I - inclination) of the principal susceptibilities and position (depth from the top in cm, last column) of all specimens of Xitle pahoehoe lava used in Chapter 3. In unit xi01, data are given for the unrotated (XI01) and tilted corrected (XR01) cases.

Spec. #	K_{max} x 10^{-3}	D_{max}	I_{max}	K_{int} x 10^{-3}	D_{int}	I_{int}	K_{min} x 10^{-3}	D_{min}	I_{min}	S P
XI01.01	4.895	133	53	4.882	12	22	4.815	269	29	9
XI01.02	4.155	101	1	4.111	195	81	4.040	11	9	58
XI01.03	8.105	277	24	8.005	118	64	7.785	10	8	118
XI01.04	14.770	271	11	14.660	117	77	14.330	2	5	200
XI01.05	10.910	270	3	10.810	17	81	10.330	179	9	300
XI01.06	6.101	266	36	6.062	73	53	5.876	172	7	400
XI01.07	7.324	342	79	7.145	90	4	6.836	180	11	500
XI01.08	4.150	265	22	4.076	142	53	4.055	8	28	540
										900
XIR1.01	4.895	43	22	4.882	194	65	4.815	309	11	
XIR1.02	4.155	99	1	4.111	9	12	4.040	195	78	
XIR1.03	8.105	304	4	8.005	35	11	7.785	190	79	
XIR1.04	14.770	291	9	14.660	23	7	14.330	145	79	
XIR1.05	10.910	279	10	10.810	11	13	10.330	149	73	
XIR1.06	6.101	303	32	6.062	44	18	5.876	159	53	
XIR1.07	7.324	4	30	7.145	271	5	6.836	170	60	
XIR1.08	4.150	288	25	4.076	62	55	4.055	188	22	
XT22.1A	4.161	115	18	4.149	23	6	4.017	275	71	490
XT22.1B	3.625	109	17	3.618	18	2	3.509	281	73	493
XT22.2A	2.594	245	18	2.583	151	12	2.534	27	68	530
XT22.2B	2.631	202	15	2.625	294	5	2.574	41	74	533
XT22.4	2.263	238	20	2.252	147	2	2.214	50	70	542
XT22.3	2.113	151	9	2.109	243	14	2.075	29	73	550
XT22.5	8.420	228	17	8.347	137	2	8.238	41	73	560
XT22.6A	17.380	239	5	17.170	147	20	16.980	342	69	572
XT22.6B	14.350	233	12	14.260	143	1	14.050	50	78	575
XT22.7	9.903	236	10	9.844	326	0	9.684	58	80	584
XT22.8A	11.560	189	24	11.500	96	7	11.440	351	65	595
XT22.8B	10.530	163	2	10.420	73	2	10.360	309	87	598
										600

TABLE A3.1 (CONTINUED) Directions of principal susceptibilities and position of specimens used in Chapter 3.

Spec. #	K_{max} x 10^{-3}	D_{max}	I_{max}	K_{int} x 10^{-3}	D_{int}	I_{int}	K_{min} x 10^{-3}	D_{min}	I_{min}	S P
XI06.01A	1.388	263	18	1.383	5	33	1.381	148	51	0
XI06.01B	1.014	189	74	1.013	279	0	1.012	9	16	5
XI06.02	5.482	183	20	5.472	84	23	5.437	310	59	32
XI06.03	4.772	150	35	4.759	55	6	4.719	317	54	50
XI06.04	5.798	140	24	5.766	47	6	5.704	304	65	62
XI06.05	4.977	124	17	4.959	27	21	4.916	249	63	79
XI06.06	5.504	278	14	5.498	10	8	5.390	130	74	97
XI06.07	5.151	297	27	5.131	38	22	5.065	162	54	114
XI06.08	4.188	273	18	4.175	16	36	4.127	161	48	127
XI06.09	4.086	183	20	4.081	62	55	4.043	284	28	141
XI06.10	2.515	132	58	2.507	339	29	2.477	242	12	152
										160
XT09.1A	4.563	226	2	4.556	135	15	4.540	322	75	30
XT09.1B	4.306	135	21	4.300	227	5	4.284	329	68	33
XT09.2A	5.130	225	13	5.099	324	35	4.999	117	52	57
XT09.2B	4.878	206	12	4.874	300	17	4.800	83	69	60
XT09.3A	3.494	30	22	3.447	122	6	3.361	226	67	155
XT09.3B	4.067	32	22	4.037	125	7	3.916	231	67	158
XT09.3C	3.527	40	22	3.489	310	1	3.406	216	68	161
XT09.4A	3.550	49	31	3.538	143	6	3.481	242	58	200
XT09.5A	2.952	113	9	2.942	206	18	2.866	358	69	300
XT09.5B	2.910	280	2	2.890	189	25	2.813	14	65	303
XT09.6A	8.002	156	23	7.976	264	36	7.962	40	45	309
XT09.7A	10.640	257	5	10.630	164	32	10.590	355	57	310
XT09.8A	2.847	269	11	2.815	359	4	2.666	108	78	350
XT09.8B	2.917	294	18	2.879	202	6	2.735	94	71	353
XT09.9A	4.316	302	4	4.255	210	22	4.023	43	68	400
XT09.10A	4.223	338	10	4.142	244	22	4.028	91	65	422
XT09.11A	4.856	196	3	4.804	295	71	4.781	105	19	450
XT09.11B	11.150	239	9	11.110	333	27	11.060	133	61	453
XT09.13A	5.031	237	15	4.984	349	54	4.960	137	32	455
XT09.12A	6.259	218	6	6.181	24	84	6.154	128	1	457
XT09.12B	3.962	233	4	3.914	8	85	3.887	143	4	460
										470

TABLE A3.1 (CONTINUED) Directions of principal susceptibilities and position of specimens used in Chapter 3.

Spec. #	K_{max} x 10^{-3}	D_{max}	I_{max}	K_{int} x 10^{-3}	D_{int}	I_{int}	K_{min} x 10^{-3}	D_{min}	I_{min}	S P
XI02.01	5.853	53	31	5.812	198	54	5.654	313	17	10
XI02.02	6.260	52	15	6.218	316	20	6.001	176	65	30
XI02.03	8.587	242	41	8.512	88	46	8.329	344	13	45
XI02.04	9.395	245	17	9.309	52	73	9.215	154	4	55
XI02.05	10.030	266	47	9.952	85	43	9.839	176	0	65
XI02.06	10.500	200	73	10.440	63	13	10.310	331	11	75
XI02.07	8.067	352	65	8.037	252	5	7.908	160	25	85
XI02.08	12.310	211	74	12.210	63	14	11.980	331	8	105
XI02.09	10.670	243	52	10.620	59	38	10.450	150	2	120
XI02.10	8.963	181	64	8.953	307	16	8.850	43	20	145
XI02.11	8.345	347	7	8.326	247	53	8.148	82	36	160
XI02.12	7.945	341	12	7.929	237	47	7.741	81	40	175
XI02.13	7.614	347	4	7.583	253	43	7.390	81	46	190
XI02.14	5.959	337	14	5.941	244	10	5.815	118	73	210
XI02.15	5.216	14	7	5.207	282	16	5.117	128	73	245
XI02.16	5.213	17	9	5.208	285	12	5.100	143	75	255
XI02.17	5.345	238	8	5.335	330	20	5.238	127	69	300
XI02.18	5.567	224	1	5.553	315	21	5.449	131	69	325
XI02.22	18.010	41	23	17.880	218	67	17.660	311	1	345
XI02.23	17.110	46	10	16.970	315	7	16.790	189	78	346
XI02.19	5.107	254	16	5.101	348	15	5.020	120	67	355
XI02.20	5.304	332	29	5.284	227	24	5.225	105	51	370
XI02.21	5.035	28	25	5.023	296	4	4.984	198	65	390
XI02.24	6.572	177	45	6.538	18	43	6.417	278	11	420
XI02.34	5.475	197	29	5.458	102	10	5.327	355	59	665
XI02.35	5.655	190	7	5.639	96	7	5.514	355	60	685
XI02.36	6.906	201	30	6.861	105	11	6.705	357	58	700
XI02.37	6.691	205	30	6.646	109	10	6.487	2	58	725
XI02.38	6.904	201	29	6.860	105	10	6.708	358	59	750
XI02.39	7.156	209	29	7.109	114	8	6.926	10	59	765
XI02.40	7.257	208	13	7.215	115	13	7.052	341	72	790
XI02.41	9.221	0	0	9.172	90	29	8.945	270	61	810

TABLE A3.2Directions (D - declination, I - inclination) of the principal susceptibilities, weigth (g) and position (height above base of unit in cm, last column) of all specimens of hawaiian S-type pahoehoe lava used in Chapter 5.

SPECIMEN	K_{max} x 10^{-3}	D_{max}	I_{max}	K_{int} x 10^{-3}	D_{int}	I_{int}	K_{min} x 10^{-3}	D_{min}	I_{min}	Weight	S P
PO02.01A	12.030	163	48	11.980	1	41	11.970	263	9	14.08	70
PO02.01B	12.290	128	68	12.220	237	7	12.210	330	20	14.87	69
PO02.02A	13.110	339	7	13.100	248	7	13.050	117	80	17.07	63
PO02.02B	11.090	297	38	11.090	169	38	11.060	53	29	16.19	62
PO02.03A	12.230	150	34	12.210	26	40	12.190	265	32	16.50	59
PO02.03B	13.410	174	55	13.390	324	31	13.370	63	15	16.99	58
PO02.04	13.160	180	41	13.130	319	41	13.130	70	22	16.52	49
PO02.05A	12.710	326	49	12.700	208	23	12.660	103	32	17.73	44
PO02.05B	12.970	344	56	12.960	196	30	12.920	97	15	18.25	43
PO02.06A	9.561	212	75	9.532	33	15	9.512	303	0	13.06	38
PO02.06B	12.060	63	89	12.060	175	0	12.030	265	1	17.40	37
PO02.06C	14.160	23	25	14.150	127	28	14.110	258	51	19.99	32
PO02.07A	11.200	162	30	11.170	54	28	11.140	290	47	16.20	31
PO02.07B	12.410	118	54	12.400	26	1	12.360	296	36	18.26	30
PO02.08	11.150	336	6	11.140	71	41	11.130	240	48	18.05	27
PO02.09	11.250	345	79	11.210	231	4	11.200	140	10	18.00	16
PO02.10A	9.492	47	57	9.466	180	24	9.445	279	21	14.40	15
PO02.10B	10.920	42	42	10.900	193	44	10.870	298	15	17.04	14
PO02.10C	11.100	51	44	11.060	213	45	11.040	312	9	17.87	13
PO02.11A	9.979	64	13	9.858	317	51	9.850	163	36	17.38	7
PO02.11B	10.280	61	24	10.210	316	30	10.200	182	50	18.04	6
PO02.12	9.479	356	6	9.477	87	15	9.230	244	74	18.73	3
											80

TABLE A3.2 (CONTINUED) Directions of the principal susceptibilities, weigth (g) and position of S-type pahoehoe (Chapter 5).

SPECIMEN	K_{max} x 10^{-3}	D_{max}	I_{max}	K_{int} x 10^{-3}	D_{int}	I_{int}	K_{min} x 10^{-3}	D_{min}	I_{min}	Weight	S P
HP07.01A	11.240	264	73	11.190	132	11	11.050	40	12	17.40	83
HP07.01B	11.780	259	81	11.710	137	5	11.580	47	7	16.11	81
HP07.01C	13.250	245	79	13.190	132	4	13.040	41	10	16.03	79
HP07.01D	14.310	276	82	14.260	133	6	14.140	43	5	16.93	77
HP07.02A	13.490	145	74	13.390	256	6	13.170	348	15	22.52	75
HP07.02B	11.700	95	12	11.680	201	53	11.630	357	34	22.60	73
HP07.03A	10.150	270	9	10.130	172	40	10.080	11	48	21.67	69
HP07.03B	10.400	163	34	10.390	274	28	10.340	34	43	22.74	67
HP07.03C	8.224	267	25	8.198	58	62	8.181	171	12	23.52	65
HP07.04A	8.729	259	50	8.715	98	39	8.677	0	9	23.22	64
HP07.04B	6.981	78	46	6.912	270	44	6.845	174	6	20.96	62
HP07.05A	9.232	74	21	9.096	235	68	8.969	341	6	19.49	60
HP07.05B	7.938	81	30	7.868	251	60	7.798	348	4	20.26	58
HP07.05C	6.807	81	9	6.762	288	80	6.668	172	4	19.83	56
HP07.06A	6.619	79	6	6.535	220	83	6.433	349	5	17.08	55
HP07.06B	6.948	251	31	6.891	83	59	6.765	344	5	19.53	54
HP07.06C	6.739	263	57	6.673	78	33	6.568	169	2	19.39	53
HP07.07A	6.048	77	58	5.996	255	32	5.914	345	1	22.17	47
HP07.07B	3.275	329	75	3.269	63	1	3.251	154	15	23.84	45
HP07.08A	2.293	359	5	2.282	201	85	2.277	90	2	22.11	38
HP07.08B	1.952	171	6	1.950	302	81	1.942	80	7	22.81	36
HP07.08C	2.470	157	2	2.464	62	71	2.454	248	19	19.65	34
HP07.09A	7.161	179	7	7.149	303	77	7.124	88	10	21.61	31
HP07.09B	5.201	4	11	5.194	116	62	5.171	268	25	20.33	29

TABLE A3.2 (CONTINUED) Directions of the principal susceptibilities, weigth (g) and position of S-type pahoehoe (Chapter 5).

SPECIMEN	K_{max} x 10^{-3}	D_{max}	I_{max}	K_{int} x 10^{-3}	D_{int}	I_{int}	K_{min} x 10^{-3}	D_{min}	I_{min}	Weight	S P
HP07.09C	4.481	35	3	4.471	128	45	4.448	301	44	21.51	27
HP07.10A	2.152	76	17	2.134	250	73	2.130	346	2	19.04	18
HP07.10B	1.818	269	11	1.814	7	36	1.807	164	52	20.48	16
HP07.10C	1.427	357	36	1.423	262	6	1.413	164	53	20.28	14
HP07.10D	2.008	0	22	2.003	268	5	1.991	165	67	19.39	12
HP07.11A	3.771	356	54	3.756	100	10	3.750	196	34	19.47	5
HP07.11B	3.885	38	63	3.878	277	15	3.847	181	22	19.66	4
HP07.11C	4.016	330	64	3.979	90	14	3.966	186	21	19.68	2
											86
PO03.01A	13.760	279	50	13.740	186	2	13.720	95	40	14.69	56
PO03.01B	12.980	317	11	12.960	226	7	12.930	105	77	14.38	55
PO03.02	14.320	243	9	14.300	152	10	14.220	13	77	19.52	46
PO03.03	12.290	222	18	12.240	129	8	12.130	15	70	18.34	36
PO03.04A	16.870	220	22	16.650	128	5	16.460	27	68	20.79	30
PO03.04B	24.320	218	25	23.400	126	6	22.600	24	65	21.85	29
PO03.05A	19.600	38	13	19.500	255	74	19.400	130	10	21.62	18
PO03.05B	15.350	42	23	15.300	223	67	15.270	132	0	21.04	17
PO03.06A	23.100	54	6	22.900	144	2	22.700	250	84	23.43	10
PO03.06B	18.390	42	16	18.260	310	9	18.190	191	72	22.63	9
PO03.07	8.460	176	8	8.456	84	17	8.439	292	71	20.07	5
PO03.08A	9.352	67	36	9.297	318	24	9.227	202	45	18.25	1
PO03.08B	11.350	88	4	11.330	356	18	11.280	190	71	22.18	0
											68

TABLE A3.2 (CONTINUED) Directions of the principal susceptibilities, weigth (g) and position of S-type pahoehoe (Chapter 5).

SPECIMEN	K_{max} x 10^{-3}	D_{max}	I_{max}	K_{int} x 10^{-3}	D_{int}	I_{int}	K_{min} x 10^{-3}	D_{min}	I_{min}	Weight	S P
PU01.01	12.060	38	16	12.030	136	23	11.960	276	61	12.72	89
PU01.02	12.610	160	7	12.550	67	25	12.460	265	64	17.70	84
PU01.03	12.750	249	16	12.730	34	70	12.500	156	11	18.14	66
PU01.04A	17.930	271	28	17.820	104	61	17.640	4	5	24.64	57
PU01.04B	19.160	194	85	19.110	293	1	18.970	23	4	20.44	55
PU01.05	13.670	89	58	13.580	235	27	13.490	333	15	25.19	51
PU01.06	13.470	260	9	13.340	164	34	13.270	3	55	24.34	46
PU01.07	19.200	125	61	19.150	248	17	19.120	346	23	23.05	37
PU01.08	14.250	90	7	14.030	357	23	13.920	196	66	22.45	27
PU01.09	15.070	88	4	14.760	356	19	14.610	189	70	22.31	17
PU01.10	14.190	97	3	14.030	4	40	13.920	190	50	20.01	7
											105
PU00.01A	22.870	351	37	22.800	81	0	22.660	171	53	12.10	34
PU00.01B	14.750	312	39	14.730	57	17	14.640	165	46	10.85	32
PU00.01C	12.910	5	49	12.880	275	0	12.840	184	41	10.40	30
PU00.02	8.301	357	49	8.288	264	2	8.269	172	41	8.04	18
PU00.03	10.650	161	6	10.640	70	11	10.590	282	78	11.40	9
PU00.04	18.230	181	2	18.180	90	15	18.040	277	75	14.33	2
PU00.05	20.920	3	2	20.730	93	9	20.510	258	81	13.46	1
											34

TABLE A3.2 (CONTINUED) Directions of the principal susceptibilities, weigth (g) and position of S-type pahoehoe (Chapter 5).

SPECIMEN	K_{max} x 10^{-3}	D_{max}	I_{max}	K_{int} x 10^{-3}	D_{int}	I_{int}	K_{min} x 10^{-3}	D_{min}	I_{min}	Weight	S P
HP02.01A	10.530	178	7	10.520	87	13	10.490	295	76	13.37	86
HP02.01B	12.470	155	6	12.460	65	2	12.420	319	84	14.53	84
HP02.02	10.140	224	0	10.140	134	3	10.110	314	87	19.36	71
HP02.03	7.194	53	11	7.191	320	15	7.170	177	71	18.25	62
HP02.04	7.296	33	18	7.286	301	6	7.264	194	71	20.66	51
HP02.05A	5.140	29	13	5.135	299	2	5.122	202	77	17.31	40
HP02.05B	4.969	14	3	4.964	284	2	4.953	156	86	16.49	38
HP02.05C	6.363	278	9	6.359	186	12	6.346	46	75	20.18	36
HP02.06	5.648	219	18	5.644	309	1	5.640	42	72	18.15	25
HP02.07	5.891	241	15	5.888	151	0	5.875	57	75	19.61	16
HP02.08	11.610	264	44	11.610	147	25	11.580	37	36	20.56	8
											87
HP06.01A	10.430	230	7	10.420	321	5	10.410	87	81	15.73	90
HP06.01B	11.180	7	62	11.160	241	18	11.140	144	21	17.20	88
HP06.01C	13.210	269	42	13.200	8	11	13.090	109	46	17.56	86
HP06.02A	8.290	22	0	8.283	292	29	8.260	112	61	14.05	77
HP06.02B	8.877	221	4	8.870	313	23	8.847	122	67	15.70	75
HP06.02C	10.360	218	3	10.360	310	30	10.330	123	59	19.03	73
HP06.03A	8.180	339	21	8.177	241	21	8.165	110	60	15.08	63
HP06.03B	9.969	339	21	9.962	241	21	9.955	110	60	18.49	61
HP06.03C	9.029	350	74	9.023	194	15	9.019	102	6	16.30	59
HP06.03D	8.160	166	59	8.156	332	30	8.149	65	6	14.52	57
HP06.03E	8.390	147	41	8.379	334	49	8.371	240	4	14.43	55

TABLE A3.2 (CONTINUED) Directions of the principal susceptibilities, weigth (g) and position of S-type pahoehoe (Chapter 5).

SPECIMEN	K_{max} x 10^{-3}	D_{max}	I_{max}	K_{int} x 10^{-3}	D_{int}	I_{int}	K_{min} x 10^{-3}	D_{min}	I_{min}	Weight	S P
HP06.04A	8.656	322	17	8.646	144	73	8.627	52	1	14.97	48
HP06.04B	8.338	140	11	8.332	293	77	8.313	49	6	14.26	46
HP06.04C	7.122	321	10	7.113	212	60	7.101	56	28	13.31	44
HP06.04D	7.643	316	5	7.634	221	49	7.619	51	40	14.45	42
HP06.04E	8.461	306	17	8.447	204	35	8.433	58	50	14.28	40
HP06.05A	7.588	332	20	7.582	207	58	7.564	71	24	15.61	31
HP06.05B	7.841	331	6	7.835	218	76	7.819	62	13	15.20	29
HP06.06A	6.963	313	63	6.945	134	27	6.921	44	0	16.91	26
HP06.06B	7.608	311	71	7.578	141	19	7.552	50	3	17.67	24
HP06.06C	7.339	311	71	7.310	138	19	7.286	47	2	17.19	22
HP06.06D	7.482	319	60	7.447	135	30	7.432	226	2	17.36	20
HP06.07A	5.146	304	69	5.110	144	20	5.086	52	7	19.15	16
HP06.07B	5.036	322	71	4.998	141	19	4.963	231	0	17.61	14
HP06.07C	5.388	322	74	5.354	135	16	5.311	226	2	19.15	12
HP06.08A	4.403	156	16	4.401	38	59	4.392	254	26	12.57	7
HP06.08B	5.808	142	18	5.803	26	53	5.795	244	31	21.87	6
HP06.08C	6.046	39	64	6.043	131	1	6.037	221	26	21.25	5
HP06.09A	5.182	55	24	5.160	152	14	5.135	269	62	19.12	4
HP06.09B	5.174	54	21	5.158	148	10	5.124	263	66	19.50	3
HP06.09C	4.647	42	17	4.637	136	12	4.600	260	69	19.14	2
											90

TABLE A3.2 (CONTINUED) Directions of the principal susceptibilities, weigth (g) and position of S-type pahoehoe (Chapter 5).

SPECIMEN	K_{max} x 10^{-3}	D_{max}	I_{max}	K_{int} x 10^{-3}	D_{int}	I_{int}	K_{min} x 10^{-3}	D_{min}	I_{min}	Weight	S P
PO01.01A	11.260	36	19	11.250	288	41	11.240	145	43	15.04	80
PO01.01B	12.670	39	19	12.650	272	60	12.650	137	22	17.40	79
PO01.02A	9.690	37	37	9.688	151	29	9.676	268	40	14.17	76
PO01.02B	10.060	37	37	10.060	151	29	10.050	268	40	14.76	75
PO01.03A	7.758	33	66	7.754	191	22	7.748	284	8	11.14	70
PO01.03B	10.080	14	0	10.080	104	37	10.080	284	53	14.34	69
PO01.03C	9.114	49	59	9.101	152	8	9.099	247	30	13.17	68
PO01.04	9.953	245	85	9.923	65	5	9.917	155	0	14.78	65
PO01.05A	9.574	335	80	9.485	243	0	9.480	153	10	14.35	54
PO01.05B	9.867	297	79	9.791	195	2	9.778	105	10	15.92	53
PO01.06A	8.605	269	81	8.544	72	9	8.534	162	3	14.03	47
PO01.06B	9.621	293	72	9.569	56	10	9.555	148	15	16.61	46
PO01.07A	8.571	275	70	8.537	169	5	8.529	77	19	16.67	38
PO01.07B	9.575	258	56	9.552	58	32	9.546	154	9	18.49	37
PO01.08A	9.471	89	49	9.454	221	30	9.441	326	25	18.09	34
PO01.08B	9.540	82	51	9.518	219	30	9.493	322	22	18.84	33
PO01.09	9.751	105	73	9.716	233	11	9.702	325	13	17.50	29
PO01.10A	8.975	353	15	8.960	90	25	8.958	234	60	15.37	24
PO01.10B	9.868	19	32	9.853	237	51	9.844	122	19	16.95	23
PO01.11A	8.906	32	38	8.899	208	52	8.871	300	2	16.09	20
PO01.11B	9.541	214	11	9.526	347	74	9.503	121	11	17.04	19
PO01.12	10.260	204	14	10.240	305	38	10.220	97	49	19.18	14
PO01.13A	5.083	91	41	5.076	218	35	5.060	332	29	15.63	8
PO01.13B	6.891	180	10	6.884	283	51	6.853	82	37	17.58	7
											84

TABLE A3.3Directions (D - declination, I - inclination) of the principal susceptibilities, weigth (g) and position (height above base of unit in cm, last column) of all specimens of hawaiian P-type pahoehoe lava used in Chapter 5.

SPECIMEN	K_{max} x 10^{-3}	D_{max}	I_{max}	K_{int} x 10^{-3}	D_{int}	I_{int}	K_{min} x 10^{-3}	D_{min}	I_{min}	Weight	S P
HP05.01A	4.570	311	32	4.554	65	32	4.538	188	41	18.73	70.0
HP05.01B	4.684	337	33	4.650	225	30	4.637	104	42	16.22	68.0
HP05.01C	5.822	54	40	5.794	147	4	5.775	241	50	17.85	66.0
HP05.01D	5.584	182	37	5.555	63	32	5.525	306	36	21.45	64.0
HP05.01E	5.307	151	32	5.302	315	57	5.294	57	7	22.27	62.0
HP05.02A	7.975	155	12	7.950	271	64	7.919	59	23	19.58	61.0
HP05.02B	5.030	144	5	5.015	237	27	5.008	45	63	22.60	59.0
HP05.02C	4.541	140	8	4.538	245	59	4.531	45	29	20.83	57.0
HP05.03A	3.197	93	31	3.190	359	7	3.177	259	59	16.33	55.0
HP05.03B	3.661	234	13	3.658	140	15	3.652	2	70	20.50	53.0
HP05.04A	5.596	240	23	5.580	145	11	5.568	31	64	20.00	51.0
HP05.04B	4.354	246	7	4.352	155	12	4.338	4	76	18.56	49.0
HP05.05A	6.456	260	30	6.447	354	8	6.444	98	58	21.79	47.0
HP05.05B	4.561	196	33	4.556	80	34	4.554	318	38	20.49	45.0
HP05.05C	5.128	86	11	5.125	181	21	5.120	330	66	21.86	44.0
HP05.06A	5.745	46	73	5.741	172	10	5.728	264	14	20.28	43.0
HP05.06B	6.403	347	34	6.391	165	56	6.382	257	1	21.59	42.0
HP05.06C	6.507	335	32	6.497	166	57	6.489	68	5	22.90	41.0
HP05.07A	6.806	125	14	6.783	24	39	6.763	230	47	23.46	25.0
HP05.07B	6.852	184	23	6.822	87	16	6.783	325	61	22.05	23.0
HP05.07C	7.606	175	8	7.586	267	13	7.551	53	74	24.87	21.0
HP05.08A	8.183	290	9	8.126	21	6	8.050	146	79	23.29	15.0
HP05.08B	8.231	293	12	8.168	24	3	8.102	127	78	22.31	13.0
HP05.08C	8.963	292	9	8.905	23	2	8.838	126	81	24.72	11.0

TABLE A3.3 (CONTINUED) Directions of the principal susceptibilities, weigth (g) and position of P-type pahoehoe (Chapter 5).

SPECIMEN	K_{max} x 10^{-3}	D_{max}	I_{max}	K_{int} x 10^{-3}	D_{int}	I_{int}	K_{min} x 10^{-3}	D_{min}	I_{min}	Weight	S P
HP05.09B	5.805	300	13	5.794	31	2	5.777	128	77	20.45	5.0
HP05.09C	6.716	98	3	6.695	7	25	6.686	196	65	22.08	4.5
HP05.10A	5.770	149	9	5.734	56	21	5.722	261	67	24.23	4.0
HP05.10B	5.255	162	9	5.223	69	18	5.194	279	70	25.03	2.0
											72.0
HP04.01A	1.854	190	67	1.845	339	20	1.833	73	11	17.85	30.0
HP04.01B	1.272	142	53	1.269	332	36	1.267	238	5	22.79	27.5
HP04.01C	1.931	26	5	1.928	116	1	1.925	213	85	20.28	25.0
HP04.02A	1.196	145	25	1.192	313	65	1.187	53	5	14.81	30.0
HP04.02B	1.807	206	67	1.793	15	23	1.790	107	4	21.97	27.5
HP04.02C	1.712	344	2	1.709	89	84	1.709	254	6	21.75	25.0
HP04.02D	2.212	49	18	2.206	178	62	2.200	312	20	19.64	22.5
HP04.02E	2.864	98	55	2.858	277	35	2.855	8	1	19.08	20.0
HP04.03A	1.727	8	5	1.726	99	15	1.725	261	74	10.55	17.0
HP04.03B	1.987	279	6	1.982	189	8	1.981	46	80	12.75	14.0
HP04.03C	2.262	117	4	2.259	209	29	2.252	20	60	13.92	11.0
HP04.03D	3.214	321	39	3.208	223	10	3.201	120	49	21.32	8.0
HP04.03E	2.915	184	16	2.912	275	2	2.906	14	74	19.19	5.0
HP04.04A	2.589	260	12	2.586	79	78	2.582	170	0	10.13	17.0
HP04.04B	3.169	94	15	3.167	212	60	3.159	357	25	14.17	14.0
HP04.04C	3.132	181	34	3.128	85	9	3.125	342	54	14.01	11.0
HP04.04D	2.864	188	22	2.863	94	10	2.857	342	66	16.77	8.0
											30.0

TABLE A3.3 (CONTINUED) Directions of the principal susceptibilities, weigth (g) and position of P-type pahoehoe (Chapter 5).

SPECIMEN	K_{max} x 10^{-3}	D_{max}	I_{max}	K_{int} x 10^{-3}	D_{int}	I_{int}	K_{min} x 10^{-3}	D_{min}	I_{min}	Weight	S P
WA00.1A	13.920	358	1	13.850	88	7	13.610	258	83	19.04	305.0
WA00.1B	15.750	185	2	15.610	95	10	15.440	285	80	19.71	303.0
WA00.2A	11.660	212	4	11.590	302	0	11.490	33	86	19.00	295.0
WA00.2B	11.060	218	4	11.000	308	7	10.940	96	82	21.74	294.0
WA00.2C	11.100	215	5	11.050	305	3	10.970	71	84	19.53	293.0
WA00.3A	21.640	219	18	21.280	311	6	21.090	57	71	20.72	292.0
WA00.3B	14.170	207	14	14.090	116	5	14.010	8	75	22.02	290.0
WA00.3C	11.660	203	12	11.580	113	2	11.530	12	78	21.83	288.0
WA00.4A	17.050	241	16	16.900	335	14	16.720	105	69	24.58	281.0
WA00.4B	12.530	215	11	12.440	307	10	12.340	79	75	22.31	279.0
WA00.4C	10.300	220	11	10.230	129	7	10.190	5	77	25.70	277.0
WA00.5B	18.080	200	17	17.910	291	2	17.860	27	73	27.41	262.0
WA00.5C	28.480	212	17	28.290	303	1	28.210	35	73	28.19	261.0
WA00.6A	20.660	210	17	20.400	117	8	20.140	4	71	24.23	241.0
WA00.6B	24.220	203	15	23.880	297	15	23.600	71	68	26.17	240.0
WA00.6C	17.690	183	10	17.530	275	14	17.310	57	73	27.95	239.0
WA00.7A	15.050	347	2	14.980	251	70	14.950	77	19	26.42	221.0
WA00.7B	16.150	149	36	16.050	6	48	15.980	254	19	29.38	220.0
WA00.8	12.910	211	19	12.640	118	9	12.460	4	69	28.34	184.0
WA00.9	15.300	194	11	15.170	306	63	14.830	99	24	26.54	150.0
WA00.10A	12.400	196	5	12.290	65	83	12.060	286	6	28.33	123.0
WA00.10B	10.670	193	7	10.600	57	81	10.410	284	6	27.65	122.0
WA00.11A	12.910	28	8	12.720	297	3	12.310	184	81	29.31	88.0
WA00.11B	12.080	29	6	11.960	120	2	11.570	225	84	29.27	87.0
WA00.12A	15.410	198	16	15.270	297	29	14.950	83	56	25.19	176.0

TABLE A3.3 (CONTINUED) Directions of the principal susceptibilities, weigth (g) and position of P-type pahoehoe (Chapter 5).

SPECIMEN	K_{max} x 10^{-3}	D_{max}	I_{max}	K_{int} x 10^{-3}	D_{int}	I_{int}	K_{min} x 10^{-3}	D_{min}	I_{min}	Weight	S P
WA00.12B	15.290	191	20	15.180	295	35	14.890	77	49	26.97	175.0
WA00.13	16.440	356	6	16.330	232	80	15.890	87	9	26.16	158.0
WA00.14	15.240	27	16	15.110	237	72	14.740	119	9	27.55	148.0
WA00.15A	11.860	25	14	11.790	289	23	11.540	144	63	24.52	131.0
WA00.15B	10.980	20	16	10.890	280	29	10.700	134	56	28.17	130.0
WA00.16A	11.370	44	13	11.290	302	39	11.050	149	48	22.46	116.0
WA00.16B	12.180	13	22	12.090	275	20	11.850	146	59	27.70	115.0
WA00.17	11.800	36	5	11.690	304	25	11.350	136	64	29.09	73.0
WA00.18	12.380	29	7	12.260	295	31	12.100	131	58	28.02	53.0
WA00.19A	8.971	168	41	8.907	56	24	8.815	304	40	20.59	33.0
WA00.19B	8.884	161	47	8.807	43	24	8.703	296	34	20.60	32.0
WA00.19C	8.914	120	60	8.851	11	11	8.796	275	28	19.94	31.0
WA00.20A	16.500	215	54	16.440	112	9	16.130	15	35	20.06	13.0
WA00.20B	17.100	154	43	17.010	262	18	16.740	9	42	19.74	12.0
WA00.20C	16.620	140	37	16.440	27	28	16.340	270	41	19.60	11.0
											305.0
HP03.01	1.025	334	3	1.023	73	70	1.022	243	19	23.46	20.0
HP03.02	1.587	130	2	1.586	32	79	1.583	220	11	22.47	14.0
HP03.03	0.997	58	64	0.995	287	18	0.995	191	18	18.59	8.0
HP03.04	0.803	184	66	0.802	7	24	0.801	277	1	24.83	10.0
HP03.05	0.800	72	31	0.800	303	47	0.798	180	27	19.97	4.0
											20.0

TABLE A3.3 (CONTINUED) Directions of the principal susceptibilities, weigth (g) and position of P-type pahoehoe (Chapter 5).

SPECIMEN	K_{max} x 10^{-3}	D_{max}	I_{max}	K_{int} x 10^{-3}	D_{int}	I_{int}	K_{min} x 10^{-3}	D_{min}	I_{min}	Weight	S P
HP01.01	10.540	180	13	10.530	271	2	10.500	11	77	19.06	111.0
HP01.02	9.523	87	14	9.514	180	10	9.478	304	72	21.12	97.0
HP01.03A	9.075	151	17	9.052	58	8	9.005	305	71	15.75	81.0
HP01.03B	8.571	134	5	8.560	44	3	8.518	282	84	20.68	80.5
HP01.04	7.849	128	14	7.843	218	0	7.806	309	76	21.17	68.0
HP01.05	8.697	173	19	8.686	266	10	8.627	22	68	22.56	52.0
HP01.06	8.800	299	10	8.781	32	13	8.753	173	73	25.15	39.0
HP01.07	8.683	283	8	8.660	16	17	8.643	168	71	23.95	33.0
HP01.08	8.169	304	25	8.142	208	12	8.097	95	62	24.58	23.0
HP01.09	8.616	293	30	8.579	201	4	8.554	104	60	23.36	17.0
HP01.10A	8.457	295	26	8.427	32	14	8.384	148	60	15.41	11.0
HP01.10B	8.842	313	16	8.816	47	13	8.784	175	69	20.04	9.0
											137.0

TABLE A3.4 Directions (D - declination, I - inclination) of the principal susceptibilities, weigth (g) and position (height above base of unit in cm, last column) of all specimens of hawaiian a'a used in Chapter 5.

SPECIMEN	K_{max} x 10^{-3}	D_{max}	I_{max}	K_{int} x 10^{-3}	D_{int}	I_{int}	K_{min} x 10^{-3}	D_{min}	I_{min}	Weight	S P
HA01.01A	25.720	239	21	25.500	147	3	25.180	49	69	22.23	124
HA01.01B	39.320	228	7	39.010	352	78	38.640	136	10	24.12	123
HA01.01C	26.190	224	29	25.910	339	37	25.780	106	39	19.74	122
HA01.02A	29.950	271	13	29.640	7	26	29.160	156	61	26.97	108
HA01.02B	34.650	269	37	34.180	62	50	33.950	169	14	25.16	106
HA01.03A	18.260	265	39	17.880	103	49	17.740	2	9	14.67	91
HA01.03B	32.290	264	30	31.600	112	56	31.360	2	13	25.29	90
HA01.04	34.200	267	15	33.550	118	72	33.230	359	9	24.41	80
HA01.05A	34.050	274	33	33.420	47	47	33.210	166	25	24.01	65
HA01.05B	46.580	276	25	45.940	11	12	45.560	125	62	25.29	64
HA01.05C	32.010	270	23	31.460	43	57	31.170	171	21	23.22	63
HA01.06A	29.590	288	12	29.110	92	77	28.870	197	3	21.75	58
HA01.06B	34.020	274	18	33.560	100	72	33.250	5	2	26.00	57
HA01.07A	38.640	82	2	38.030	175	55	37.890	350	35	27.15	48
HA01.07B	37.770	79	9	37.320	173	26	37.020	331	63	23.98	47
HA01.08A	42.850	255	16	42.450	158	24	41.750	15	60	26.81	33
HA01.08B	43.560	244	4	43.140	151	36	42.650	340	53	24.84	32
HA01.09A	38.240	245	7	37.880	335	5	37.210	103	81	27.53	22
HA01.09B	31.150	242	8	30.830	152	0	30.410	61	82	25.00	20
HA01.09C	32.120	245	9	31.770	338	20	31.180	133	68	25.16	18
HA01.10A	27.640	225	10	27.250	319	21	26.980	111	66	25.08	6
HA01.10B	31.060	220	0	30.600	130	12	30.370	312	78	27.40	4
											130

TABLE A3.4 (CONTINUED) Directions of the principal susceptibilities, weigth (g) and position of a'a (Chapter 5).

SPECIMEN	K_{max} x 10^{-3}	D_{max}	I_{max}	K_{int} x 10^{-3}	D_{int}	I_{int}	K_{min} x 10^{-3}	D_{min}	I_{min}	Weight	S P
HA02.01A	27.730	271	28	27.560	98	62	27.210	3	3	15.93	30
HA02.01B	39.570	258	18	39.200	64	72	39.000	167	4	23.23	29
HA02.01C	30.170	83	2	29.810	327	86	29.620	173	4	24.67	28
HA02.01D	24.360	68	3	23.900	338	3	23.830	205	86	25.29	27
HA02.02A	19.240	51	20	19.070	310	28	18.960	172	54	21.43	18
HA02.02B	18.990	48	31	18.750	302	25	18.560	180	48	20.86	17
HA02.02C	34.680	115	33	34.500	343	47	34.260	223	25	23.59	16
HA02.03A	24.060	67	41	23.740	324	14	23.330	219	46	18.82	17
HA02.03B	29.420	44	14	29.050	309	22	28.440	164	64	26.60	16
HA02.03C	34.920	246	1	34.550	337	20	33.840	153	70	23.32	15
HA02.04A	28.970	237	8	28.660	330	20	28.080	125	68	24.73	8
HA02.04B	29.610	239	17	29.340	335	20	28.820	111	63	24.18	7
HA02.04C	27.450	252	10	27.030	343	6	26.400	105	79	25.77	6
HA02.05A	17.740	263	28	17.470	169	8	17.380	65	61	19.35	4
HA02.05B	20.730	261	37	20.580	156	18	20.260	46	47	22.72	3
HA02.05C	31.070	175	31	30.900	289	34	30.160	54	40	19.70	2
											30
HA03.01A	7.126	161	60	7.122	300	23	7.097	38	17	12.70	25
HA03.01B	7.589	292	75	7.571	120	15	7.550	29	2	13.82	24
HA03.01C	8.167	286	25	8.149	158	53	8.141	28	25	14.47	23
HA03.01D	13.790	297	52	13.710	207	0	13.620	117	38	13.92	22
HA03.02A	4.238	139	59	4.235	262	18	4.223	0	24	9.73	20
HA03.02B	5.632	85	65	5.611	232	21	5.605	327	12	12.29	19
HA03.02C	5.977	64	53	5.957	192	25	5.943	295	26	12.52	18

TABLE A3.4 (CONTINUED) Directions of the principal susceptibilities, weigth (g) and position of a'a (Chapter 5).

SPECIMEN	K_{max} x 10^{-3}	D_{max}	I_{max}	K_{int} x 10^{-3}	D_{int}	I_{int}	K_{min} x 10^{-3}	D_{min}	I_{min}	Weight	S P
HA03.02D	5.890	56	53	5.869	172	18	5.862	273	31	12.35	17
HA03.03A	5.177	117	3	5.150	285	87	5.144	27	1	8.10	13
HA03.03B	5.982	101	14	5.976	200	32	5.973	351	54	12.21	14
HA03.03C	6.716	50	65	6.685	172	14	6.675	267	20	12.47	13
HA03.03D	12.530	84	52	12.490	341	10	12.450	244	36	16.66	12
HA03.04A	29.710	132	10	29.560	246	67	29.300	38	21	19.07	7
HA03.04B	36.490	248	52	36.210	150	6	36.020	56	37	17.80	6
HA03.04C	30.280	296	42	30.020	206	0	29.900	116	48	17.94	5
											29
HA04.01A	63.950	329	48	63.540	119	38	63.010	221	15	20.17	161
HA04.01B	60.700	113	86	59.370	11	1	59.020	281	4	23.35	160
HA04.01C	61.130	288	45	60.870	171	25	59.980	62	35	23.21	159
HA04.02A	36.410	234	41	36.200	349	25	36.140	101	38	19.28	147
HA04.02B	42.740	292	58	42.450	174	16	42.160	76	27	24.95	145
HA04.02C	42.080	278	67	41.910	164	10	41.470	70	20	24.35	143
HA04.02D	40.890	176	33	40.660	303	42	40.340	64	30	24.71	141
HA04.02E	42.800	251	60	42.540	349	4	42.120	81	30	26.85	139
HA04.03A	32.660	320	70	32.260	57	3	32.120	148	20	17.17	130
HA04.03B	36.580	22	30	36.420	239	55	36.140	123	18	25.35	129
HA04.04A	34.130	251	22	34.060	354	30	33.920	131	51	23.55	116
HA04.04B	39.490	213	5	39.140	310	55	38.970	120	34	27.65	115
HA04.04C	40.220	214	32	39.620	324	29	39.040	86	44	28.39	114
HA04.05A	55.530	73	1	55.480	163	5	54.920	332	85	19.11	105
HA04.05B	76.040	142	16	75.890	245	39	75.750	34	47	25.23	103

TABLE A3.4 (CONTINUED) Directions of the principal susceptibilities, weigth (g) and position of a'a (Chapter 5).

SPECIMEN	K_{max} x 10^{-3}	D_{max}	I_{max}	K_{int} x 10^{-3}	D_{int}	I_{int}	K_{min} x 10^{-3}	D_{min}	I_{min}	Weight	S P
HA04.05C	64.220	257	30	64.190	132	45	63.920	6	30	23.85	101
HA04.05D	57.670	230	45	57.120	137	3	56.780	44	45	25.11	99
HA04.05E	69.950	200	28	69.640	304	25	69.420	68	51	24.48	97
HA04.06A	28.470	201	32	27.870	310	28	27.610	72	45	18.81	100
HA04.06B	42.540	295	57	42.320	187	12	41.800	90	31	26.36	98
HA04.06C	51.820	298	52	51.210	187	15	50.800	87	34	27.38	97
HA04.07A	42.280	358	15	42.010	254	43	41.110	102	43	24.17	80
HA04.07B	56.950	323	40	56.440	214	21	55.320	104	43	28.44	79
HA04.07C	55.470	325	38	54.680	219	19	53.710	109	45	29.57	78
HA04.08A	49.840	39	41	49.330	226	49	48.790	132	4	26.84	68
HA04.08B	57.070	44	14	56.840	221	76	56.280	313	1	27.97	67
HA04.08C	58.040	36	18	57.620	263	65	56.930	132	17	28.66	66
HA04.09	44.060	44	14	43.390	311	13	42.810	180	71	27.04	52
HA04.10A	48.770	168	21	48.550	69	22	47.060	296	59	26.09	44
HA04.10B	44.710	156	18	44.070	58	23	42.980	282	60	28.17	43
HA04.11A	32.540	132	13	31.880	41	5	31.370	292	76	18.76	41
HA04.11B	56.240	147	17	53.650	244	22	52.200	23	62	26.56	40
HA04.11C	49.360	145	4	48.220	236	10	47.500	34	80	28.83	39
HA04.12A	31.460	134	8	30.310	242	66	30.250	40	23	15.49	30
HA04.12B	42.460	132	6	41.470	224	11	41.040	16	77	28.00	29
HA04.12C	39.630	122	6	38.940	213	10	38.360	1	78	27.52	28
HA04.13A	43.020	295	6	41.560	202	26	40.970	37	63	15.78	24
HA04.13B	35.190	285	3	34.450	195	10	33.920	33	79	26.42	22
HA04.13C	42.060	288	4	40.930	198	9	40.430	39	80	29.81	20
HA04.13D	45.280	288	17	44.290	198	2	44.080	100	73	28.92	18

TABLE A3.4 (CONTINUED) Directions of the principal susceptibilities, weigth (g) and position of a'a (Chapter 5).

SPECIMEN	K_{max} x 10^{-3}	D_{max}	I_{max}	K_{int} x 10^{-3}	D_{int}	I_{int}	K_{min} x 10^{-3}	D_{min}	I_{min}	Weight	S P
HA04.14A	45.250	354	7	44.370	264	1	43.970	164	83	28.32	10
HA04.14B	48.500	344	7	47.390	78	28	47.010	241	61	28.28	8
											171
PO04.01A	15.400	48	28	15.060	286	45	14.930	158	32	17.89	91
PO04.01B	20.010	48	19	19.560	294	50	19.380	152	34	23.53	90
PO04.01C	18.390	50	20	17.910	286	58	17.760	149	25	20.42	89
PO04.02A	24.320	344	5	24.040	253	13	23.540	93	76	21.38	80
PO04.02B	26.790	325	3	26.700	234	4	26.100	84	85	21.59	79
PO04.03A	30.820	330	45	30.400	221	18	29.820	115	40	23.15	70
PO04.03B	30.670	329	38	30.220	221	21	29.710	109	44	25.01	69
PO04.04	25.780	324	6	25.350	233	12	24.950	82	76	24.43	62
PO04.05A	20.310	321	28	19.920	226	8	19.480	123	61	19.50	54
PO04.05B	28.260	317	25	27.620	224	7	26.830	120	64	25.64	53
PO04.06	21.760	321	5	21.320	230	12	20.940	74	77	25.29	44
PO04.07A	18.140	323	11	17.760	229	19	17.310	81	68	21.80	32
PO04.07B	20.570	321	17	20.110	225	19	19.650	90	65	25.39	31
PO04.08	20.050	314	9	19.730	218	33	19.410	58	55	25.92	12
PO04.09A	18.470	162	9	18.220	253	7	17.930	22	79	20.98	9
PO04.09B	33.060	129	18	32.940	31	23	32.470	254	60	26.87	8
PO04.09C	33.470	146	2	33.290	236	14	32.720	47	76	26.69	7
											111

TABLE A3.4 (CONTINUED) Directions of the principal susceptibilities, weigth (g) and position of a'a (Chapter 5).

SPECIMEN	K_{max} x 10^{-3}	D_{max}	I_{max}	K_{int} x 10^{-3}	D_{int}	I_{int}	K_{min} x 10^{-3}	D_{min}	I_{min}	Weight	S P
PU02.01	12.340	248	15	12.310	344	19	12.220	123	66	18.00	47
PU02.02	14.300	295	40	14.260	190	17	14.190	83	45	21.14	43
PU02.03	13.820	139	4	13.790	32	75	13.710	230	14	20.53	37
PU02.04	15.130	279	6	15.100	187	14	14.980	29	75	21.70	36
PU02.05	15.580	234	9	15.540	109	75	15.470	325	12	23.00	25
PU02.06	14.470	265	11	14.420	175	4	14.400	62	79	21.72	18
PU02.07	13.700	92	31	13.680	182	1	13.630	274	59	20.36	14
											70

TABLE A3.5 Directions (D - declination, I - inclination) of the principal susceptibilities, weigth (g) and position (height above exposed base of unit in cm, last column) of all specimens of hawaiian toothpaste lava used in Chapter 5.

SPECIMEN	K_{max} x 10^{-3}	D_{max}	I_{max}	K_{int} x 10^{-3}	D_{int}	I_{int}	K_{min} x 10^{-3}	D_{min}	I_{min}	Weight	S P
HTB0.1A	16.870	141	44	16.820	291	42	16.790	36	16	23.28	94
HTB0.1B	10.310	284	14	10.300	135	74	10.140	16	8	23.20	93
HTB0.2	9.266	119	18	9.188	263	68	9.028	25	12	25.89	73
HTB0.3	12.700	241	28	12.670	113	50	12.490	347	27	24.82	70
HTB0.4A	8.950	246	28	8.886	107	55	8.846	347	19	16.89	63
HTB0.4B	6.994	95	61	6.940	235	23	6.759	333	17	26.29	62
HTB0.5A	14.370	337	74	14.340	230	5	14.200	138	15	19.61	52
HTB0.5B	7.793	199	76	7.751	60	11	7.682	328	9	23.63	51
HTB0.6A	10.330	235	9	10.270	350	69	10.200	142	19	18.24	42
HTB0.6B	5.877	262	75	5.855	77	15	5.721	168	1	27.08	41
HTB0.7A	12.520	54	17	12.380	304	48	12.160	157	37	16.54	25
HTB0.7B	7.212	313	80	7.199	70	4	7.012	161	9	25.90	24
HTB0.8A	11.610	339	55	11.490	74	3	11.310	166	35	16.10	16
HTB0.8B	7.218	65	24	7.173	251	66	7.070	156	2	28.14	15
HTB0.9A	13.480	43	36	13.220	279	38	12.990	160	32	20.63	5
HTB0.9B	7.914	76	12	7.849	227	76	7.703	344	6	27.80	4
											100
HTF0.1A	20.910	116	38	20.610	0	30	20.480	244	38	25.01	108
HTF0.1B	20.420	129	22	20.200	22	36	19.980	244	45	24.07	106
HTF0.2A	31.480	109	84	31.040	343	3	30.650	253	5	17.67	91
HTF0.2B	21.940	176	73	21.510	350	17	21.280	81	2	27.67	89
HTF0.3A	23.060	328	56	22.910	155	34	22.660	63	3	28.28	82
HTF0.3B	24.540	302	63	24.210	161	22	23.970	64	15	28.77	80

TABLE A3.5 (CONTINUED) Directions of the principal susceptibilities, weigth (g) and position of toothpaste lava (Chapter 5).

SPECIMEN	K_{max} x 10^{-3}	D_{max}	I_{max}	K_{int} x 10^{-3}	D_{int}	I_{int}	K_{min} x 10^{-3}	D_{min}	I_{min}	Weight	S P
HTF0.4	22.390	294	49	22.100	183	17	21.840	80	36	27.77	72
HTF0.5	23.460	272	78	23.120	152	6	22.670	61	10	28.92	66
HTF0.6A	21.070	285	76	20.650	150	10	20.550	58	9	13.61	58
HTF0.6B	24.170	282	74	23.750	171	6	23.530	79	15	29.44	56
HTF0.7	26.730	265	47	26.390	168	7	25.870	72	42	29.10	50
HTF0.8	24.110	272	28	23.580	178	8	23.350	74	60	28.87	40
HTF0.9	21.430	280	29	20.970	75	59	20.870	184	11	28.45	26
											120
TP00.01	6.190	100	32	6.155	200	15	6.083	312	54	23.58	110
TP00.02	6.282	132	26	6.245	235	26	6.232	4	52	23.05	105
TP00.03	6.876	113	31	6.867	209	11	6.795	316	57	20.23	99
TP00.04	5.033	198	25	5.032	91	32	4.979	318	48	24.69	96
TP00.05	8.261	207	6	8.226	115	21	8.191	313	68	23.80	88
TP00.06	8.726	305	1	8.697	35	10	8.572	209	80	27.41	81
TP00.07	6.958	180	25	6.929	87	6	6.821	346	64	27.27	72
TP00.08	9.875	261	9	9.825	158	55	9.662	357	33	25.95	63
TP00.09	9.009	157	58	8.997	45	13	8.950	307	28	26.94	56
TP00.10	8.980	98	22	8.947	203	33	8.801	341	49	27.48	55
TP00.11	8.533	104	31	8.452	215	31	8.314	339	44	26.49	49
TP00.12	9.135	125	6	9.031	215	4	8.972	339	82	25.55	42
TP00.13	7.698	102	30	7.627	216	35	7.480	343	40	27.80	36
TP00.14	7.646	111	36	7.614	229	33	7.512	348	37	27.63	26
TP00.15	6.079	152	86	6.062	280	3	6.007	10	3	23.47	18
											115

TABLE A3.5 (CONTINUED) Directions of the principal susceptibilities, weigth (g) and position of toothpaste lava (Chapter 5).

SPECIMEN	K_{max} x 10^{-3}	D_{max}	I_{max}	K_{int} x 10^{-3}	D_{int}	I_{int}	K_{min} x 10^{-3}	D_{min}	I_{min}	Weight	S P
TP01.01	6.713	128	25	6.690	30	16	6.676	271	60	23.61	53
TP01.02	5.542	171	3	5.512	281	82	5.508	80	8	22.72	48
TP01.03	5.633	175	17	5.604	80	19	5.557	305	65	22.78	43
TP01.04	5.962	143	22	5.934	50	7	5.892	303	67	22.55	37
TP01.05	7.221	94	26	7.202	184	0	7.144	274	64	23.14	26
TP01.06	7.475	175	21	7.448	69	36	7.373	289	47	24.97	19
TP01.07	6.569	96	36	6.563	286	54	6.554	189	5	24.07	13
TP01.08	3.726	101	47	3.709	207	14	3.704	309	39	22.37	9
TP01.09	4.409	240	19	4.408	139	27	4.397	1	56	21.02	4
											58

TABLE A3.6 Directions (D - declination, I - inclination) of the principal susceptibilities, weigth (g) and position (last column: lower section (CR0.001-CR0.023B): height above base of outcrop; upper section (CR0.138A - CR0.101): depth below top of unit, in m) of all specimens from the Birkett flow, CRB, used in Chapter 7.

SPECIMEN	K_{max} x 10^{-3}	D_{max}	I_{max}	K_{int} x 10^{-3}	D_{int}	I_{int}	K_{min} x 10^{-3}	D_{min}	I_{min}	Weight	S P
CR0.001	2.066	338	5	2.058	76	57	2.055	245	32	21.96	7.86
CR0.002A	1.552	87	41	1.532	339	20	1.511	230	43	14.68	8.04
CR0.002B	2.720	282	4	2.713	189	41	2.706	17	49	19.19	8.06
CR0.003	2.549	55	18	2.542	152	21	2.537	288	62	21.28	8.08
CR0.004	1.639	142	39	1.638	29	26	1.634	275	40	17.29	8.36
CR0.005A	1.533	229	56	1.529	319	0	1.527	49	34	17.80	8.47
CR0.005B	2.259	172	13	2.255	76	25	2.254	286	62	21.83	8.49
CR0.006A	2.309	341	55	2.305	80	7	2.304	175	34	20.44	8.55
CR0.006B	3.860	58	22	3.852	291	56	3.835	159	25	24.29	8.57
CR0.007A	3.842	270	36	3.838	168	17	3.831	57	49	24.10	8.84
CR0.007B	4.202	104	13	4.196	215	56	4.196	6	31	21.26	8.86
CR0.008	6.250	63	68	6.238	213	19	6.231	307	10	23.11	8.93
CR0.009	3.532	37	55	3.526	137	6	3.520	231	34	24.37	9.08
CR0.010	7.034	272	18	7.023	33	58	6.940	173	26	26.90	9.60
CR0.011	2.185	156	25	2.181	53	26	2.177	284	52	18.55	9.83
CR0.012	2.729	93	9	2.718	188	32	2.716	350	57	18.64	9.85
CR0.013	4.919	246	15	4.914	10	63	4.827	150	21	21.72	9.99
CR0.014	2.272	289	5	2.269	22	34	2.260	192	56	21.61	10.07

TABLE A3.6 (CONTINUED) Directions of the principal susceptibilities, weigth (g) and position of Birkett flow (Chapter 7).

SPECIMEN	K_{max} x 10^{-3}	D_{max}	I_{max}	K_{int} x 10^{-3}	D_{int}	I_{int}	K_{min} x 10^{-3}	D_{min}	I_{min}	Weight	S P
CR0.015	2.493	280	1	2.488	12	64	2.477	190	26	21.80	10.13
CR0.016	2.810	275	4	2.799	86	85	2.793	185	1	25.88	10.21
CR0.017	2.122	275	13	2.112	17	43	2.108	172	44	24.45	10.22
CR0.018	4.656	28	77	4.622	257	9	4.525	165	10	27.43	10.29
CR0.019	5.991	26	77	5.955	254	9	5.829	162	9	27.32	10.36
CR0.020A	2.308	263	12	2.306	24	68	2.301	169	18	23.92	10.42
CR0.020B	4.544	337	72	4.514	68	0	4.433	158	18	21.37	10.44
CR0.021	3.947	32	59	3.933	273	17	3.885	175	26	25.82	10.52
CR0.022	3.565	1	24	3.547	121	48	3.478	255	32	22.50	10.58
CR0.023A	5.403	42	70	5.360	260	16	5.175	167	11	26.25	10.64
CR0.023B	9.322	309	76	9.267	77	8	8.798	168	11	25.84	10.66
CR0.138A	1.800	203	44	1.795	44	44	1.790	304	11	24.61	22.50
CR0.138B	1.839	189	46	1.836	11	42	1.833	280	1	26.11	22.48
CR0.137	6.187	270	19	6.145	1	3	6.126	99	71	25.96	22.50
CR0.136	3.074	15	54	3.073	147	26	3.069	249	24	24.30	21.80
CR0.135	6.576	69	48	6.548	279	38	6.502	176	15	29.33	22.00
CR0.134	5.632	44	41	5.624	284	30	5.613	171	34	24.18	21.50
CR0.133	6.180	183	1	6.147	93	2	6.117	300	88	22.69	20.60

TABLE A3.6 (CONTINUED) Directions of the principal susceptibilities, weigth (g) and position of Birkett flow (Chapter 7).

SPECIMEN	K_{max} x 10^{-3}	D_{max}	I_{max}	K_{int} x 10^{-3}	D_{int}	I_{int}	K_{min} x 10^{-3}	D_{min}	I_{min}	Weight	S P
CR0.132	3.460	313	74	3.447	78	9	3.433	170	13	19.41	20.50
CR0.131	12.340	281	77	12.240	64	10	12.130	155	8	28.49	19.90
CR0.130	10.200	83	43	10.160	254	47	10.030	349	4	29.85	19.80
CR0.129	19.270	266	75	18.720	95	15	17.480	5	2	29.89	19.25
CR0.128	18.250	47	76	18.040	248	13	17.020	157	5	29.82	19.10
CR0.127	8.888	1	81	8.853	236	5	8.547	146	7	28.13	18.45
CR0.126	6.124	181	27	6.080	351	63	6.024	89	4	19.35	17.30
CR0.125	6.042	185	12	6.017	277	7	5.951	35	76	26.31	16.60
CR0.124	14.360	189	15	13.950	98	4	13.540	354	74	28.57	15.10
CR0.123	10.930	359	2	10.750	268	20	10.380	95	70	27.49	14.90
CR0.122	9.216	322	26	9.135	89	51	9.045	218	27	24.38	13.70
CR0.121	4.103	314	68	4.066	81	13	4.038	175	17	19.51	12.60
CR0.120	4.405	167	50	4.394	303	31	4.386	47	23	26.11	12.10
CR0.119	8.579	204	13	8.487	113	4	8.441	8	76	23.28	11.50
CR0.118	8.743	357	3	8.419	88	12	8.268	256	78	20.73	11.20
CR0.117	4.547	5	55	4.499	100	3	4.493	192	35	30.23	10.60
CR0.116	6.468	316	78	6.459	175	9	6.442	84	7	22.39	10.15
CR0.115	6.022	305	41	5.984	122	49	5.955	213	1	26.04	9.60
CR0.114	6.262	254	42	6.206	72	48	6.180	163	1	22.46	9.10

TABLE A3.6 (CONTINUED) Directions of the principal susceptibilities, weigth (g) and position of Birkett flow (Chapter 7).

SPECIMEN	K_{max} x 10^{-3}	D_{max}	I_{max}	K_{int} x 10^{-3}	D_{int}	I_{int}	K_{min} x 10^{-3}	D_{min}	I_{min}	Weight	S P
CR0.113	6.263	154	60	6.210	268	13	6.130	4	26	28.75	8.50
CR0.112	8.516	259	59	8.400	107	28	8.309	11	12	27.58	7.70
CR0.111	10.060	55	61	9.875	264	26	9.466	168	12	29.72	7.30
CR0.110	16.570	299	41	16.490	99	47	16.200	200	10	29.50	6.45
CR0.109	12.350	178	77	12.260	331	12	11.990	62	6	28.38	5.90
CR0.108	24.210	108	78	23.220	330	9	22.800	239	8	29.61	5.00
CR0.107	13.520	315	83	13.190	87	4	12.710	178	5	30.04	4.40
CR0.106	12.980	252	60	12.730	68	30	12.480	159	1	29.53	3.80
CR0.105	16.620	21	85	16.190	278	1	15.930	188	5	29.69	2.80
CR0.104	15.940	209	56	15.680	71	27	15.510	331	20	29.41	2.50
CR0.103	17.650	290	89	17.380	94	1	17.020	184	0	29.89	1.80
CR0.102	15.740	32	18	15.530	189	70	15.290	299	7	30.00	1.30
CR0.101	27.010	351	55	26.650	157	34	26.050	251	7	30.69	0.79

REFERENCES

Abouzakm, A.G., 1974. Magnetic anisotropy studies in the Whin sill. MS thesis, University of Newcastle upon Tyne; 93p.

Aubele, J.C., Crumpler, L.S., and Elston, W.E., 1988. Vesicle zonation and vertical structure of basalt flows. J. Volcanol. Geotherm. Res., 35; 349-374.

Baer, G., and Reches, Z., 1987. Flow patterns of magma in dikes, Makhtesh Ramon, Israel. Geology, 15; 569-572.

Baloga, S., and Pieri, D., 1986. Time dependent profiles of lava flows. Jour. Geophys. Res. 91; 9543-9552.

Batchelor, G.K., 1991. An introduction to fluid dynamics. Cambridge University Press, Cambridge; 615pp.

Borradaile, G.J., 1988. Magnetic susceptibility, petrofabrics and strain. Tectonophysics, 156; 1-20.

Brailsford, F., 1966. Physical principles of Magnetism. D VanNostrand Company LTD, London; 274 pp.

Brown, H.C., Khan, M.A., and Stacey, F.D., 1964. A search for flow structure in columnar basalt using magnetic anisotropy measurements. Pure Appl. Geophys., 57; 61-65.

Cañón-Tapia, E., 1992. Applications to volcanology of palaeomagnetic and rock-magnetic techniques. MS thesis, Univ. of Hawaii; 146 p.

Cañón-Tapia, E., 1994. AMS parameters: guidelines for their rational selection. Pure App. Geophys., 142; 365-382.

Cañón-Tapia, E., Walker, G.P.L., and Herrero-Bervera, E., 1993. Magnetic properties of two flow units of Xitle volcano, Mexico: structural correlations and flow direction. EOS, 74 (spring meeting suppl.); 115.

Cañón-Tapia, E., Herrero-Bervera, E., and Walker, G.P.L., 1994. Flow directions and paleomagnetic study of rocks from Azufre volcano, Argentina. J. Geom. Geoelectr., 46; 143-159.

Carmichael, R.S., 1984. CRC Handbook of physical properties of rocks v. III. CRC Press Inc., Boca Ratón; 340 pp.

Cas, R.A.F., and Wright, J.V., 1988. Volcanic susccessions, modern and ancient. Unwin Hyman, London; 528 pp.

Centeno-García, E., Urrutia-Fucugauchi, J., and Herrero-Bervera, E., 1986. Diferenciación y caracterización de flujos de lava por medio de sus propiedades magnéticas: Pedregal de San Angel, México. Memoria de la reunión anual de la Unión Geofísica Mexicana; 464-471.

Clift 1978

Collinson, D.W., 1983. Methods in rock magnetism and palaeomagnetism. Techniques and instrumentation. Chapman and Hall, London; 503 pp.

Constable, C., and Tauxe, L., 1990. The bootstrap for magnetic susceptibility tensors. J. Geophys. Res. 95; 8383-8395.

Coward, M.P., 1980. The analysis of flow profiles in a basaltic dyke using strained vesicles. J. Geol. Soc. London, 137; 605-615.

Dutton, C.E.,1884.Hawaiian volcanoes. U.S. Geol. Surv., 4th annual report; 75-219.

Ellwood, B.B., 1978. Flow and emplacement direction determined for selected basaltic bodies using magnetic anisotropy measurements. Earth Planet. Scie. Lett., 41; 254-264.

Ellwood, B.B., 1979. Sample shape and magnetic grain sizes: two possible controls on the anisotropy of magnetic susceptibility variability in deep-sea sediments. Earth Planet. Scie. Lett., 43; 309-314.

Ellwood, B.B., 1982. Estimation of flow directions for calk-alkaline welded tuffs and paleomagnetic data reliability from anisotropy of magnetic susceptibility measurements: central San Juan mountains, southwest Colorado. Earth Planet. Scie. Lett. 35; 116-122.

Ernst, R.E., and Baragar, W.R.A., 1992. Evidence from magnetic fabric for the flow pattern of magma in the Mackenzie giant radiating dyke swarm. Nature 365; 511-513.

Ernst, R.E., and Pearce, G.W., 1989. Averaging of anisotropy of magnetic susceptibility data. In F.P. Agterberg and G.F. Bonham-Carter (eds.) Statistical applications in the Earth Sciences. Geol. Surv. Canada Paper 89-9; 297-305.

Fink, J.H., and Griffith, R.W., 1990. Radial spreading of viscous-gravity currents with solidifying crust. J. Fluid. Mech., 221; 485-509.

Fisher N.I., Lewis, T., and Embleton, B.J.J., 1993. Statistical analysis of spherical data. Cambridge University Press, Cambridge; 329 pp.

Gauthier, F., 1973. Field and laboratory studies of the rheology of Mount Etna lava. Phil. Trans. Roy. Soc. London, A274; 83-98.

Godinot, A., 1988. Comment on "Pipe vesicles in hawaiian basaltic lavas: their origin and potential as paleoslope indicators". Geology, 16; 90.

Grabovsky, M.A.,1956 Magnetic anisotropy of rocks. Bull. Acad. Scie. USSSR, Geophys. Ser. 4.

Grabovsky, M.A., and Brodskaya, S.Y., 1958. Normal magnetization and thermomagnetization of anisotropic rocks. Izv. Geophys. Ser. 10; 977-988.

Graham, J.W., 1966. Significance of magnetic anisotropy in Appalachian sedimentary rocks, in J.S. Steinhart and T.J. Smith (eds.) The earth beneath the continents, Geophys. Monogrr. 10; 627-648.

Gunn, B.M., and Mooser, F., 1970. Geochemistry of the volcanics of central Mexico. Bull. volcanol. 34; 577-616.

Halvorsen, E., 1974. The magnetic fabric of some dolerite intrusions, northesat Spitsbergen. Implications for their mode of emplacement. Earth Planet. Scie. Lett., 21; 127-133.

Hargraves, R.B., Johnson, D., and Chan, C.Y., 1991. Distribution anisotropy: the cause of AMS in igneous rocks? Geophys. Res. Lett., 18; 2193-2196.

Hext, G.R., 1963. The estimation of second-order tensors, with related tests and designs. Biometrika 50; 353-373

Hatcher, R.D., Jr., 1990. Structural Geology: Principles, concepts and problems. Merrill Publishing Co., Columbus; 531 pp.

Hillhouse J.W., and Wells,R.E., 1991.Magnetic fabric, flow direction and source area of the lower Miocene Peach Springs tuff in Arizona, California and Nevada. J. Geophys. Res., 96; 124443-12460.

Hrouda, F., 1982. Magnetic anisotropy of rocks and its application in geology and geophysics. Geophys. Surv. 5; 37-82.

Hulme, G., 1974 The interpretation of lava flow morphology. Geophys. Jour. R. astr. Soc. 39; 361-383.

Husch, J.M., 1990. Palisades sill: origin of the olivine zone by separate magmatic injection rather than gravity settling. Geology, 18; 699-702.

Incoronato, A., Addison, F.T., Tarling, D.H., Nardi, G., and Pescatore, T., 1983.Magnetic fabric investigations of pyroclastic deposits from Phlegrean fields, southern Italy. Nature, 306; 461-463.

Jackson, M., and Tauxe, L., 1991. Anisotropy of magnetic susceptibility and remanence: developments in the characterization of tectonic, sedimentary and igneous fabric. Rev. Geophys. 29 Supp.; 371- 376.

Jeffery, G.B., 1922. The motion of ellipsoid particles immersed in a viscous fluid. Proc. R. Soc. Lond., A102; 162-179.

Jelinek, V., 1978. Statistical processing of anisotropy of magnetic susceptibility measured on groups of specimens. Studia geoph. et geod. 22; 50-62.

Jelinek, V., 1981. Characterization of the magnetic fabric of rocks. Tectonophysics 79; T63-T67.

Khan, M.A., 1962. The anisotropy of magnetic susceptibility of some igneous and metamorphic rocks. J. Geophys. Res. 67; 2873-2885.

Kilburn, C.R.J.,1981. Pahoehoe and aa lavas: adiscussion and continuation of the model of Peterson and Tilling. Jour. Volcanol. Geotherm. Res., 11; 373-382.

Kilburn, C.R.J., and Lopes, R.M.C., 1991. General patterns of flow field growth: aa and blocky lavas. J. Geophys. Res., 96; 19721-19732.

Kilburn, C.R.J., and Luongo, G., 1993. Preface in "Active lavas: monitoring and modelling" (KilburnC.R.J., and Luongo, G., eds.) University College London Press, London; ix.

Knight, M.D., and Walker, G.P.L., 1988. Magma flow directions in dikes of the Koolau complex, Oahu, determined from magnetic fabric studies. J. Geophys. Res. 93; 4301-4319.

Knight, M.D., Walker, G.P.L., Ellwood, B.B., and Diehl, J., 1986. Stratigraphy, paleomagnetism, and magnetic fabric of the Toba tuffs: constraints on the sources and eruptive styles. Jour. Geophys. Res. 91; 10355-10382.

Kolofikova, O., 1976. Geological interpretations of magnetic properties of basalts: examples of the Chibsky Les lava flow of the Velky Roudny volcano (Nizky Jesenik) Cas. Min. Geol. 21; 387-396 (In Czech)

Komar, P.D., 1976. Phenocryst interactions and the velocity profile of magma flowing though dikes or sills. Geol. Soc. Am., Bull., 87; 1336-1342.

Kuno, H., 1965. Fractionation trends of basalt magmas in lava flows. J. Petrol. 6; 302-321.

Landon, R.D., and Long, P.E., 1989. Detailed stratigraphy of the N2 Grande Ronde Basalt, Columbia River Basalt Group, in the central Columbia Plateau. In Reidel, S.P., and Hooper, P.R., (eds.) Volcanism and tectonism in the Columbia River flood - basalt province. Geol. Soc. Am., Spec. Pap. 239; 55-66.

Libby, W.F., 1951. Radio carbon dating. Chicago, 124 pp.

Lienert, B.R., 1991. Monte Carlo simulation of errors in the anisotropy of magnetic susceptibility: a second-rank symmetric tensor. J. Geophys. Res., 96; 19539-19544.

Long, P.E., and Wood, B.J., 1986. Structures, textures, and cooling histories of Columbia River basalt flows. Geol. Soc. Am., Bull., 97; 1144-1155.

MacDonald, G.A., 1953. Pahoehoe, aa and block lava. Am. J. Sci., 251; 169-191.Menke, W., and Abbott, D., 1981. Geophysical Theory. Columbia University Press, New York; 458 pp.

MacDonald, G.A., and Katsura, T., 1964. Chemical composition of Hawaiian lavas. Jour. Petrol. 5; 82-133.

MacDonald, W.D., and Palmer, H.C, 1990. Flow directions in ash-flow tuffs: a comparison of geological and magnetic susceptibility measurements, Tshirege member (upper Bandelier tuff), Valles caldera, New Mexico, USA. Bull. Volcanol., 53; 45-59.

MacDonald, W.D., Palmer, H.C., and Hayatsu, A. 1992. Egan range volcanic complex, Nevada: geochronology, paleomagnetism and magnetic fabrics. Phys. Earth Plant. Int. 74; 109-126.

Manga, M., and Stone, H.A., 1994. Interactions between bubbles in magmas and lavas: effects of bubble deformation. J. Volcanol. Geotherm. Res., 63; 267-279.

Martin del Pozzo, A.L., 1982. Monogenetic Vulcanism in Sierra Chichinautzin, México. Bull. Volcanol. 45; 9-24.

Maxwell, J.C., 1904. A treatise on electricity and magnetism II. Clarendon Press, Oxford; 500 pp.

McMillan , K., Cross, R.W., and Long, P.E., 1987. Two-stage vesiculation in the Cohassett flow of the Grande Ronde Basalt, south-central Washington. Geology, 15; 809-812.

Menke and Abbot, 1981.

Naranjo, J.A., Sparks, R.S.J., Stasiuk, M.V., Moreno, H., Ablay, G.J., 1992. Morphological, structural and textural variations in the 1988-1990 andesite lava of Lonquimay volcano, Chile. Geol. Mag. 129; 657-678.

Noe-Nygaard, 1968. On extrusion forms in plateau basalts. Shield volcanoes of the "scutulum" type. Science in Iceland Anniversary volume, 10-13. Societas Scientarum Islandica, Rekjavik.

Noltimier, H.C., 1971. Magnetic rock cylinders with negligible shape anisotropy. J. Geophys. Res., 76; 4035-4037.

Nye, J.F., 1960. Physical properties of crystals. Oxford University Press, London; 323 pp.

O'Really, W., 1984. Rock and mineral magnetism. Blackie and son, LTD, Glasgow; 220 pp.

Osborn, J.A., 1945. Demagnetizing factors for the general ellipsoid. Phys. Rev., 67; 351-357.

Park, J.K., Tanczyk, E.I., and Desbarats, A., 1988. Magnetic fabric and its significance in the 1400 Ma Mealy diabase dykes of Labrador, Canada. J. Geophys. Res., 93; 13689-13704.

Park, S., and Iversen, J.D., 1984. Dynamics of lava flow: thickness growth characteristics of steady two-dimensional flow. Geophys. Res. Let. 11; 641-644.

Petersen, N., 1976. Notes in the variation of magnetization within basalt lava flows and dikes. Pure App. Geophys. 114; 177-193.

Peterson, D.W., and Tilling, R.I., 1980. Transition of basaltic lava from pahoehoe to aa, Kilaue volcano, Hawaii: field observations and key factors. J. Volcanol. Geotherm. Res., 7; 271-293.

Philpotts, A.R., and Lewis, C.L., 1987. Pipe vesicles-an alternate mode for their origin. Geology, 15; 971-974.

Pinkerton, H., and Wilson, L., 1994. Factors controlling the lenths of channel-fed lava flows. Bull. Volcanol., 56; 108-120.

Porath, H., Stacey, F.D., and Cheam, A.S., 1968. The choice of specimen shape for magnetic anisotropy measurements on rocks. Earth Planet. Scie. Lett., 1; ???

Puranen, R., Pekkarinen, L.J. and Pesonen, L.J. 1992. Interpretation of magnetic fabrics in the early proterozoic diabase dykes of Keuruu, central Finland. Phys. Earth Plant. Int. 72; 68-82.

Rees, 1968.

Rochette, P., 1988. Inverse magnetic fabric in carbonate-bearing rocks. Earth Planet. Scie. Lett. 90; 229-237.

Rochette, P., Jackson, M., and Aubourg, C., 1992. Rock magnetism and the interpretation of anisotropy of magnetic susceptibility. Rev. Geophys., 30; 209-226.

Rowland, S.K., and Walker, G.P.L., 1987. Toothpaste lava: characteristics and origin of a lava structural type transitional between pahoehoe and aa. Bull. Volcanol., 49; 631-641.

Rowland, S.K., and Walker, G.P.L., 1990. Pahoehoe and aa in Hawaii: volumetric flow rate controls the lava structure. Bull. Volcanol., 52; 615-628.

Sahagian, D.L., 1985. Bubble migration and coalescence during the solidification of basaltic lava flows. J. Geol., 93; 205-211.

Sahagian, D.L., Anderson, A.T., and Ward, B., 1989. Bubble coalescence in basalt flows: comparison of a numerical model with natural examples. Bull. Volcanol., 52; 49-56.

Seaman, S.J., McIntosh, W.C., Geissman, J.W., Williams, M.L., and Elston, W.E., 1991. Magnetic fabrics of the Bloodgood Canyon and Shelley Peak tuffs southwestern New Mexico: implications for emplacement and alteration processes. Bull. Volcanol., 53; 460-476.

Shcherbakov, V.P., Lamash, B.E., and Sycheva, N.K., 1995. Monte Carlo modelling of thermoremanence acquisition in interacting single domain grains. Phys. Earth Plant. Int., 87; 197-211.

Smith, E.I., and Rhodes, R.C., 1972. Flow direction determination of lava flows. Geol. Soc. Am. Bull., 83; 1869-1873.

Smith, J.V., Miyake, Y., and Yamauchi, S., 1993. Flow direction and groundmass shear zones in dykes, Shimane Peninsula, Japan. Geol. Mag., 130; 117-120.

Sprowl, D.R., 1990. Numerical estimation of interactive effects in single-domain magnetite. Geophys. Res. Lett., 17; 2009-2012.

Stacey, F.D., 1963. The physical theory of rock magnetism. Adv. Phys., 12; 45-133.

Stacey, F.D., and Banerjee, S.K., 1974. The physical principles of rock magnetism. Elsevier, Amsterdam; 195 pp.

Staudigel, H., Gee, J., Tauxe, L., and Varga, R.J., 1992. Shallow intrusive directions of sheeted dikes in the Troodos ophiolite:anisotropy of magnetic susceptibility and structural data. Geology 20; 841-844.

Stein, D.J., and Spera, F.J., Rheology and microstructure of magmatic emulsions: theory and experiments. J. Volcanol. Geotherm. Res., 49; 157-174.

Stephenson, A. 1994. Distribution anisotropy: two simple models for magnetic lineation and foliation. Phys. Earth Planet. Int. 82; 49-53.

Stoner, E.C., 1945. The demagnetizing factors for ellipsoids. Phil. Mag., 36; 803-821.

Symons, D.T.A., 1975. Age and flow direction from magnetic measurements on the historic Aiyansh flow, British Columbia. J. Geophys. Res. 80; 2622-2626.

Tarling, D.H., and Hrouda, F., 1993. The magnetic anisotropy of rocks. Chapman and Hall, London; 217pp.

Taylor, G.I., 1923. The motion of ellipsoidal particles in a viscous fluid. Proc. Roy. Soc. London A103; 58-61.

Tormey, D.R., Frey, F.A., and López-Escobar, L., 1989. Geologic history of the active Azufre-Planchon-Peteroa volcanic center (35°15'S, southern Andes), with implications for the development of compositional gaps. Asoc. Geol. Argentina, Rev. 44; 420-430.

Verma, S.P., and Armienta, M.A., 1985. 87Sr/86Sr, alkali and alkaline earth element geochemistry of Chichinautzin Sierra, Mexico. Geofis. Int. 24; 665-678.

Walker, G.P.L., 1987. Pipe vesicles in Hawaiian basaltic lavas: their origin and potential as paleoslope indicators. Geology, 15; 84-87.

Walker, G.P.L., 1989. Spongy pahoehoe in Hawaii: a study of vesicle-distribution patterns in basalt and their significance. Bull. Volcanol., 51; 199-209.

Walker, G.P.L. 1991. Structure, and origin by injection of lava under surface crust, of tumuli, "lava rises", "lava-rise pits", and "lava-inflation clefts" in Hawaii. Bull. Volcanol. 53; 546-558.

Walker, G.P.L., 1995a. Origin of vesicle types and distribution patterns in the Xitle pahoehoe basalt, in Mexico City. Bull. Volcanol., in press

Walker, G.P.L. 1995b. Recognition of lava rises: an alternative mode of lava flow growth. (in prep.)

Waters, A.C., 1960. Determining direction of flow in basalts. Am. J. Sci., 258; 350-366.

Wilmoth, R.A., and Walker, G.P.L., 1993. P-type and S-type pahoehoe: a study of vesicle distribution patterns in hawaiian lava flows. J. Volcanol. Geotherm. Res., 55; 129-142.

Williams, and McBirney, 1979. Volcanology. Freeman and Cooper, San Francisco, 397 pp.

Wolff, J.A., Ellwood, B.B., and Sachs, S.D., 1989. Anisotropy of magnetic susceptibility in welded tuffs: application to a welded-tuff dyke in the tertiary Trans-pecos Texas volcanic province, USA. Bull. Volcanol., 51; 299-310.